Spectral and Physicochemical Characteristics of nC$_{60}$ in Aqueous Solutions

Xiaojun Chang

Dissertation submitted to the faculty of the Virginia Polytechnic Institute and State University in partial fulfillment of the requirement of the degree of

Doctor of Philosophy

In

Civil and Environmental Engineering

Peter J. Vikesland
Linsey C. Marr
John C. Little
John R. Morris

July 21st, 2011
Blacksburg, VA

Keywords: Fullerene nanoparticles (nC$_{60}$), UV-Vis spectra, extinction coefficient, citrate, carboxylic acids.

Spectral and Physicochemical Characteristics of nC$_{60}$ in Aqueous Solutions

Xiaojun Chang

ABSTRACT

Despite its extremely low solubility in water, fullerite C_{60} can form colloidally stable aqueous suspensions containing nanoscale C_{60} particles (nC$_{60}$) when it is subject to contact with water. nC$_{60}$ is the primary fullerene form following its release to the environment. The aim of the present study was to provide fundamental insights into the properties and environmental impacts of nC$_{60}$. nC$_{60}$ suspensions containing negatively charged and heterogeneous nanoparticles were produced via extended mixing in the presence and absence of citrate and other carboxylates. These low-molecular weight acids were employed as simple surrogates of natural organic matter. The properties of nC$_{60}$ were characterized using dynamic light scattering (DLS), transmission electron microscopy (TEM), and UV-Vis spectroscopy. nC$_{60}$ produced in the presence of carboxylate differs from that produced in water alone (aq/nC$_{60}$) with respect to surface charge, average particle size, interfacial properties, and UV-Vis spectroscopic characteristics. Importantly, regularly shaped (spheres, triangles, squares, and nano-rods) nC$_{60}$ nanoparticles were observed in carboxylate solutions, but not in water alone. This observation indicates that a carboxylate-mediated 'bottom-up' process occurs in the presence of carboxylates. Changes in the UV-Vis spectra over time indicate that reactions between C_{60} and water or other constituents in water never stop, potentially leading to significant morphologic changes during storage or as a

result of simple dilution. These results suggest that studies examining the transport, fate, and environmental impacts of nC$_{60}$ should take the constituents of natural waters into consideration and that careful examination on the properties of the tested nC$_{60}$ should be conducted prior to and during each study.

Acknowledgements

I would like to thank my advisor, Dr. Peter Vikesland for his guidance and encouragement throughout my research. Without his help, this dissertation would not have been possible. Despite his busy schedule, he has always been supportive and ready to help me figure out my problems. Chemistry and research methods are not the only thing that I have learnt from him. His enthusiasm and attitude towards research work inspired me a lot and prepared me well for the future.

I would also like to thank the members of my committee Dr. Linsey Marr, Dr. John Little, and Dr. John Morris who have provided valuable advice on this dissertation.

I acknowledge the National Science Foundation, Environmental Protection Agency, Center for the Environmental Implications of Nanotechnology, and Institute for Critical Technology and Applied Science for providing funding for this research.

I owe my gratitude to Julie Petruska and Jody Smiley. I could not have finished without their non-ending help in the lab. My thanks also go to Matt Hull, Matt Chan, Weinan Leng, Becky Halvorson, Rob Rebodos, and Krista Rule, who has been always offering me help and suggestions.

Lastly, I would like to thank my friends and family. I especially want to thank my parents for their love, support and confidence in me. I also want to dedicate this dissertation to my grandparents who loved me unconditionally and taught me to be a decent person.

Table of Contents

List of Figures

List of Tables

Attribution Page

Chapter 3, 4, 6, and 7 are the manuscripts prepared for *Environmental Science and Technology*.

Chapter 5 is reproduced with permission from *Environmental Pollutions.* **2009**, Issue 157, pp. 1072-1080.

Chapter 1 Introduction

1.1 Background

Buckminsterfullerene $C_{60,}$ discovered by Kroto et al.[1] in 1985, has attracted extensive attention due to the unique physical, chemical, optical, and structural properties imparted by its structure. The potential applications of C_{60} in various fields, including electronics,[2] medicines,[3-5] biological techniques,[6,7] solar cells,[8,9] sensors,[10,11] water and wastewater treatment,[12] and cosmetics,[13,14] have a promising future based on results from fundamental studies of C_{60}. As of the year 2010, the production of C_{60} has reached tons per year.[15,16] The increases in production and the number of applications will inevitably lead to release of C_{60} to the environment, which elicits concerns about the environmental, health, and safety impacts of C_{60}.

C_{60}, a cage-like molecule containing twenty six-member and twelve five-member rings, consists entirely of sp^2-hybridized carbon.[17] Each carbon atom has two different kinds of bonds: two short C-C bonds (1.40 Å) shared by adjacent hexagons and one long C-C bond (1.45 Å) fusing a pentagon and a hexagon.[18] The former bond has a prevalent double-bond character, while the latter one has substantial single-bond character. The pentagons dominate the curvature of the cage.[19] Because of the curvature of the C_{60} molecule, the σ orbitals are not coplanar and have a tangential component. The π cloud surrounding the cage molecule is therefore not the same as that of other aromatic molecules. NMR studies have shown that C_{60} has an icosahedral point group symmetry (I_h).[20,21]

Although fullerite C_{60} has extremely low solubility in water (1.3×10^{-11} ng/mL),[22-24] it can form stable colloidal suspensions containing fullerene nanoparticles (nC_{60}) when it is subject to contact with water.[25-28] Therefore, we could expect that when fullerite C_{60} is released to

environmental waters, nC$_{60}$ would be the main form existing in aqueous solutions. To investigate the transport, fate, and environmental impacts of fullerite C$_{60}$, it is imperative to understand the properties of nC$_{60}$ and the interactions between C$_{60}$ and other constituents in natural waters. Natural organic matter (NOM), one of the most important constituents in environmental waters, has been reported as having the ability to stabilize nC$_{60}$ particles.[29-31] The mechanism(s) by which NOM interacts with nC$_{60}$ and how it stabilizes nC$_{60}$, however, are still unknown. Due to the complicated structure of NOM, it is difficult to investigate its effect on the formation and properties of nC$_{60}$.

1.2 Research Objectives

At the time this dissertation was undertaken there were a number of published papers on the formation, properties, transport, and toxicity of nC$_{60}$. However, variations in preparation method and the lack of consistency and collaboration between different analytic methods prevent us from fundamentally understanding and accurately estimating the environmental impact of C$_{60}$. The overall goal of this study was to better understand the formation and properties of nC$_{60}$ in aqueous solutions. Stable colloidal suspensions consisting of C$_{60}$ nanoparticles were prepared via extended mixing. Dynamic light scattering (DLS), transmission electron microscopy (TEM), and UV-Vis spectroscopy were employed to characterize the as produced nC$_{60}$. Small molecular weight carboxylic acids, as simplified surrogates of NOM, were used in the present study to investigate their effects on nC$_{60}$ formation. The objectives of this research were:

(1) To better understand the UV-Vis spectra of aq/nC$_{60}$ (produced via extended mixing in water alone) and to establish relationships between its spectral properties and its colloidal properties;

(2) To investigate the properties of nC$_{60}$ produced in the presence of citrate and to determine the effects of different types of carboxylic acids on the formation of nC$_{60}$;

(3) To evaluate the stability of nC$_{60}$ suspensions;

1.3 Dissertation Outline

This dissertation contains a total eight chapters including this introductory chapter. **Chapter 2** provides a brief literature review presenting the background of nC$_{60}$ and the current state of knowledge in the field of the properties of nC$_{60}$ and its environmental impacts. A study on the UV-Vis spectra of aq/nC$_{60}$ suspensions is described in **Chapter 3**. The temporal changes in aq/nC$_{60}$ properties were evaluated and the effects of particle size and preparation method were observed. **Chapter 4** notes the challenge of reproducing nC$_{60}$ via extended mixing and calculates extinction coefficients for various aq/nC$_{60}$ suspensions. According to the results presented in this chapter, extinction coefficients for aq/nC$_{60}$ are significantly dependent upon its colloidal properties, and therefore they should be carefully used when trying to determine the C$_{60}$ concentration for different suspensions. nC$_{60}$ suspensions were produced in the presence of different carboxylic acids in **Chapter 5**. The identities and concentrations of carboxylic acids greatly affect the formation of nC$_{60}$. In **Chapter 6** nC$_{60}$ were produced in the presence of citrate and other carboxylates via extended mixing. Solution chemistries dictate the formation of nC$_{60}$ in salt solutions and also alter their interfacial and morphological properties. Changes in properties of nC$_{60}$ during dilution were investigated in **Chapter 7**. According to the results from this chapter, simple dilution has the potential to greatly alter the surface charge, particle size, and particle morphology of nC$_{60}$. **Chapter 8** summarizes the collected results and discusses the environmental implications of the present study.

Chapter 2 Literature Review

2.1 Solubility of C_{60}

A 'real' solution of fullerite C_{60} is homogeneous and fully solvated. To produce such solutions, the fullerite C_{60} crystal lattice breaks down, forms individual molecules, and these molecules are individually dispersed in the solvent. The solubilization of C_{60} in a liquid solvent involves three kinds of interactions: (i) solute-solvent, (ii) solvent-solvent, and (iii) solute-solute. Interactions (i) and (iii) are of van der Waals type and weak, while interaction (ii) in a polar solvent can be relatively strong. Since a C_{60} molecule is much larger than most solvent molecules, its solubilization greatly disrupts the local solvent structure. For polar solvents with a dielectric permittivity larger than 13, interactions between C_{60} and the solvent molecules are too weak to compensate for reduced solvent-solvent interactions. The interactions between C_{60} molecules are therefore favored and the fullerene molecules associate to form aggregates.[32-34] Dynamic light scattering (DLS) and static light scattering (SLS) have shown that dilute solutions of C_{60} aggregate slowly in benzene[35] at room temperature. The formed aggregates are weakly held together and unstable against mechanical shaking. Nath et al.[36] confirmed similar reversible C_{60} aggregation in benzonitrile by DLS, UV-VIS, and scanning electron microscopy (SEM). Recently, formation of C_{60} aggregates in various organic solvents (such as carbon disulfide,[37,38] toluene,[39] and *N*-methylpyrrolidinone[40]) and their mixtures[33,40-42] have been studied. Therefore, organic solutions of C_{60} reported in many studies are actually colloidal solutions containing both dissolved C_{60} molecules and C_{60} aggregates.[35,43]

Ruoff et al.[44] have shown that C_{60} has high solubility in solvents with a large refractive index, a dielectric constant around 4, a large molecular volume, a Hildebrand solubility parameter equal

to 10 $cal^{1/2}cm^{-3/2}$, and a tendency to act as a moderate nucleophile. As a result, aromatic compounds are better solvents for C_{60} than alkanes or polar organic solvents (e.g., alcohols). They concluded that the solubility of C_{60} is a complicated function of solvent properties and cannot be uniformly predicted by a single solvent parameter (e.g., refractive index or molecular weight).

2.2 Formation of *n*C_{60} in Water

The solubility of fullerite C_{60} is the highest in nonpolar solvents and solvents of low polarity, while C_{60} solubility in water is extremely low (1.3×10^{-11} ng/mL).[22] The high hydrophobicity of C_{60} impedes its dispersion in aquatic systems, which is required in most applications, especially in biological systems. Accordingly, several methods have been used to increase C_{60} solubility in aqueous solutions: (i) introduction of hydrophilic groups to C_{60} by covalent functionalization;[45-48] (ii) formation of water soluble host-guest complexes (e.g., with γ-cyclodextrins[49,50] or polyvinylpyrrolidone[51,52]); and (iii) facilitation of C_{60} solubilization by the addition of surfactants.[53-55]

Although solutions of pristine molecular C_{60} in aquatic systems have proven difficult to produce, it is possible to disperse un-derivatized C_{60} in water as stable colloidal nanoparticles using solvent exchange, extended mixing, or sonication, each of which is discussed in the following section. *n*C_{60} suspensions produced using these methods have C_{60} concentrations ([C_{60}]) up to 100 mg/L, [25,27,56,57] which is ~11 orders of magnitude higher than its estimated molecular solubility.[22,44] Brant et al. developed the notation *n*C_{60} to describe a stable colloidal nanoparticle of C_{60} in aqueous systems and the notation "initial solvent/colloidal species".[58] The prefix designates the production methods or solution wherein the *n*C_{60} is formed. For instance, THF/*n*C_{60} refers to *n*C_{60} produced via solvent exchange with THF; SON/*n*C_{60} is *n*C_{60} produced

by ultrasonicating a mixture of C_{60} powder and water; and aq/$n$$C_{60}$ is $n$$C_{60}$ produced by extended mixing in water alone.

Solvent Exchange. In 1994, Scrivens and Tour[25] were the first to produce aqueous dispersions of C_{60} without the use of stabilizers in the final suspension. In this protocol, an aqueous C_{60} suspension was prepared by adding a saturated benzene solution of C_{60} into THF. The resulting light purple solution was then added dropwise to rapidly stirred acetone. Addition of water to this mixture resulted in the formation of a fine mustard yellow suspension and the organic solvents were removed by distillation. The final BTA/$n$$C_{60}$ (where BTA refers to Benzene-Toluene-Acetone) suspension was stable for more than 3 months.

In 1995, Andrievksy and co-workers produced an aqueous colloidal solution of fullerenes via a simpler solvent exchange method.[26] In their procedure, the only organic solvent employed was toluene, which was then removed through evaporation by sonication. A brownish-orange and slightly opalescent Tol/$n$$C_{60}$ suspension was obtained after filtration through a 0.22 μm filter.

The two methods described above provide a facile way to prepare aqueous C_{60} suspensions with regularly shaped particles[59,60] for biological applications. However, the use of potentially toxic organic solvents such as benzene and toluene has the potential to produce materials with toxicity to biological systems. In 2001, Deguchi *et al*. published another solvent exchange method involving a comparatively less toxic solvent, THF, to produce THF/$n$$C_{60}$.[27] In this method, C_{60} saturated THF was injected into an equal amount of water. The THF was then removed by purging the solution with nitrogen. This protocol involves a bottom-up process (Figure 2.1), during which fullerite C_{60} molecules dissolved in organic solvents aggregate into larger regularly shaped $n$$C_{60}$.

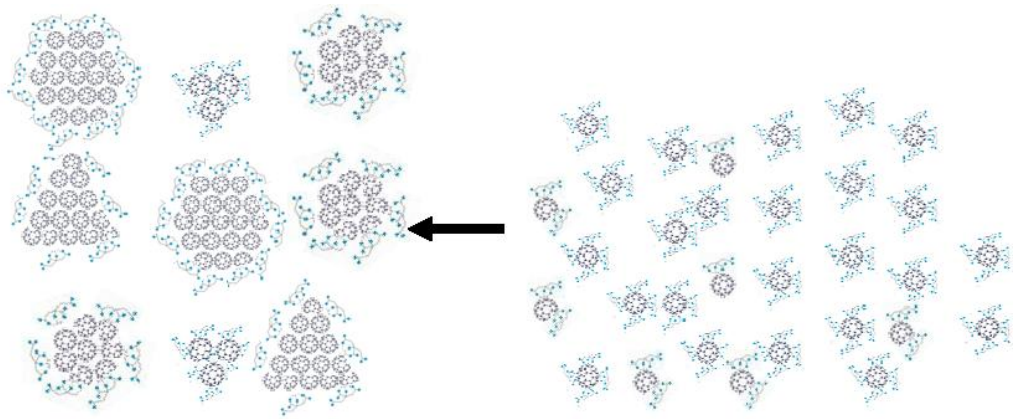

Figure 2.1 The bottom-up process.

While the details of each solvent exchange method to form nC$_{60}$ may differ slightly, these methods all include three main steps: (i) dissolution of fullerite C$_{60}$ in an organic solvent (e.g. benzene,[61] toluene,[26] THF,[27] ethanol,[62] chlorobenzene[63]) or a combination of organic solvents (e.g. benzene-THF-acetone[25] and toluene-THF-acetone[64]); (ii) mixing the C$_{60}$ solution with water; and (iii) removing organic solvents by distillation,[25,61] evaporation,[64] purging gas,[27] or sonication.[26] HPLC, FTIR, and UV-Vis data have confirmed that nC$_{60}$ produced via solvent exchange consists of unmodified C$_{60}$ molecules.[27,65]

Sonication. Compared with the multi-step solvent exchange technique, the sonication method is much simpler and only involves direct dispersion of fullerite C$_{60}$ in water. Ko et al.[66] added 20 mg of C$_{60}$ to 10 mL of concentrated sulfuric acid and nitric acid at a volumetric ratio of 3:1. The mixture was ultrasonicated for 3 days in air at 25-43 ºC. After neutralization by NaOH, a dark brownish-orange nC$_{60}$ suspension was obtained. In recent studies by Belousova et al.[67] and Labille et al.,[68] SON/nC$_{60}$ was prepared by sonicating a mixture of fullerite C$_{60}$ and water alone for a time period longer than 10 hours. TEM images (Figure 2.2) of these SON/nC$_{60}$ indicate that irregularly shaped nC$_{60}$ are formed during sonication.

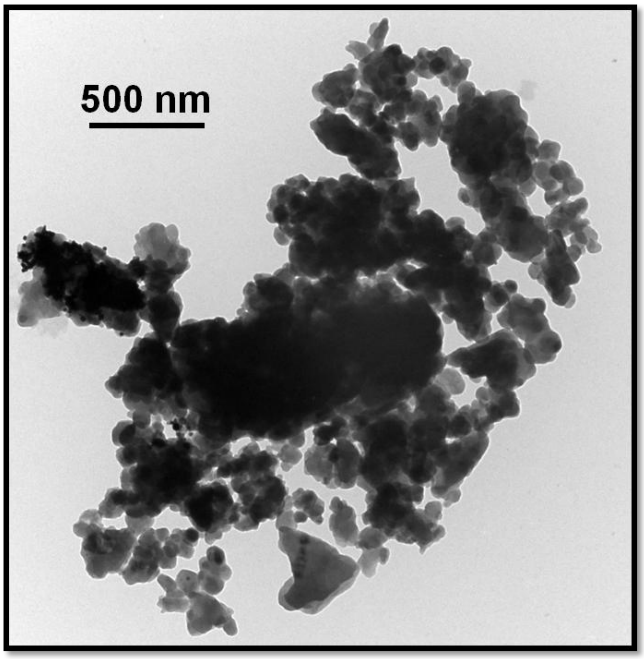

Figure 2.2 TEM image of SON/*n*C_{60}.

Extended Mixing. Compared with sonication, extended mixing produces *n*C_{60} under milder conditions. Cheng et al.[28] were the first to employ extended mixing to prepare *n*C_{60} suspensions in 2004. As-purchased C_{60} was mixed with a solution of NaCl and NaN_3 by magnetic stirring for 2 days and the resulting suspension was turbid and brownish. Labille et al. stirred 200 mg of C_{60} powder in 250 mL ultrapure water for 14 days and obtained a 500 mg/L *n*C_{60} suspension after filtration and concentration.[69] Several recent studies[58,59] have shown that aq/*n*C_{60} obtained by extended mixing has different surface charge, size, structure, morphology and toxicity from that prepared via solvent exchange. During the stirring process, bulk fullerite C_{60} starting material is weathered into small particles by the mechanical forces provided by magnetic stirring. This top-down process (Figure 2.3) results in the formation of irregularly shaped heterogeneous *n*C_{60} particles.

Each of the techniques for preparing nC$_{60}$ has their advantages and disadvantages. Solvent exchange produces regular, homogenous nC$_{60}$ particles, which are easy to characterize and to use in transport studies. However, the use of intermediate organic solvents may introduce unexpected adverse effects and toxicity to aqueous systems. Sonication is a fast and convenient way to prepare nC$_{60}$ suspensions;[59] however, the high temperature and pressure created by cavitation bubbles produced during ultrasonic treatment[70] may facilitate chemical reactions between C$_{60}$ and water or other constituents in aquatic systems, which subsequently alter the properties of nC$_{60}$. Of the different methods, extended mixing is the simplest and it may provide a more intuitive simulation of the slow process when C$_{60}$ is released to the environment. But the resulting highly heterogeneous nC$_{60}$ particles are not expected to be useful for industrial applications.

2.3 Properties of nC$_{60}$

To fully evaluate the environmental impact of nC$_{60}$ formation, its physicochemical properties, which ultimately determine its transport, fate, and toxicity, are the key parameters needed for well-designed studies. However, the application of various preparation pathways may result in different physicochemical characteristics for the nC$_{60}$ suspensions[71] and have led to difficulties in comparing and interpreting data from different studies. Table 2.1 summarizes the spectroscopic, surface charge, and size data from a number of previous studies.

Absorbance Spectra. The spectral properties of nC$_{60}$ obviously differ from those of molecular C$_{60}$ solutions. A true solution of molecular C$_{60}$ solution in *n*-hexane exhibits three primary peaks in its UV-Vis spectrum.[65] The 260- and 330-nm bands correspond to the strong allowed electronic transitions $6^1T_{1u} \rightarrow 1^1A_g$ and $3^1T_{1u} \rightarrow 1^1A_g$,[72] respectively. These two peaks are characteristic of the C$_{60}$ molecule and are highly sensitive to its local environment. Relative to

molecular C_{60}, the absorption bands of nC_{60} are broader, less intense, and red-shifted (Figure 2.4).[27] The broadening of the absorbance bands is caused by the strong light scattering of nC_{60} particles[65] and the decrease in intensity is purported to result from the reduced excited state energy caused by nanoparticle aggregation.[73] The red shift and band broadening are typical for colloidal C_{60} solutions.[74] The sharp spike at around 405 nm, which corresponds to the interaction of C_{60} with its environment, disappears completely, while a broad low intensity absorption band between 400-600 nm appears.[25,58,67,75,76] There are two possible origins of this band: Some attribute it to the formation of weak donor-acceptor (D-A) complexes of C_{60} with water or other aqueous constituents that have the ability to serve as electron donors.[65,77] The second hypothesis explains the origin of this band as arising from the appearance of solid and crystalline C_{60},[59-61,78] in which close electronic interactions between adjacent C_{60} molecules result in the absorbance in this range.

Although spectra of nC_{60} show similar general properties, they differ from each other slightly because of the different preparation methods and solution chemistries (Table 2.1). Comparison between aq/nC_{60} and THF/nC_{60} also shows that aq/nC_{60} suspensions have a broad absorption band between 400 and 600 nm. However, there has been no systematic study of nC_{60} UV-Vis spectra before now. The origins of the differences in peak position, intensity, and shape are still unknown. The lack of full interpretation of nC_{60} spectra reduces the power of the UV-Vis spectrometer. Better understanding of UV-Vis spectra will provide more specific information about nC_{60} in aqueous solutions.

Surface Charge. Several studies[25-27,56,60] have reported that nC_{60} suspensions produced either via solvent exchange or extended mixing were colloidally stable for months. The concentrations and average particle sizes of these suspensions did not change much during storage periods of up

to several months. The principal reason for the stability of these suspensions is the electrostatic repulsive force between particles that occurs due to their negatively charged surfaces. There are several possible mechanisms to explain the origins of the negative charge, such as electron donor-acceptor (D-A) interaction induced charge transfer and adsorption of other ionic species,[27] clathrate formation, and protolytic processes (i.e., localized hydrolysis) stemming from water structure at the C_{60} surface,[65] by which nC_{60} obtains its surface charge. However, chemical modification has been ruled out.[27,79]

Table 2.1 UV-Vis, surface charge, and average size data of nC_{60} in aqueous solutions

	Absorption maxima of UV-Vis spectra (nm)	Surface charge (ζ-potential, mV)	Size (nm)
BTA/nC_{60}	(227, 280, and 360)[25]		
SON/SDS/nC_{60}		(-39.0 ± 1.4[a])[79]	(229[a,b])[79]
EthOH/nC_{60}		(-31.6 ± 2.3[a])[62]	(121.8 ± 0.8[a,b])[62]
TTA/nC_{60}		(-36[c]) [60] (~-30[e])[59]	(100 ± 10[d])[60] (170 ± 20[b])[59]
Tol/nC_{60}	(265,345, and 454)[75] (265, 345, and 450)[76]	(~-30[e,f])[59]	(~27[d]; ~66[b])[48] (160 ± 20[b,f])[59]
THF/nC_{60}	(312-218, 257-265, and 330-339)[27] (200, 260, and 349)[58]	(-30)[27] (-25 to -50[g])[58] (~-50[e])[59]	(62.8[b])[27] (160 ± 20[b])[59] (219 ± 2.2[a,b])[80]
aq/nC_{60}	(223, 286, and 361)[58]	(~-30[e])[59] (-13.5 ± 1.1[a])[62] (-26.4[a], -45.5[h])[80] (-55.7 ± 1.0 [a])[81] (-47.0 ± 4.9[h]; -39.0 ± 7.2[a])[82]	(180 ± 20[b])[59] (178.6 ± 1.2[a,b])[62] (186 ± 12.6[a,b]; 392[b, h])[80] (193 ± 2[a,b])[81] (514 ± 17[b,h,i]; 171 ± 13[a,b, i])[82]
SON/nC_{60}			(152[b])[83]

[a]samples were filtered through a 0.45 μm filter before the measurement; [b]measured by DLS (Hydrodynamic diameter, Z_{ave}); [c]at pH = 5; [d]measured by TEM; [e]at pH = 7 and I = 0.0001 M NaCl; [f]referred to as SON/nC_{60} in this paper; [g]depending on solution chemistry; [h]data of supernatant from a suspension settled for 1 hour; [i]at pH =7.

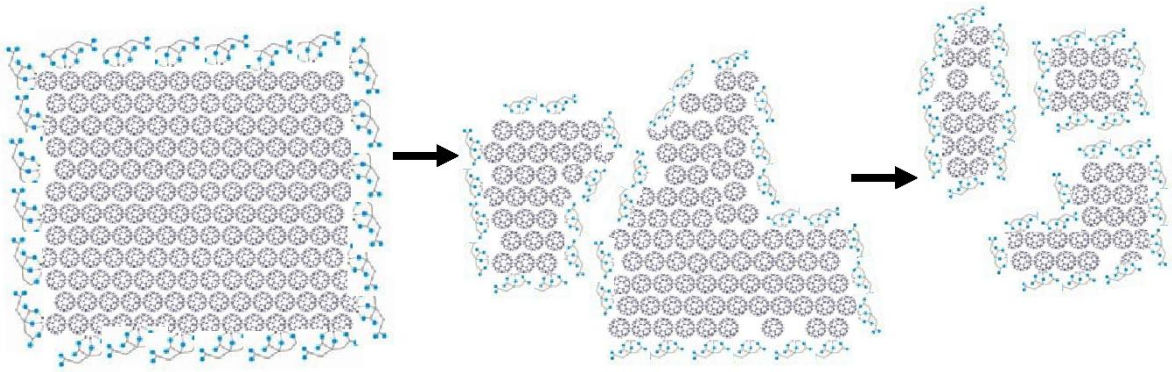

Figure 2.3 The top-down process.

C_{60} has a high electron affinity (2.7 eV)[84] that provides it with the capacity to participate in D-A interactions. Charge transfer between C_{60} and γ-cyclodextrin has been confirmed by Yoshida et al.[85] In aquatic systems, charge transfer introduced by weak D-A interactions between the unpaired electrons of the oxygen atom in H_2O with C_{60} molecules could be one of the sources of the negatively charged surfaces.[65] The observation that Tol/$n$$C_{60}$[65] and THF/$n$$C_{60}$[27] can only be extracted by toluene when $n$$C_{60}$ is precipitated by the addition of inorganic cations indicates that $n$$C_{60}$ is surrounded by a stable hydrophilic shell of water molecules. The strongly polar H_2O molecules at the surface lead to an overall negative surface charge and enhance $n$$C_{60}$ stability by preventing direct interactions between $n$$C_{60}$ particles and hydrophobic constituents in aquatic environment.[59,65] The grater surface charge of THF/$n$$C_{60}$ relative to aq/$n$$C_{60}$ indicates that charge transfer due to the D-A interaction between ether oxygen in THF and C_{60} is one way for $n$$C_{60}$ to acquire a surface charge.[58] The results of conductometric and potentiometric studies by Brant et al.[58] and Ma et al.[82] have shown the existence of strong acidic groups at the surface of $n$$C_{60}$, indicating that $n$$C_{60}$ does not obtain its surface charge through adsorption of hydroxyl ions alone.

The surface charge of $n$$C_{60}$ is greatly affected by solution pH, ionic strength, and ion composition. The ζ-potential of THF/$n$$C_{60}$ and aq/$n$$C_{60}$ increase with an increase in solution

pH.[58,81,82] In monovalent electrolyte solutions, the surface charge of THF/nC$_{60}$ decreases with an increase in ionic strength and large aggregates (e.g., weakly held together particles) produced by coagulation are observed when the ionic strength is larger than 10^{-2} M. Similar behaviors have been observed for TTA/nC$_{60}$,[64] Tol/nC$_{60}$, EtOH/nC$_{60}$,[62] and aq/nC$_{60}$.[59] Compared with monovalent cations, divalent electrolytes are more efficient in screening the negative surface charge.[58] These behaviors of nC$_{60}$ are consistent with classic colloid theory.[86]

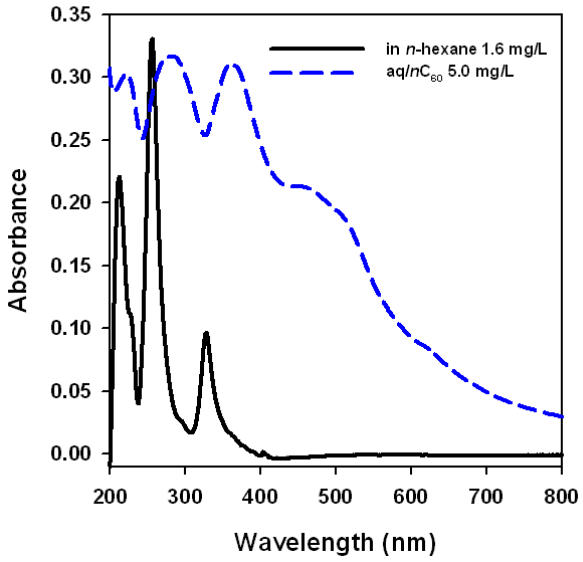

Figure 2.4 UV-Vis absorption spectra of C$_{60}$-*n*-hexane solution and aq/*n*C$_{60}$.

Size, Structure, and Morphology. Properties of nC$_{60}$ of environmental concern, such as toxicity and ability to absorb other contaminants, greatly depend on their size, structure, and morphology.[87,88]

Both TEM and DLS characterizations show that nC$_{60}$ suspensions produced via either solvent exchange or extended mixing have a broad size range,[87] In many studies, hydrodynamic diameter (Z_{ave}) is used to represent the average sizes of nC$_{60}$ in a suspensions which depends upon the procedures used for preparing suspensions, physicochemical properties of the solvent employed

in the procedure, solution chemistries, and the pre-treatments prior to characterization (e.g., filtration or settling). As shown in Table 2.1, average particles sizes of nC$_{60}$ produced by extended mixing are mostly larger than those of nC$_{60}$ produced via solvent exchange. And aq/nC$_{60}$ has smaller average particle size after filtration than after 1-h settling. In accordance with the reduction in its surface charge, the size of TTA/nC$_{60}$ decreases with increasing pH.[60]

nC$_{60}$ produced by different pathways show great varieties in structure and morphology.[59,89] nC$_{60}$ obtained by solvent exchange undergoes a bottom-up process and most of its particles are regularly shaped (spherical, triangular, rectangular, or hexangular). While aq/nC$_{60}$, produced through a top-down process, is highly polydisperse and regular shaped particles are seldom observed.[59,80] TEM[62] and HRTEM[80] studies confirm that aq/nC$_{60}$ has a crystalline nature, as does THF/nC$_{60}$,[27,60] tol/nC$_{60}$,[67] and SON/nC$_{60}$.[67] However, aq/nC$_{60}$ nanoparticles do not exhibit the symmetry and regularity observed in solvent exchange produced nC$_{60}$.[80] The differences in structure and morphology indicate that different mechanisms of formation and interactions between C$_{60}$ and other constituents are involved in various preparation techniques.

Many studies[25-27,56,60] have claimed that nC$_{60}$ suspensions are stable over months. Here the definition of 'stable' is only based on the unchanged average size of nC$_{60}$. nC$_{60}$ suspensions are complicated colloidal systems, where dissolution and re-aggregation occur constantly. Therefore, in a 'stable' nC$_{60}$ suspension, each individual particles is not necessarily in a stable status.

2.4 Environmental Impacts

The formation of negatively charged nC$_{60}$ provides a mechanism by which C$_{60}$ can be dispersed in aquatic environments when it is released. The stabilization of nC$_{60}$ in aquatic systems with ionic strength below 0.05 M,[60] which includes typical groundwaters and surface

waters indicates that they could exist ubiquitously in the environment. Lecoanet and Wiesner reported that nC$_{60}$ has the ability to migrate through a well-defined porous medium, which is similar to a sandy ground water aquifer.[90] These particles are capable of adsorbing other constituents in natural waters. On one hand, the adsorption of some organic compounds, such as NOM and proteins, will increase the stability of nC$_{60}$.[80,83] One the other hand, the adsorption of organic contaminants, such as naphthalene[28], chlorobenzene,[88] and polycyclic aromatic hydrocarbons (PAHs),[91] will increase the mobility of the pollutants.[92] The presence of these absorbed contaminants has the potential to elevate the toxicity of nC$_{60}$.

Chapter 3: UV-Vis Spectroscopic Properties of *n*C_{60} Produced via Extended Mixing

Xiaojun Chang and Peter J. Vikesland

(Submitted to *Environmental Science and Technology* for review)

3.1 Introduction

The ultraviolet-visible (UV-Vis) spectra of fullerene C_{60} in the gas phase and organic solvents[72,93] have been extensively studied since the discovery of C_{60} in 1985. In the gas phase, C_{60} exhibits sharp absorption bands that broaden when C_{60} is dispersed in liquids or solutions due to solvation effects as well as the increased number of interactions between neighboring C_{60} molecules.[94,95] Accordingly, the absorption spectra of C_{60} in a solution are highly dependent upon the properties of the solvent.[96] Fullerene C_{60} has appreciable solubility in aromatic and nonpolar solvents (e.g., 2150 mg/L in toluene, 1440 mg/L in benzene, and 40 mg/L in *n*-hexane[97]), but is only sparingly soluble in polar solvents (e.g., 35 μg/L in methanol and 800 μg/L in ethanol[24]). For true C_{60} solutions, in which C_{60} is dispersed as individual molecules, the shape, the position of adsorption maximum, and the relative absorbance of each band in the UV-Vis spectrum change with solvent identity.[93] Previous studies[93,96,98] have reported the effect of solvent properties (e.g., polarizability parameter, polarity parameter, molecular volume, Hildebrand solubility, etc.) on the spectra of fullerene solutions.

Although it has extremely low solubility in water, C_{60} forms colloidally stable aqueous suspensions consisting of nanoscale particles (*n*C_{60}) [25-27,80] instead of a true solution of dispersed individual molecules. As a result, *n*C_{60} exhibit UV-Vis spectra that differ from that of true C_{60} solutions in organic solvents. Although the spectra of *n*C_{60} reported in the literature are generally

similar, they often subtly differ from one another depending upon the preparation methods (solvent exchange, sonication, or extended mixing) and solution chemistries employed.[25,27,58,99] Compared with the well-characterized spectra of C_{60} in organic solvents, the spectral properties of nC_{60} suspensions are still not well understood. As documented herein, interpretation of UV-Vis spectra can be a powerful tool to investigate the properties of nC_{60} suspensions.

Both transmission electron microscopy (TEM) and dynamic light scattering (DLS) are commonly used to characterize the size and structure of nC_{60} suspensions; however, TEM requires the use of dried samples and DLS is inherently challenged by highly heterogeneous suspensions such as nC_{60}. The drying process may induce artifacts that reduce the reliability of the collected images,[100] and the hydrodynamic diameter (Z_{ave}) determined by DLS is an average of all peaks in the particle size distribution for a highly polydisperse solution such as nC_{60}.[80] As a result, two nC_{60} samples with similar Z_{ave} values may have very different structural characteristics due to their inherent heterogeneity. UV-Vis spectroscopy is an *in situ* technique that measures the spectroscopic properties of solutions and provides direct information that can provide insights into the interactions between C_{60} and solution constituents.

Recently Kato et al.[74] and Deguchi et al.[79] provided the first attempts to systematically evaluate the UV-Vis spectra of nC_{60} solutions produced by THF solvent exchange and sonication/surfactant stabilization, respectively. Each of these studies indicates that the spectral properties of nC_{60} suspensions are a function of the nC_{60} particle size with the measured absorption bands blue-shifting as the particle size decreases. Both Kato et al.[74] and Deguchi et al.[79] hypothesize that these changes in the absorption properties reflect an increase in the number of interactions between water molecules and the C_{60} surface that occur concomitant with a decrease in agglomerate size. Unfortunately because their nC_{60} suspensions were produced either

by solvent exchange or sonication/surfactant stabilization it is not clear how readily their conclusions translate to aqueous systems devoid of residual solvents (e.g., THF) or surfactants (sodium dodecylsulfate). In the present study, we provide the first detailed analysis of the UV-Vis spectroscopic properties of nC$_{60}$ produced via extended mixing in water in the absence of any organic solvents or surfactants.

3.2 Materials and Methods

Materials. Sublimed C$_{60}$ (> 99.9% pure) was purchased from Materials Electronics Research Corporation (Tucson, AZ). Reagent grade toluene and ACS grade *n*-hexane were purchased from Sigma Aldrich and Mallinckrodt Chemical, respectively. All glassware was washed with aqua regia and rinsed thoroughly before use. All water (> 18.2 MΩ-cm) used in this study was obtained from a Barnstead NANOpure water purification system.

Sample Preparation. C$_{60}$-*n*-hexane and C$_{60}$-toluene solutions were prepared by directly dissolving as purchased fullerene C$_{60}$ powder in solvents. Stable aqueous C$_{60}$ colloidal suspensions (aq/nC$_{60}$) were prepared via extended mixing.[28,80,101] As purchased fullerene C$_{60}$ was pulverized (amplitude 0.5 mm for 20 minutes) in a Fritsch pulverisette 0 ball mill to reduce its irregularity and initial size. The resulting powder was sieved through a 63 μm metal sieve and stored in the dark. ICP-MS analysis of the pulverized material did not indicate the presence of any residual metals within the resultant C$_{60}$ powder. Pulverized powder was added to nanopure water at a concentration of 400 mg C$_{60}$/L. The mixture was magnetically stirred at 500 rpm in the dark at room temperature. To characterize changes in aq/nC$_{60}$ properties over time, sample aliquots of 2.5 mL were removed periodically and settled for 24 hours before 2.0 mL samples of supernatant were characterized. The supernatant of an aq/nC$_{60}$ suspension prepared using a 30-

day stirring time and a 15-day settling period was transferred to a clean glass vial and stored in the dark as stock aq/nC$_{60}$.

Particle Size Discrimination by Centrifugation. Aliquots (5 mL) of stock aq/nC$_{60}$ were centrifuged at 7000 rpm for time periods of 1-40 min in a Beckman J2-HS centrifuge and 3.5 mL of the supernatant was transferred to a test tube for characterization. In a second experiment, stock aq/nC$_{60}$ suspension was diluted by nanopure water at a dilution ratio (= final suspension volume/stock aq/nC$_{60}$ volume) of 4:1. The resulting suspension was then subjected to the same centrifugation and characterization procedures.

***n*C$_{60}$ Characterization.** The average size (represented by hydrodynamic diameter, Z_{ave}) and the average surface charge (represented by the electrophoretic mobility, EM) of the aq/nC$_{60}$ suspensions were measured using a Malvern NanoZS dynamic light scattering (DLS) instrument and a disposable folded capillary cell. Details regarding the DLS measurements are found elsewhere (Chapter 5).[101] UV-Vis absorption spectra of aq/nC$_{60}$ were recorded using a Cary 5000 UV-Vis-NIR spectrophotometer at room temperature using a quartz cuvette with a pathlength of 1 cm. The cuvette was filled with 2.5 mL of aq/nC$_{60}$ solution and scanned over a range of 200-800 nm at a bandwidth of 1 nm using double beam mode. Each of the spectra of aq/nC$_{60}$ was obtained using a nanopure water background. Absorption spectra of C$_{60}$ in toluene and *n*-hexane were measured using the same spectrophotometer, with background corrections of toluene and *n*-hexane, respectively.

3.3 Results and Discussion

A true solution of C$_{60}$ in *n*-hexane exhibits a characteristic spike in the UV-Vis spectrum at 404 nm as well as three major absorption bands at 211, 257, and 328 nm (Figure 3.1). The UV-

Vis spectrum of a C_{60}-toluene solution shows a similar spike at 407 nm and an additional absorption band at 336 nm. The C_{60}-toluene solution does not exhibit absorption bands at lower wavelengths (<280 nm) because of the intrinsic absorption of the toluene aromatic ring. Compared with the spectra of well-dispersed C_{60} in organic solvents, aq/*n*C_{60} exhibits three absorption peaks at 221, 288, and 369 nm. As previously described,[27,59,60,67] these absorption bands are red-shifted and broader than the corresponding absorption bands in either toluene or *n*-hexane. These differences occur as a result of the extended electronic interactions possible within the crystalline lattice of *n*C_{60} as well as light scattering by the *n*C_{60} particles.

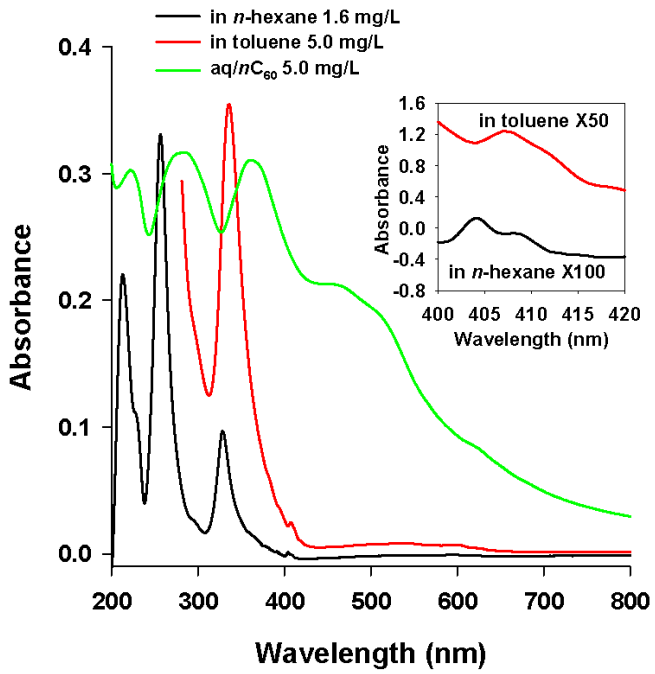

Figure 3.1 UV-Vis spectra of C_{60} in *n*-hexane, toluene, and aq/*n*C_{60}.

In aq/*n*C_{60} the spike in the 400-410 nm region, which is a vibronic signal (reflecting changes in vibrational energy under irradiation[94]) observed in the C_{60}-organic solutions, disappears while a continuous absorption band is observed in the 400-600 nm region. The vibronic signal results from coupling of the weak symmetry-allowed 1^1T_{1u}-1^1A_g electronic transition with

intramolecular vibrational features.[93] When C_{60} is present in nanoparticle form the molecular orbitals arising from π-orbital interactions between fullerene molecules become broader. These intermolecular effects perturb the 1^1T_{1u}-1^1A_g transition to such a degree that it is no longer visible for nC_{60}.[54] The appearance of the continuous absorption band between 400-600 nm has been previously assigned to the parity forbidden HOMO-LUMO transition ($h_u - t_{1u}$) in C_{60} thin films[102] or to the formation of weak donor-acceptor complexes between C_{60} and water.[65] The origins of this band are discussed in more detail in the sections that follow.

Our negatively charged aq/nC_{60} nanoparticles were obtained by magnetic stirring. The surface charge (represented by the measured electrophoretic mobility) of aq/nC_{60} is stable during the extended mixing period, while the average particle size (represented by the hydrodynamic diameter, Z_{ave}) decreases from >550 nm at the beginning of the stirring period to 270 nm after 15 days (Figure A.1). During the extended mixing period, the absorbance of the aq/nC_{60} suspensions increases with stirring time (Figure 3.2A). This increase in absorption reflects the increase in C_{60} concentration that occurs during mixing;[103] however, there are also subtle changes in the absorption spectra that occur over the mixing period. Figure 3.2B illustrates normalized absorption spectra produced by dividing the absorbance at each wavelength by the measured absorbance at 360 nm (ABS(360)). This normalization scheme accounts for the change in absorbance due to the increase in the nC_{60} concentration over time. As shown, there are readily discernible changes in the normalized spectra over time: (1) the spectra in the 240-290 nm region exhibit a general decline in relative intensity; (2) the peak in the 360 nm region shifts to shorter wavelengths; and (3) the relative intensity of the 400-600 nm absorption band decreases. In the sections that follow we systematically examine these changes in the spectra.

Changes in the 240-290 nm Region. The collected spectra in the 240-290 nm region are time-dependent (Figure A.2A). After one day of stirring, the position of absorption maximum (λ_{max}) in this region was at 255 nm with a shoulder band at ≈280 nm. The relative absorbance of these peaks also changed over time. On days 2 and 3, there were two peaks (at 255 and 277 nm) in the normalized spectra. As stirring time increased, however, the 255 nm peak shrank to become a shoulder of the peak at 284 nm by day 4. After day 4 the peak at 255 nm had completely disappeared and λ_{max} in this region was stable at 288 nm (Figure 3.2B).

Leach et al.[72] have assigned the absorption bands of the spectra of C_{60}-*n*-hexane solutions to their corresponding electronic and vibrational transitions. In *n*-hexane, the peak at 257 nm is assigned to the allowed 6^1T_{1u}-1^1A_g transition and the absorption peak in the 285-305 nm region corresponds to the allowed 4^1T_{1u}-1^1A_g and 5^1T_{1u}-1^1A_g transitions. These transitions can be assigned to bands with slightly different λ_{max} values in other organic solvents.[96] Unfortunately, no similar work has been done in aqueous nC_{60} suspensions to date. Although we do not know the exact origins of these absorption bands and the reason(s) for their spectral variation over time, it is reasonable to assign the bands at 255 nm and 288 nm to different electronic transitions. The temporal change in the relative intensities of these bands indicates that the interaction between C_{60} and water progressively alters the spectroscopic properties of aq/nC_{60}.

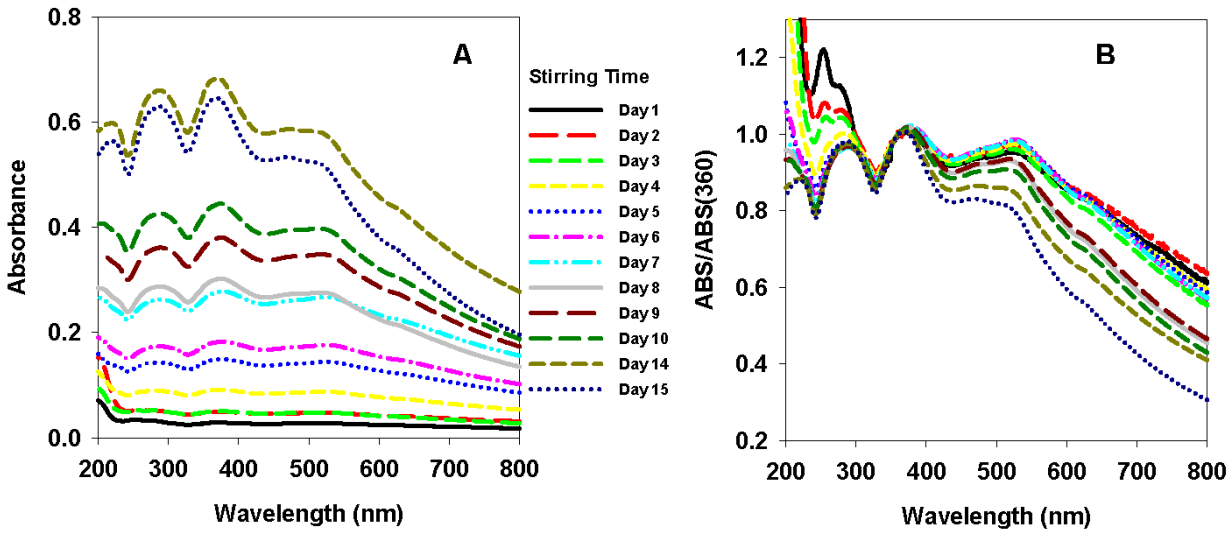

Figure 3.2 (A) UV-Vis spectra and (B) normalized spectra of aq/*n*C_{60} produced by extended mixing

Changes in the 360 nm Absorption Band. The position of absorption maximum of the ≈360 nm band (λ_{max}(360)) decreased from 378 to 369 nm between day 5 and day 15 (Figure A.2B; Note: (1) the *n*C_{60} concentrations prior to day 5 were too low to determine exact λ_{max}(360) values and (2) As discussed in the following sections, λ_{max} depends upon the average particle size. We note that although the wavelength range noted here is >360 nm, we use the term "360 nm band" to define this particular band later in the chapter and use it here for consistency). As discussed *vide infra* this blue shift is both the result of the progressive change in the interaction between aq/*n*C_{60} and water and of the decrease in the size of the *n*C_{60} particles that occurs over time due to mixing (Z_{ave} = 390 nm on day 5 and Z_{ave} = 272 nm on day 15).

A centrifugation experiment was conducted to fractionate the aq/*n*C_{60} suspensions to investigate whether mixing mediated changes in particle size were responsible for the blue shift of the 360 nm absorption band. Aq/*n*C_{60} suspensions subject to differential centrifugation periods had similar surface charges (≈3.0 × 10^{-8} m^2/V-s, Figure A.3), but their average particle size decreased from 245 to 114 nm as the centrifugation time increased from 0 to 40 min. Over this

centrifugation period the absorbance at a fixed wavelength of 360 nm decreased from 1.52 to 0.04 (Figure A.4). This decrease in absorbance is the result of the declining total C_{60} concentration as a result of centrifugation. Normalized spectra (Figure 3.3A), obtained by dividing the absorbance at each wavelength by its ABS(360), show that two major absorption bands shift to shorter wavelengths with a decrease in particle size. $\lambda_{max}(360)$ and $\lambda_{max}(275)$ decrease from 361 to 350 nm and from 285 to 268 nm, respectively (Figure 3.3B). To confirm this result and test the reproducibility of the relationship between λ_{max} and Z_{ave}, the centrifugation experiment was repeated, but using a diluted aq/*n*C_{60} suspension (as described in the Experimental Section). The lack of any measurable difference between the results of the centrifuged diluted aq/*n*C_{60} and the centrifuged stock aq/*n*C_{60} suspensions (Figure A.5) indicates that the relationship between λ_{max} and Z_{ave} is not concentration dependent.

A comparison of the blue shift of the 360 nm absorption band observed herein and that reported elsewhere[74,79] is shown in Figure 3.4A. The three curves shown are regression lines indicating the relationship between λ_{max} and Z_{ave} obtained in the present study and those of Deguchi et al.[79] and Kato et al.[74] These relationships are expressed by Eqns. 3.1, 3.2, and 3.3, respectively

$$\lambda_{max}(360) = 0.087\ Z_{ave} + 340.1\ \text{nm}\ (R^2 = 0.9074) \quad (3.1)$$

$$\lambda_{max}(360) = (0.065 \pm 0.009)\ Z_{ave} + (337.1 \pm 1.4)\ \text{nm} \quad (3.2)$$

$$\lambda_{max}(360) = 0.1429\ Z_{ave} + 325.7\ \text{nm} \quad (3.3)$$

The slope of the regression line indicates the extent of the blue shift that occurs for a given decrease in average particle size. The slopes from Deguchi et al. and our study are similar, yet

smaller than that from Kato et al. This difference reflects the different methods used to size fractionate the nC$_{60}$ suspensions. Centrifugation and centrifugation/filtration were used in our experiments and the Deguchi et al.[79] study, respectively, while Kato et al.[74] employed the Asymmetrical Flow Field Flow Fractionation (AF4) technique. Centrifugation and filtration selectively remove the largest particles from a suspension and thus may only slightly reduce the polydispersity of a highly heterogeneous suspension. In contrast, AF4 is known to produce suspensions with narrower particle size distributions.[104] As a result, size fractionated nC$_{60}$ obtained by AF4 is expected to be less polydisperse than that obtained via centrifugation. For two suspensions with similar Z_{ave} values, the more polydisperse one will generally have a greater amount of large particles. The presence of these large particles would decrease the extent of the blue shift and alter the observed slope.

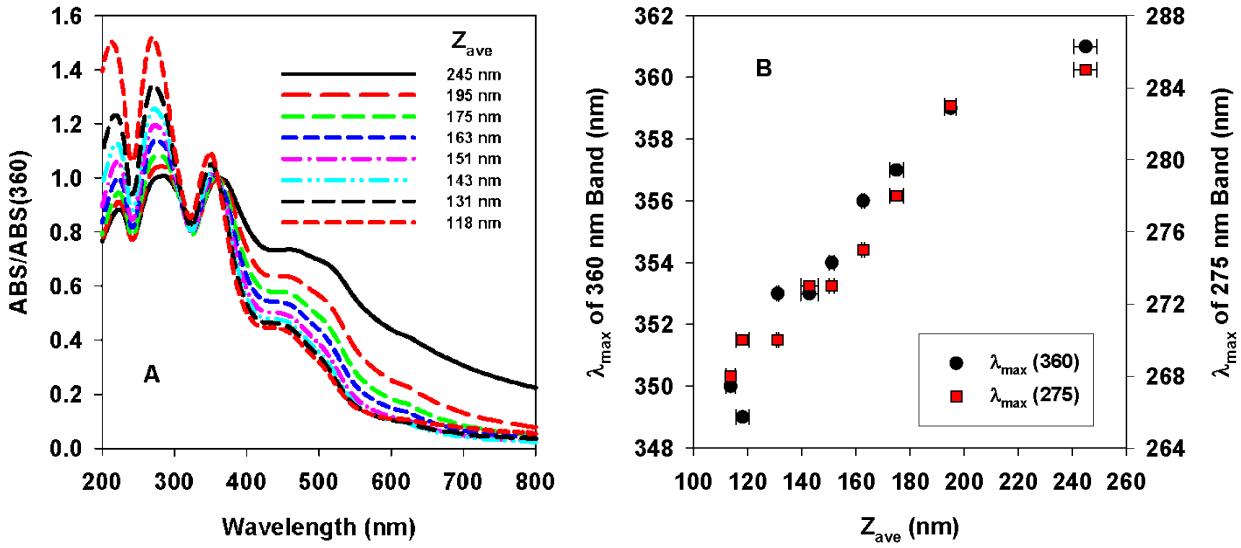

Figure 3.3 (A) Normalized UV-Vis spectra of centrifuged aq/nC$_{60}$ and (B) λ_{max}(360) and λ_{max}(275) as a function of Z_{ave}. (The Z_{ave} value represented in this figure is the average of three measurements and the error bar represents the standard deviation of three measurements.)

Absorption spectra of C$_{60}$ in organic solvents, micelles, and colloidal liposome solutions have been recorded at room temperature.[77,93,96,98] In these solvents, fullerene C$_{60}$ is primarily dispersed

as individual molecules. Across this set of solvents there is a red shift of the 330 nm band that generally correlates with an increase in the solvent polarizability parameter (Figure 3.4B). The solvent polarizability parameter is derived from the Lorentz-Lorenz relation: $\phi\,(n^2) = (n^2-1)/(n^2+2)$, where n is the refractive index of the solvent. This red shift corresponds to a decrease in the electrostatic work required to produce the solute transition dipole in the dielectric medium in contact with each C_{60} molecule,[105] thus indicating that the position of this absorption band provides information about the interaction between fullerene and the solvent molecules. For instance, the large red shift observed in aromatic solvents (λ_{max} = 335.0 and 335.5 nm for C_{60} in benzene and toluene, respectively[93]) has been attributed to complex formation between C_{60} and aromatic solvent molecules through π-π interactions.[106] Using data from the literature that is summarized in Figure 3.4B we obtained the following regression relating solvent polarizability to $\lambda_{max}(360)$:

$$\lambda_{max}(360) = (84.18 \pm 25.68)\,\phi(n^2) + (307.84 \pm 6.4) \qquad (3.4)$$

For water the polarizability parameter (n=1.33) is 0.204. Based upon this value and through the use of Eqn. 3.4, the $\lambda_{max}(360)$ of a "hypothetical" aqueous molecular-C_{60} solution is predicted to be 325 ± 6.4 nm.

A previous study[78] reported that $\lambda_{max}(360)$ for a series of C_{60}-SDBS solutions decreased from 344 to 330 nm as the concentration of SDBS increased from 0.5 to 50 g/L. Across this concentration range the aggregation of C_{60} becomes increasingly sterically inhibited and C_{60} becomes more finely dispersed. If we consider the linear trends obtained from the regression of $\lambda_{max}(360)$ and Z_{ave} (Figure 3.4A) and extrapolate to Z_{ave} = 0.7 nm, (e.g., the diameter of one C_{60} molecule), the calculated $\lambda_{max}(360)$ value should represent the position of the 360 nm absorption

band for a "hypothetical" aqueous molecular C_{60} solution, wherein C_{60} is dispersed in water as individual molecules. The three experimentally predicted values, obtained via this approach, increase in the order of Kato (326 nm) < Deguchi (337 nm) ≈ our study (340 nm). The differences between these values presumably reflect the different *n*C_{60} preparation procedures employed. Kato et al. produced their *n*C_{60} via solvent exchange with tetrahydrofuran (THF/*n*C_{60}). This protocol involves the initial dissolution of fullerene C_{60} in THF, mixing the solution with water, and then removing the THF by sonication.[59] In this synthesis approach, THF residues (e.g., THF[59,60,65] or its derivatives[59,107]) potentially surround C_{60} and therefore may prevent it from fully interacting with water. As a result, the calculated λ_{max}(360) value for THF/*n*C_{60} may actually reflect interactions between C_{60} molecules and residual organic solvent rather than just C_{60} and water. This hypothesis is supported by the fact that the calculated λ_{max}(360) of the 'molecular C_{60} aqueous solution' determined for THF/*n*C_{60} (=326 nm) is close to that of a C_{60}-THF solution (=328 nm) as reported by Gun'kin and Longinova.[77] SDS/SON/*n*C_{60}, which was obtained by ultrasonicating fullerene C_{60} powder in 40 mM sodium dedecylsulfate (SDS) in the Deguchi et al. study, has a similar λ_{max}(360) to aq/*n*C_{60} despite the fact that the interactions between a C_{60} molecule and water are expected to be altered by the presence of the surfactant.

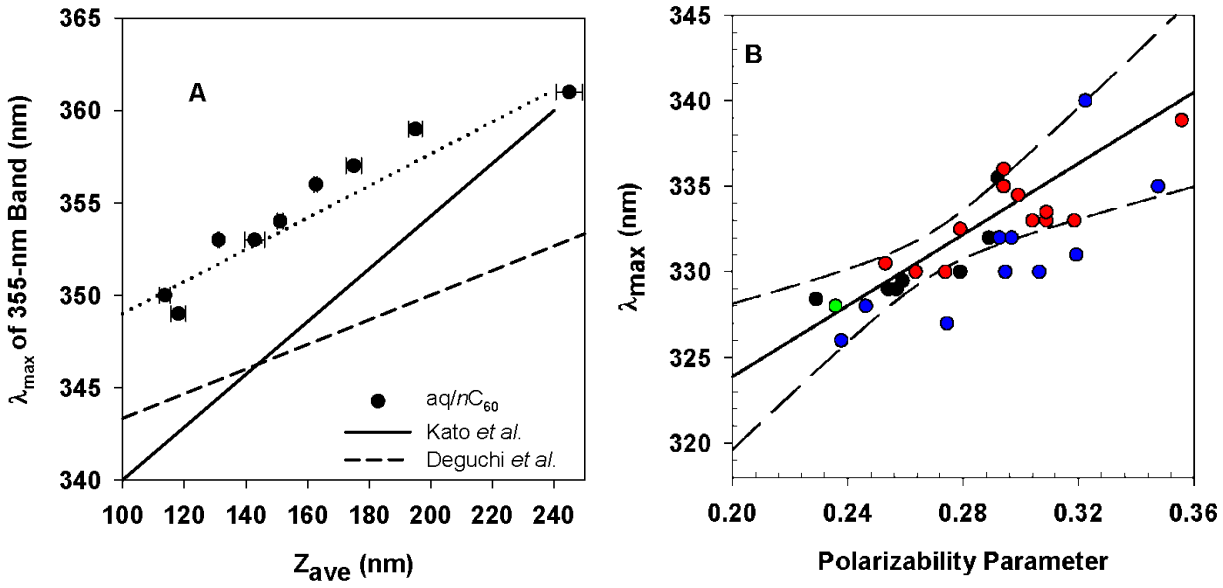

Figure 3.4 (A) λ_{max} as a function of Z_{ave} (The Z_{ave} value represented in this figure is the average of three measurements and the error bar represents the standard deviation of three measurements), and (B) Polarizability parameter vs. λ_{max} (Black dots are from Bensasson et al.;[93] Red dots are from Gallagher et al.;[98] The green dot is from Renge;[96] And the blue dots are from Gun'kin and Loginova.[77] These data are summarized in Table A.1; The solid line represents a linear fit of all data and the dashed lines represent the 95% confidence interval).

Compared with THF/nC$_{60}$ and SDS/SON/nC$_{60}$, there were no other constituents in the aq/nC$_{60}$ suspensions except for C$_{60}$ and water. Therefore, the aq/nC$_{60}$ particles/agglomerates are surrounded by water and the only interaction at the water-solid interface is the C$_{60}$-water interaction. The value for λ_{max} (=340 nm) obtained by extrapolation of the trends in Figure 3.4A is much larger than that predicted based solely upon the polarizability parameter (=325 nm). This difference is indicative of a strong interaction between water and C$_{60}$.[108] In aromatic solvents, strong π-π interactions increase C$_{60}$ solubility and are responsible for the red shift.[97] In polar solvents (e.g., THF), charge-transfer interactions[60] account for the red shift. The large red shift for C$_{60}$-water solutions is at least partially the result of charge-transfer interactions. Recently it was found that hydration of C$_{60}$ results in surface hydroxylation and a fullerenol-like nC$_{60}$ surface.[68] In addition, Wi et al.[108] recently reported the presence of ordered water molecules at the aq/nC$_{60}$ surface that could be responsible for the observed red shift.

Changes in the 400-600 nm Region. In Figure 3.2B and Figure A.2C, the normalized spectra of aq/*n*C_{60} in the 400-600 nm region are presented. The relative intensity of this broad continuous absorption band decreases during the extended mixing period concomitant with the observed decrease in the average particle size (Figure A.1). In addition, the shape of this absorption band changes over time with its λ_{max} shifting from 540 to 460 nm.

The origin of this continuous band in the aq/*n*C_{60} spectrum has been under debate for some time. Some studies attribute it to the formation of weak donor-acceptor complexes of C_{60} with water or other aqueous constituents that have the ability to serve as electron donors.[65,77] A second hypothesis suggests that this band arises due to the presence of solid and crystalline C_{60},[59,60,99] in which close electronic interactions amongst adjacent C_{60} molecules produce the measured absorbance.[109]

In the present study, the relative intensity of this band was used to determine its origin. Bensasson et al.[93] have shown that aggregation of C_{60} in organic solvents has a strong effect on the oscillator strength of the intense 6^1T_{1u}-1^1A_g (≈257 nm) allowed transition, but a lesser effect on the weaker 3-$^1T_{1u}$-1^1A_g (≈330 nm) transition. This result indicates that the 330-nm absorption band is less sensitive to solute-solute interactions (i.e., nanoparticle formation) than the 257 nm band. Given this fact, we calculated the ratio of the absorbance at 450 nm to the absorbance at 360 nm to determine the relative intensity of the broad absorption band from 400 to 600 nm.

Electron donor/acceptor interactions should occur primarily at the surfaces of nC$_{60}$. As a result, an absorption band produced in response to donor-acceptor complex formation should exhibit an increase in relative intensity as the fraction of C$_{60}$ molecules at the particle surface (f_s) increases. A simple calculation to estimate f_s for a spherical nC$_{60}$ nanoparticle can be readily derived:

$$n_{total} = \frac{4\pi}{3}\left(\frac{Z_{ave}}{2}\right)^3 \frac{4}{l^3} \tag{3.5}$$

$$n_{surface} = n_{total} - \frac{4\pi}{3}\left(\frac{Z_{ave}}{2} - l\right)^3 \frac{4}{l^3} \tag{3.6}$$

$$f_s = \frac{n_{surface}}{n_{total}} = 1 - \left(1 - \frac{2l}{Z_{ave}}\right)^3 \tag{3.7}$$

Where n_{total} is the total number of C$_{60}$ molecules contained in a spherical nC$_{60}$ nanoparticle of diameter Z_{ave} (nm); l is the lattice constant of an aq/nC$_{60}$ particle (=1.417 nm[110]) with *fcc* crystallinity; and $n_{surface}$ is the number of C$_{60}$ molecules present in the surface layer of the spherical particle. Figure 3.5A shows that the relative intensity of the 400-600 nm absorption band decreases with f_s. A recent paper[111] provided another method to estimate f_s. Although this method could increase the accuracy of our estimates since it takes the fractal dimension of the nanoparticle into consideration, we were unable to use it herein since we do not know the fractal dimension of our aq/nC$_{60}$. Regardless of which method to estimate f_s is used, however, f_s is expected to decrease with Z_{ave} and the predicted trend of a decrease in relative intensity with an increase in f_s remains. This finding indicates that donor-acceptor complex formation is not the origin of this band.

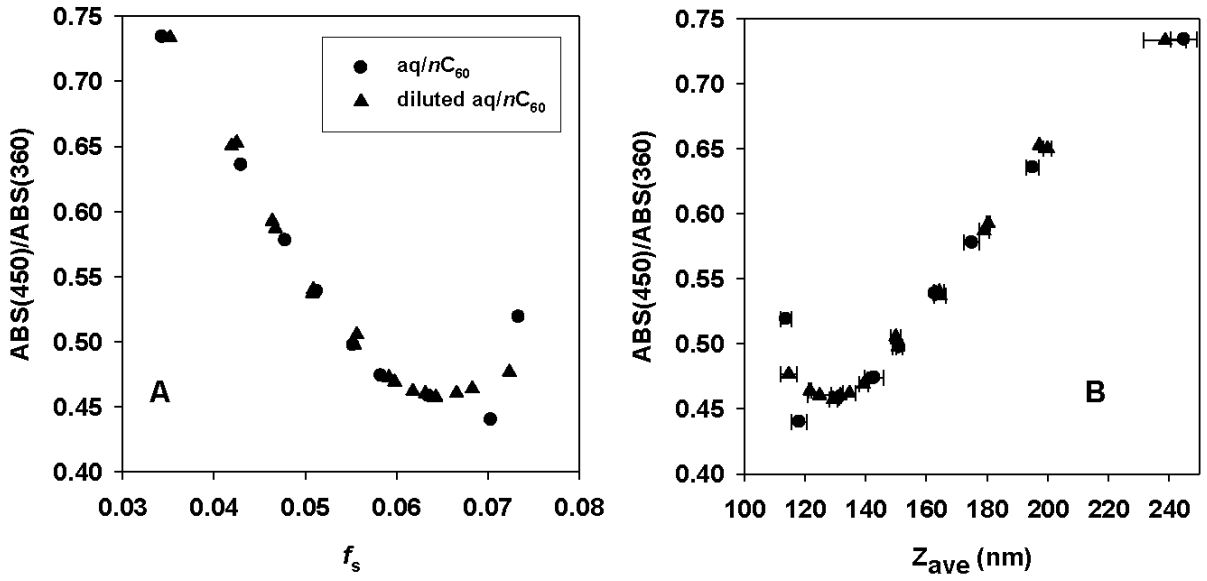

Figure 3.5 Relative intensity of 400-600 absorption band as a function of (A) fraction of surface C_{60} molecules and (B) Z_{ave} (The Z_{ave} value represented in this figure is the average of three measurements and the error bar represents the standard deviation of three measurements).

If the interactions between C_{60} molecules in a crystalline nC_{60} particle are the origin of the 400-600 nm absorption band, the relative intensity should increase with an increase in Z_{ave}.[74] Data from our centrifugation experiments (Figure 3.5B) fit this predicted trend well. This calculation thus supports the hypothesis that the close association between individual C_{60} molecules in aq/nC_{60} is responsible for the 400-600 nm continuous absorption band. Importantly, according to Figure 3.5B, the ABS(450)/ABS(360) ratio increases proportionally with the average particle size for Z_{ave} values larger than 120 nm. Calculation of this ratio can thus be made to estimate the average size of nC_{60} suspensions that meet this criterion. This prediction should be more reliable than that obtained from the relationship between $\lambda_{max}(360)$ and Z_{ave} (i.e., Figure 3.4A) since $\lambda_{max}(360)$ is strongly affected by solution chemistry. It has previously been established that absorbance ratios are generally more robust and less subject to variation.[93]

3.4 Environmental Implications

Aq/*n*C_{60} produced via extended mixing is arguably a better approximation of the nanoparticles that will form when C_{60} is released to the environment than *n*C_{60} produced via methodologies involving the use of organic solvents or under intense sonication conditions. During its formation, aq/*n*C_{60} exhibits progressive changes in its UV-Vis spectra. The changes in the 250-290 nm region imply that the interaction between C_{60} and water is a temporal process and that the affinity of C_{60} with water varies over time. The rate at which this process occurs in natural waters could be either diminished or accelerated depending upon the solution composition. In any case, however, the progressive nature of the reaction should be considered to truly evaluate the reactivity and fate of C_{60} in aqueous environments.

As documented herein, the *n*C_{60} particle size is an important factor that dictates its UV-Vis spectroscopic properties. The relative intensity of the continuous absorption band in the 400-600 nm region and the position of absorption maximum of 360 nm band are proportional to the Z_{ave} of *n*C_{60}. With continued development, these relationships have the potential to be used to predict particle sizes in the absence of DLS data. However, $\lambda_{max}(360)$ is affected by the presence of other constituents in solution, indicating that size prediction by $\lambda_{max}(360)$ should be carefully conducted with continual awareness of the sample preparation methodology. Extrapolation of the relationship between $\lambda_{max}(360)$ and Z_{ave} reveals that the strong interaction between C_{60} and water is different from the interactions between C_{60} and organic solvents.

Chapter 4 Uncontrolled Variability in the Extinction Spectra of aq/nC$_{60}$

Xiaojun Chang and Peter J. Vikesland

4.1 Introduction

Following its discovery in 1985,[1] fullerene C_{60} has drawn intense research and industrial attention because of its unique properties. As a result of increases in C_{60} production and the number of applications in which it is being employed there is concern about the potential environmental and health effects of C_{60}. Although C_{60} has extremely low solubility in water,[22] it forms stable colloidal suspensions containing fullerene nanoparticles (nC$_{60}$) in aqueous solutions when subject to extended mixing, sonication, or solvent exchange.[25-27,80] To better understand the behavior and fate of C_{60}, numerous studies have been conducted to investigate the physicochemical and morphological properties of nC$_{60}$.[60,80,112-114]

The concentration of C_{60} ([C_{60}]) in an aqueous solution is one of the most important parameters that needs to be determined to facilitate the study of the behavior, transport and fate of C_{60} and nC$_{60}$.[115] Unfortunately, this fundamental parameter has proven experimentally challenging to quantify. To measure [C_{60}] in water, several analytical methods have been established. In a majority of these methods, nC$_{60}$ in aquatic matrices is extracted into non-polar toluene by liquid-liquid extraction[103,116,117] or solid phase extraction[103,116,118] and then quantified using high-performance liquid chromatography (HPLC) coupled with UV-Vis detection or mass spectrometry. These methods, however, are time consuming and are highly dependent upon the extraction efficiency. Past studies have shown that the extraction efficiency, as low as 40% from tap water[103] and as high as 85% from surface and groundwater,[116] is strongly affected by solution

composition. Because of these challenges, many researchers instead have attempted to employ UV-Vis spectroscopy to directly quantify [C_{60}] in aqueous solutions. In this approach, a calibration curve correlating solution absorbance at a specific wavelength to the total carbon concentration of a series of nC_{60} 'standards' is used to determine [C_{60}] for an unknown sample based upon its absorbance at the same wavelength.[87,89,119] Implicit in this approach is the assumption that similarly prepared solutions should provide comparable results. Unfortunately, this assumption has never been experimentally verified.

Heterogeneous nC_{60} suspensions have UV-Vis spectra that differ from those of C_{60}-organic solutions. Their spectra exhibit spectroscopic properties that are dependent upon particle size, particle concentration, preparation method, and solution chemistry.[27,67,74,79,120] For instance, aq/nC_{60}, produced in water via extended mixing, has red-shifted absorption bands relative to C_{60} dissolved in toluene and *n*-hexane and there are quantifiable changes in relative absorbance that occur with an increase in average particle size.[121] Because of the complicating effects of concentration and particle size on the UV-Vis spectra of nC_{60} it is potentially challenging to directly compare the absorption spectrum of one nC_{60} suspension to another. In an attempt to quantify the impacts of concentration and particle size on the UV-Vis spectrum, we obtained extinction spectra, which are UV-Vis spectra that have been normalized either by [C_{60}] or particle concentration. To our knowledge, there have previously been no systematic studies examining the validity of using the same extinction coefficients for nC_{60} suspensions with various [C_{60}] or nC_{60} particle sizes in quantitative determinations of [C_{60}]. As shown herein, extreme care should be taken when attempting to determine nC_{60} concentrations based solely on UV-Vis measurements.

4.2 Materials and Methods

Materials. Sublimed fullerene C_{60} (99.9%) was purchased from Materials Electronics Research Corporation (Tucson, AZ). Reagent grade toluene and ACS grade *n*-hexane were purchased from Sigma Aldrich and Mallinckrodt Chemical, respectively. The water (>18.2 MΩ-cm) used in this study was obtained from a Barnstead NANOpure water purification system. All solutions and suspensions were prepared and stored in glassware washed with aqua regia and rinsed thoroughly before use.

C_{60} Solution and *n*C_{60} Suspension Preparation. Stock C_{60}-organic solutions were prepared by dissolving 16 mg/L and 50 mg/L as purchased C_{60} in *n*-hexane and toluene, respectively. Stable colloidal fullerene C_{60} suspensions in water (*n*C_{60}) were produced via extended mixing (aq/*n*C_{60})[28,80,101] and sonication (SON/*n*C_{60}).[67,68] As purchased C_{60} was pulverized in a Fritsch pulverisette 0 ball mill at an amplitude of 5 mm for 20 min and sieved through a 38 μm metal sieve to remove large unpulverized materials. ICP-MS measurements of the pulverized materials indicated that no metal contaminants were transferred during ball milling and sieving. Aq/*n*C_{60} suspensions were produced by mixing the resultant C_{60} powder with nanopure water (400 mg C_{60}/1000 mL water) using magnetic stirring at 30 °C in the dark for at least two weeks. SON/*n*C_{60} suspensions, prepared at the same initial C_{60}/water concentration, were sonicated for 6 hours in 1.5 h cycles with a 5 min interruption between each cycle.

***n*C_{60} Characterization.** The total mass concentration of C_{60} [C_{60}] in an *n*C_{60} suspension was obtained as the concentration of total organic carbon (TOC, as mg C/L) determined by a Shimadzu TOC-VCSN. The size distribution, average size (represented by hydrodynamic diameter, Z_{ave}) and the average surface charge (represented by the electrophoretic mobility, EM) of the *n*C_{60} suspensions were measured using a Malvern NanoZS dynamic light scattering (DLS)

instrument and a disposable folded capillary cell. Details regarding the EM and DLS measurements are found elsewhere.[101]

UV-Visible Spectrophotometry. Absorption spectra of nC$_{60}$ were recorded with a Cary 5000 UV-Vis-NIR spectrophotometer at room temperature using a quartz cuvette with a light pathlength of 1 cm. The cuvette was filled with a 2.5 mL aliquot of suspension and scanned over the spectral range of 200-800 nm at a bandwidth of 1 nm in double beam mode. Each nC$_{60}$ spectrum was measured using a nanopure water background correction. Absorption spectra of C$_{60}$ in toluene and *n*-hexane were measured using the same spectrophotometer, with background corrections of toluene and *n*-hexane, respectively.

Extinction Coefficient Determination. Herein we define two extinction coefficients: the extinction coefficient per mole of C$_{60}$ (molar extinction coefficient, ε, mole^{-1}·cm^{-1}·L) and the extinction coefficient per nC$_{60}$ particle (particle extinction coefficient, γ, particle^{-1}·cm^{-1}·L). Particle extinction coefficients, defined as the extinction intensity per mole of nanoparticle or mole of nanocrystal in previous studies,[122,123] have the same units as the molar extinction coefficient ε. To avoid confusion, in the present study, we define the particle extinction coefficient γ as the extinction intensity of one nC$_{60}$ particle. The two extinction coefficients were determined based upon the Beer-Lambert Law:

$$A = \varepsilon l c \tag{4.1}$$

$$A = \gamma l N \tag{4.2}$$

where A is the absorbance at a given wavelength; l is the light path length (= 1 cm in our study); c is [C$_{60}$] determined by TOC (mol/L); and N is the nC$_{60}$ particle number concentration (particles/L).

Due to the extreme heterogeneity of aq/nC$_{60}$,[101] it was experimentally difficult to accurately determine N for an aq/nC$_{60}$ suspension. Therefore, in an effort to estimate this important parameter we used the measured [C$_{60}$] value and a DLS determined hydrodynamic diameter (Z_{ave}), to estimate N under the simplifying assumption that we have a monodisperse suspension of spherical nC$_{60}$ particles with diameter Z_{ave}. Particles of aq/nC$_{60}$ exhibit a face centered cubic[80] crystalline habit and accordingly each unit cell contains four C$_{60}$ molecules. The number of C$_{60}$ molecules in a spherical aq/nC$_{60}$ particle (n, molecules/particle) with diameter Z_{ave} can be calculated as:

$$n = \frac{4\pi}{3}\left(\frac{Z_{ave}}{2}\right)^3 \frac{4}{L^3} \tag{4.3}$$

where L is 1.417 nm, the lattice constant of C$_{60}$.[110] The particle number concentration N (particle/L) is defined as:

$$N = \frac{C}{n/N_A} \tag{4.4}$$

where N_A is Avogadro's number. We emphasize that due to the inherent heterogeneity of aq/nC$_{60}$ suspensions, the N values obtained using Eqn. (4.4) are approximate. Accordingly, the γ value calculated using this approach is a general index that reflects the intensity of light extinction per particle for a hypothetical nC$_{60}$ suspension with [C$_{60}$] = c mol/L consisting of spherical particles with diameter of Z_{ave}.

To determine the extinction coefficient for a particular sample, each sample was diluted to six different concentrations (relative concentrations of 0.1, 0.3, 0.5, 0.7, 0.9, and 1.0) and their UV-Vis spectra were recorded. Extinction coefficients ε and γ were obtained as the slopes of regressions of UV-Vis absorbance vs. [C$_{60}$] and UV-Vis absorbance vs. N, respectively. Each

regression was linear with correlation coefficients very close to 1 (for most samples $R^2 > 0.99$ and the minimum R^2 value was 0.96.). A representative set of curves is shown in Figure B.1 in Appendix B.

4.3 Results and Discussion

Extinction Spectra for C_{60}-toluene and C_{60}-*n*-hexane. Extinction spectra for C_{60} dissolved in *n*-hexane and toluene are presented in Figure 4.1. Under our experimental conditions, the concentration of C_{60} ($[C_{60}]$) in each of these solvents was well below its solubility limit (e.g., 23.3 mM in toluene and 0.46 mM in *n*-hexane[97]) and C_{60} was primarily dispersed in these solutions as individual molecules. The true solution of C_{60} in *n*-hexane shows three peaks at 211, 257, and 328 nm that correspond to the symmetry-allowed transitions 8^1T_{1u}-1^1A_g, 6^1T_{1u}-1^1A_g, and 3^1T_{1u}-1^1A_g, respectively.[72] Compared with sharp peaks observed in *n*-hexane (an aliphatic solvent), there is a broadened peak at 336 nm for the C_{60}-toluene solution, and no peaks are observed in the short wavelength region (< 280 nm) because of the intrinsic light absorption of the aromatic ring of the solvent. The molar extinction coefficients of the 3^1T_{1u}-1^1A_g transition (≈330 nm absorption band) are 4.9×10^4 and 5.2×10^4 $mole^{-1} \cdot cm^{-1} \cdot L$ for C_{60}-*n*-hexane and C_{60}-toluene, respectively. These values are consistent with previous studies[65,77,79] and this consistency illustrates that it is possible to obtain reproducible extinction spectra for C_{60} when it is fully dissolved in a solvent.

Extinction Spectra for aq/*n*C_{60}. The collected extinction spectra for aq/*n*C_{60} differ significantly from those obtained for C_{60} in organic solvent. The extinction spectrum shown in Figure 4.1 for an aq/*n*C_{60} suspension ($[C_{60}]$ = 0.027 mM and Z_{ave} = 177 nm) has three absorption peaks at around 220, 280, and 360 nm that are broader and red shifted relative to the spectra

obtained in the organic solvents. In addition, the vibronic features due to the HOMO-LUMO A_0 transition (1^1T_{1u}-1^1A_g, symmetry-allowed) around 405 nm (inset Figure 4.1) in both C_{60}-organic solutions disappear in aq/*n*C_{60}, while a broad absorption band from 400 to 600 nm is now observed.

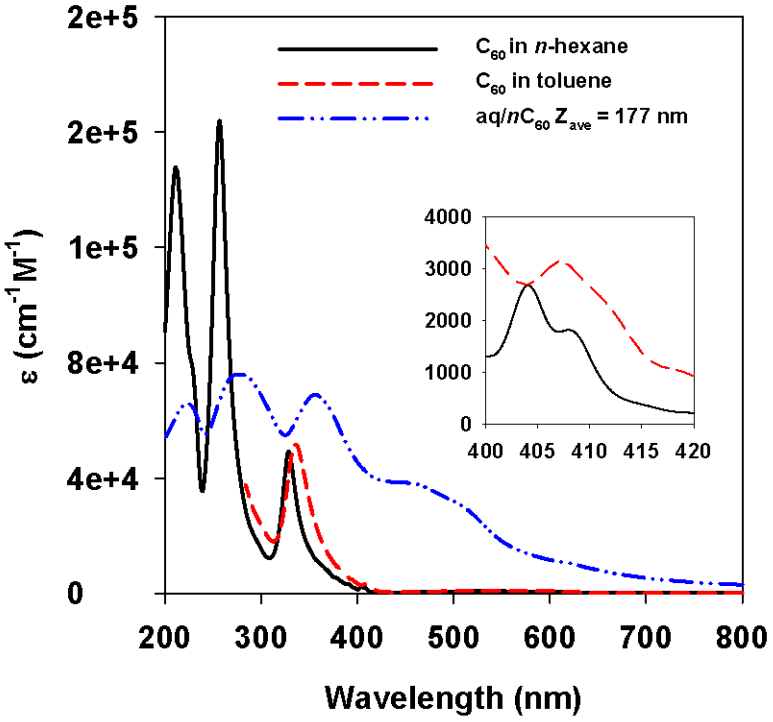

Figure 4.1 Extinction spectra of C_{60} dissolved in toluene and *n*-hexane compared to the spectrum of aq/*n*C_{60}; Inset: Detailed extinction spectra of C_{60}-oragnic solutions in the vicinity of 405 nm.

The shape and position of the absorption maximum of the 330-nm peak (symmetry-allowed transition 3^1T_{1u}-1^1A_g), are solvent-dependent.[96,98] For aq/*n*C_{60} the maximum of this transition is found at ≈ 360 nm. This significant red shift is likely caused by the interactions between C_{60} and water as well as light scattering by aq/*n*C_{60} particles. The magnitude of the molar absorptivity (ε) of this peak for aq/*n*C_{60} is similar to that measured in the organic solvents, while the ε values of the 280- and 220-nm peaks are considerably smaller than those of the corresponding peaks in C_{60}-*n*-hexane. This result is consistent with a previous study, in which Bensasson et al.[93]

proposed that particles of C_{60} exhibit reduced oscillator strengths (i.e., the intensity of the transition) for the 6^1T_{1u}-1^1A_g (260 nm) allowed transition, yet less dampening is observed for the 3^1T_{1u}-1^1A_g (330 nm) transition.

The 1^1T_{1u}-1^1A_g transition results from intramolecular vibrations (within the C_{60} cage) and has been previously shown to be suppressed by intermolecular solute-solute interactions in C_{60} aggregates. Torres et al.[124] observed the disappearance of vibronic features in the 400-410 nm region and the appearance of a broad continuous absorption band in the 400-600 nm region, a sign of C_{60} aggregation, in PVP/*n*C_{60}, SDS/*n*C_{60}, and THF/*n*C_{60} suspensions. Similar changes have also been reported for C_{60}-liposome solutions, C_{60} films,[93] and C_{60}-alcohol solutions[109] as aggregation occurs. The ε at 450 nm (4.0×10^4 $mole^{-1} \cdot cm^{-1} \cdot L$) for aq/*n*$C_{60}$ with Z_{ave} of 177 nm in Figure 4.1 is two orders of magnitude larger than those observed for C_{60}-*n*-hexane and C_{60}-toluene, which are 260 and 360 $M^{-1}cm^{-1}$, respectively. As shown in our previous study (Chapter 3),[121] the increase in the relative intensity of this continuous absorption band is indicative of an increase in average particle size.

Reproducibility of aq/*n*C_{60} via Extended Mixing. Although extreme care was taken to produce aq/*n*C_{60} suspensions with identical spectral and colloidal properties, we were consistently unable to do so. Four 'identical' batches of aq/*n*C_{60} were prepared in replicate bottles with a fixed stir rate, stir-bar size, solid to solution ratio (40 mg C_{60} in 100 mL water), stirring period of 21-days, and 24-hour settling period. Although consistent EM values were obtained for the different batches, Z_{ave}, [C_{60}], and the UV-Vis spectra for each solution varied considerably (Figure B.2). These results corroborate previous studies by our group[80] obtained with a different C_{60} material (e.g., Sigma-Aldrich instead of MER as used herein). Collectively,

these results show that the highly stochastic processes involved in the top-down production of nC$_{60}$ are challenging, if not impossible, to systematically reproduce.

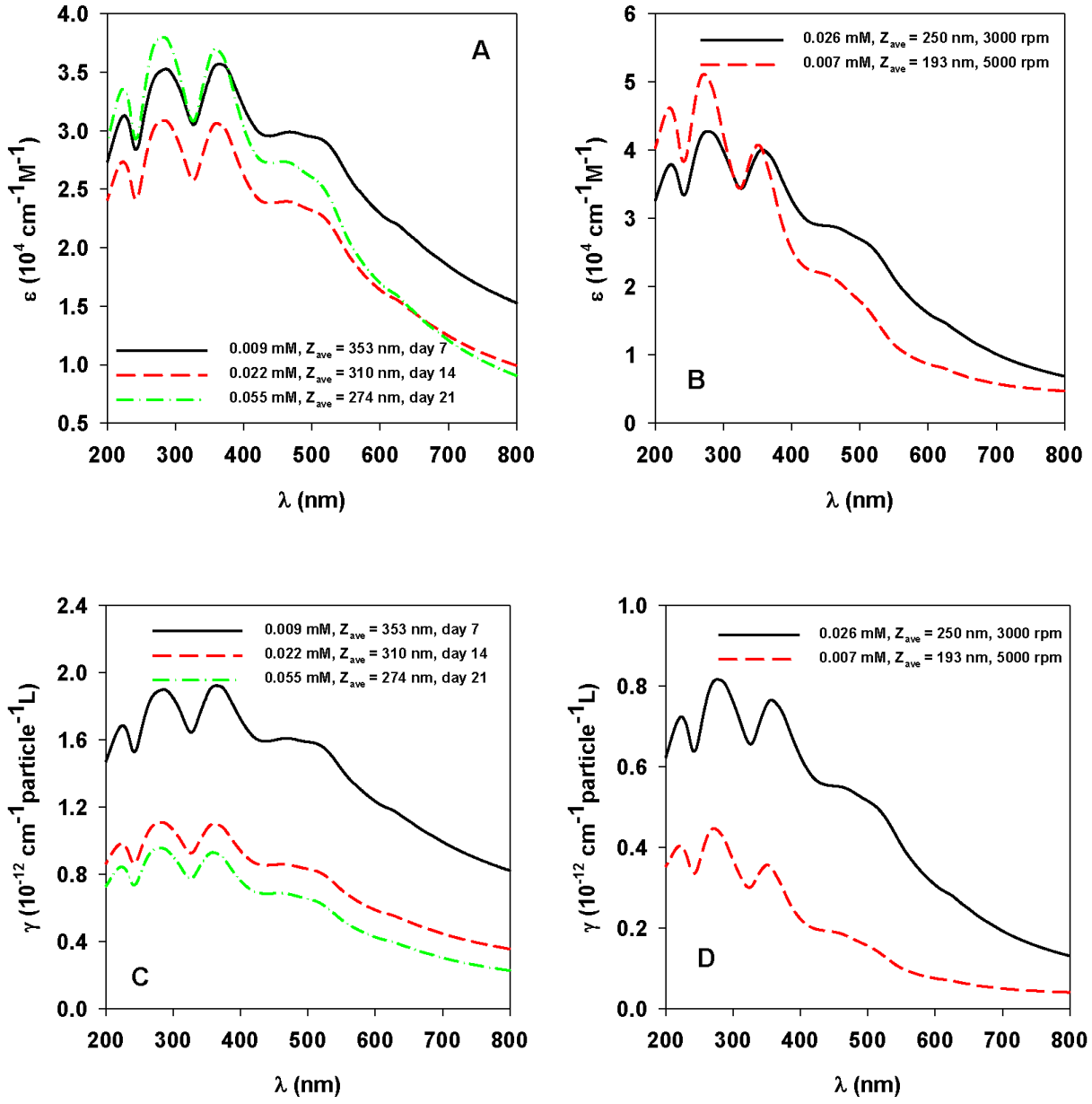

Figure 4.2 Molar extinction spectra for aq/nC$_{60}$ suspensions (A) from the same batch, but different stirring periods and (B) from the same batch, centrifuged at different speeds. Particle extinction spectra for aq/nC$_{60}$ suspensions (C) from the same batch, but different stirring periods and (D) from the same batch, centrifuged at different speeds.

It could be hypothesized that the differences in the spectra shown in Figure B.2 are the result of minute variations in solution characteristics and not differences in the spectral properties of aq/*n*C_{60}. To address this possibility, Figure 4.2A shows three molar extinction curves for samples from the same batch, yet variable stirring periods. In this batch, Z_{ave} for the aq/*n*C_{60} suspension decreased from 353 to 274 nm, while [C_{60}] increased from 0.009 to 0.055 mM over the 7- to 21-day stirring period. Normalization by [C_{60}] at each time point is insufficient to produce a consistent extinction spectrum. To eliminate the potential effects of time dependent variations in the spectral properties of aq/*n*C_{60}, a second experiment was conducted wherein a single *n*C_{60} sample was centrifuged at different speeds. As shown in Figure 4.2B, extinction curves for the centrifuged samples also do not converge.

The results shown in Figure 4.2 indicate that aq/*n*C_{60} suspensions, unlike C_{60} solutions in toluene and *n*-hexane, exhibit highly variable extinction spectra. We note that this observation is not limited to aq/*n*C_{60} produced by extended mixing, but also reflects SON/*n*C_{60} suspensions (See Appendix B). The formation of SON/*n*C_{60} and aq/*n*C_{60} occur via top-down processes, during which the bulk starting materials (up to 30 μm in size[80]) are weathered into smaller particles due to mechanical forces. The inherent randomness of the top-down process and the resultant heterogeneities of the final suspensions are the main reasons for the poor reproducibility observed in the formation of SON/*n*C_{60} and aq/*n*C_{60} suspensions.

Particle Extinction Coefficients. Compared with molecular C_{60}-toluene and C_{60}-*n*-hexane solutions, whose extinction spectra are simply concentration normalized absorption spectra, the *n*C_{60} suspensions have UV-Vis spectra with contributions from both absorption and scattering. In a colloidal system, the particle concentration, as well as the molar concentration of the solute, determine the solution spectral properties.[125] In an attempt to estimate the absorptivity of an

aq/nC$_{60}$ particle (extinction coefficient per particle, γ), we normalized the collected spectra to a calculated particle number concentration N. Using Eqns. 4.2-4.4, we calculated γ at each wavelength and the γ vs. λ curves for the aq/nC$_{60}$ suspensions in Figures 4.2A and 4.2B are presented in Figures 4.2C and 4.2D, respectively. Particle concentration normalized spectra also did not converge, indicating that aq/nC$_{60}$ suspensions from the same original batch, but with variable stirring periods or centrifugation conditions have variable particle absorptivities.

It could be argued that the disparity between spectra for samples from the same batch could be a result of the decision to neglect the polydispersity of each sample when determining N. Therefore in an attempt to account for the broad size distributions of aq/nC$_{60}$, we used the size distribution data obtained from DLS measurements to calculate an average particle extinction coefficient Γ (particle^{-1} cm^{-1}L, detailed information about this calculation is presented in Appendix B) for an aq/nC$_{60}$ suspension consisting of spherical particles of variable sizes. These calculation results showed that similar to ε and γ, the spectra of Γ for different aq/nC$_{60}$ suspensions did not converge.

As discussed previously, aq/nC$_{60}$ suspensions obtained via extended mixing exhibited various [C$_{60}$] and average sizes. As a result, two aq/nC$_{60}$ suspensions having the same [C$_{60}$] may have very different aq/nC$_{60}$ particle number concentrations and thus it can be expected that ε and γ have different changing patterns with aq/nC$_{60}$ particle size. As shown in Figure 4.3A, the molar extinction coefficients determined at 280, 360, and 460 nm (which represent the intensities of the strong 6^1T_{1u}-1^1A_g, 3^1T_{1u}-1^1A_g bands, and the continuous band ranging from 400 to 600 nm, respectively) generally decline with an increase in Z_{ave}. ε, which is the absorbance normalized by the C$_{60}$ molar concentration, reflects the intensity of light absorbed and scattered by an aq/nC$_{60}$ solution with a [C$_{60}$] of 1 M. Although such a trend has never been published for C$_{60}$, similar

decreases in ε with particle size have been reported for colloidal CdSe nanocrystals by Striolo et al..[126]

In contrast to what is observed with ε, there is an increase in γ with Z_{ave} (Figure 4.3B). This result indicates that a larger aq/nC$_{60}$ nanoparticle has increased capacity to absorb and scatter light compared to a smaller aq/nC$_{60}$ nanoparticle. The data in Figure 4.3B were fitted to an empirical function relating the average size of an aq/nC$_{60}$ suspension to γ:

$$\gamma(280\text{ nm}): \quad \gamma = (5.9674 \times 10^{-17}) Z_{ave}^{1.72} \qquad R^2 = 0.85 \qquad (4.5)$$

$$\gamma(360\text{ nm}): \quad \gamma = (1.9575 \times 10^{-17}) Z_{ave}^{1.91} \qquad R^2 = 0.86 \qquad (4.6)$$

$$\gamma(460\text{ nm}): \quad \gamma = (7.6175 \times 10^{-19}) Z_{ave}^{2.43} \qquad R^2 = 0.87 \qquad (4.7)$$

The particle extinction coefficients at these three wavelengths exponentially increased with particle size. A linear dependence of the particle extinction coefficient on the volume, which is predicted based upon Mie theory,[127] has been reported for monodisperse spherical gold nanoparticles (AuNP) with sizes ranging from 9 to 99 nm.[128] The size dependence of the extinction coefficients of one molar nanoparticles of AuNP,[128-130] Cd nanocrystals,[122,126,131] PbSe semiconductor nanocrystals,[132] and PbS quantum dots[123,133] was found to follow a power law with exponents between 2-3 and R^2 close to 1. In the present study, the regression results for γ at three specific wavelengths for nC$_{60}$ have smaller R^2 values (≈ 0.86). These relatively poor fits can be attributed to the heterogeneity of the suspensions and to the simplifying assumption that we have spherical nanoparticles. Each of the previous studies[122,123,126,128-133] investigated the particle extinction coefficients of highly monodisperse spherical nanoparticles. For aq/nC$_{60}$, however, the size distribution of the irregularly shaped particles ranged from less than 100 to 500 nm according to the DLS and TEM results (not shown). As a result, the estimated N is

approximate and the resultant γ is a general index of the absorptivity of an aq/nC$_{60}$ solution. Because of the lower absorbance and the wider absorption bands that result from the broader particle size distribution[132] and the irregular shape of the particles,[128,134,135] aq/nC$_{60}$ suspensions do not exhibit the same degree of regularity in their spectral properties as monodisperse spherical nanoparticles. This result clearly shows that it is challenging to predict the spectroscopic properties of aq/nC$_{60}$; nonetheless, consideration of the particle size distribution substantially improves the correlation between size and the absorptivity and this normalization should be considered when dealing with aq/nC$_{60}$ solutions (Details can be found in Appendix B).

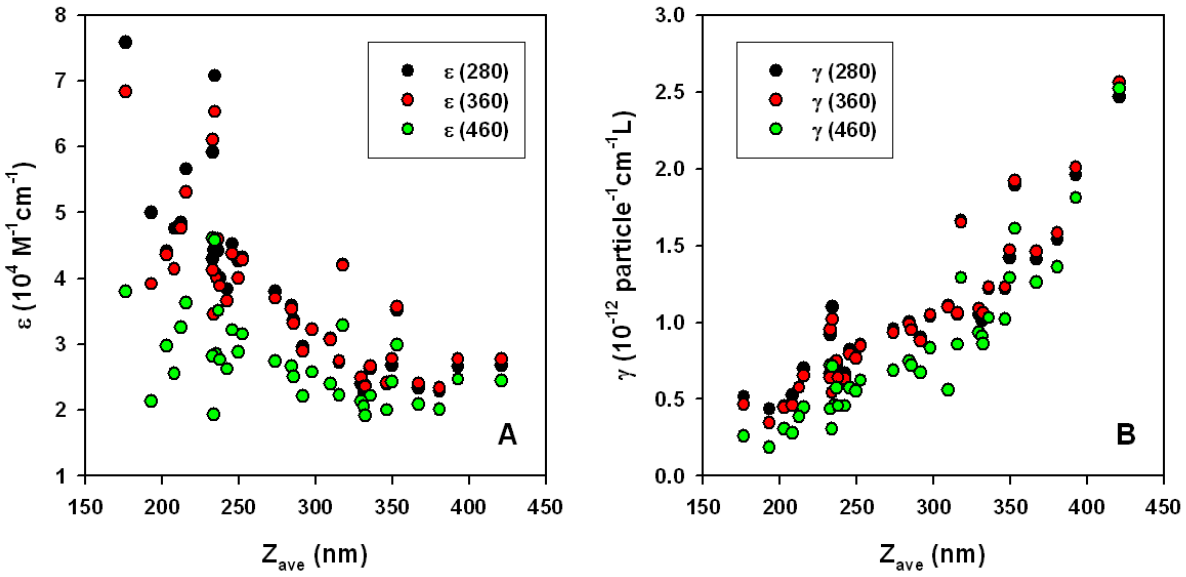

Figure 4.3 (A) ε and (B) γ as a function of average particle size.

Jain et al.[130] calculated the absorption and scattering efficiency of AuNP using Mie theory and the discrete dipole approximation (DDA) method and demonstrated that an increase in the AuNP size resulted in an increase in the extinction and the relative contribution of scattering. We employed MiePlot software (Philip Laven, Geneva, Switzerland) to calculate the absorption, scattering, and extinction of a hypothetically monodisperse aq/nC$_{60}$ suspension consisting of

spherical particles. In this calculation, the real and imaginary refractive indices for fullerene films[136] were used as representative of those for aq/nC$_{60}$ particles in the Mie calculation. Because of size limitations inherent to Mie theory (i.e., it is not valid for particles with sizes similar to or larger than the incident light wavelength), the spectra for aq/nC$_{60}$ with particle sizes larger than 300 nm predicted by MiePlot were quite dissimilar from those experimentally obtained (Figure B.12). For aq/nC$_{60}$ particles smaller than 300 nm, however, MiePlot results show similar increases in the extinction coefficient with particle size as was observed experimentally (Figure B.12). The consistency between the experimental results and the theoretical calculations suggests that despite the various shapes of aq/nC$_{60}$ formed via extended mixing, particles with larger sizes have a greater propensity to extinct incident light. Spectra for monodisperse aq/nC$_{60}$ from MiePlot (Figure B.13) also indicate that the increase in extinction spectra with particle size mainly results from enhanced scattering.

Widths of Absorption Bands. Absorption bands for aq/nC$_{60}$ suspensions are generally broader than those for C$_{60}$-organic solutions (Figure 4.1). This broadness can be attributed to C$_{60}$-water interaction induced higher electronic transition densities[72] and the particle size increase due to the aggregation of C$_{60}$.[132,137] Figure 4.4A shows that the absorption bandwidths (represented as the full width at half maximum, FWHM) of the 6^1T_{1u}-1^1A_g, and 3^1T_{1u}-1^1A_g transitions of nC$_{60}$ generally increased with an increase in average particle size. Similar increases reported in the spectra of AuNP were accounted for in terms of the phase-retardation effects of large nanoparticles and the growing contribution of scattering to the extinction spectrum.[138] In general, samples with greater polydispersity (e.g., larger PDI) exhibit broader absorption bands (Figure B.14). This observation is consistent with previous studies.[138,139] Interestingly, the centrifuged nC$_{60}$ samples do not follow the same trends (Figure 4.4B). Centrifuged nC$_{60}$ samples,

unlike the settled ones, did not exhibit an increase in PDI with Z_{ave} (Figure B.15). The relatively random PDIs of the centrifuged samples in the present study likely result from the re-entrainment of large particles from the sediment to the supernatant during transfer from the centrifuge tube for further characterization. Interestingly, except for the bandwidth, the centrifuged samples did not show many differences in their spectral properties relative to the settled samples, suggesting that the overall heterogeneity of an aq/nC$_{60}$ suspension primarily affects the absorption bandwidth, while the average particle size of the suspension determines the majority of its spectral properties.

The position of absorption maximum and the bandwidth of an absorption band, each of which is affected by solute-solvent interactions and the size of particles, follow a linear relationship despite different pretreatments prior to UV-Vis and DLS characterization (Figure 4.4C). Although the mechanism of this concurrent change is unknown, Bensasson et al.[93] reported a similar relationship for C_{60} in different organic solvents and solutions with surfactants. With the relationships shown in Figures 4.4A and 4.4C, it is possible to approximately estimate the average particle size of an aq/nC$_{60}$ sample based on its UV-Vis spectrum (Details in Appendix B).

Size Effects on the Position of Absorption Maximum in Extinction Spectra. The size of an nC$_{60}$ particle not only alters the extinction coefficient of the suspension at a given wavelength, but also affects the shape of the collected extinction spectra. The main absorption bands resulting from the 6^1T_{1u}-1^1A_g (280 nm) and 3^1T_{1u}-1^1A_g (360 nm) transitions red shift from 270 to 290 nm and from 350 to 370 nm as Z_{ave} increases from 180 to 450 nm, respectively (Figure 4.5A). Similar bathochromic effects have been reported in previous studies.[74,79,121] The red shift in the present study, however, does not exhibit the linear relationship with an increase in average

particle size described elsewhere. This result may reflect the high polydispersity of aq/nC$_{60}$ suspensions produced via extended mixing and gravitational settling without further fractionation. Large particles, the irregular shape of these particles, and the higher heterogeneity of aq/nC$_{60}$ result in a broader absorption band[127,132,134] and therefore reduce the capacity of the UV-Vis absorption spectra to differentiate average particle size based upon the position of absorption maximum.

Relative absorption intensity is calculated by dividing the ε value at a certain wavelength by ε(360). Similar to previous studies,[74,121] the relative 280-nm absorbance decreases with average particle size (Figure 4.5B). Bensasson et al.[93] have reported the decreasing relative intensity of this peak with red shifted maximum absorption in different C$_{60}$-organic solutions or C$_{60}$-liposome solutions. Currently the reason for the changing relative intensity of this peak in aqueous nC$_{60}$ suspensions is not known.

The relative intensity of the broad absorption band from 400 to 600 nm, represented by ε(450)/ε(360) increases with particle size (Figure 4.5B). The decrease shown in Figure 4.5B confirms that this band is due to the close electronic interactions among adjacent C$_{60}$ molecules in aq/nC$_{60}$ naoparticles.[27,59,140] It also explains the poor decrease of ε(460) with Z_{ave} shown in Figure 4.3A. Because of the stronger ability of larger particles to extinct incidental light in this region, the decrease in the molar concentration normalized light absorption intensity at 460 nm is not as large as that observed for ε(280) and ε(360).

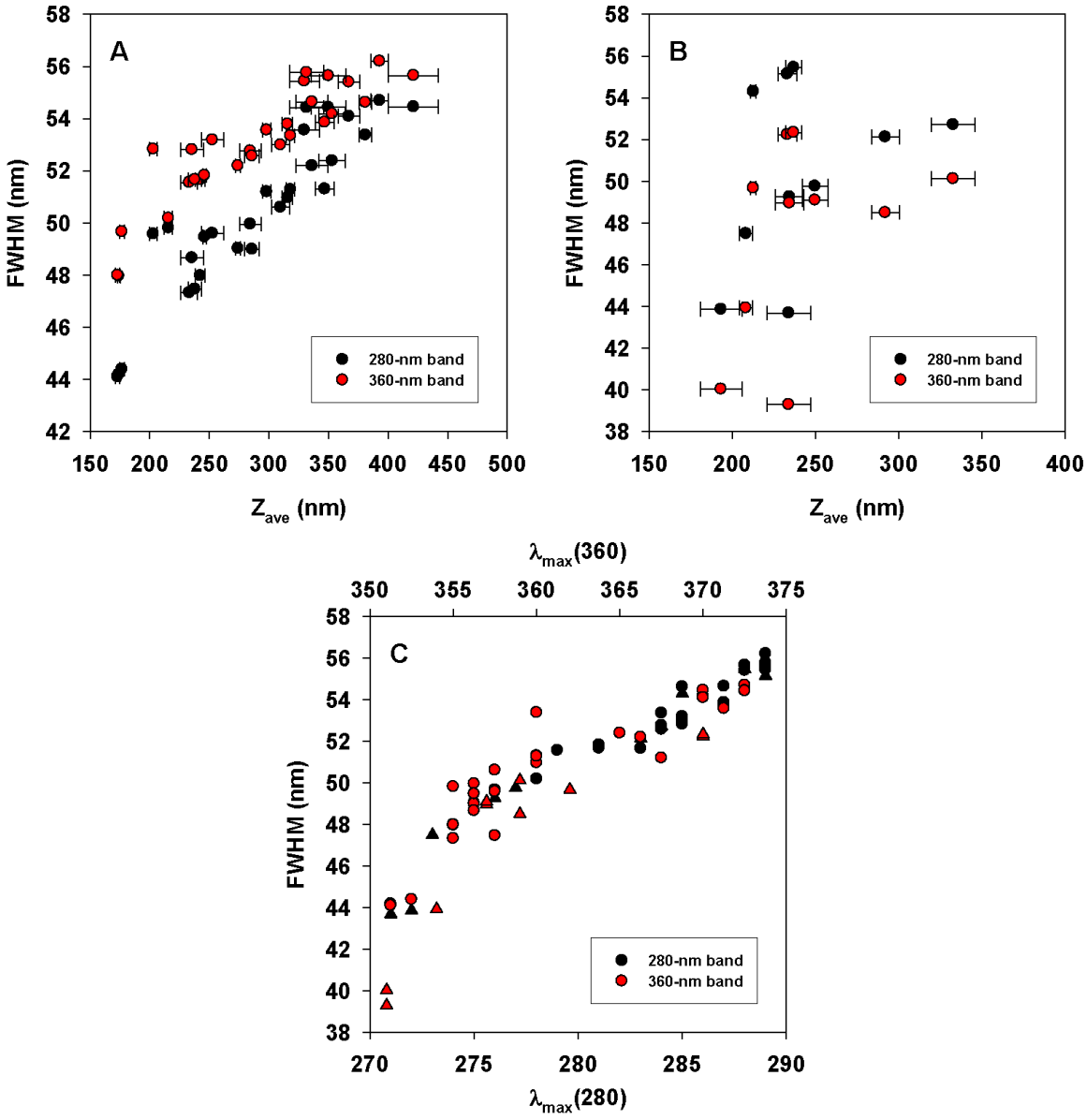

Figure 4.4 The full width at half maximum (FWHM) of the 360- and 280-nm bands as a function of the average particle size: (A) gravitational settled samples and (B) centrifuged samples. The horizontal error bar represents the standard deviation of three measurements for each sample. (C) FWHM of the 360 and 280 nm bands as a function of the position of the absorption maximum (Dots: gravitational settled samples; and triangles: centrifuged samples).

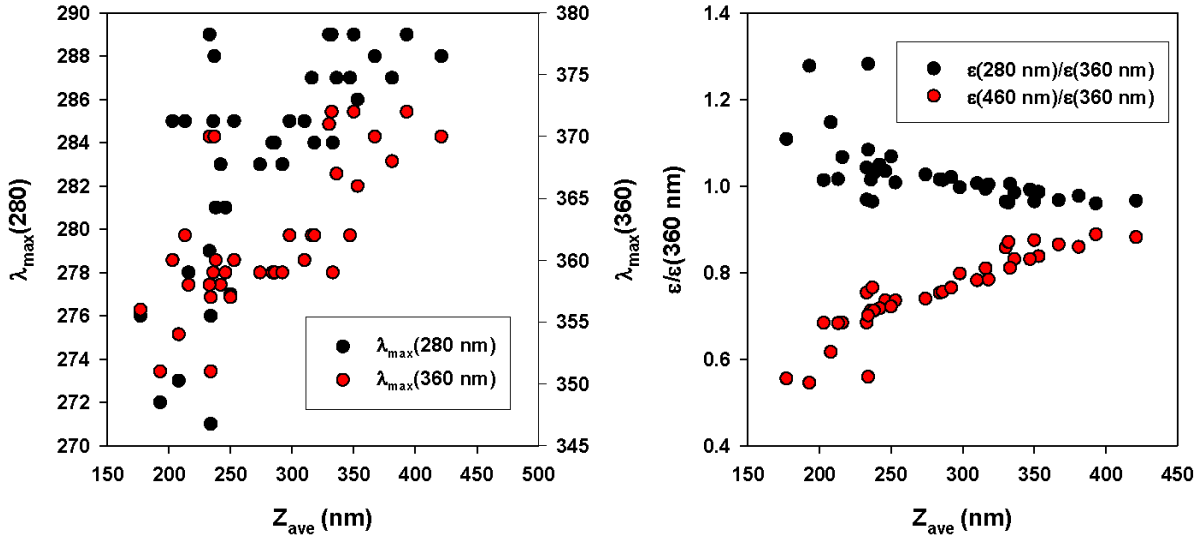

Figure 4.5 (A) The position of absorption maximum of 280 and 360 nm absorption bands as a function of average particle size; (B) relative intensities at 280 nm and 450 nm as a function of average particle size.

4.4 Environmental Implications

In the present study, we have made extensive efforts to obtain extinction spectra for aq/*n*C_{60} by normalizing collected UV-Vis spectra by either the C_{60} concentration or the particle concentration. However, neither of these attempts was successful at obtaining a single extinction spectrum that could be used to describe different aq/*n*C_{60} suspensions. Besides the variations in the extinction intensity other spectral properties, including the position of absorption maximum,, bandwidths, and relative absorption intensities, all change as a function of the particle size and particle size distribution. Therefore, for aq/*n*C_{60} produced via extended mixing it is challenging, if not impossible to obtain a single extinction spectrum for different samples.

It is of significant importance to both the research and industrial communities to reproducibly produce *n*C_{60} suspensions. Unfortunately, due to the random nature of the top-down process, it is extremely difficult to produce identical *n*C_{60} suspensions via extended mixing or sonication. The general lack of reproducibility of aq/*n*C_{60} is likely a significant factor in the observed variability

of nC$_{60}$ toxicity: Oberdörster et al.[141] reported that the morality of *Daphnia magna* increased in aq/nC$_{60}$ suspensions (500 mg C$_{60}$/L water, stirred for two months, particle size 10-200 nm), while aq/nC$_{60}$ produced (20 mg C$_{60}$/L water, stirred for 4-6 weeks, Z_{ave} = 448.2 ± 33.1 nm, ζ potential = -17.8 ± 7.1 mV) by Spohn et al.[119] did not show any toxic effect to *D. magna*. When studies investigating the behavior, transport, and environmental impacts of aq/nC$_{60}$ or SON/nC$_{60}$ are conducted, researchers must be aware that the data obtained using different batches of aq/nC$_{60}$ and SON/nC$_{60}$ may not be comparable. Particle size, [C$_{60}$], nC$_{60}$ particle concentration, and other colloidal properties, collectively determine the properties of nC$_{60}$ with respect to its transformation, transport, and toxicity. Furthermore, as shown in Figures 4.2A and 4.2C, even for samples from the same batch, temporal effects can have a dramatic impact on these parameters.

Although UV-Vis spectroscopy can be employed to directly measure the concentration of a number of chemicals in aqueous solutions,[142-144] it is inappropriate to use the UV-Vis absorbance of nC$_{60}$ suspensions to determine their C$_{60}$ concentration unless extreme care has been taken to fully characterize the system with respect to particle size, solution chemistry, and aggregation state. The decrease in the molar extinction coefficient with particle size implies that when an extinction coefficient of a suspension is used to calculate the [C$_{60}$] of a suspension with a larger particle size, the calculated value would be larger than the actual [C$_{60}$]. For example, if we use the ε(360) of the aq/nC$_{60}$ suspension with the smallest Z_{ave} (177 nm) in the present study to calculate [C$_{60}$] for aq/nC$_{60}$ suspensions with larger Z_{ave} (up to 421 nm), the calculated [C$_{60}$] is up to 70% lower than the actual [C$_{60}$] of these aq/nC$_{60}$ suspension (Figure B.16). Particle extinction coefficients that are dependent upon particle size and size distribution cannot be directly used to determine [C$_{60}$] either. For studies in which the size and other properties of nC$_{60}$ may change

either temporally or spatially (e.g., column studies), extreme care should be taken in data interpretation and comparison when UV-Vis absorbance is used to calculate or represent [C_{60}]. To obtain more reliable [C_{60}] results for a *n*C_{60} suspension based upon its UV-Vis spectra, the calibration curve must be constructed such that both concentration and size information of the *n*C_{60} standards are considered. Finally, the average particle size for the to-be-determined sample should be determined as well and should be similar to that of the standards.

Chapter 5 Effects of Carboxylic Acids on nC$_{60}$ Aggregate Formation

Reproduced with permission from

Environmental Poluution **2009**, issue *157*, pp. 1072-1080.

5.1 Introduction

As a result of its unique cage-like structure, remarkable electrochemical properties, and its anti-oxidant capabilities, C_{60} fullerene is now being exploited in a growing number of products and applications in various fields including biomedicine,[145] optoelectronics,[146] sensors,[10] and cosmetics.[13] Increasing industrial-scale production and applications of C_{60} fullerene suggest that considerable amounts of C_{60} will be released into natural systems. Currently, however, little is known about the interactions of fullerene with the constituents of natural waters and thus the potential environmental impacts of C_{60} are unclear.

C_{60} fullerene, which is virtually insoluble in water,[22] can form stable colloidal solutions containing high concentrations of C_{60} nanoparticles (nC$_{60}$). In the majority of the studies employing nC$_{60}$, a solvent exchange method has been used to produce nC$_{60}$. Although regularly shaped nC$_{60}$ nanoparticles can be produced quickly through this protocol, the use of organic solvents such as tetrahydrofuran (THF), toluene, and acetone raise concerns that organic residuals in nC$_{60}$ may cause or enhance its toxicity.[87,147] Several previous studies have shown that nC$_{60}$ formed by directly mixing C_{60} with water (e.g., aq/nC$_{60}$) has different size, morpholologic,[59,80] toxicologic,[87] and UV-Vis characteristics[58] than nC$_{60}$ produced by organic solvent exchange methods (e.g., THF/nC$_{60}$, Tol/nC$_{60}$).

In practice, because of its low solubility in water, it is unlikely that C_{60} that has not been functionalized to improve its solubility will be employed in many products. Accordingly, it is presently unclear whether either aq/*n*C_{60} or the *n*C_{60} nanoparticles produced in the presence of organic solvents will directly correspond to the *n*C_{60} nanoparticles that will be found in the environment. However, because even "soluble" derivatives of C_{60} aggregate in aqueous solutions,[148] a fundamental understanding of the processes dictating the formation of these nanoparticles is of importance. In this study, the method of long-term stirring of C_{60} powder in aqueous solutions was employed.

When materials containing C_{60} are released in natural aqueous environments, there will be interactions between C_{60} and natural components. Several recent studies have suggested that natural organic matter (NOM) can enhance the apparent water solubility of C_{60}[29] and result in the formation of smaller and more stable *n*C_{60} nanoparticles.[30,80,89] Given these observations, it is possible that release of C_{60} fullerene in natural, aqueous environments may have unexpected consequences. Unfortunately, because of the complex nature of NOM, the mechanism by which C_{60} interacts with NOM is currently unknown.

As a first step towards an improved understanding of *n*C_{60} formation in the presence of NOM, the effects of carboxylic acid groups, which are highly prevalent in NOM,[149,150] were studied. *n*C_{60} were produced in three carboxylic acid solutions: sodium acetate, sodium tartrate, and sodium citrate. These three organic acids contain one, two, and three carboxylic acid groups, respectively. As documented herein, as the carboxylic acid type and concentration change, *n*C_{60} of different sizes and morphologies are observed.

5.2 Materials and Methods

Chemicals and Glassware. Sublimed C_{60} fullerene powder was purchased from Materials and Electrochemical Research (MER) Corporation (Tucson, AZ). Experiments were conducted using ACS grade sodium citrate, sodium acetate, tartaric acid, and sodium hydroxide (Fisher Scientific, Fair Lawn, NJ). All water used in these experiments was obtained from a NANOpure Ultrapure water system (Apple Scientific Inc., Chesterland, OH). The resistivity of the water was always greater than 18.3 MΩ•cm. All *n*C_{60} solutions were prepared and stored in glass containers that had been washed with aqua regia and rinsed thoroughly prior to use. Sodium citrate and sodium acetate were dissolved directly to obtain solutions with concentrations ranging from 5 to 25 mM. Sodium tartrate stock was produced by using NaOH to adjust the pH of a tartaric acid solution. Each of these solutions was filtered through a 0.2 μm nylon membrane prior to use.

***n*C_{60} Suspension Preparation.** The general method for production of *n*C_{60} aqueous suspensions is based on that described in Cheng et al..[28] Dry sublimed C_{60} fullerene (fullerite C_{60}) was pulverized to a very fine powder using a Fritsch pulverizette 0 ball mill at amplitude 0.5 mm. The resulting fine powder was sieved through a 63 μm metal sieve. To produce *n*C_{60}, 40 mg of pulverized and sieved fullerite C_{60} was added to 50 mL of nanopure water or carboxylic acid solution in a 75 mL glass vial. A PTFE magnetic stir-bar was added and the solution was stirred in the dark at 30 ºC for two weeks. To maintain consistency between experiments, the stirring intensity, sample vial type, and sample volume were the same for each experiment.

***n*C_{60} Production Variables.** The general *n*C_{60} production procedure was modified to test the effects of the following variables on *n*C_{60} formation: (1) Pulverization time: As received C_{60} was pulverized for 5 to 60 min. (2) Effect of carboxylic acid: C_{60} was added to solutions containing 1-25 mM sodium acetate, sodium tartrate, or sodium citrate to evaluate the effect of these

constituents on particle size and surface charge. (3) Settling Time: Periodic samples were settled for 1 hour, 24 hours, or 10 months, and the respective supernatants were characterized. At each sample point, 2.5 mL of suspension was taken from a continuously stirred sample vial. This aliquot was then transferred to a test tube and, following the settling period, 2 mL of supernatant was characterized.

Characterization of *n*C_{60}.

UV-Visible Spectrophotometry. UV-Vis absorption spectra of *n*C_{60} were acquired using a Cary 5000 UV-Vis-NIR spectrophotometer (Varian Analytical Instruments, Walnut Creek, CA). A quartz cuvette with a 10 mm pathlength was used to measure solution absorbance over the spectral range of 200-800 nm.

Dynamic Light Scattering (DLS) and Electrophoretic Mobility. A Nano Zeta-sizer (Malvern Instruments, Worcestershire, United Kingdom) with a 633 nm laser source, a detection angle of 173º, and a folded capillary cell was employed to measure particle size distributions of undiluted, settled *n*C_{60} solutions. The reported range of detection of this instrument is 0.6 nm to 6 µm. The intensity-based hydrodynamic diameter (Z_{ave}) and second-order polydispersity index (PDI) were obtained by using the CONTIN algorithm to develop the size distribution of the *n*C_{60} nanoparticles. The Nano ZS was also used for electrophoretic mobility (EM) measurements. Temperature was maintained at 25 ºC by the instrument. A minimum of three measurements, each consisting of at least 12 subruns for size measurement and 23 subruns for EM measurements, were made on each sample to ensure accuracy and reproducibility.

Transmission Electron Microscopy (TEM). TEM samples were imaged using a Zeiss 10 CA TEM operated at 60 kV. Samples were prepared by placing 5-10 µL of sample on a

Formvar/carbon coated 200-mesh copper grid. The grid was then dried in a desiccator at room temperature for a period of at least 12 hours.

5.3 Results and Discussion

Pulverization Time. Prior to conducting experiments with our chosen carboxylic acids, we examined the effects of pulverization time on nC$_{60}$ formation in the absence of organic materials. Previous research has shown that pulverization of fullerite C$_{60}$ results in a visible increase in the speed and extent that C$_{60}$ becomes stabilized in solution and makes it possible to reach higher concentrations of nC$_{60}$ more rapidly.[80] To further evaluate the effects of pulverization, fullerite C$_{60}$ was pulverized for 5, 10, 20, 30, or 60 minutes and the resulting powders were added to nanopure water and stirred for 14 days.

Aq/nC$_{60}$ produced in this study has broad UV-Vis peaks at 223, 287, and 370 nm (Figure 5.1A). Compared with nC$_{60}$ produced by solvent exchange methods (peaks at 223, 286 and 349 nm[58]), the absorbance band at 370 is red-shifted and an additional broad band at 400-600 nm is observed. The occurrence of this absorbance band has been suggested to be the result of the formation of weak donor-acceptor complexes of C$_{60}$ with water.[65]

With extended stirring, the apparent nC$_{60}$ concentration of each pulverized sample increases. Direct comparison of the measured UV-Vis absorbance at 370 nm (Figure 5.1B), which reflects both light scattering by the nC$_{60}$ nanoparticles and light absorption by C$_{60}$, suggests that although differences in pulverization time alter the apparent nC$_{60}$ concentration that these effects do not follow a simple trend. As shown in Figure 5.1B, the longest pulverization time did not lead to the most rapid stabilization nor the most concentrated aq/nC$_{60}$ solution. Furthermore, the least concentrated aq/nC$_{60}$ solution was not produced by the shortest pulverization time. A relatively

short pulverization period of only twenty minutes was sufficient to produce the most concentrated solution after fourteen days of stirring. We note that although extreme care was taken to replicate the mixing conditions in each sample vial that there are inherent difficulties associated with reproducible production of nC$_{60}$ solutions of a given concentration. Past experience[80] has shown that final solution concentrations can vary by an order of magnitude for solutions prepared under 'identical' conditions. This variability makes quantitative comparison of solution concentrations for different sample vials, such as that shown in Figure 5.1B, difficult. It is thus impossible to definitively say whether different pulverization times alter the rate at which nC$_{60}$ forms.

Figure 5.1C shows volume weighted size distributions of these five samples after fourteen days of stirring and a 1 hour settling period. Each particle size distribution consists of three broad peaks with diameters in the general size ranges: 115-211, 457-548, and 5058-5560 nm. Given the polydisperse nature of these suspensions, direct comparison of the particle size distributions is complex and thus we determined average hydrodynamic diameters (Z_{ave}) for each suspension (Table 5.1). For polydisperse systems, rather than corresponding to any one peak in the particle size distributions, Z_{ave} represents an average of all peaks. As shown in Table 5.1, as the pulverization time is increased there is a statistically significant decrease in the hydrodynamic diameter. With 5 min of pulverization, Z_{ave} is 425 ± 4 nm, while 60 min of pulverization results in a Z_{ave} of 286 ± 16 nm. In addition to a decrease in particle size with increased pulverization time, the polydispersity index (PDI) decreases concomitantly. This result suggests that increased pulverization times facilitate the more rapid production of smaller and more homogeneous nC$_{60}$ nanoparticles.

One potential explanation for the smaller nC$_{60}$ nanoparticles observed in the more extensively pulverized samples is that the physical act of pulverization alters the surface chemistry of C$_{60}$. However, we do not believe this to be the case since the measured surface charges (electrophoretic mobilities or EM) of the different suspensions were statistically indistinguishable (Table 5.1) and averaged -2.85 ($\pm$ 0.4) $\times$ 10^{-8} m^2/Vs over the 14 day stirring period. (In determining this average we did not consider the measured electrophoretic mobility for the 5 minute pulverized sample obtained on day 14. For unknown reasons this value was considerably higher than that measured any other day and was thus considered an outlier.) Although the reactions responsible for setting the surface potential are currently unexplained,[58-60] one would expect that they should be affected by the surface chemistry of the material. To our knowledge, no one has previously looked at the impacts of pulverization on the interfacial chemistry of C$_{60}$ and such an effort was beyond the scope of the present experiments.

Collectively considering the data presented in Figure 5.1 and Table 5.1, it is apparent that the pulverization period does not change the measured surface charge, but does affect the average particle size. Pulverization does not alter the surface chemistry of C$_{60}$, but it does decrease the size of the fullerite C$_{60}$ starting material, which in turn affects particle size and possibly the rate at which nC$_{60}$ is formed. Unfortunately, because UV-vis absorbance measurements incorporate both light scattering and molecular absorption phenomena, each of which is a function of particle size, they are not reliable as a tool to determine the rates at which nC$_{60}$ forms. Given these findings, we chose to employ a 20 min pulverization time in our experiments with carboxylic acids. This period is sufficient to rapidly produce nC$_{60}$ suspensions with relatively high concentrations.

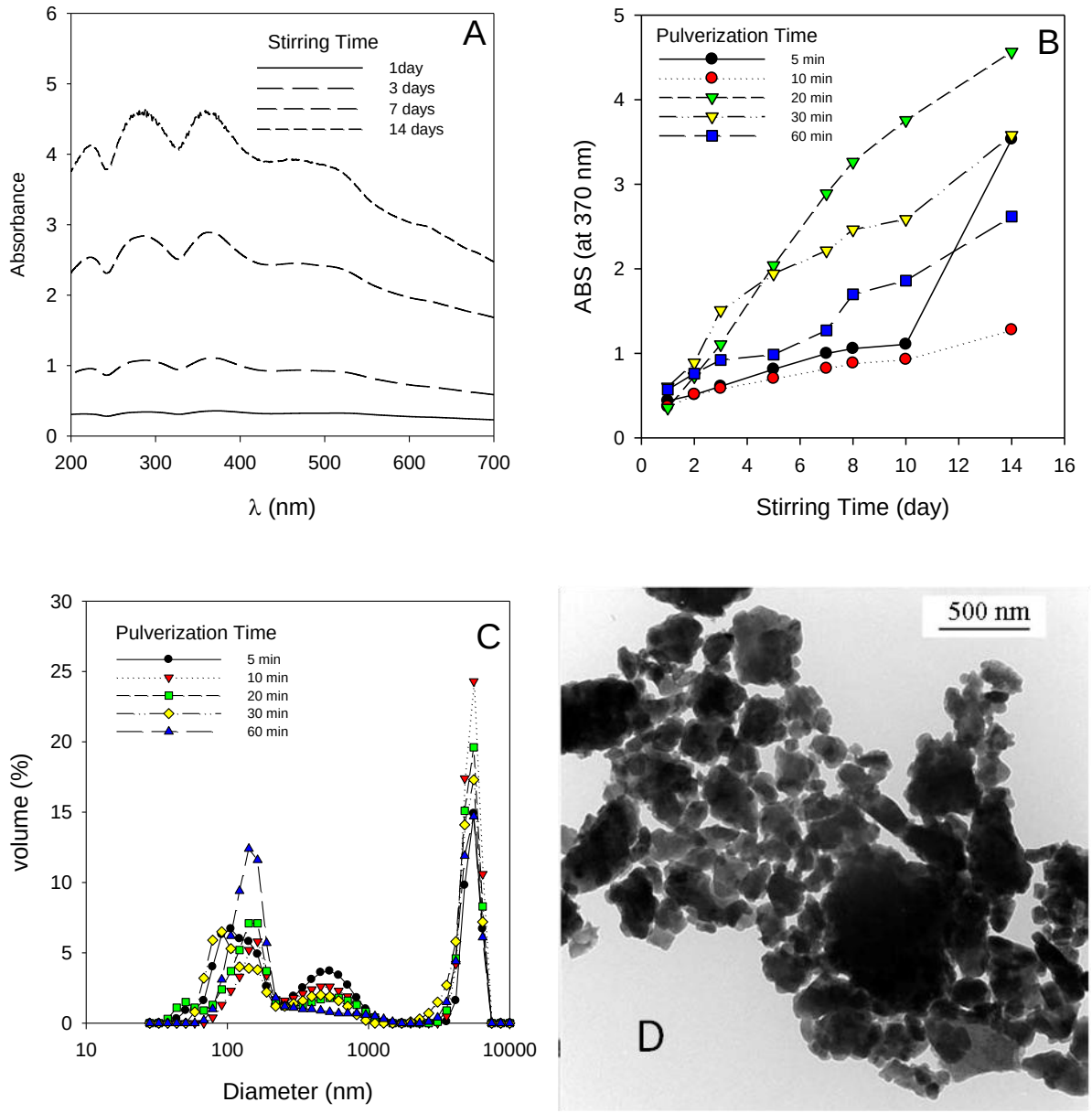

Figure 5.1 (A) UV-Vis absorption spectra of aq/*n*C_{60}. (B) Sample absorbance increases with extended stirring time. (C) Size distributions of samples after stirring for 14 days and settling for 1 hour. (D) TEM image of aq/*n*C_{60}. Compared with *n*C_{60} formed in carboxylic acid solutions, aq/*n*C_{60} aggregates have tighter structure and are consisted of larger irregularly shaped primary particles.

Effects of Carboxylic Acids. We have determined that the identity and the concentration of carboxylic acids present in solution affects *n*C_{60} formation. To investigate the effects of these acids, pulverized fullerite C_{60} was added to sodium acetate, sodium tartrate, and sodium citrate solutions of different concentrations. Table 5.2 lists average EM, Z_{ave}, and PDI values for *n*C_{60} in

these carboxylic acid solutions during the 14 day stirring period. For those suspensions containing higher concentrations of nC$_{60}$, as indicated by a yellow or light brown color (Figure 5.2), these three parameters were quite stable during the 14 day stirring period (data not shown). However, for those samples where the final concentration of nC$_{60}$ was lower, these three values varied with time, as might be expected for a precipitating solution.

Table 5.1 Electrophoretic mobilities, hydrodynamic diameters, and polydispersity indices of aq/nC$_{60}$. Errors reflect the standard deviations of replicate measurements.

Pulverizing Time	Electrophoretic Mobility (10^{-8} m^2/Vs)				Hydrodynamic Diameter (nm)				Polydispersity Index			
	Stirring time				Stirring time				Stirring time			
	3 days	8 days	14 days	Average	3 days	8 days	14 days	Average	3 days	8 days	14 days	Average
5 min	-2.72	-3.16	-5.88	-3.92±1.71	421	426	428	425±4	0.440	0.421	0.438	0.433±0.010
10 min	-2.35	-2.51	-3.22	-2.69±0.46	349	347	389	362±24	0.394	0.403	0.432	0.410±0.020
20 min	-2.77	-2.52	-3.58	-2.96±0.55	307	381	358	349±38	0.286	0.447	0.403	0.379±0.083
30 min	-2.47	-2.45	-3.30	-2.74±0.49	310	327	355	331±23	0.326	0.417	0.395	0.379±0.047
60 min	-2.72	-2.57	-3.26	-2.85±0.36	269	301	288	286±16	0.275	0.411	0.354	0.347±0.068

Table 5.2 Electrophoretic mobilities, hydrodynamic diameters, and polydispersity indices of nC$_{60}$ in carboxylic acid solutions. Errors reflect the standard deviations of replicate measurements.

Concentration of Carboxylate		Electrophoretic Mobility (10^{-8} m^2/Vs)	Hydrodynamic Diameter (nm)	Polydispersity Index (PDI)
Sodium Acetate	5 mM	-4.02±0.15	636±115	0.477±0.019
	10 mM	-4.30±0.29	516±44	0.540±0.100
	15 mM	-4.20±0.36	565±39	0.532±0.069
	20 mM	-3.80±0.43	1252±536	0.377±0.061
	25 mM	-3.41±0.26	1754±153	0.630±0.176
Sodium Tartrate	1 mM	-4.39±0.35	492±22	0.477±0.019
	5 mM	-3.67±0.88	875±637	0.540±0.100
	10 mM	-3.46±0.46	1744±93	0.532±0.069
	15 mM	-2.74±0.15	2183±356	0.377±0.061
	25 mM	-3.29±0.47	1803±291	0.630±0.176
Sodium Citrate	5 mM	-5.28±0.31	548±239	0.495±0.018
	10 mM	-5.00±0.40	874±94	0.452±0.045
	15 mM	-4.44±0.59	1218±267	0.484±0.084
	20 mM	-4.00±1.00	1527±166	0.528±0.121
	25 mM	-3.32±0.21	1590±82	0.577±0.085

In general, as shown in Figure 5.3A and in Table 5.1, the average EM values for nC$_{60}$ increase (become less negative) as the concentration of a given carboxylic acid increases. This trend can be attributed to the charge neutralizing effect of sodium ion. As the carboxylic acid concentration increases from 1 to 25 mM, the sodium ion concentration increases concomitantly. Past studies

have shown that sodium ion levels in excess of 10 mM can lead to destabilization[59] and aggregation[64] of nC$_{60}$.

For a fixed carboxylic acid concentration, the EM values for nC$_{60}$ follow the trend: nC$_{60}$ in sodium citrate < nC$_{60}$ in sodium acetate < nC$_{60}$ in sodium tartrate (Figure 5.3A). This trend, which does not follow what might be expected based on the total number of carboxylic acid groups in each molecule (acetate = 1, tartrate = 2, citrate = 3) can nonetheless be explained by differences in the solution pH. As shown in Figure 5.3B, when solution pH is considered, the nC$_{60}$ nanoparticles clearly fall into three distinct groups. nC$_{60}$ produced in sodium tartrate solutions (pH range = 5.5-5.6) is generally less negatively charged than that in sodium acetate solutions (pH range = 6.8-7.2), which in turn is less negatively charged than nC$_{60}$ in sodium citrate solutions (pH range = 7.8-8.3). Both the identity of the carboxylic acid and the solution pH, which for this set of experiments was set by the carboxylic acid concentration, affect the nC$_{60}$ surface charge.

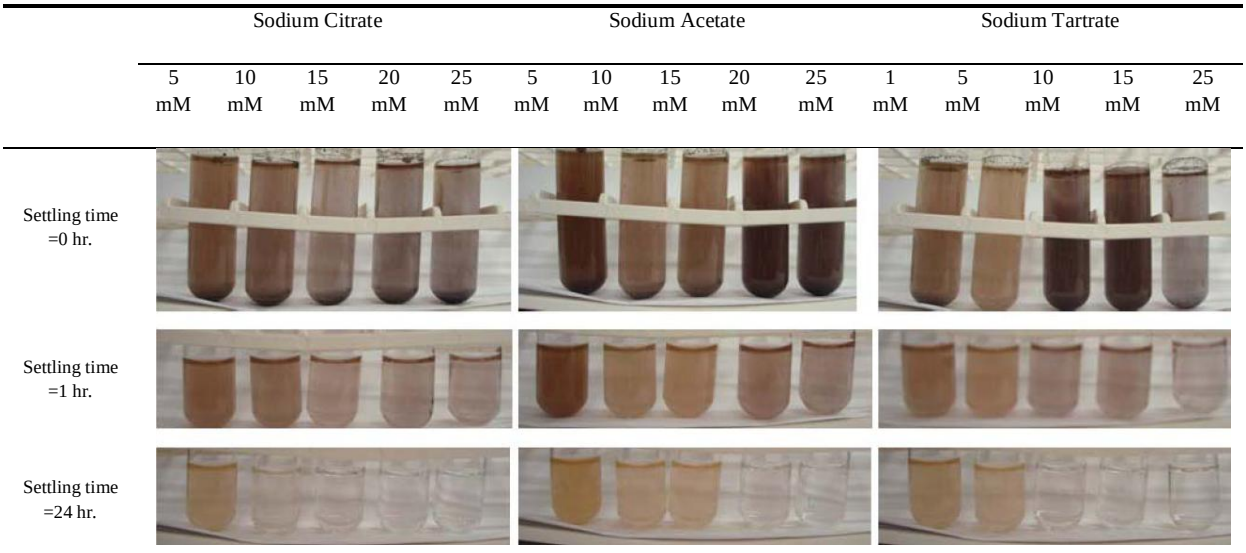

Figure 5.2 Visual images of nC$_{60}$ solutions after stirring for 7 days and settling for various times.

As shown in Figures 5.3A and 5.3C, Z_{ave} values for the different samples generally correlate with the trends observed in the EM values. For a given carboxylic acid, as the EM value becomes increasingly negative, the nC$_{60}$ have smaller average sizes. In contrast, nC$_{60}$ with EM values closer to zero have larger Z_{ave} values. This result is a direct ramification of the charge neutralizing effect of increasing concentrations of sodium ion and is consistent with the observations of Chen and Elimelech.[30] When nC$_{60}$ has greater surface charge (the EM value is more negative), strong electrostatic repulsive forces keep the nanoparticle away from each other, resulting in a stable suspension with a higher nC$_{60}$ concentration and smaller particle size. When the EM value approaches zero, however, the particles lose the ability to repulse nearby particles and they form larger particles, and as a result, larger Z_{ave} values are observed. When the particles are large enough, they can settle, leading to decreased nC$_{60}$ concentrations and transparent supernatants (Figure 5.2).

In the experiments depicted in Figure 5.3, when the carboxylic acid concentration is increased, the pH and sodium ion concentration simultaneously increase. To decouple these variables we conducted an additional set of experiments wherein the pH of 10-25 mM sodium acetate, sodium tartrate, and sodium citrate solutions was fixed between 6.95 and 7.23 by the addition of NaOH. Under these conditions, the measured EM values of the different suspensions do not vary significantly and an average EM value of -3.83 ($\pm$ 0.5) $\times$ 10^{-8} m^2/Vs was measured. Furthermore, the Z_{ave} values are also insensitive to the carboxylic acid concentration or identity (Z_{ave} = 557 $\pm$ 115 nm). At their surface, these findings suggest that the primary role that the carboxylic acids play in these experiments is to fix the solution pH and alter the particle surface charge. However, the role of these acids is not that simple since the acid identity affects the nC$_{60}$ morphology as determined by TEM (Figure 5.4).

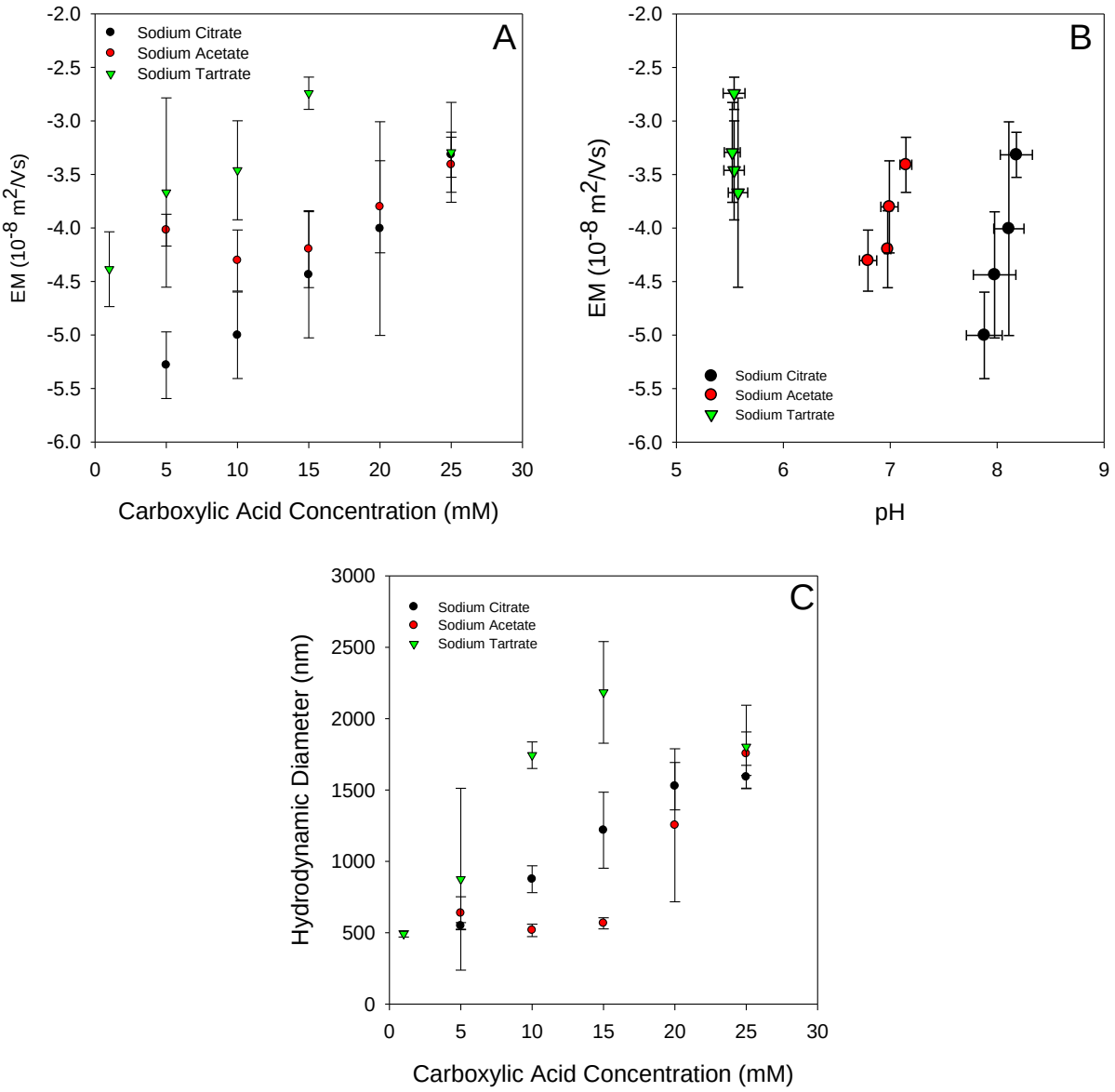

Figure 5.3 (A) Electrophoretic mobilities of nC_{60} vs. carboxylic acids concentration. (B) EM vs. pH of solutions. (C) Hydrodynamic diameters of nC_{60} vs. carboxylic acid concentration. Data points represent average values after stirring for 3, 7 and 14 days. The error bars represent the standard deviation.

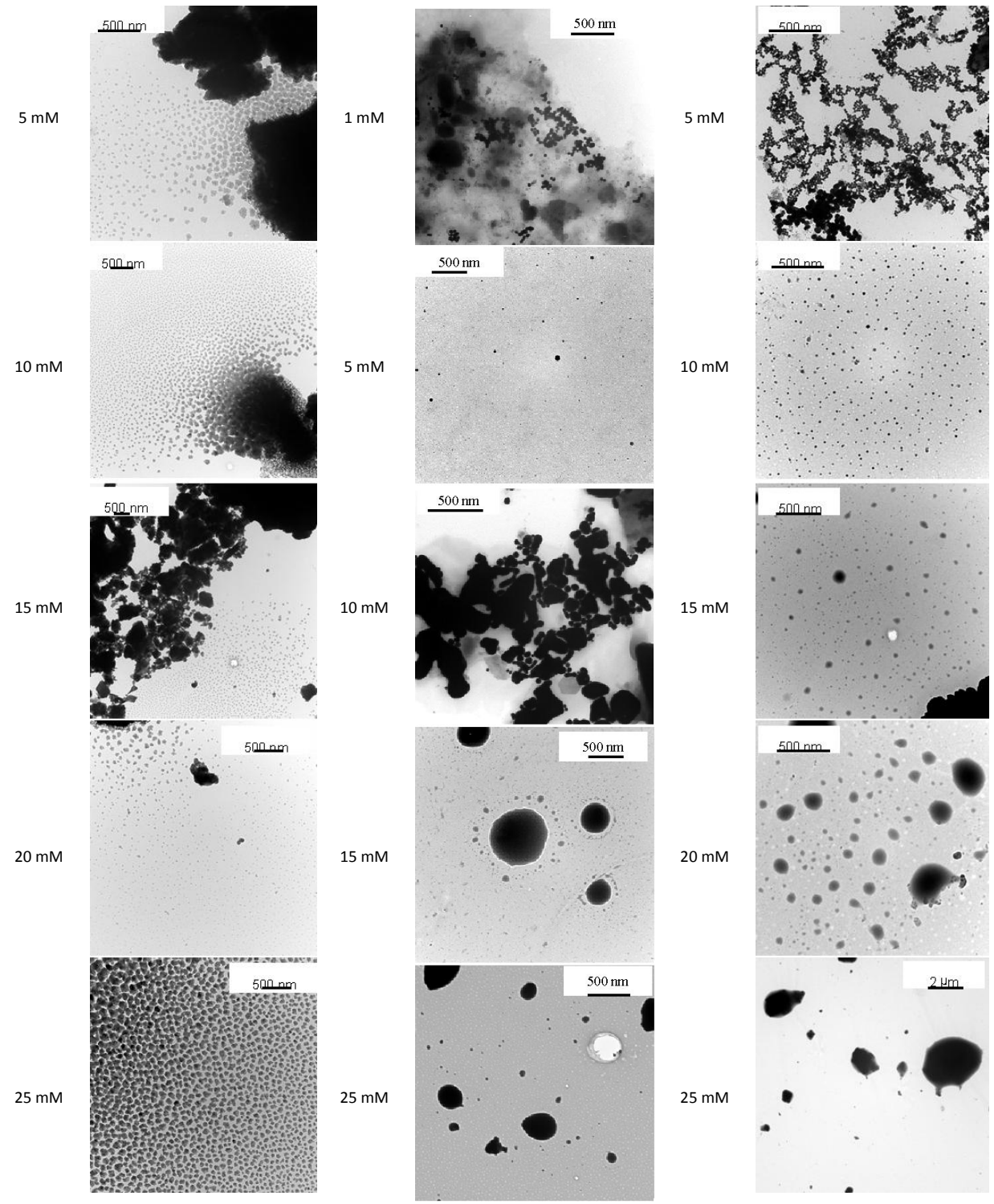

Figure 5.4 TEM images of nC_{60} in carboxylic acid solutions, stirred for 14 days and sampled without settling.

In the sodium acetate solutions, small angular, irregularly shaped particles are distributed around larger bulk sized particles. Interestingly, the size of these particles appears to get smaller as they get further away from a bulk particle. This trend is presumed to be the result of the effects of drying on the sample, yet is instructive because it illustrates the facile nature of nC$_{60}$ – showing that something as simple as drying can result in significant disaggregation. In contrast, nC$_{60}$ produced in solutions of sodium citrate and sodium tartrate exhibit both irregular shaped and spherical morphologies. At higher sodium citrate and sodium tartrate concentrations, although a few smaller nanoparticles (<100 nm) are observed, the majority of the particles are close to or larger than 1 μm.

The variation in nC$_{60}$ morphology for these solutions is hypothesized to be the result of differences in the structures of these carboxylic acids. Acetic acid has only one carboxylic group and apparently interacts with C$_{60}$ as a "trimmer" that takes large pieces of fullerite C$_{60}$ apart. Tartaric acid and citric acid, having two and three carboxylic groups, respectively, also have this ability, but simultaneously seem to possess the capability to build new highly structured aggregates. As shown in Figure 5.4, the particles formed in the presence of these acids exhibit spherical morphologies that differ significantly from those formed in the presence of acetic acid or water alone (Figure 5.1D). At the present time, it is not known if this effect is a direct result of these molecules having multiple carboxylic acid groups that can simultaneously interact with multiple C$_{60}$ atoms or is indicative of other phenomena. Ongoing studies in our laboratory seek to answer this important question.

To illustrate temporal trends in the formation of nC$_{60}$, TEM images of aggregates in 5 mM carboxylic acid solutions on days 3, 7, and 14 are shown in Figure 5.5 and particle size distributions for these samples are shown in Figure 5.6. For nC$_{60}$ in 5 mM sodium citrate solution,

on days 3 and 7, angular particles (≤100 nm) and very small spherical ones surrounding them were observed. By day 14, the number of small spherical particles had increased and become larger. Although a large number of tiny spherical nanoparticles (≤10 nm) were observed in TEM images from this sample, the total volume of these particles was not large enough to be discerned in the volume weighted particle size distribution (Figure 5.6A).

The morphology of nC_{60} in 5 mM sodium acetate solution changed remarkably during the 14 day stirring period. On day 3, the nC_{60} nanoparticles were very similar to those in 5 mM sodium citrate. By day 7, however, rod-like nanoparticles appeared, but by day 14, only large particles surrounded by small ones (~10 nm) were found. Again, as observed for sodium citrate, although TEM images showed different shaped particles as a function of stirring time, DLS results for these three days are remarkably similar (Figure 5.6B).

For tartaric acid, there were no obvious differences in nC_{60} structure between day 3 and day 7. Most of the aggregates were around 500 nm, and were composed of primary particles that are approximately 100 nm in size. These two kinds of aggregates correspond to the two peaks found by DLS (Figure 5.6C). On day 14, an increase in the number of large particles, as indicated by the Z_{ave} value (Table 5.2) and size distribution, led to a dramatic decrease in the nC_{60} concentration (as determined by visual observation of the suspension color). As a result, particle density on the TEM grids was lower. Although lower in number, aggregates with similar structure to those observed on days 3 and 7 remained.

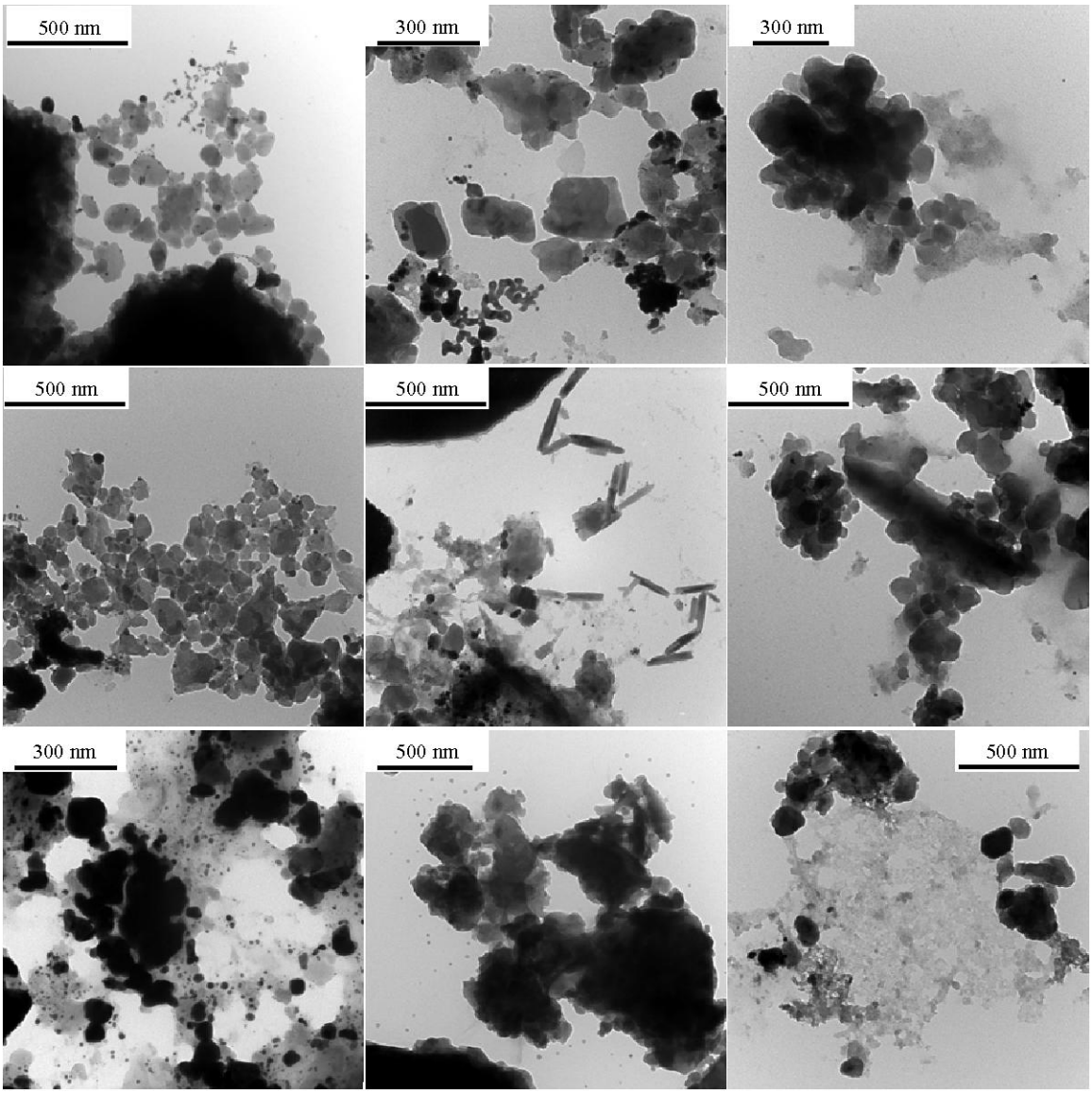

Figure 5.5 TEM Images of nC$_{60}$ produced in the presence of three carboxylic acids on days 3, 7, and 14. Left column: 5 mM sodium citrate; Middle column: 5 mM sodium acetate; Right column: 5 mM sodium tartrate.

Comparing the results obtained by analysis of the TEM images with that obtained via DLS, it is apparent that DLS does not capture the facile nature of these suspensions. Although the TEM results clearly show nC$_{60}$ breaking, forming, and reforming, this behavior was not captured by the DLS. This discrepancy could be caused by the conversion from intensity weighted results to a volume weighted result based on Mie theory. This theory, which is suitable for spherical particles, may lead to inaccuracies for nC$_{60}$ that have complex structures. This comparison

indicates that for nC_{60} nanoparticles formed in aqueous carboxylic acid solutions, size distributions developed from DLS measurements alone are insufficient to accurately characterize these suspensions.

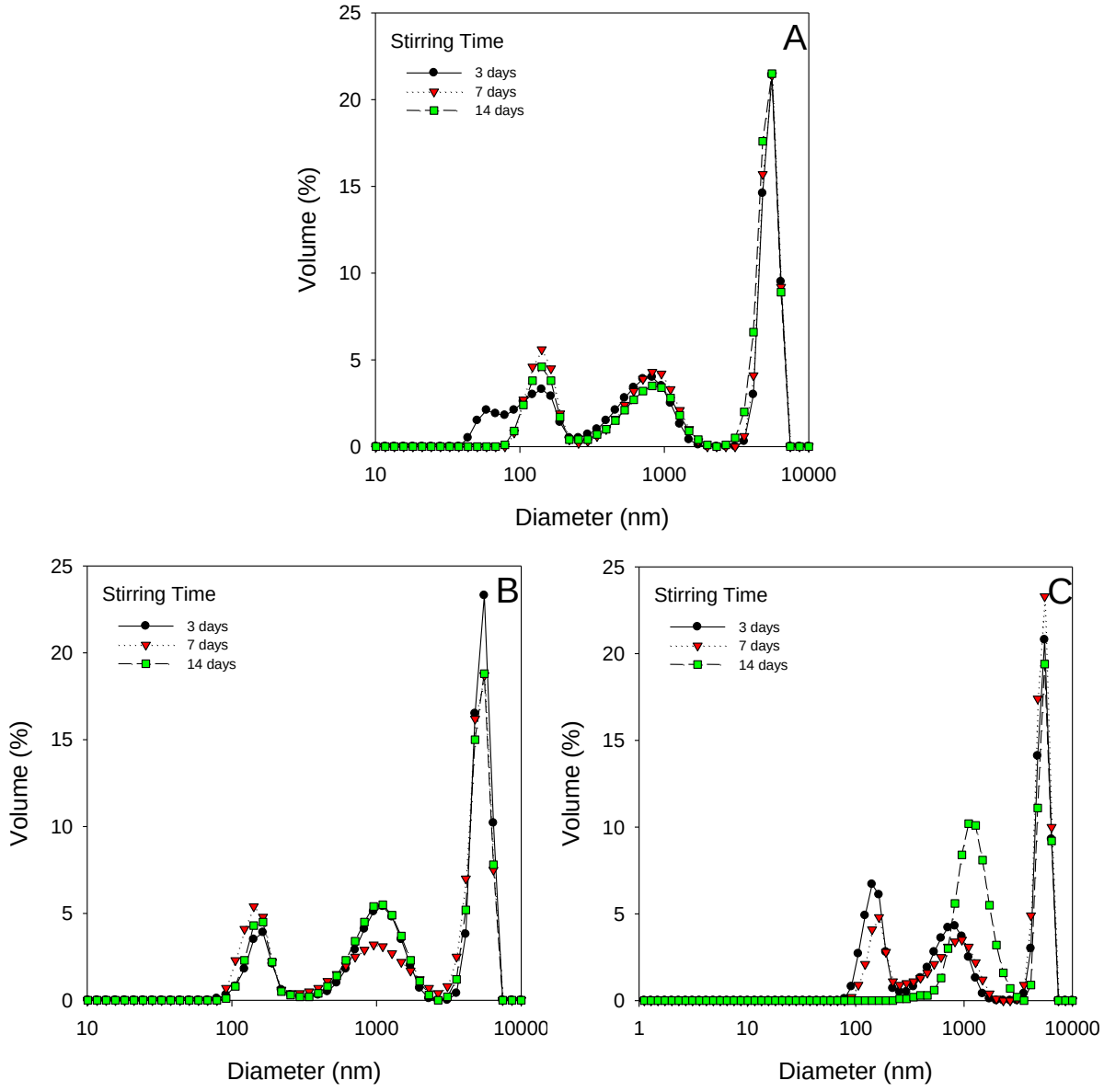

Figure 5.6 Size distributions of nC_{60} after different stirring times in (A) 5 mM sodium citrate, (B) 5 mM sodium acetate, and (C) 5 mM sodium tartrate.

Settling Time. In this study, no artificial method (such as filtration or centrifugation) was used to obtain stable nC_{60} solutions. However, in our analyses the settling time used prior to sample

characterization is a critical factor that may affect the characteristics of the suspensions. Figure 5.1 shows that: (1) unsettled suspensions contain numerous large particles that can be observed by eye; (2) after one hour of settling, many of the very large particles have precipitated, but some remain in suspension and produce a brown or light black color in the supernatants. These large particles result in the large peaks at about 5 μm in Figure 5.1 and Figure 5.6; and (3) after 24 hours, very stable supernatants are obtained. These supernatants can be light yellow or transparent. In general, longer settling times allow larger, unstable particles to settle out of the solutions, resulting in less polydisperse (decreased PDI) systems. As the large particles settle, Z_{ave} values for nC_{60} in 5 mM sodium citrate, sodium acetate and sodium tartrate solutions decrease remarkably. However, there are no obvious trends with respect to EM (Table 5.3).

Table 5.3 Hydrodynamic diameter (Z_{ave}, nm), Polydispersity Index (PDI), Electrophoretic Mobility (EM, 10^{-8} m^2/Vs) of nC_{60} solutions after stirring for 14 days and settling for different times. Errors reflect the standard deivations of replicate measurements.

	Settled for 1 hour			Settled for 24 hour			Settled for 10 months		
	Z_{ave}	PDI	EM	Z_{ave}	PDI	EM	Z_{ave}	PDI	EM
nC_{60} in 5 mM sodium citrate	533±26	0.492±0.025	-5.32±0.21	409±20	0.374±0.075	-4.95±0.17	343±1	0.488±0.001	-4.08±0.17
nC_{60} in 5 mM sodium acetate	644±27	0.478±0.072	-4.00±0.04	329±9	0.331±0.029	-3.96±0.11	170±3	0.171±0.009	-3.75±0.02
nC_{60} in 5 mM tartaric acid (pH adjusted)	1609±240	0.655±0.061	-2.68±0.06	585±31	0.590±0.042	-4.40±0.25	180±2	0.111±0.009	-4.03±0.15

TEM images of the nC_{60} from a 5 mM sodium acetate solution with different settling times are shown in Figure 5.7. Figures 5.7A and 5.7B are images of samples without settling and after settling for 1 hour, respectively. Aggregates in these two images have very similar morphologies: they consist of large, solid and irregularly shaped particles surrounded by tiny spherical ones. After 24 hours of settling, not only does the average size of nC_{60} decrease (from 644 to 328 nm) as determined by DLS, but the shape and structure of these particles also change. Besides the irregular angular primary particles, rectangular ones have also formed (Figure 5.7C). When the settling time is extended to 10 months, only loose aggregates composed of similar sized and

shaped primary particles are observed (Figure 5.7D). Morphologic changes based on TEM images suggest that even in a "stable" solution where no particle settling appears to occur, the interaction between nC$_{60}$ and water or other constituents in the solution never stops.

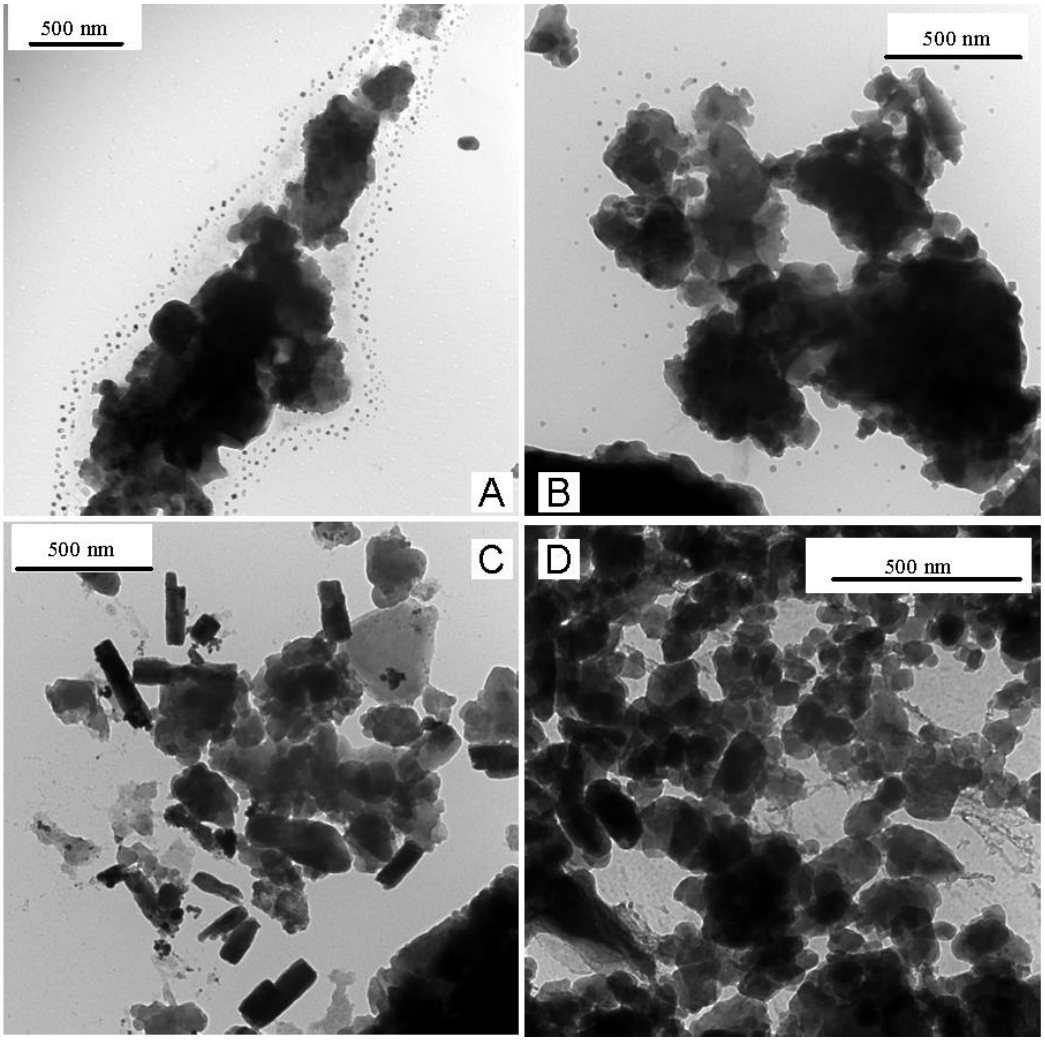

Figure 5.7 TEM images of nC$_{60}$ in 5 mM sodium acetate after stirring for two weeks (A) unsettled; (B) settled for 1 hour; (C) settled for 24 hours; and (D) settled for 10 months.

5.4 Conclusions

When produced in the presence of carboxylic acids, nC$_{60}$ have properties that differ significantly from those produced in its absence. In general, nC$_{60}$ formed in the presence of these acids have more negative surface charges and are more homogeneous than those produced in

water alone. Carboxylic acid identity and solution pH, which are intricately connected, play an important role, with the surface charge on nC$_{60}$ following the trend: citric acid (highest pH) < acetic acid < tartaric acid (lowest pH). These results suggest that the ultimate fate of C$_{60}$ in aqueous environments is likely to be significantly affected by the quantities and types of carboxyl moieties present in natural systems and by the solution pH. Additional studies to further evaluate the effects of these acids are required to determine how they affect the fate and transport of C$_{60}$ in aqueous environments.

Chapter 6 Association of Citrate with nC$_{60}$: Surface Charge, Morphology, and Spectral Characteristics

Xiaojun Chang and Peter J. Vikesland

6.1 Introduction

The increases in production and use of fullerite C_{60} will result in its discharge to the environment. Recent studies[27,59,60,69] have documented that despite its extreme hydrophobicity and virtual insolubility,[22] fullerite C_{60} can form colloidally stable nanoparticles (nC$_{60}$) in aqueous solutions. In general, two methodologies have been developed to disperse this hydrophobic material in water. The solvent exchange method, which involves the dissolution of C_{60} in a favorable solvent that is then exchanged with water, rapidly produces small, regularly shaped nC$_{60}$ particles.[57,59,60,64] The extended mixing method, an entirely different approach, requires no intermediate solvent, but simply involves mixing of C_{60} powder in aqueous media for extended periods.[28,80,101] During extended mixing, stochastic grinding processes result in the breakdown of fullerite C_{60} to produce polydisperse un-structured nC$_{60}$ (Figure 6.1A). In contrast, the production of highly regular (i.e., spherical, cuboidal)[60] aggregates by solvent exchange suggests a bottom-up process (Figure 6.1B) that involves C_{60} molecules as the nC$_{60}$ building blocks. These two processes are not necessarily exclusive and, as we show herein, may occur simultaneously under some solution conditions. nC$_{60}$ produced via solvent exchange and extended mixing differ with respect to surface charge, size, and structure.[58,59,62,80,87] These properties then dictate the aggregation and deposition behavior of nC$_{60}$[30,31,112] thus determining its mobility and toxicity.[87,151,152]

Upon release into natural waters, C_{60} interacts with water and other aqueous constituents. These interactions dictate nC_{60} formation and its transport, fate, and environmental impacts. Studies have shown that the presence of natural organic matter (NOM) enhances the apparent solubility of C_{60},[29] alters the morphology of nC_{60},[89] facilitates formation of highly regular (i.e., spherical, cuboidal) nC_{60} particles,[80,89,153] and produces more stable nC_{60} suspensions.[30,31] Chen and Elimelech[30,31] hypothesized that the stability enhancement was the result of electrosteric repulsion induced by adsorption of charged humic macromolecules to nC_{60} surfaces. However, this explanation fails to explain the observed formation of small regularly shaped aggregates. In our previous study (Chapter 5),[101] we observed that the presence of carboxylic acids altered the surface charge, particle size, and particle structure of nC_{60}. This latter result suggests that carboxyl groups affect nC_{60} formation.

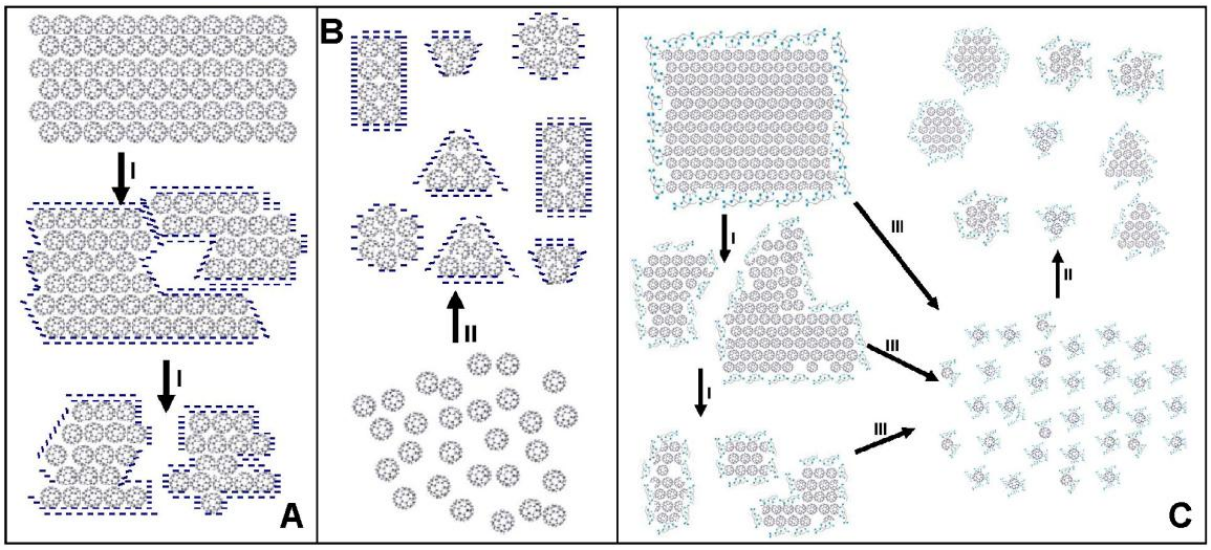

Figure 6.1 (A) nC_{60} formation via extended mixing (I, top-down process); (B) nC_{60} formation via solvent exchange (II, bottom-up process); and (C) nC_{60} formation in the presence of citrate via extended mixing (III, citrate facilitated dissolution).

Herein we employed citric acid and other small molecular weight carboxylic acids as chemically simple surrogates for the carboxyl groups prevalent within NOM and other abundant

macromolecules (e.g., proteins, carbohydrates). Based upon our past results[101] we hypothesized that the carboxylic acid moieties present in these macromolecules can directly interact with the C_{60} surface such that its properties are altered. Citric acid possesses three carboxyl groups (Figure C.1) and in its own right is a ubiquitous component of environmental systems and biological fluids.[154] To test our hypothesis, we conducted extended mixing experiments to produce $n$$C_{60}$ in the presence of variable concentrations of citrate and other carboxylates and tested the properties of the $n$$C_{60}$ particles formed in these solutions. We report the electrophoretic mobility, hydrodynamic diameter, and structure of $n$$C_{60}$ as a function of the carboxylate and sodium concentrations as well as the solution pH. Most interestingly, spherical and other regularly shaped $n$$C_{60}$ were commonly observed in carboxylate solutions. The $n$$C_{60}$ produced in carboxylate solutions exhibit differential UV-Vis spectral and interfacial properties from $n$$C_{60}$ produced in water alone.

6.2 Materials and Methods

All experiments were conducted using 99.9% pure sublimed C_{60} purchased from Materials and Electrochemical Research Corporation (MER, Tucson, AZ). ACS grade sodium citrate (Na_3Cit), sodium acetate, (NaAce), citric acid (H_3Cit), sodium chloride (NaCl), potassium phosphate (KH_2PO_4), and phosphoric acid (H_3PO_4) were purchased from Fisher Scientific (Fair Lawn, NJ). 98% sodium formate (NaFor), 99% sodium propionate (NaPro) and 99% sodium butyrate (NaBut) were purchased from Alfa Aesar (Ward Hill, MA). Sodium hexanoate (NaHex), sodium decanoate (NaDec), and sodium laurate (NaLau) were purchased from Spectrum Chemical (Gardena, CA). Reagent grade toluene was purchased from Sigma Aldrich. All water used in the present study had a resistivity greater than 18.2 MΩ-cm and was obtained from a NANOpure water system (Apple Scientific Inc., Chesterland, OH). Aqueous salt solutions and $n$$C_{60}$

suspensions were prepared and stored in glass containers that were copiously washed with aqua-regia and rinsed thoroughly before use.

***n*C$_{60}$ Suspension Preparation**. *n*C$_{60}$ suspensions were produced via the extended mixing method based on previously described protocols.[28,80,101] Herein we refer to *n*C$_{60}$ produced in water alone as aq/*n*C$_{60}$ and *n*C$_{60}$ produced in the presence of citrate as cit/*n*C$_{60}$. *n*C$_{60}$ produced in the presence of the other carboxylates is distinguished using similar three letter notations (e.g., for/*n*C$_{60}$, ace/*n*C$_{60}$, pro/*n*C$_{60}$, but/*n*C$_{60}$, hex/*n*C$_{60}$, dec/*n*C$_{60}$, and lau/*n*C$_{60}$). Concentrations indicated immediately prior to the term cit/*n*C$_{60}$ (e.g., X mM cit/*n*C$_{60}$) represent the citrate concentration employed to produce a particular suspension of cit/*n*C$_{60}$.

A Fritsch pulverisette 0 ball mill was utilized to reduce the initial irregularity and size of fullerite C$_{60}$. As purchased C$_{60}$ powder was pulverized at an amplitude of 0.5 mm for 20 minutes. The resulting fine powder was sieved through a 63 μm metal sieve and stored in the dark. ICP-MS measurements of the pulverized materials indicated that no metal contaminants were transferred during ball milling and sieving.

Sieved C$_{60}$ powder was mixed in aqueous solutions at a ratio of 400 mg C$_{60}$/L solution. Mixtures were magnetically stirred for at least two weeks in the dark at 30 °C. To investigate temporal effects on the properties of *n*C$_{60}$ during extended mixing, sample aliquots of 2.5 mL were transferred periodically from stirred mixtures to aqua-regia cleaned test tubes and settled for 24 hours prior to characterization for their supernatants. Preliminary experiments established that this settling period was sufficient to allow a majority of the large particles to settle out of solution and thus to produce stable *n*C$_{60}$ suspensions that could be subsequently characterized.

Characterization. To quantify the apparent surface charge, we measured the electrophoretic mobility (EM) of the suspensions. We refrain from reporting ζ-potentials because the heterogeneous nature of nC$_{60}$ suspensions makes the Smoluchowski approximation inappropriate.[155] The EM of a suspension was measured using a Malvern Nano ZS equipped with a helium/neon laser (λ = 633 nm) and disposable folded capillary cells. Using the same Nano ZS and a detection angle of 173º, dynamic light scattering (DLS) was employed to determine the particle size distribution of nC$_{60}$. The Stokes-Einstein equation was used to determine the hydrodynamic diameter (Z_{ave}) of the nC$_{60}$ particles based upon diffusivities determined by the method of cumulants. The temperature was automatically maintained at 25 °C by the instrument. Three measurements, each consisting of at least 23 subruns for surface charge and 12 subruns for size, respectively, were made on each sample. The averages of these measurements are presented along with errors representing the standard deviations of the measurements.

TEM samples were prepared by placing 5-10 μL of nC$_{60}$ suspension on a formvar/carbon coated 200-mesh copper grid and the grid was dried in a room temperature desiccator. Grids were imaged with a Zeiss 10 CA TEM operated at 60 kV. 400-mesh copper grids with ultrathin carbon film on a holey carbon support (Ted Pella, Inc.) were used for the HRTEM sample preparation. A FEI Titan scanning/transmission electron microscope was operated at 200 kV to obtain high-resolution transmission electron microscope (HRTEM) images of a limited subset of samples. A representative selection of particle images was obtained from multiple sites on each grid.

An HP 1090 HPLC with an acid column (Restek Pinnacle ODS Amine) coupled with a refractive index detector was used to measure citrate concentration ([citrate]) in aqueous phase. Phosphate buffer with pH = 3.0 was used as mobile phase at a flow rate of 1.0 mL/min.

Extraction. An aliquot (3mL) of nC_{60} was mixed with the same volume of toluene by vortexing in a test tube for 1 min. And the mixture was settled for 15 min to allow the two phases to separate. Then the toluene phase was transferred to an aqua-regia cleaned test tube. The extraction operation was repeated for two more times. The C_{60} concentration ($[C_{60}]_{tol}$) in each toluene extract was determined based upon its UV-Vis absorbance at 336 nm and a calibration curve established by a series of C_{60}-toluene solutions with known $[C_{60}]$. The recovery efficiency of each extraction is defined as the ratio of $[C_{60}]_{tol}$ in each toluene extract to the total nC_{60} concentration ($[nC_{60}]_{TOT}$) for each nC_{60} suspension. $[nC_{60}]_{TOT}$ in an aqueous solution was determined by exhaustive extraction with toluene in the presence of 200 mM NaCl (Details can be found in Appendix C).

6.3 Results and Discussion.

Our previous study (Chapter 5)[101] established that low molecular weight carboxylic acids such as citric acid can affect the surface charge, average particle size, and morphology of nC_{60}. Herein we show in greater depth that changes in pH and solution chemistry mediated by the sodium citrate concentration affect nC_{60} formation and then evaluate the impacts of these changes on the spectral and interfacial properties of nC_{60}. Regularly shaped nC_{60} particles were observed frequently in the presence of citrate and other carboxylates, clearly indicating that there is a bottom-up process involving C_{60} molecules or their clusters as building blocks that can occur during extended mixing.

Extended mixing experiments of 14-day duration were carried out in solutions with $[Na_3Cit]$ ranging from 0 to 25 mM. As discussed in the sections that follow, Na_3Cit significantly alters the surface charge, average size, and morphology of nC_{60} and these changes result in quantifiable

alterations to the UV-Vis spectral properties of nC$_{60}$ and its susceptibility to salt induced aggregation.

Surface Charge. In general, the electrophoretic mobility (EM) of each nC$_{60}$ suspension was stable over a fourteen day stirring period (Figure C.2). To simplify our discussion, we focus our analysis on EM values measured at the end of the stirring period. In the absence of Na_3Cit, the EM of aq/nC$_{60}$ was -3.03 (± 0.03) × 10^{-8} m^2/V-s. This value is consistent with that of aq/nC$_{60}$ obtained by extended mixing of unpulverized fullerite C$_{60}$.[62,82] As shown in Figure 6.2A, the cit/nC$_{60}$ surface charge was greatly affected by [Na_3Cit]. At low Na_3Cit loadings (< 10 mM), cit/nC$_{60}$ had a more negative surface charge than aq/nC$_{60}$ with a maximum of -5.03 (± 0.11) × 10^{-8} m^2/V-s for 0.7 mM cit/nC$_{60}$. Because Na_3Cit is the salt of a weak acid (Figure C.1), altering its concentration simultaneously changes solution pH (Figure 6.2A-inset) and sodium ion concentration ([Na^+]). Previous studies[58,82] have suggested that nC$_{60}$ is more negatively charged at higher pH. In solutions with low [Na_3Cit] (≤ 3 mM), our results are consistent with these studies (A detailed discussion of how pH changes regulated by [Na_3Cit] affect nC$_{60}$ formation can be found in Appendix C). However, when [Na_3Cit] exceeded 3 mM, EM became less negative as [Na_3Cit] increased. As discussed in Appendix C, this effect can be attributed to the elevated [Na^+] under these conditions.

Average Particle Size. In contrast to EM, which was independent of stirring time, the hydrodynamic diameters (Z_{ave}) of the nC$_{60}$ suspensions and their polydispersity indices (PDI) both decreased over time for [Na_3Cit] ≤ 3 mM (Figures C.3A and C.3C). The temporal decreases in both Z_{ave} and PDI and the blunt irregular particles detected in these solutions (discussed in detail in the next section) suggest that nC$_{60}$ was primarily produced by a top-down process (Figure 6.1A) wherein large crystals of C$_{60}$ break apart due to continual agitation. The resultant

nC_{60} particles then acquired a stabilizing surface charge through the contact with water and other aqueous constituents.[69,156] As shown in Figure C.3A, Z_{ave} decreased during the first week of the stirring period; but was fairly stable during the second week. This observation is similar to a previous study, in which Ma et al.[82] reported that the nC_{60} particle size became stable after 8-day magnetic stirring. The observed plateau in particle size is presumably dictated by the mixing intensity of the system. Reactors with higher shear rates might be expected to produce smaller particles.

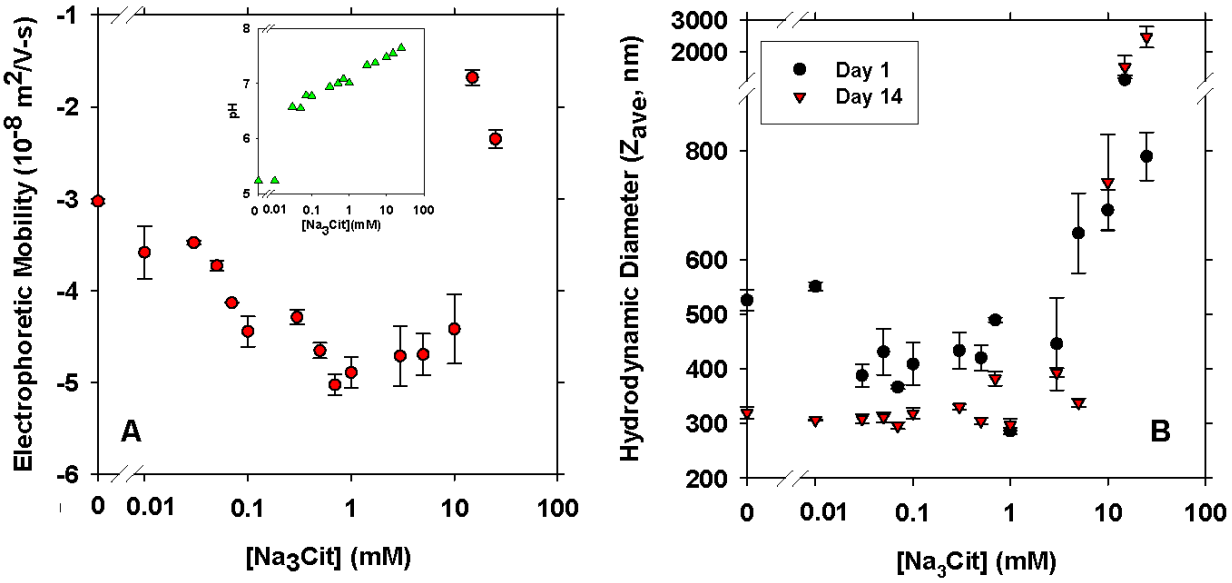

Figure 6.2 (A) Electrophoretic mobility of nC_{60} produced in the absence and presence of Na_3Cit; inset: the pH of the nC_{60} suspension as a function of [Na_3Cit]; (B) Average particle size as a function of [Na_3Cit] after 1 and 14 days stirring. (Note: For 15 mM Na_3Cit the day 2 Z_{ave} value is reported due to an error in the day 1 measurement. Each data point represents the average of three measurements for one sample and the error bar represents the standard deviation.)

To summarize the temporal trends in Z_{ave} we report values after 14-day stirring and compare them to values measured on day 1 in Figure 6.2B. As discussed previously, nC_{60} produced in solutions with low and moderate [Na_3Cit] levels ($\leq$ 3 mM) had smaller average particle sizes after 14-day of stirring than when these suspensions were only mixed for 1 day. However, at the

end of the stirring period, nC$_{60}$ produced in solutions with [Na$_3$Cit] = 0-5 mM had similar average sizes (≈ 300 nm) despite the fact that EM and solution pH varied considerably. This result illustrates that Z_{ave} is relatively insensitive to surface charge and pH over this [Na$_3$Cit] range.

Instead of decreasing over time, Z_{ave} for cit/nC$_{60}$ produced in solutions with [Na$_3$Cit] ≥ 10 mM fluctuated widely over the stirring period (Figure C.3B). Relatively large cit/nC$_{60}$ clusters (≥ 1000 nm) were frequently detected throughout the 14-day stirring period in these concentrated Na$_3$Cit solutions. After 24-h settling, a majority of these large particles settled leaving clear and transparent supernatants. The resultant low nC$_{60}$ concentrations in these supernatants resulted in wide variability in the three DLS measurements for each sample thus producing large error bars. Quantitative trends with respect to EM and Z_{ave} were therefore difficult to discern at high [Na$_3$Cit] levels. Nonetheless, despite their inherent instability, cit/nC$_{60}$ produced in solutions with high [Na$_3$Cit] were statistically less negatively charged and larger than those produced at more moderate [Na$_3$Cit] levels (Figure 6.2).

Morphologies and Structures. EM and Z_{ave} values represent the average properties of all nC$_{60}$ particles present in the supernatant. As such, they do not provide detailed information at the single particle scale. We characterized the structure and morphology of the nC$_{60}$ particles using TEM and HRTEM to better elucidate how citrate affects nC$_{60}$ formation. We note that artifacts associated with the drying of the TEM grids may have affected the collected images.[100] However, each grid was acquired and handled in exactly the same manner and thus comparisons between the collected images should reflect differences in solution phase particles. Cryo-TEM, which has the purported capacity to better characterize the *in situ* morphology of nC$_{60}$, was not possible for these samples. Nonetheless, past studies have generally shown that the nC$_{60}$

nanoparticles observed via cryo-TEM are typically morphologically similar to those obtained using normal TEM as employed herein.[60]

As described by both DLS and TEM, the nC$_{60}$ samples produced via extended mixing were highly polydisperse with the particle sizes falling in the range from <100 nm to several microns. In the absence of Na_3Cit, large aq/nC$_{60}$ clusters (several microns in diameter) were composed of a number of angular particles (diameter: 100-500 nm) tightly packed together (Figure 6.3A). At [Na_3Cit] = 0.01 mM, similar clusters were observed; however, these clusters were generally more loosely packed (Figure 6.3B). In 0.1, 0.5, and 1.0 mM Na_3Cit, ≈1 μm clusters composed of a few irregular particles were the primary type observed by TEM (Figures 6.3C-E). The existence of these angular particles is indicative of mixing heterogeneity and provides evidence for the top-down process shown in Figure 6.1A. Comparatively speaking, the tighter more compact structure of the aq/nC$_{60}$ clusters may be the result of their relatively slower aggregation during drying.[157] In the presence of Na_3Cit, the local [Na^+] concentration rapidly increased during drying and may have induced more pronounced aggregation of cit/nC$_{60}$, thus producing clusters with a looser structure.

Interestingly, small spherical particles (15-50 nm) were frequently observed in cit/nC$_{60}$ samples produced at [Na_3Cit] = 0.1-10 mM (Figures 6.3C-G). Although spherical particles have been observed in nC$_{60}$ samples produced via solvent exchange[59,60] or sonication,[89] this is to our knowledge the first time such highly regular nC$_{60}$ nanoparticles have been reproducibly produced in large quantities via extended mixing. Despite dissimilarities in their sizes, the appearance of spherical cit/nC$_{60}$ particles in solutions with sufficient [Na_3Cit] suggests the existence of a bottom-up process wherein C$_{60}$ molecules or small clusters of C$_{60}$ molecules self-assemble into regular shapes (Figure 6.1B). Although one could theorize that capillary forces elicited during

drying were responsible for production of these regularly shaped particles, we were unable to find any evidence in the literature to support this hypothesis. Our extensive literature search indicated that capillary force induced aggregation generally produces highly regular nanoparticle clusters.[158,159] We thus discount the possibility that capillary forces could produce the spherical clusters observed in Figure 6.3. In addition, observation of other types of regularly shaped particles (Figure C.8) further supports the existence of the bottom-up process. The self-assembly of nanoscale particles into regularly shaped objects is a commonly observed phenomenon and is indicative of interfacial forces driving formation of nanoparticle clusters that minimize the overall surface energy.[160,161]

Because of the stochastic nature of nC$_{60}$ production via the top-down process, a majority of the cit/nC$_{60}$ particles in each solution retained their irregular form and thus formation of the generally small highly regular particles was not apparent in the DLS results. Detailed imaging of large apparently unweathered nanoparticles, however, often illustrated the localized formation of highly regular nanoparticles (Figure C.9). As we have noted previously,[80] Z_{ave} represents an average of all of the peaks in the particle size distribution of a highly polydisperse sample and does not match any one peak. As discussed elsewhere,[155] the scattering intensity of a particle scales to the sixth power of its hydraulic radius and thus it is generally impossible to detect small particles in the presence of larger particles without resorting to highly specialized DLS instrumentation. Collectively these results illustrate the importance of multiple lines of inquiry to characterize nanoparticle suspensions.[162]

To investigate the nature of the highly regular particles, HRTEM was employed to probe their crystal structure. Fast Fourier transformations (FFT)[80] of a HRTEM image of cit/nC$_{60}$ (Figure 6.4A) indicate that these highly regular particles exhibit a hexagonally closest packed (*hcp*)

crystal structure that differs from the face centered cubic (*fcc*) habit of either fullerite C_{60}[163] or aq/*n*C_{60} (Figure 6.4B). The *fcc* habit is the thermodynamically stable form of C_{60}, while the *hcp* habit is typically observed at high temperatures and pressures.[163] The presence of citrate apparently stabilizes the higher energy phase, aiding in the formation of the highly regular particle structures shown in Figures 6.3 and 6.4A.

Spectral Properties of cit/*n*C_{60}. Previous studies by our group and others have shown that detailed interpretation of the UV-Vis spectrum of *n*C_{60} solutions can provide information about the average particle size, heterogeneity, and water affinity of *n*C_{60}.[74,79,121,164] The spectra of *n*C_{60} vary as a function of the *n*C_{60} concentration, average particle size, particle size distribution, and solution chemistry. As shown in Figure C.10, normalized UV-Vis spectra of aq/*n*C_{60} and 0.1, 1, and 5 mM cit/*n*C_{60} differ from one another with respect to the position of the absorption maxima (λ_{max}), relative absorbance, and absorption bandwidths. These changes are indicative of an alteration in the interfacial properties of *n*C_{60} as a function of [Na_3Cit].

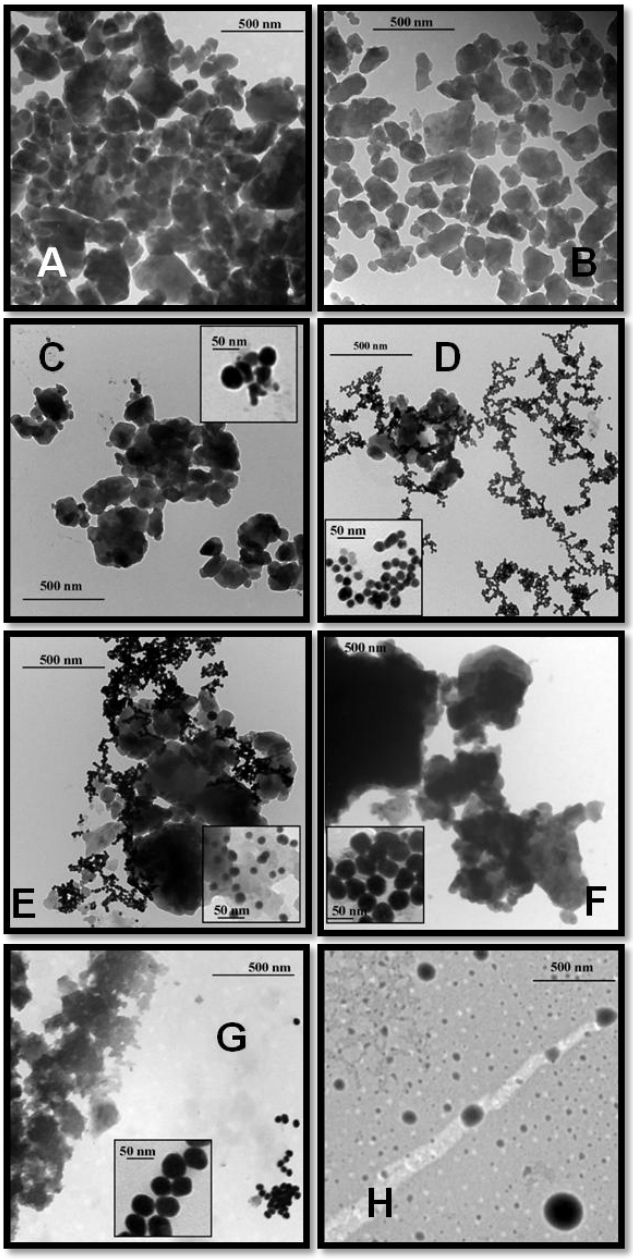

Figure 6.3 TEM images of nC_{60} formed in solutions with different sodium citrate concentrations: 0, 0.01, 0.1, 0.5, 1, 5, 10, and 25 mM (A to H).

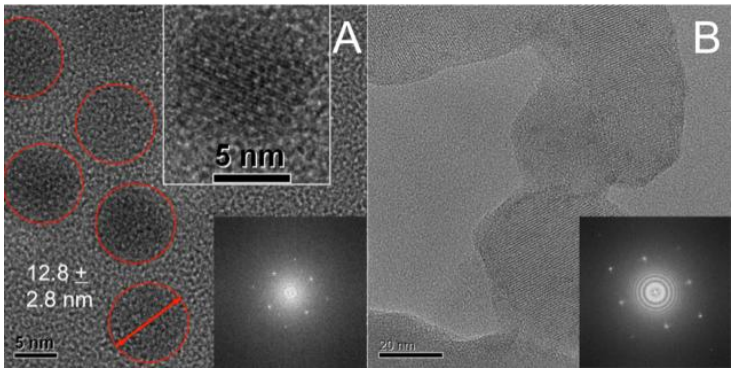

Figure 6.4 (A) HRTEM image of spherical cit/*n*C_{60} particles formed in 10 mM Na_3Cit solution. Upper inset shows visible lattice fringing and lower inset shows the FFT of a spherical cit/*n*C_{60} particle. (B) HRTEM image and FFT of aq/*n*C_{60}.

To further probe the spectral characteristics of the cit/*n*C_{60} and aq/*n*C_{60} suspensions they were subject to centrifugation mediated size fractionation (Figure C.11). UV-Vis spectra of the fractionated *n*C_{60} suspensions recorded over the spectral range of 200 to 800 nm (Figure C.12) revealed that as [*n*C_{60}] decreased and the average particle size decreased that the absorption maxima for the centrifuged *n*C_{60} suspensions shifted to shorter wavelengths. Decreases in particle size are responsible for these blue shifts.[74,79,121,164] Importantly, there were perceptible differences in the extent of the blue-shift as a function of [Na_3Cit]. To illustrate these differences the absorption maximum of the 3^1T_{1u}-1^1A_g absorption band ($\lambda_{max}(360)$) was plotted versus Z_{ave} for four *n*C_{60} suspensions (Figure 6.5) and linear regressions for each curve were obtained (Table 6.1). As shown, as [Na_3Cit] increases there is a statistically significant increase in the measured slope, indicating a larger blue shift for a given decrease in average particle size. The differences in slope suggest that *n*C_{60} produced in solutions with different [Na_3Cit] levels have various morphologies and structures, which is consistent with the TEM results.

The position of the absorption maximum for the 360-nm absorption band of a molecular C_{60} solution is indicative of interactions between C_{60} and the solvent or other solutes in solution.[79,93,105,121] If we extrapolate the linear relationships in Table 6.1 to Z_{ave} = 0.7 nm (e.g.,

the diameter of one C_{60} molecule), the calculated $\lambda_{max}(360)$ value should represent the position of the absorption maximum for a 'hypothetical' molecular C_{60} solution in a given aqueous solvent. According to previous studies (Chapter 3), the larger $\lambda_{max}(360)$ value of a molecular C_{60} solution indicates strong interactions between C_{60} and the solvent. The smaller calculated $\lambda_{max}(360)$ values for "molecular C_{60}-citrate solutions" obtained by the relationships listed in Table 6.1 can be interpreted as evidence that the interactions between C_{60} and citrate molecules are weaker than those between C_{60} and water. This conclusion is consistent with the results discussed in the following section.

Interfacial Properties of cit/*n*C_{60}. The results presented thus far have shown that the presence of citrate alters the surface charge, size, and morphology of *n*C_{60} and these changes result in alterations to its spectral properties and, as discussed in Appendix C, its proclivity to salt induced aggregation. Past studies have shown that citrate associates with metal[165-167] and metal oxide nanoparticles,[154] as well as carbon nanotubes.[168] These associations in turn alter the interfacial properties of these materials. Similarly citrate is potentially able to alter the interfacial properties of cit/*n*C_{60} by associating with C_{60}.

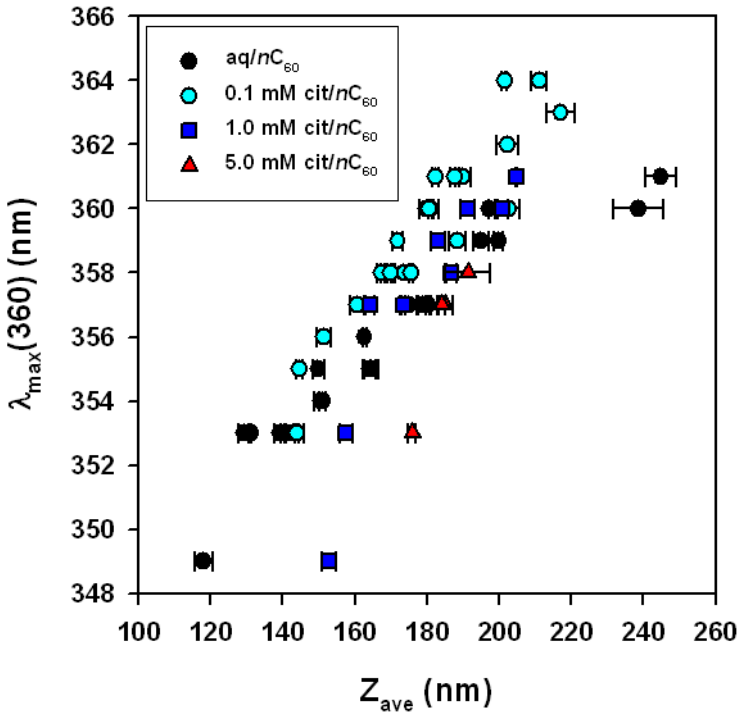

Figure 6.5 Position of absorption maximum of 360 nm absorption band as a function of average particle size. (The error bar represents the standard deviation of three measurements.).

Table 6.1 Linear relationship between the position of absorption maximum of 360 nm band ($\lambda_{max}(360)$) and the average particle size (Z_{ave}) of a nC_{60} suspension.

Suspension	Linear Relationship between $\lambda_{max}(360)$ and Z_{ave}	R^2
aq/nC_{60}	$\lambda_{max}(360) = (0.0851 \pm 0.0143)\ Z_{ave} + (341.4 \pm 2.4)$[a]	0.8970
0.1 mM cit/nC_{60}	$\lambda_{max}(360) = (0.1292 \pm 0.0226)\ Z_{ave} + (336.1 \pm 4.1)$	0.8702
1.0 mM cit/nC_{60}	$\lambda_{max}(360) = (0.1885 \pm 0.0808) Z_{ave} + (323.3 \pm 14.6)$	0.8106
5.0 mM cit/nC_{60}	$\lambda_{max}(360) = (0.3312 \pm 0.3325)\ Z_{ave} + (295.3 \pm 61.2)$	0.9018

[a]The error of the fit parameters represents 95% confidence interval.

The hydrophobicity/hydrophilicity of nC_{60} can be evaluated by determining its extraction efficiency from water to an organic phase.[59,113] Past studies have shown that toluene is an appropriate solvent as an extractant and it has thus been commonly used to quantify nC_{60}.[115-117] In the present study, we compare the extraction efficiency of aq/nC_{60} and 1.0 mM cit/nC_{60} to toluene in the absence of added salt. After three extraction cycles, only 4.3% ($[C_{60}]_{tol}$ = 1.2 mg/L) of aq/nC_{60} ($[C_{60}]_{TOT}$ = 27.6 mg/L) partitioned to the toluene phase. In contrast, 22%

($[C_{60}]_{tol}$ = 3.9 mg/L) of 1 mM cit/$n$$C_{60}$ ($[C_{60}]_{TOT}$ = 12.9 mg/L) partitioned to toluene after the same three cycles, thus indicating that cit/$n$$C_{60}$ has a greater affinity to toluene than aq/$n$$C_{60}$. Previous studies[27,103,116] have reported that toluene does not efficiently extract $n$$C_{60}$ in the absence of salt due to the presence of an adsorbed water layer that hinders C_{60} solvation in the moderately apolar solvent. According to our extraction experiments conducted in the absence of NaCl, surface charge is not the only factor dictating the extraction efficiency of $n$$C_{60}$. As shown in Figure 6.2A, 1.0 mM cit/$n$$C_{60}$ has a more negatively charged surface than aq/$n$$C_{60}$, while considerably more cit/$n$$C_{60}$ was extracted to the toluene phase. This result suggests that the association of trace quantities of citrate to the surface of $n$$C_{60}$ enhances its relative extraction efficiency (A detailed calculation of the quantity of surface associated citrate is provided in Appendix C). One could argue that the enhanced solubility of 1.0 mM cit/$n$$C_{60}$ is due to the higher ionic strength of the solution and the higher propensity for the particles to 'salt-out'. To test this possibility, additional extraction experiments were conducted in the presence of a substantial excess of NaCl (200 mM) and the increased recovery efficiency of cit/$n$$C_{60}$ relative to aq/$n$$C_{60}$ was still observed (See the Appendix C for details of these experiments). We thus attribute the enhanced extraction efficiency of cit/$n$$C_{60}$ to the presence of an adsorbed citrate layer that enhances the affinity of $n$$C_{60}$ to moderately apolar toluene.

Role of Citrate/Carboxylate. Cit/$n$$C_{60}$ produced in the presence of citrate exhibits characteristics (e.g., surface charge, average particle size, particle morphology, UV-Vis spectra, aggregation behavior, and interfacial properties) that differ from aq/$n$$C_{60}$. Citrate not only regulates solution pH and solution chemistry, thus dictating the surface charge of $n$$C_{60}$, but also facilitates the formation of regularly shaped cit/$n$$C_{60}$ particles. Although only a small amount of citrate associates with $n$$C_{60}$ based on our calculations (See Appendix C), it nonetheless is

sufficient to greatly alter the properties of nC$_{60}$. We propose Figure 6.1C to explain cit/nC$_{60}$ nanoparticle formation. In this mechanism, citrate associates with fullerite C$_{60}$ and enhances its dissolution, the resulting molecular clusters or molecules of C$_{60}$ then undergo crystallization to produce cit/nC$_{60}$. The mechanism by which citrate associates with C$_{60}$ is presently unknown; however, we theorize that it involves a weak association between the carboxyl groups of citrate and the π electron cloud of the fullerene. This type of non-bonding interaction has recently been shown to enhance formation of supramolecular anthraquinone structures.[169] Jiang et al.[170] recently determined that citric acid treated carbon nanotubes (CNT) exhibit more negative zeta potentials than pristine CNT. They hypothesized that citrate associated with the CNT surface, but did not suggest a mechanism. It is well established that C$_{60}$ serves as an electron acceptor in electron donor-acceptor complexes with a variety of organic molecules (e.g., benzene,[171] ferrocene,[172] phenol,[173] cubane[174]) and it appears that citrate can interact in a similar manner. As a result of continuous agitation and carboxyl facilitated dissolution, the top-down and bottom-up processes occur simultaneously during extended mixing. Therefore, the resultant cit/nC$_{60}$ suspensions were highly heterogeneous, containing both irregularly shaped particles (sizes ranged from less than 100 nm to several microns) and small regularly shaped nanoparticles (e.g., spheres, rectangles, triangles, etc.).

To test the generalizability of our findings, nC$_{60}$ suspensions were also produced in the presence of other carboxylate solutions. As expected, the nC$_{60}$ surface charge and average particle size varied with carboxylate identity and concentration (Figure C.21). Importantly, regularly shaped nC$_{60}$ nanoparticles were repeatedly observed in these suspensions (Figure 6.6). To our knowledge, Figure 6.6 provides the first evidence for the formation of large numbers of nC$_{60}$ nanorods with similar size under any conditions. As discussed previously, these highly

regular structures cannot be conceivably formed by capillary forces elicited during the drying process and thus are representative of nanostructures formed *in situ*. The existence of nanorods, squares, and other regularly shaped nC$_{60}$ nanoparticles supports the bottom-up process in the presence of carboxyl group described in Figure 6.1C.

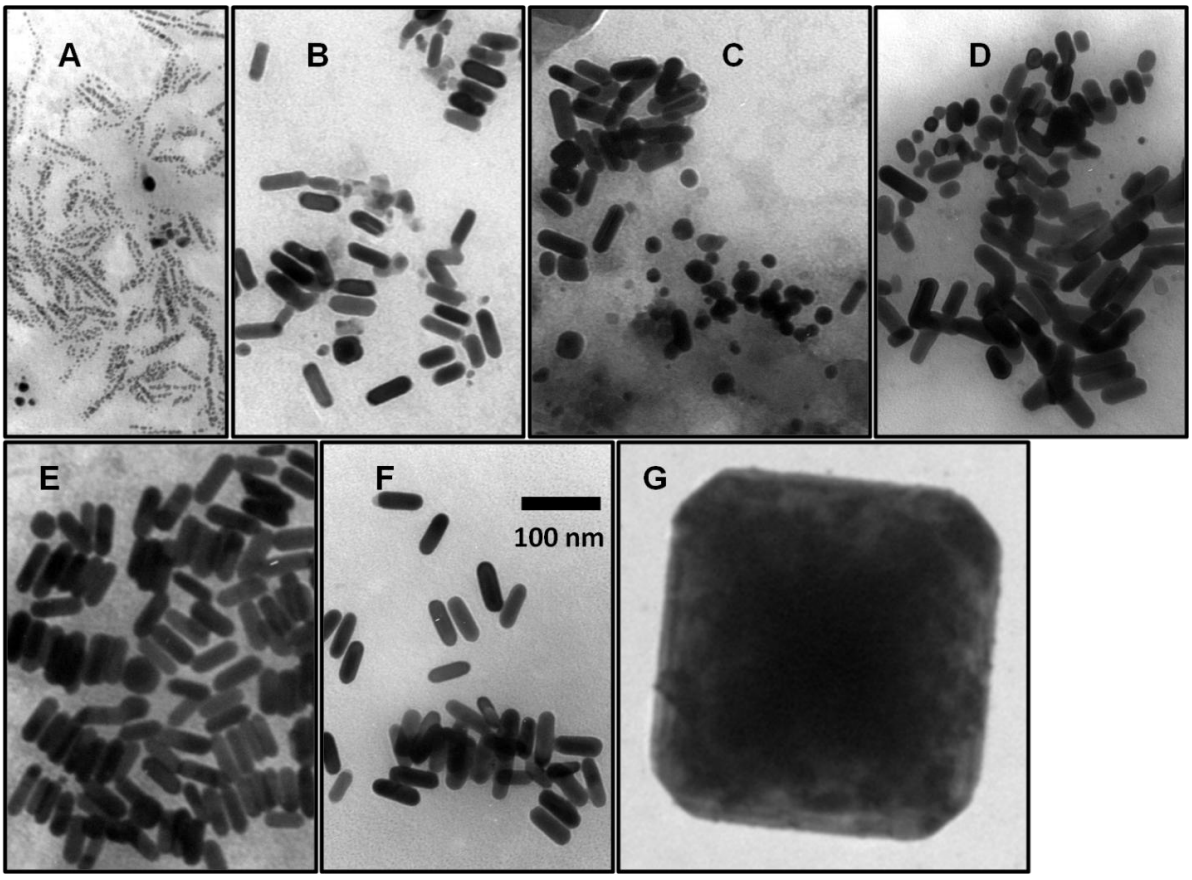

Figure 6.6 TEM images of nC$_{60}$ produced in various carboxylate solutions. (A): Small clusters (< 10 nm) of C$_{60}$ in 3.0 mM sodium acetate; (B): nanorods in 1.5 mM sodium propionate; (C): nanorods, squares, and spheres in 1.5 mM sodium butyrate; (D): nanorods, elongated spheres, and spheres in 3.0 mM sodium butyrate; (E): nanorods in 10 mM sodium decanoate; (F): nanorods in 0.5 mM sodium propionate; and (G): large square in 10 mM sodium formate.

6.4 Environmental Implications

We have shown that nC$_{60}$ produced in the presence of citrate and other carboxylates exhibits properties that differ from aq/nC$_{60}$. The different surface charges, sizes, morphologies, and interfacial characteristics of cit/nC$_{60}$ and the other carboxylate nC$_{60}$ will alter their various

transport paths and interactions with organisms in the environment. Accordingly, studies investigating the fate and environmental impacts of nC$_{60}$ must carefully take the constituents of natural waters fully into consideration. Otherwise, results based solely on aq/nC$_{60}$ are not fully representative of scenarios where C$_{60}$ is released into the environment.

nC$_{60}$ nanoparticles produced in the presence of citrate or other carboxylates via extended mixing are subjected to weathering by continuous agitation as well as dissolution-recrystallization induced by the association between carboxyl groups and C$_{60}$. The dissolution-recrystallization mechanism depicted in Figure 6.1C has implications for the cellular uptake of C$_{60}$ and the environmental fate of C$_{60}$. Porter et al.[175,176] detected C$_{60}$ crystals within sub-cellular compartments (e.g., secondary lysosomes, nuclei) of human monocyte macrophages and hypothesized that these C$_{60}$ crystals were produced in the cell following uptake of individual C$_{60}$ molecules through ion channels or membrane pores. Their large crystals of C$_{60}$ were often surrounded by smaller C$_{60}$ particles, suggesting that the acidic environment of the secondary lysozymes can break-down C$_{60}$ crystals. Such a mechanism is consistent with citrate (or other carboxylate) mediated dissolution and re-crystallization. Similar dissolution-recrystallization reactions are feasible in any environment where carboxyl containing moieties come in contact with C$_{60}$. Because molecular C$_{60}$ and small clusters of C$_{60}$ are more efficient at producing reactive oxygen species (ROS) than large nC$_{60}$ particles[177,178] the production of molecular C$_{60}$ or their small clusters via Figure 6.1C could result in greater levels of toxicity than expected based on measurements for nC$_{60}$ alone. Accordingly, studies examining the potential cellular toxicity of C$_{60}$ or its environmental implications should consider the role of molecular C$_{60}$ and small clusters of C$_{60}$ molecules. Finally, the observation that carboxyl functional groups help to stabilize

molecular C_{60} may lead to the development of alternative strategies to produce novel C_{60} based crystals.

Chapter 7 Changes in the Properties of nC$_{60}$ Following Dilution

Xiaojun Chang and Peter Vikesland

7.1 Introduction

Since its discovery in 1985,[1] fullerene C_{60} has attracted extensive attention in both research and industrial fields due to its unique properties. Because of the increases in production and the number of applications of C_{60}, its release to the environment is inevitable. Although C_{60} is virtually insoluble in water,[22] it forms colloidal suspensions consisting of fullerite C_{60} nanoparticles (nC$_{60}$) when it is subject to the contact with water during solvent exchange[25-27,59] or extended mixing.[28,59,80,101] nC$_{60}$ are the main form of C_{60} existing in the environment and they have elicited concerns with respect to their environmental, health, and safety (EHS) impacts. Therefore there have been a number of studies on the aggregation and deposition behaviors,[31,112] transport,[179,180] interactions with other constituents in water,[181,182] and toxicity of nC$_{60}$.[183,184]

The nC$_{60}$ suspensions are oftentimes colloidally stable for long periods of time.[30,83] For these samples, there is no noticeable precipitation or measurable increase in average particle size during the storage period. However, the changes in structure and morphology for nC$_{60}$ suspensions after different storage times, as described in our previous study (Chapter 5),[101] indicate that the interactions between C_{60} and water or other constituents in solutions continually occur even under apparently quiescent conditions. In a majority of the recent studies on nC$_{60}$, stock nC$_{60}$ suspensions were usually produced in big batches and then employed in different experiments that oftentimes involve alterations in solution chemistry and nC$_{60}$ concentration (e.g., pH adjustment,[58,59] dilution for aggregation kinetics experiments,[30,112,185] nC$_{60}$ concentration adjustment for adsorption experiments,[28,88,91] etc…). A number of these studies used the

properties of stock nC_{60} suspension to represent those of the modified nC_{60} suspensions, assuming that these properties, including surface charge, particle size, and particle morphology, do not change during dilution or the addition of other solutes. Unfortunately, to date there has been no study affirming this assumption. In the present study, to test the validity of this hypothesis we evaluated the effects of dilution on the measured properties of nC_{60}.

7.2 Materials and Methods

Materials and Chemicals. Sublimed 99.9% fullerene C_{60} (Materials and Electrochemical Research Corporation, MER, Tucson, AZ) was used to produce nC_{60} suspensions. ACS grade sodium citrate (Na_3Cit) and sodium chloride (NaCl) were purchased from Fisher Scientific (Fair Lawn, NJ). All water used in the present study was obtained from a Barnstead NANOpure water purification system and had resistivity greater than 18.2 mΩ-cm. nC_{60} suspensions and salt solutions were produced and stored in glass containers washed copiously with aqua-regia and thoroughly rinsed prior to use.

***n*C$_{60}$ Suspension Preparation.** Stable fullerene nC_{60} suspensions were produced via extended mixing. To distinguish nC_{60} produced in water alone from that produced in Na_3Cit solutions, they are referred to herein as aq/nC_{60} and cit/nC_{60}, respectively. The concentration listed immediately prior to cit/nC_{60} reflects the concentration of Na_3Cit ([Na_3Cit]) in a solution wherein cit/nC_{60} was produced (e.g., 1 mM cit/nC_{60} represents nC_{60} produced in 1 mM Na_3Cit).

The method to prepare stock nC_{60} suspensions in the present study was based upon that from our previous studies.[80,101,186] Pulverized and sieved fullerene powder was mixed with water alone or Na_3Cit at a concentration of 400 mg C_{60}/L. The mixtures were magnetically stirred for 1 month and settled for at least 1 month prior to the supernatants being characterized and used in

subsequent experiments. These stock nC$_{60}$ suspensions were produced and stored in the dark at 30 ºC.

Characterization.

Surface Charge and Size. A Malvern Nano ZS equipped with a helium/neon laser (λ = 633 nm) and a disposal folded capillary cell were employed to characterize the surface charge. We report electrophoretic mobility (EM) instead of ζ-potential because the heterogeneous nature of nC$_{60}$ makes the Smoluchowski approximation inappropriate.[155] The same Nano ZS with a detection angle of 173º (dynamic light scattering, DLS) was used to determine the size distribution for an nC$_{60}$ sample using the cumulant algorithm. We report average particle size (hydrodynamic diameter, Z_{ave}) based upon the measured particle diffusivities and the Stokes-Einstein equation. Temperature was automatically maintained by the instrument at 25 ºC. The average of three measurements for each sample is presented along with the error representing the standard deviation of the measurements. Each measurement consists of at least 23 subruns for EM and 12 subruns for size characterization.

Transmission Electron Microscope (TEM). An aliquot of an nC$_{60}$ suspension (5-10 µL) was placed on a formvar/carbon coated 200-mesh copper grid and dried in a desiccator at room temperature overnight. Grids were then imaged using a Zeiss 10 CA TEM at 60 kV. All TEM grids were acquired and handled exactly the same way and a representative selection of particle images was obtained from multiple sites on each grid.

UV-Visible Spectrophotometry The absorbance of the nC$_{60}$ suspensions was recorded using a Cary 5000 UV-VIS-NIR spectrophotometer at room temperature. Sample aliquots (2.5 mL) were added to a quartz cuvette with a light pathlength of 1 cm and scanned over the spectral range of

200-800 nm at a bandwidth of 1 nm using double beam mode. All of the nC$_{60}$ spectra were background corrected by the spectrum of nanopaure water.

Dilution. Three types of dilution experiments were conducted in the present study: direct dilution, re-suspension, and centrifugation.

Direct dilution. In the direct dilution experiments, stock nC$_{60}$ suspensions were simply mixed with water or Na$_3$Cit. Aq/nC$_{60}$ stock suspensions were diluted with nanopure water, while the cit/nC$_{60}$ suspensions were diluted either in nanopure water or in the same Na$_3$Cit solutions in which they were produced. The dilution factor (DF = final volume/volume of aliquot) varied from 1 to 20.

Re-suspension. A re-suspension experiment was conducted to evaluate how changes in solution chemistry affect the properties of nC$_{60}$. Aliquots (2.0 mL) of stock 1.0 mM cit/nC$_{60}$ suspension were centrifuged at 20,000 rpm for one hour. Supernatants were carefully decanted and their UV-Vis spectra showed no characteristic absorption bands for nC$_{60}$, thus indicating that virtually all of the cit/nC$_{60}$ nanoparticles had precipitated on the bottom of the centrifuge tubes. Na$_3$Cit solutions (2.0 mL) with different [Na$_3$Cit] levels (0.2 to 1.0 mM) were then added to the centrifuge tubes to re-suspend the settled cit/nC$_{60}$ nanoparticles immediately after centrifugation. These suspensions were then characterized by DLS and TEM.

Centrifugation. Aliquots (5 mL) of the stock nC$_{60}$ suspensions were centrifuged at 7000 rpm for different time periods and their supernatants (≈ 3.5 mL) were transferred to aqua-regia cleaned test tubes for characterization.

7.3 Results and Discussion

Direct Dilution. The electrophoretic mobility (EM) and average particle size (Z_{ave}) of un-diluted aq/nC$_{60}$ stock suspension (DF = 1) were -3.07 (± 0.03) × 10^{-8} m^2/V-s and 245.4 (± 3.7) nm, respectively. Dilution of aq/nC$_{60}$ in water did not alter either its surface charge or its average particle size. Over the tested range of dilutions (DF = 1 to 20) the measured EM remained stable at approximately -3.50 (± 0.22) × 10^{-8} m^2/V-s and their Z_{ave} values were constant at 243.4 (± 3.7) nm (Figure 7.1). Importantly, the cit/nC$_{60}$ suspensions diluted in water did not exhibit measurable changes in either EM or Z_{ave} even though the pH, ionic strength, and [Na_3Cit] levels changed dramatically due to dilution (Table 7.1).

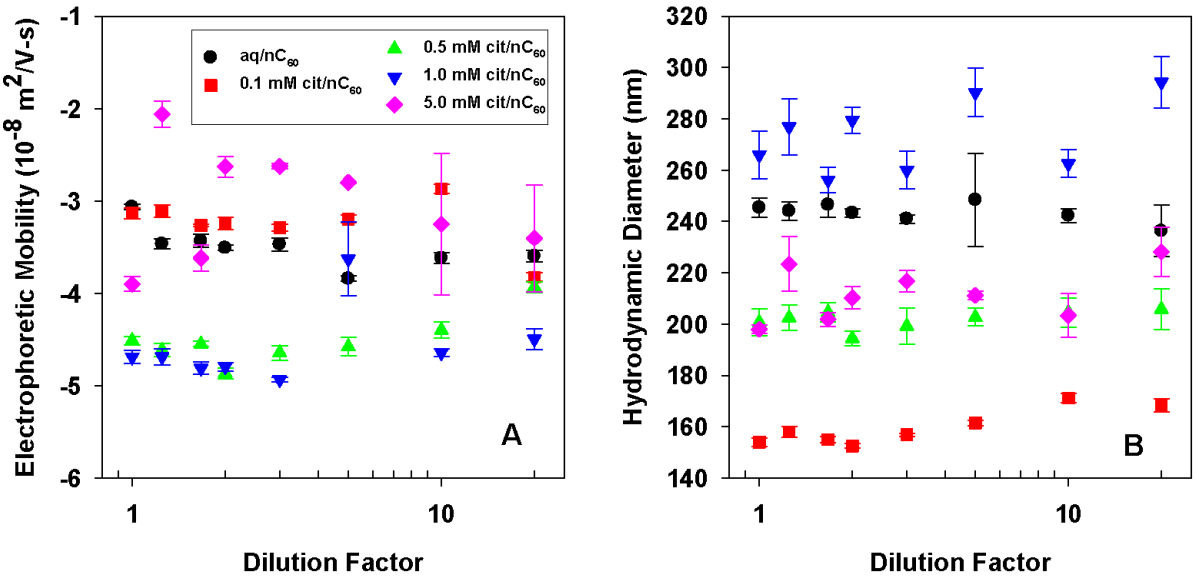

Figure 7.1 (A) Surface charge and (B) average particle size of nC$_{60}$ after dilution by water as a function of the dilution factor. (Data point represents the average of three measurements for each sample and the error bar represents the standard deviation.)

Previous studies[58,82] have shown that the surface charge of nC$_{60}$ nanoparticles becomes more negative with an increase in pH. And our previous study[186] of nC$_{60}$ formation in the presence of citrate suggested that as long as the sodium ion concentration ([Na^+]) remained < 30 mM, the

solution pH dictates nC_{60} surface charge. After direct dilution by water, [Na_3Cit] and pH of cit/nC_{60} suspensions decreased with the dilution factor. For instance, 5.0 mM cit/nC_{60} had a total citrate concentration ([Na_3Cit]) of 0.25 mM when the DF was 20 and its pH dropped from 7.4 to 6.9. However, the EM and Z_{ave} of diluted 5 mM cit/nC_{60} at this dilution factor were very close to those of the 5.0 mM cit/nC_{60} stock suspension. The fact that the EM and Z_{ave} did not change following dilution suggests that the factors responsible for surface charge development and the size of the nanoparticles are not affected within the timescale (< 48 hrs) of the dilution experiments.

Table 7.1 [Na_3Cit], pH, and ionic strength of diluted cit/nC_{60} as a function of the diluted factor.

Dilution Factor	Parent nC_{60} suspension											
	0.1 mM cit/nC_{60}			0.5 mM cit/nC_{60}			1.0 mM cit/nC_{60}			5.0 mM cit/nC_{60}		
	[Na_3Cit] (mM)	pH	Ionic strength (mM)	[Na_3Cit]	pH	Ionic strength (mM)	[Na_3Cit]	pH	Ionic strength (mM)	[Na_3Cit]	pH	Ionic strength (mM)
1	0.100	6.75	0.52	0.500	7.01	2.75	1.000	7.12	5.59	5.000	7.37	28.76
1.25	0.080	6.71	0.41	0.400	6.97	2.18	0.800	7.08	4.45	4.000	7.34	22.93
1.67	0.060	6.67	0.31	0.300	6.92	1.62	0.600	7.03	3.31	3.000	7.29	17.12
2	0.050	6.64	0.25	0.250	6.90	1.34	0.500	7.01	2.75	2.500	7.26	14.22
3	0.033	6.58	0.17	0.167	6.83	0.88	0.333	6.94	1.81	1.667	7.20	9.41
5	0.020	6.49	0.10	0.100	6.75	0.52	0.200	6.86	1.07	1.000	7.12	5.59
10	0.010	6.38	0.05	0.050	6.64	0.25	0.100	6.75	0.52	0.500	7.01	2.75
20	0.005	6.27	0.02	0.025	6.53	0.12	0.050	6.64	0.25	0.250	6.90	1.34

Direct dilution by Na_3Cit solution. In direct contrast to the results obtained when the nC_{60} suspensions were diluted in water, the dilution of cit/nC_{60} in Na_3Cit solutions resulted in quantifiable changes in EM and Z_{ave} (Figure 7.2). This result was not anticipated since the solution chemistry (e.g., [Na_3Cit], ionic strength, and pH) was unaltered by the dilution process. Instead the only variable that changed in these dilutions was the Na_3Cit to C_{60} molar ratio. For cit/nC_{60} produced in solutions with low [Na_3Cit] levels (0.1 and 0.5 mM), the measured EM of the cit/nC_{60} nanoparticles were statistically stable while 1.0 and 5.0 mM cit/nC_{60} became much less negatively charged with an increase in DF (Figure 7.2A). Concomitant with the decrease in

surface charge was an increase in Z_{ave}. For cit/nC$_{60}$ produced in low [Na_3Cit] levels, the extent of the increase in Z_{ave} was moderate (≈ 20 nm); while 5.0 mM cit/nC$_{60}$ stock suspension diluted in 5.0 mM Na_3Cit had average particle size 300 nm larger than the Z_{ave} of undiluted 5.0 mM cit/nC$_{60}$ stock suspension (Figure 7.2B inset). These changes in EM and Z_{ave} are consistent with the increase in the ratio of Na^+ to C$_{60}$ ([Na^+]/[C$_{60}$]) for the diluents with high [Na^+] (e.g., 3.0 mM Na^+ in 1.0 mM Na_3Cit solution and 15.0 mM Na^+ in 5.0 mM Na_3Cit solution).

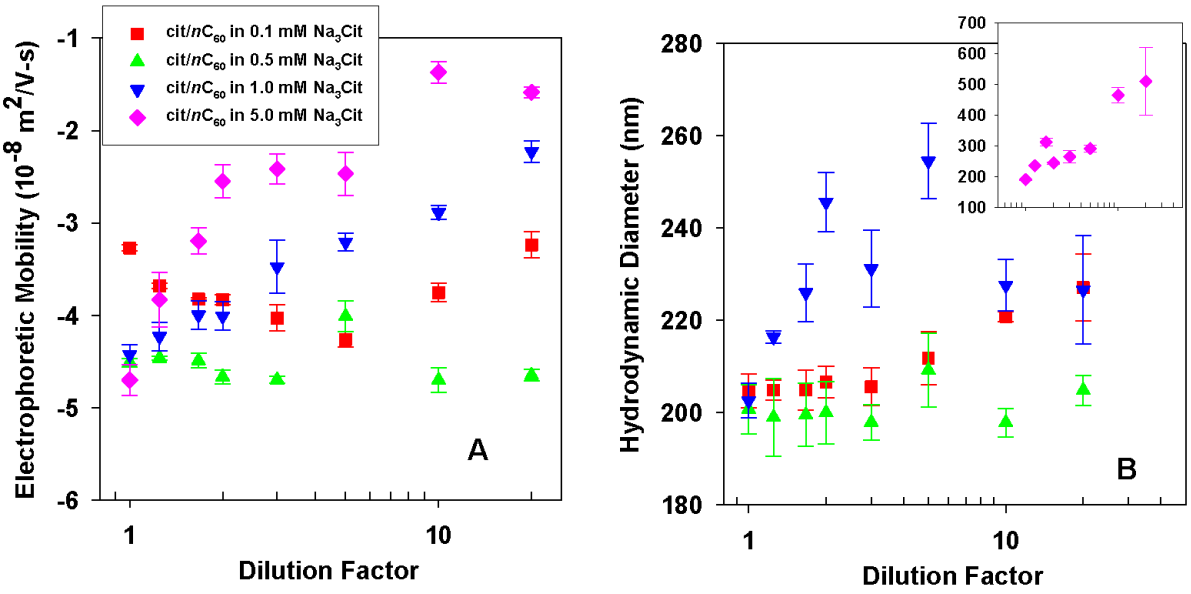

Figure 7.2 (A) Surface charge and (B) average particle size of nC$_{60}$ after dilution by the same solution wherein nC$_{60}$ was produced as a function of the dilution factor. (Data point represents the average of three measurements for each sample and the error bar represents the standard deviation.)

Centrifugation. According to the results in the previous sections, the decreases in [C$_{60}$]/[Na^+] or [Na^+]/[other constituents] in the diluted suspension seems to be the most important factor determining their colloidal properties. To test this conclusion, we conducted a series of centrifugation experiments in which nC$_{60}$ suspensions were fractionated based upon size (Figure 7.3A). In terms of [C$_{60}$], centrifugation of the nC$_{60}$ suspensions results in a decrease in concentration and thus samples centrifuged for longer periods of time can be regarded as more

dilute than samples centrifuged for shorter periods. This conclusion is supported by the observed decrease in the solution absorbance at 355 nm (i.e., the 3^1T_{1u}-1^1A_g absorption band[121]; Figure 7.3A inset). An increase in the centrifugation time, and the concomitant decreases in particle size and [nC$_{60}$], did not alter the EM for aq/nC$_{60}$ or 0.1 mM cit/nC$_{60}$. However, for cit/nC$_{60}$ produced in solutions with [Na_3Cit] ≥ 1.0 mM there was a significant decrease in EM with an increase in centrifugation time (Figure 7.3B). This latter result is similar to the results of the direct dilution experiments involving dilution in the Na_3Cit solution of the same concentration in which cit/nC$_{60}$ was produced.

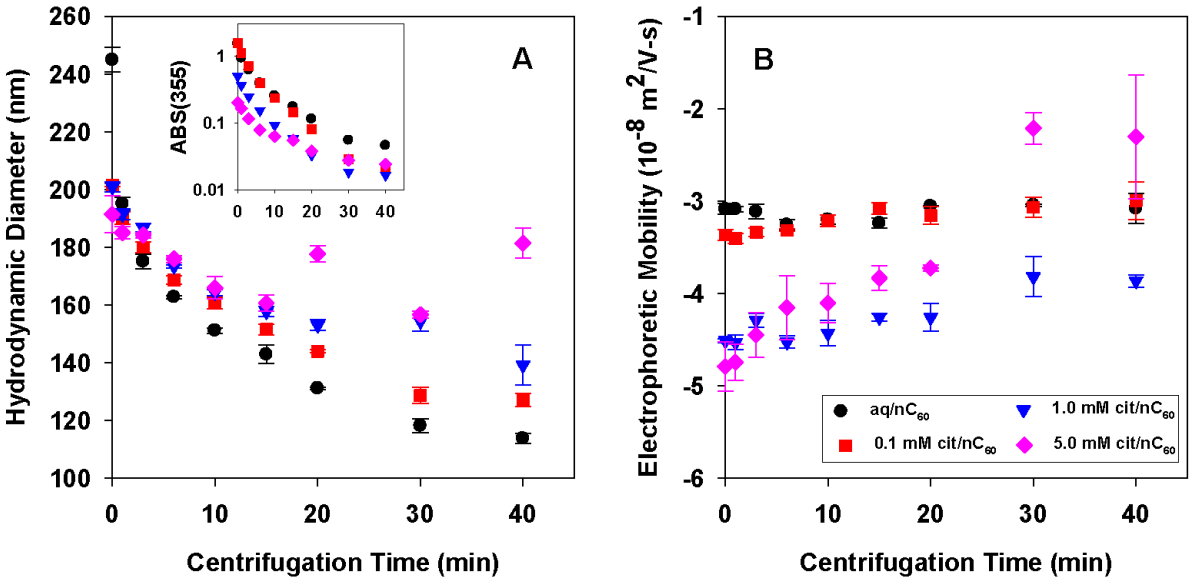

Figure 7.3 (A) Average particle size of nC$_{60}$ as a function of centrifugation time. Inset in (A) is the absorbance at 355 nm for centrifuged nC$_{60}$ determined by UV-Vis spectrophotometer. (B) Surface charge as a function of centrifugation time. (Data point represents the average of three measurements for each sample and the error bar represents the standard deviation)

Re-suspension. In both the direct dilution and centrifugation experiments the [C$_{60}$] in the final suspensions were reduced, thus altering the ratio of [C$_{60}$] to the concentrations of the other solution constituents. To keep [C$_{60}$] constant, while solely altering the solution chemistry, a re-suspension experiment was conducted. In this experiment, 1.0 mM cit/nC$_{60}$ was isolated from

suspension via centrifugation and then the pellet was re-suspended in solutions with different [Na_3Cit] levels. Following re-suspension for 24 hours the EM of re-suspended 1 mM cit/nC_{60} was statistically stable despite the fact that [Na_3Cit] varied from 0.2 to 0.8 mM (Figure 7.4A). The DLS determined average sizes (Z_{ave} ≈ 197 nm) were also independent of [Na_3Cit] and their intensity weighted size distribution curves were quite similar too (Figure 7.4B).

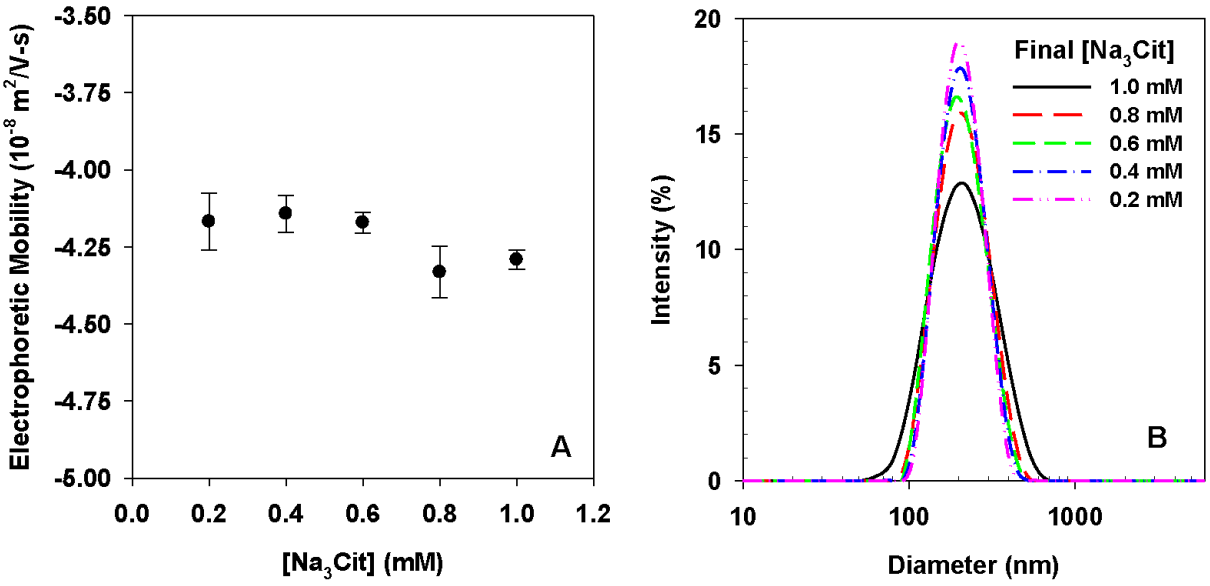

Figure 7.4 (A) Surface charge (Data point represents the average of three measurements for each sample and the error bar represents the standard deviation) and (B) size distribution curve of re-suspended cit/nC_{60}.

Table 7.2 Changes in solution chemistries, colloidal properties, [C_{60}], and concentration ratios during different types of dilution experiments

	EM	Z_{ave}	pH	[Na_3Cit]	[C_{60}]	[C_{60}]:[H_2O]	[C_{60}]:[citrate]	[C_{60}]:[Na^+]
Direct dilution by water	No change	No change	↓ [c]	↓	↓	↓	No change	No change
Direct dilution by same solution wherein it was produced	less negative[a]	↑	No change	No change	↓	↓	↓	↓
Centrifugation	less negative[a]	↓ [b]	No change	No change	↓	↓	↓	↓
Re-suspension	No change	No change	↓	↓	No change	No change	↑	↑

[a] EM became less negative in the cases of cit/nC_{60} produced in solutions with high [Na_3Cit] levels (≥ 1.0 mM); [b] Z_{ave} decreased because of centrifugal forces. [c] For cit/nC_{60} samples, pH decreased after dilution by water. For aq/nC_{60} samples, pH stayed unchanged after dilution by water.

Table 7.2 summarizes the changes in nC$_{60}$ properties, solution chemistries, and concentration ratios over the four different types of dilution experiments. Despite the fact that pH, ionic strength, and [Na_3Cit] changed during direct dilution by water, two commonly reported properties of the diluted nC$_{60}$ samples, EM and Z_{ave}, were similar to the parent cit/nC$_{60}$ stock suspensions. We attribute the stability of these colloidal properties to the two parameters that were unchanged in these suspensions: the ratio of [C$_{60}$]/[citrate] and the ratio of [C$_{60}$]/[Na^+]. In contrast, during direct dilution by the same solution in which an nC$_{60}$ suspension was produced, the surface charge of the diluted cit/nC$_{60}$ samples became less negative even though the solution chemistries did not change during dilution. The increase in the average particle size when cit/nC$_{60}$ was diluted in citrate solutions is likely a direct result of its less negatively charged surface that occurs in response to the increase in [Na^+] thus reducing the energy barrier for cit/nC$_{60}$ particles to aggregate. In the re-suspension experiment, although changes in the solution chemistries were similar to those in the direct dilution by water, the EM of the re-suspended 1 mM cit/nC$_{60}$ did not become less negative and these particles did not aggregate according to the DLS results. The lack of change in EM and Z_{ave} in this experiment was likely due to the increases in the ratios of [C$_{60}$]/[citrate] and [C$_{60}$]/[Na^+]. Diluted aq/nC$_{60}$ and 1 mM cit/nC$_{60}$ after centrifugation also exhibited less negatively charged surfaces (data not shown), indicating that the ratio of nC$_{60}$ to water is also important to determine the surface charge of nC$_{60}$. Similar decreases in surface charge have been observed for aq/nC$_{60}$ after filtration.[82] Our previous studies[101,186] suggested that solution chemistry (e.g., pH, carboxylate identity, and [Na^+]) dictates the formation of nC$_{60}$. According to the dilution experiment results, however, [C$_{60}$] and the ratio of [C$_{60}$] to other constituents in solutions are also important in determining the final measured properties of nC$_{60}$.

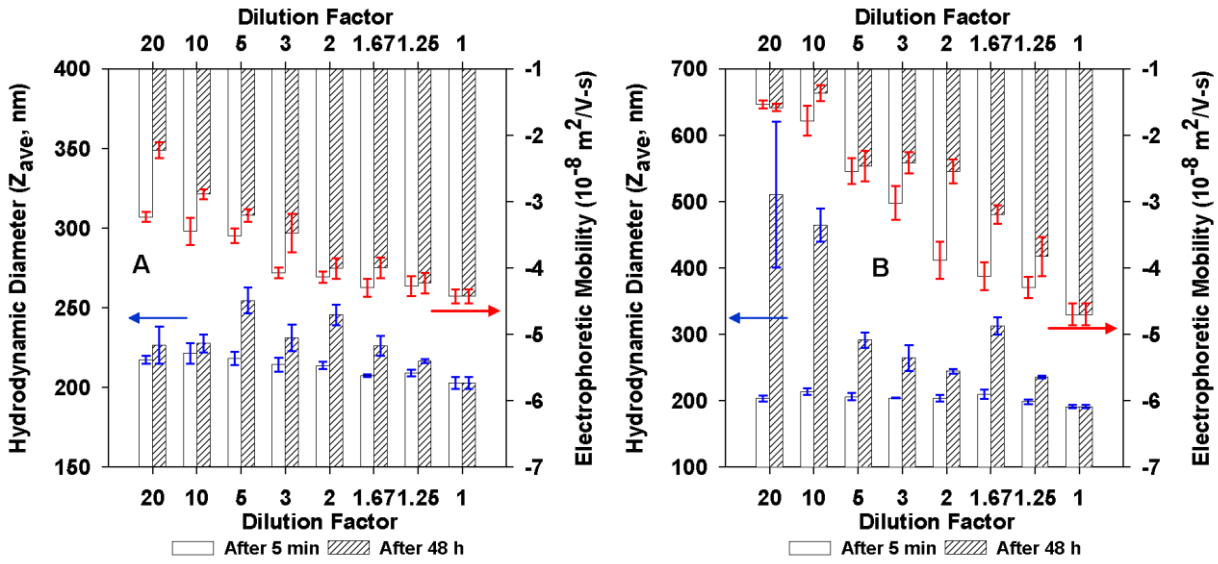

Figure 7.5 Surface charge and average particle size of diluted (A) 1.0 mM cit/*n*C_{60} and (B) 5.0 mM cit/*n*C_{60} after 5 min and 48-h storage. The two cit/*n*C_{60} stock suspensions were respectively diluted by 1.0 and 5.0 mM Na_3Cit solutions. (The vertical bar represents the average of three measurements for each sample, and the error bar represents their standard deviation.)

Results reported for both direct dilution experiments in previous sections were measured 48 hours after dilution. We also measured their EM and Z_{ave} 5 minutes after dilution in order to evaluate any temporal effects. For aq/*n*C_{60} and cit/*n*C_{60} produced in solutions with low [Na_3Cit] levels (0.1 and 0.5 mM) the values for samples after 5-min and 48-h storage were statistically the same (data not shown). However, for cit/*n*C_{60} produced in 1.0 and 5.0 mM Na_3Cit, we observed slightly less negative surface charges and increases in Z_{ave} after 48-h storage (Figures 7.5A and 7.5B). Changes in surface charges with DF occurred immediately after dilution. Diluted 5.0 mM cit/*n*C_{60} suspensions after 48-h storage were less negatively charged than their counterparts measured immediately after dilution (Figure 7.5B). This decrease in surface charge was presumably related to the larger particle sizes after storage. The increase in the average particle size was only observed 48-h after dilution due to the progressive aggregation process. When DF was greater than 10, the average particle sizes of the diluted 5.0 mM cit/*n*C_{60} suspensions grew from 200 nm to 500 nm during 48-h storage.

UV-Vis Spectra of Direct Diluted *n*C_{60}. UV-Vis spectra of *n*C_{60} suspensions reveal information about their sizes and the interactions of *n*C_{60} with water and other constituents.[74,79,93,121] In the present study, the changes in UV-Vis spectra of diluted *n*C_{60} samples collaborated the changes in their surface charges and average particles sizes.

Similar to our previous study (Chapters 3 and 6),[121] we examined changes in the UV-Vis spectra for the *n*C_{60} suspensions. Due to the differences in UV-Vis absorbance caused by various [C_{60}] in diluted *n*C_{60} suspensions, it is difficult to tell subtle differences in collected UV-Vis spectroscopic properties. To better present the variation in UV-Vis spectra for diluted *n*C_{60} suspensions, each spectrum was divided by its absorbance at 360 nm (ABS(360)) to obtain a normalized spectrum of an *n*C_{60} sample. Despite changes in [C_{60}], the spectra for all five types of *n*C_{60} suspensions diluted by water showed no difference from those of their respective stock *n*C_{60} suspension (data not shown). This observation was consistent with the unchanged surface charges and average particle sizes of these suspensions. Similarly, because of their stable EM and Z_{ave} values, almost identical normalized spectra were observed for 0.1 mM cit/*n*C_{60} suspensions diluted by 0.1 mM Na_3Cit solutions (data not shown). However, when 1.0 and 5.0 mM cit/*n*C_{60} were diluted by the same Na_3Cit solutions in which they were produced, after 5-min storage, their normalized spectra had no obvious difference from those of their respective parent suspensions (Figures 7.6A and 7.6B). However, after a 48-h storing period, changes in their spectral properties occurred (Figures 7.6C and 7.6D). The increase in relative intensity for the broad absorption band in the range of 400-600 nm corresponds to an increase in average particle size.[121]

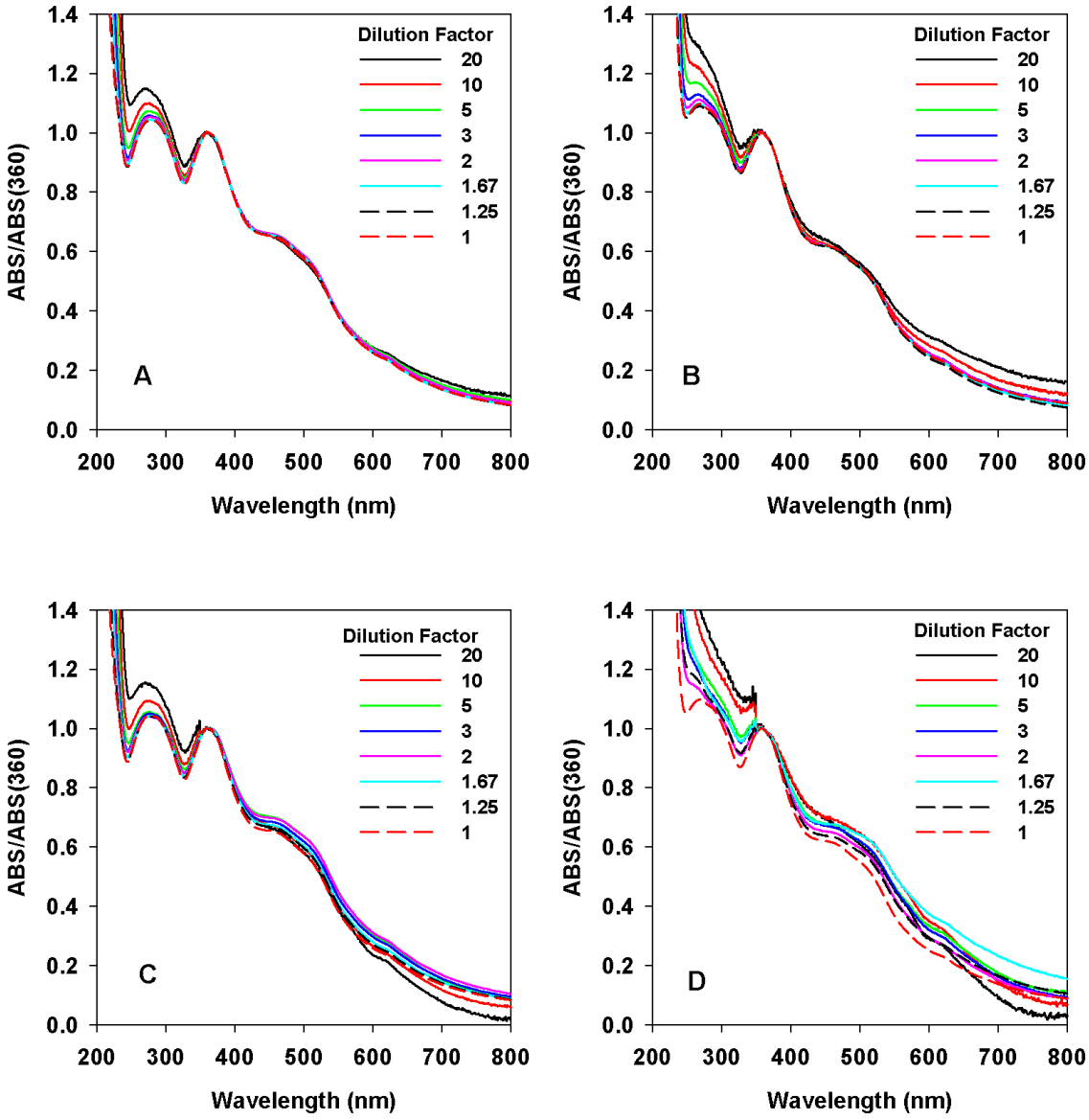

Figure 7.6 Normalized UV-Vis spectra of nC$_{60}$ diluted by the same solution wherein it was produced. (A) 1.0 mM cit/nC$_{60}$ after 5 min; (B) 5.0 mM cit/nC$_{60}$ after 5 min ; (C) 1.0 mM cit/nC$_{60}$ after 48-h;and (D) 5.0 mM cit/nC$_{60}$ after 48-h.

TEM Images of Diluted nC$_{60}$. As we have noted previously,[186] surface charge and average particle size only represent the average properties of all of the nC$_{60}$ nanoparticles in a suspension and these parameters fail to provide detailed information at the single particle scale. In the present study, we employed transmission electron microscopy (TEM) to characterize the structure and morphology of selected dilute nC$_{60}$ samples.

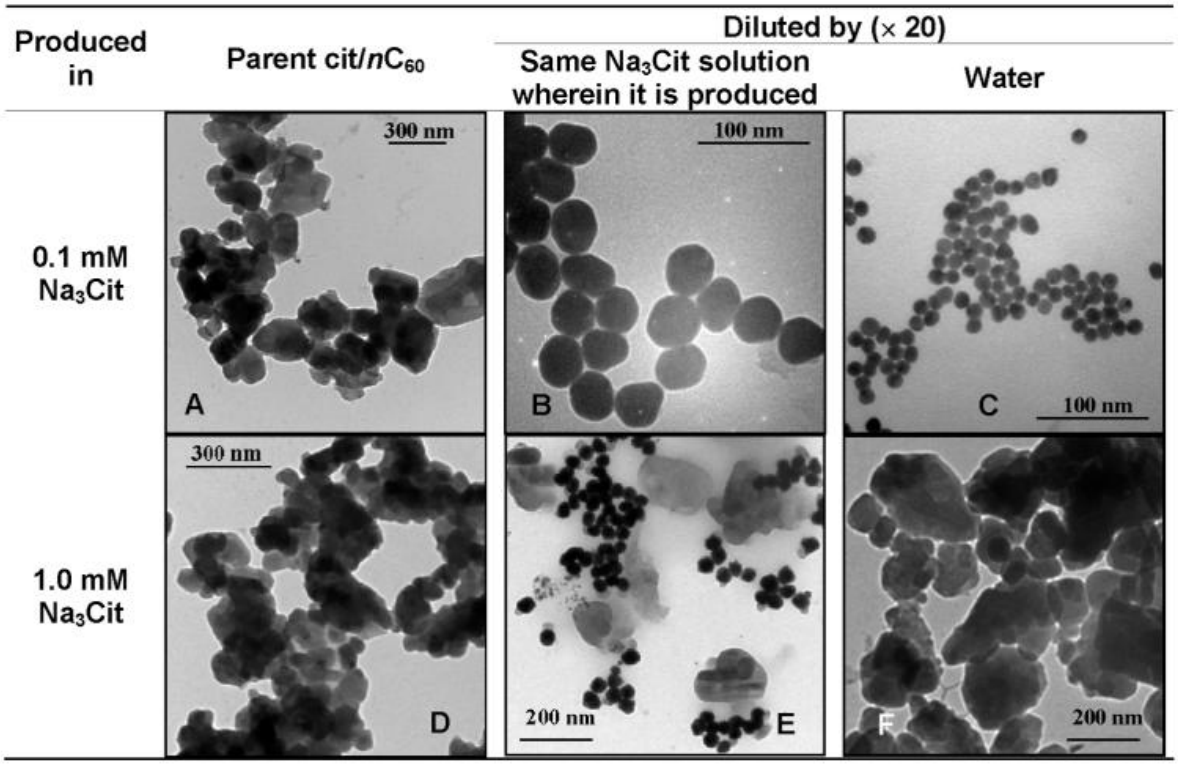

Figure 7.7 TEM images of cit/nC$_{60}$ produced in 0.1 mM Na_3Cit (A) diluted by 0.1 mM Na_3Cit (B) and water (C); TEM images of cit/nC$_{60}$ produced in 1.0 mM Na_3Cit (D) diluted by 1.0 mM Na_3Cit (E) and water (F).

TEM images of samples obtained from the direct dilution experiments indicate that the identity of the diluent (either Na_3Cit or water) greatly affects the size, structure, and morphology of the final cit/nC$_{60}$ nanoparticles. For the 0.1 mM cit/nC$_{60}$ sample, which primarily existed as irregularly shaped particles in the parent solution (Figure 7.7A), spherical particles of 40 nm diameter were observed when this sample was diluted 20× by 0.1 mM Na_3Cit (Figure 7.7B); however, 12 nm diameter particles were observed when this sample was diluted 20× by nanopure water (Figure 7.7C). Despite the fact that there was no change in EM and Z_{ave} for both diluted samples, 1.0 mM cit/nC$_{60}$ (Figure 7.7D) produced spherical particles when diluted 20× by 1 mM Na_3Cit (Figure 7.7E), while only large angular nanoparticles were observed when the suspension was diluted by nanopure water (Figure 7.7F). We note that in those diluted cit/nC$_{60}$ suspensions,

wherein spherical particles formed, a majority of the particles observed under TEM were irregularly shaped ones.

In re-suspension experiments, TEM examination shows that despite the stable Z_{ave} and EM values (Figure 7.4), the structure and morphology of cit/*n*C_{60} were dramatically affected by the final solution chemistry. When 1.0 mM cit/*n*C_{60} (Figure 7.7D) were re-suspended in 0.8 mM Na_3Cit, a number of regularly shaped (triangular, hexagonal, spherical, and semispherical) particles with sizes around 100 nm were observed 1.5 h after re-suspension (Figure 7.8A and inset). Characterization of this sample 24 h after re-suspension showed the loss of these particles and the appearance of small spherical particles (~ 15 nm, Figure 7.8B inset) and large irregular ones (100-500 nm; Figure 7.8B). For the sample re-suspended in a solution with a lower final [Na_3Cit] of 0.4 mM, regularly shaped nanoparticles similar to those in the 0.8 mM [Na_3Cit] sample were observed 1.5 h after re-suspension; however, small spherical particles (~ 15 nm) were also present (Figure 7.8C and inset). In this latter sample after 24-h reaction time, only large aggregates with a size of several microns, consisting of irregular particle, were observed (Figure 7.8D). In general after 24-h, cit/*n*C_{60} re-suspended in solutions with higher final [Na_3Cit] levels exhibited morphologic characteristics (Figures 7.9A, 7.9B and insets) similar to that of the original cit/*n*C_{60} produced in 1 mM Na_3Cit (i.e., both small spherical particles and loose compact aggregates). In contrast, cit/*n*C_{60} re-suspended in solutions with lower final [Na_3Cit] levels became increasingly irregular in shape and exhibited a highly compact structure (Figures 7.9C, 7.9D and insets) that resembles the morphology of aq/*n*C_{60}.[186]

The formation and gradual disappearance of highly ordered cit/*n*C_{60} particles in these samples after dilution and during the storage period were similar to that observed in our previous study (Chapter 5),[101] which reported the morphological changes of *n*C_{60} produced in 5 mM sodium

acetate during 10-month storage. These changes indicate that apparently stable nC_{60} suspensions undergo dissolution and re-crystallization constantly. We reiterate, as mentioned previously, the small regular particles only constitute a small portion of the cit/nC_{60} particles observed via TEM. This fact is likely the reason that no discernable differences with respect to average size or UV-Vis characteristics were apparent between the parent solution and the solutions after dilution. The appearance of regularly shaped particles also indicates that in the presence of citrate there is a bottom-up process that involves C_{60} molecules or small clusters as the building blocks of the regular nanoparticles.[186] Although our evidence implicating molecular C_{60} in these transformations is circumstantial there is no currently available analytical tool to definitively detect molecular C_{60} in water.

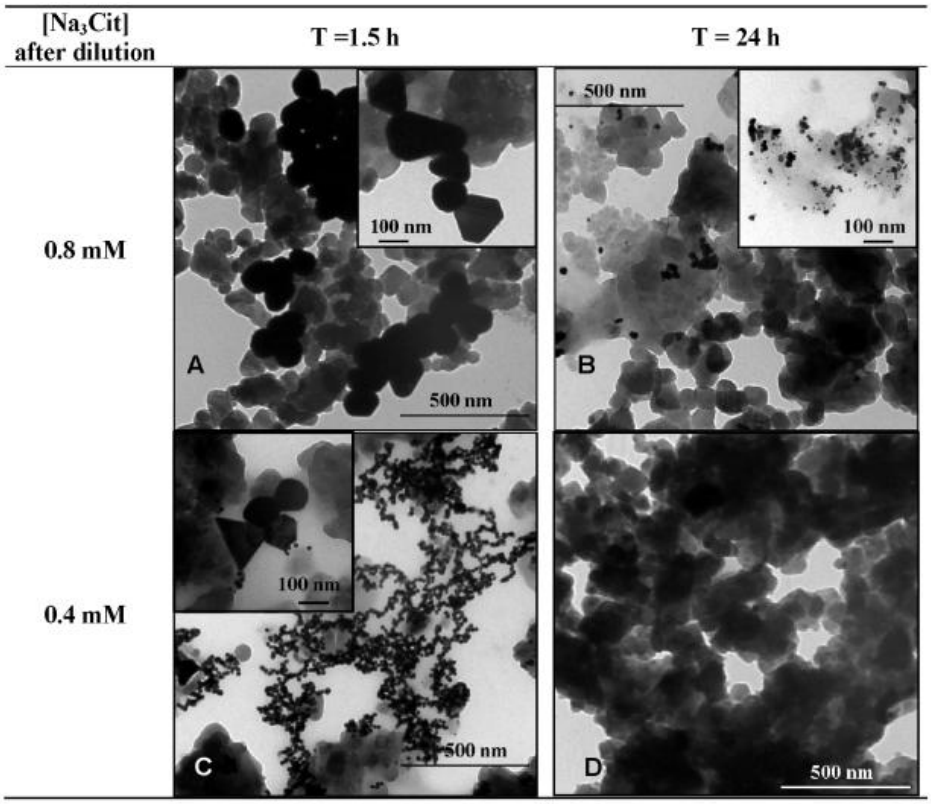

Figure 7.8 TEM image of 1.0 mM cit/nC_{60} re-suspended in the solution with [Na_3Cit] = 0.8 mM (A)1.5-h and (B) 24 h after dilution; TEM image of 1.0 mM cit/nC_{60} re-suspended in the solution with [Na_3Cit] = 0.4 mM (A)1.5-h and (B) 24 h after dilution. (Insets: close-ups of regularly shape particles)

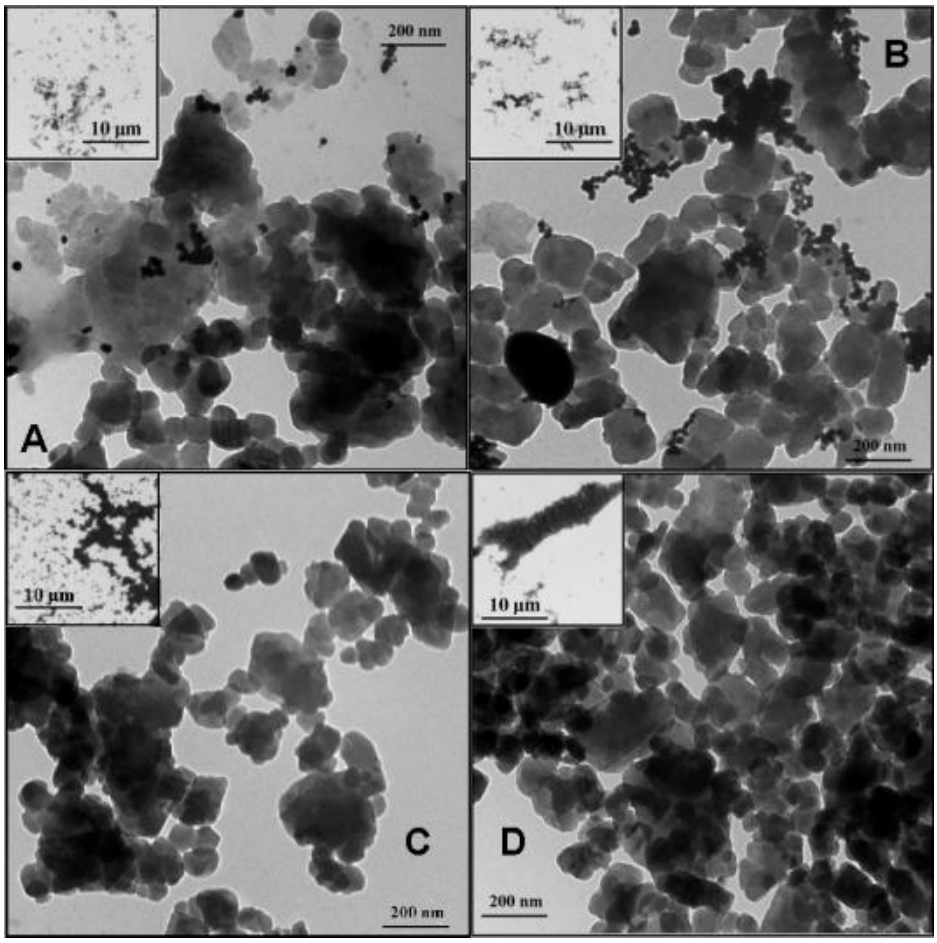

Figure 7.9 TEM images 1 mM cit/nC$_{60}$ re-suspended in solutions with final [Na$_3$Cit] of (A) 0.8 mM, (B) 0.6 mM, (C) 0.4 mM , and (D) 0.2 mM. (General views of one representative mesh on the TEM grids).

7.4 Environmental Implications.

The present study indicates that dilution of nC$_{60}$ suspensions will readily cause measurable changes in their colloidal properties, including surface charge and particle size. The most important factor dictating these properties in the diluted samples are the ratio of [C$_{60}$] to the concentration of other constituents in solution. In some cases, although general indices such as EM and Z_{ave} remained unchanged after dilution, the structure and morphology of nC$_{60}$ were greatly altered.

In current studies of nC$_{60}$ environmental impacts, stock nC$_{60}$ suspensions usually undergo pre-treatment before characterization or further investigation: nC$_{60}$ suspensions have been

centrifuged[64] or diluted (1:40)[184] for TEM sample preparation; experiments involving the adsorption of organic contaminants on nC$_{60}$ required the adjustment of nC$_{60}$ concentration;[28,88,91,187] aggregation kinetic experiments of nC$_{60}$[30,112,185] and their toxicity studies[184,188] involved dilution of nC$_{60}$; the pH and ionic strength of nC$_{60}$ suspensions were adjusted by adding acid, base, or electrolyte solutions.[58,59,64] All of these operations result in dilution effects and alter the concentration ratios between C$_{60}$ and other constituents, potentially leading to changes in the properties of nC$_{60}$, which will ultimately affect the transport, fate, and environmental impacts of nC$_{60}$. According to the results of the present study, we suggest that extreme care should be taken when stock nC$_{60}$ suspensions are diluted for further investigations and that changes in nC$_{60}$ properties should be considered when interpreting data obtained from experiments involving diluted nC$_{60}$ suspensions.

Chapter 8 Conclusions and Environmental Implications.

8.1 Summary of Findings

In the present study, colloidally stable nC$_{60}$ suspensions were produced via extended mixing in both the presence and absence of carboxylates. Under all but the highest salt concentrations the as produced nC$_{60}$ nanoparticles exhibited a negative surface charge and remained stable in suspension after a long storage period.

Aq/nC$_{60}$, which is produced by magnetic stirring for an extended period in water alone, is the simplest form of nC$_{60}$. Its surface charge was independent of stirring time while its average particle size decreased with stirring time. Changes in the UV-Vis spectral properties of aq/nC$_{60}$ over the stirring period indicated that the interactions between C$_{60}$ and water are progressive and do not occur immediately. nC$_{60}$ produced in citrate or other low molecular weight carboxylate solutions differ from aq/nC$_{60}$ with respect to surface charge, average particle size, interfacial properties, spectral characteristics, and resistance to salt induced aggregation. Interestingly, in the presence of citrate or other carboxylates, regularly shaped (spherical, triangular, square, hexangular, or rod-like) nC$_{60}$ nanoparticles formed through a bottom-up process. This process involves individual C$_{60}$ molecules or C$_{60}$ clusters as building blocks. Irregularly shaped nC$_{60}$ nanoparticles produced through a top-down process induced by continuous agitation were also observed concurrently.

Our study on the stability of nC$_{60}$ suggests that simple dilution of nC$_{60}$ suspensions will readily cause changes in surface charge and particle size. The most important factor determining these properties of the diluted sample is the ratio of [C$_{60}$] to the concentrations of other constituents in solutions. Importantly, in some cases, although general indices such as surface charge and

particle size remained unchanged after dilution, the structure and morphology of nC$_{60}$ were greatly altered.

In addition to DLS and TEM we employed the UV-Vis spectrophotometer as a supplemental tool to probe the properties of nC$_{60}$. The spectra of aq/nC$_{60}$ depend upon the average particle size, size distribution, and interactions between C$_{60}$ and water. With an increase in average particle size, the absorption maxima of the two main absorption bands for nC$_{60}$ shift to shorter wavelengths. The extent of the blue shift for the 360 nm absorption band is determined by the methods used to prepare and fractionate nC$_{60}$ suspensions. The results of the UV-Vis study confirm the argument that the origin of the continuous broad absorption in the 400-600 nm region is due to the aggregation of C$_{60}$.

8.2 Environmental Implications.

This study has clearly shown that the UV-Vis spectrum provides information about fullerene nanparticles (nC$_{60}$). The UV-Vis spectrum of an nC$_{60}$ suspension is dependent upon its interfacial properties as determined by the interaction between C$_{60}$ and other constituents, and as illustrated herein, the spectral characteristics of a nC$_{60}$ suspension have the potential to be used to predict the average particle size of the suspension in the absence of dynamic light scattering (DLS) data. Clearly the potential exists to use UV-Vis as a powerful tool to investigate the properties of nC$_{60}$.

nC$_{60}$ produced via extended mixing is arguably a better approximation of the particles that will form when C$_{60}$ is released to the environment than nC$_{60}$ produced via methodologies involving the use of organic solvents or under intense sonication conditions. Changes in its UV-Vis spectral properties over the stirring period imply that the formation of nC$_{60}$ is a temporal process.

The rate at which this process occurs in natural waters could be either diminished or accelerated depending upon the solution composition. In any case, however, the progressive nature of the reaction should be considered to truly evaluate the reactivity and fate of C_{60} in aqueous environments.

In natural waters, the existence of a variety of constituents will change the properties of nC_{60} formed after C_{60} release and will alter their transport paths and interactions with organisms in the environment. Accordingly, studies investigating the fate and environmental impacts of nC_{60} must take the constituents in natural waters into consideration. Without such consideration the results based on aq/nC_{60} may not fully represent the scenarios when C_{60} is released into the environment.

The concomitant occurrence of irregularly and regularly shaped nC_{60} nanoparticles produced in the presence of citrate or other carboxylates via extended mixing indicates that fullerite C_{60} is subject to weathering by continuous agitation as well as recrystallization through a bottom-up process involving clusters or individual C_{60} molecules. The morphological changes and appearance of regularly shaped nC_{60} nanoparticles in diluted nC_{60} samples confirm the dissolution-crystallization induced by association between carboxyl groups and C_{60}. Clusters or individual C_{60} molecules, the building blocks of those regularly shaped nC_{60} nanoparticles have great implications for the cellular uptake of C_{60}, the toxicity of C_{60} in aqueous solutions, and therefore its environmental fate. These clusters or molecules are small enough to enter cells through ion channels or membrane pores.[175,176] Molecular C_{60} and small clusters of C_{60} are more efficient at producing reactive oxygen species (ROS) than large nC_{60} particles.[177,178] Therefore, the production of molecular C_{60} or their small clusters could result in greater levels of toxicity than expected based on measurements for nC_{60} alone. Accordingly, studies examining the

potential cellular toxicity of C_{60} or its environmental implications should consider the role of molecular C_{60} and small clusters of C_{60} molecules.

The non-stop dissolution-recrystallization process determines the instability of $n$$C_{60}$ suspensions during storage or due to simple changes in solution chemistry. As a result, the colloidal properties and morphology of stock $n$$C_{60}$ suspensions can readily change during storage. According to the results of the present study, we suggest that it is not appropriate to use the data for a stock $n$$C_{60}$ suspension to represent the properties of the $n$$C_{60}$ in the tested aqueous solutions. Changes in $n$$C_{60}$ properties should be fully taken into consideration during the interpretation of data obtained from experiments involving dilution or other aqueous solution additions.

It is of significant importance to both the research and industrial communities to reproducibly produce $n$$C_{60}$ suspensions. Unfortunately, due to the random nature of the top-down process, it is extremely difficult to produce identical $n$$C_{60}$ suspensions via extended mixing or sonication. The differences in the properties of $n$$C_{60}$ produced in different batches ultimately lead to their varied extinction coefficients. As a result, it is inappropriate to use the UV-Vis absorbance of $n$$C_{60}$ suspensions to determine their C_{60} concentration unless extreme care has been taken to fully characterize the system with respect to particle size, solution chemistry, and aggregation state. Particle extinction coefficients that are dependent upon particle size and size distribution cannot be directly used to determine [C_{60}] either. The general lack of reproducibility of aq/$n$$C_{60}$ is also likely a significant factor in the observed variability of $n$$C_{60}$ toxicity. When studies investigating the behavior, transport, and environmental impacts of $n$$C_{60}$ are conducted, researchers must be aware that the data obtained using different batches of $n$$C_{60}$ may not be comparable. Particle size,

[C_{60}], $n$$C_{60}$ particle concentration, and other colloidal properties, collectively determine the properties of $n$$C_{60}$ with respect to its transformation, transport, and toxicity.

Appendix A: Supporting Information for Chapter 3

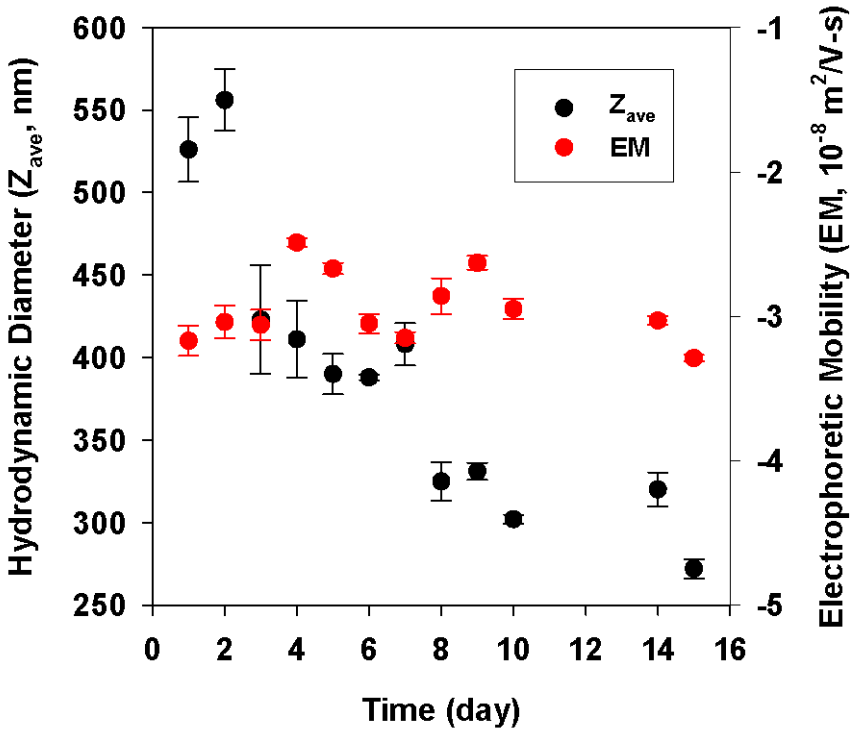

Figure A.1 Average particle size (Z_{ave}) and surface charge (EM) of aq/nC_{60} as a function of extended mixing time. (Each data point represents the average of three measurements and the error bar represents the standard deviation of three measurements.)

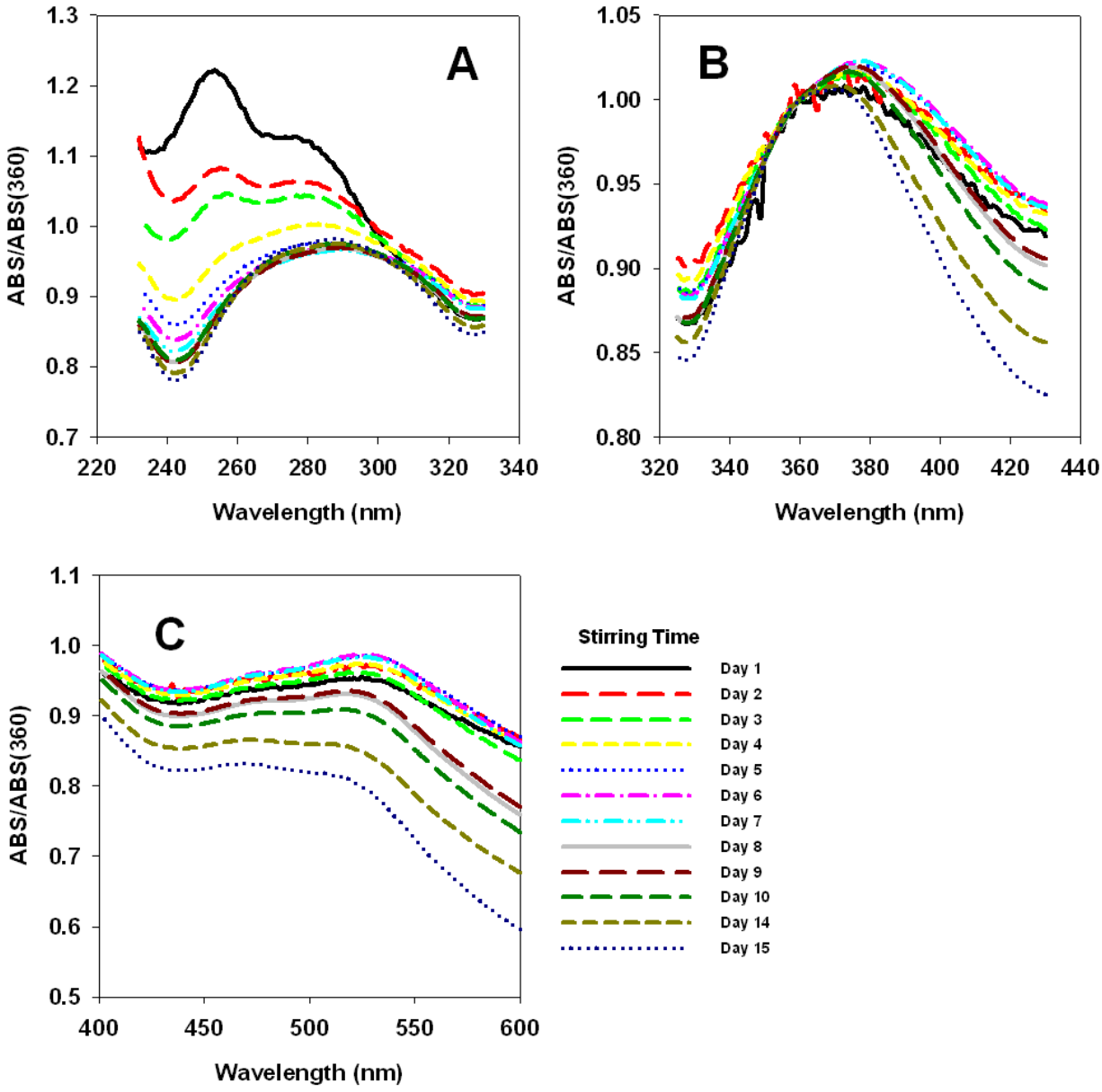

Figure A.2 Normalized UV-Vis spectra of aq/nC_{60} produced via extended mixing. Spectra are normalized by the measured absorbance at 360 nm: (A) 240-290 nm; (B) 330-410 nm; and (C) 400-600 nm.

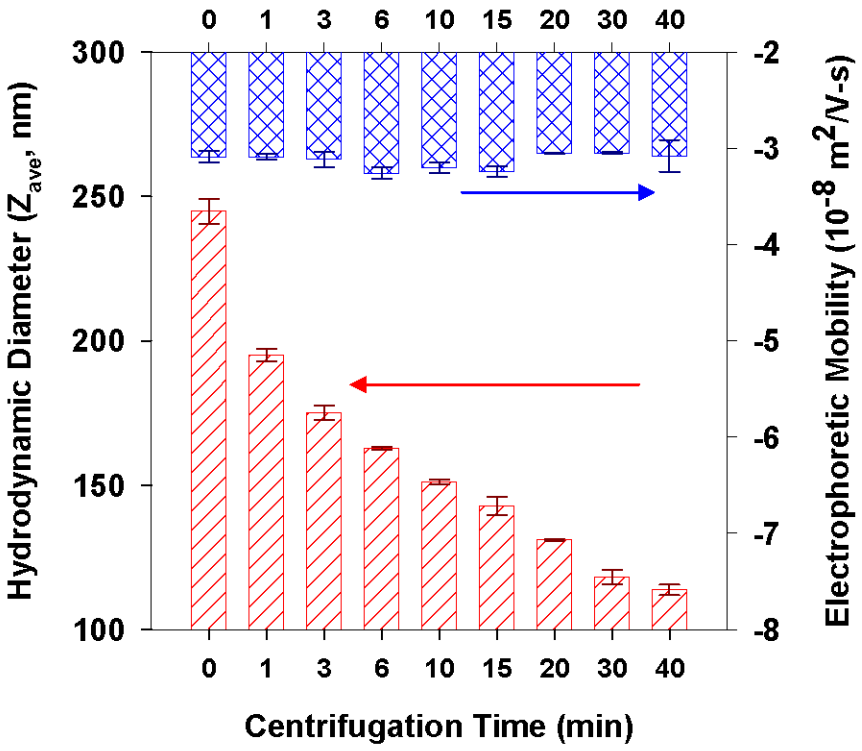

Figure A.3 Electrophoretic mobility and hydrodynamic diameter of aq/*n*C_{60} as a function of centrifugation time. (Each vertical bar represents the average of three measurements and the error bar represents the standard deviation of three measurements.)

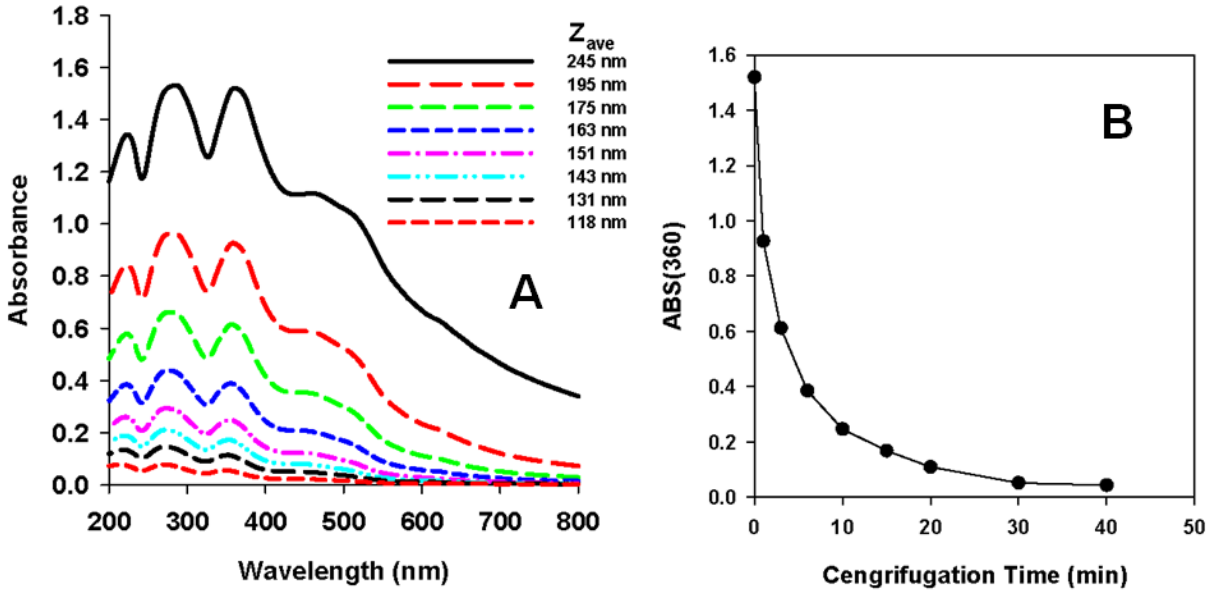

Figure A.4 (A) UV-Vis spectra of stock aq/*n*C$_{60}$ after different periods of centrifugation; and (B) The absorbance at 360 nm as a function of centrifugation time.

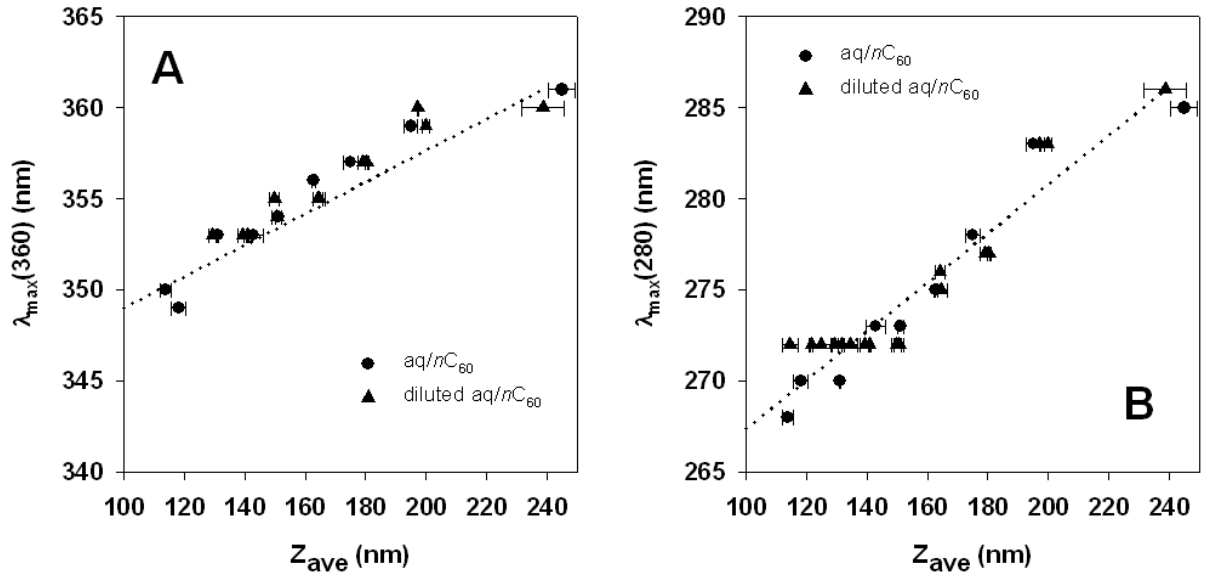

Figure A.5 (A) λ_{max}(360) and (B) λ_{max}(280) as a function of the particle size of centrifuged aq/*n*C$_{60}$ suspensions. Both a full strength solution as well as a diluted solution were tested. (The Z_{ave} value represented in this figure is the average of three measurements and the error bar represents the standard deviation of three measurements.)

Table A.1 The positions of absorption maxima of C_{60} in organic solutions

Solvent	λ_{max}	n	Reference
benzene	330	1.501	
toluene	332	1.497	
chlorobenzene	330	1.5248	
o-dichlorobenzene	331	1.5514	
o-xylene	332	1.5054	[77]
N,*N*-dimethylaniline	340	1.5580	
1-methylnaphthalene	335	1.612	
carbon tetrachloride	327	1.461	
isooctane	326	1.3914	
THF	328	1.4072	
n-heptane	328	1.3876	[96]
carbon tetrachloride	330.0039	1.46	
1,4-dioxane	330.4947	1.42	
N,*N*-dimethylaniline	330.0039	1.44	
fluorobenzene	332.5057	1.47	
anisole	333.004	1.52	
benzonitrile	333.004	1.53	
o-dichlorobenzene	333.004	1.55	[98]
chlorobenzene	333.5038	1.53	
pyridine	334.4966	1.51	
benzene	335.0009	1.5	
toluene	336.0027	1.5	
mesitylene	336.0139	1.5	
carbon disulfide	338.8605	1.63	
n-hexane	328.4	1.3749	
cyclohexane	329	1.4465	
1-octanol	329.5	1.4295	
2-octanol	329	1.4234	[93]
benzene	335	1.501	
toluene	335.5	1.497	
Triton X-100	332		
decalin	330	1.318	

Appendix B: Supporting Information for Chapter 4

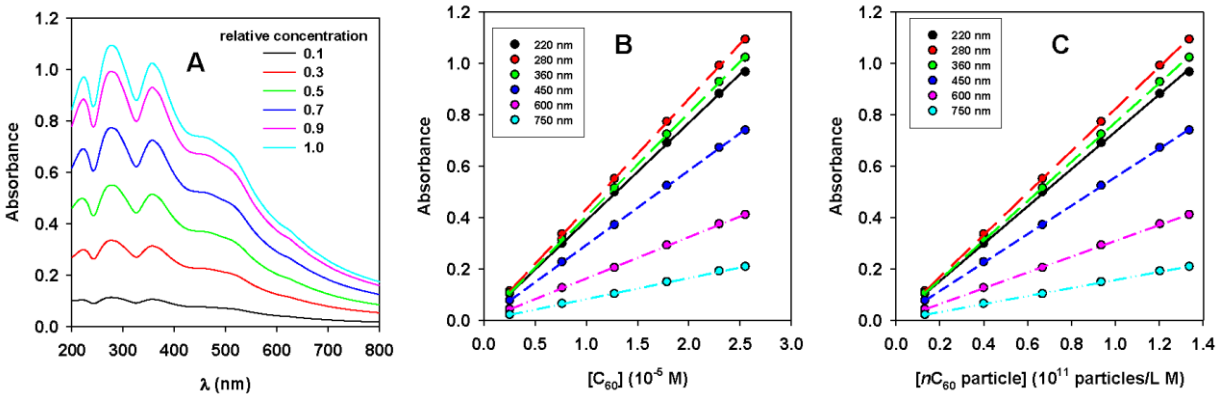

Figure B.1 (A) UV-Vis spectra of a series of diluted aq/*n*C_{60} suspension, the [C_{60}] and particle concentration in the original suspension were 2.55 × 10^{-5} M and 1.34 × 10^{12} particles/L, respectively; the regression curves of (B) absorbance vs. [C_{60}] and (C) absorbance vs. particle concentration at different wavelengths.

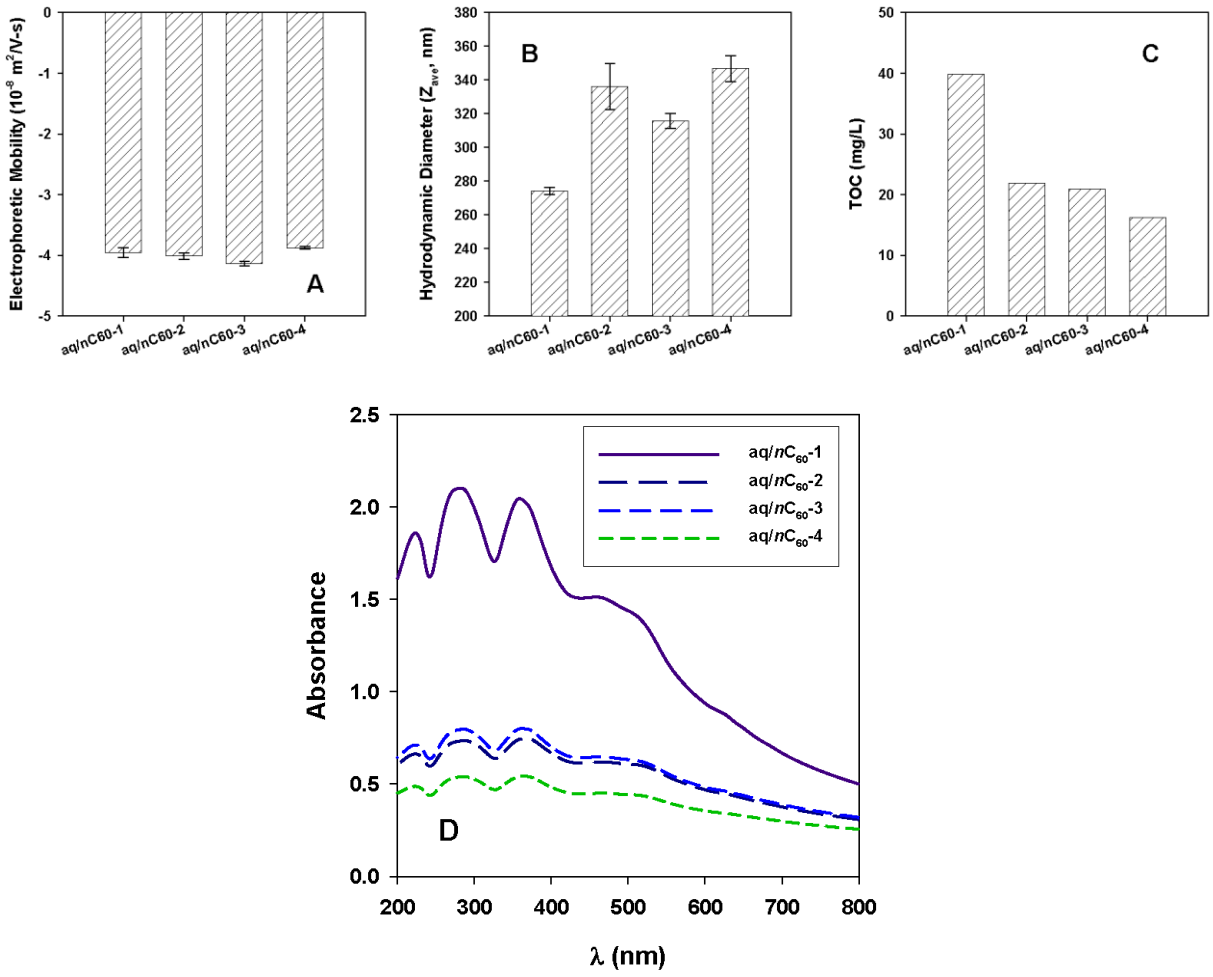

Figure B.2 (A) Surface charge, (B) average particle size (Each vertical bar represents the average of three measurements and the error bar represents the standard deviation of three measurements.), (C) C_{60} concentration, and (D) UV-Vis absorption spectra of aq/nC_{60} from four batches after 21-day stirring.

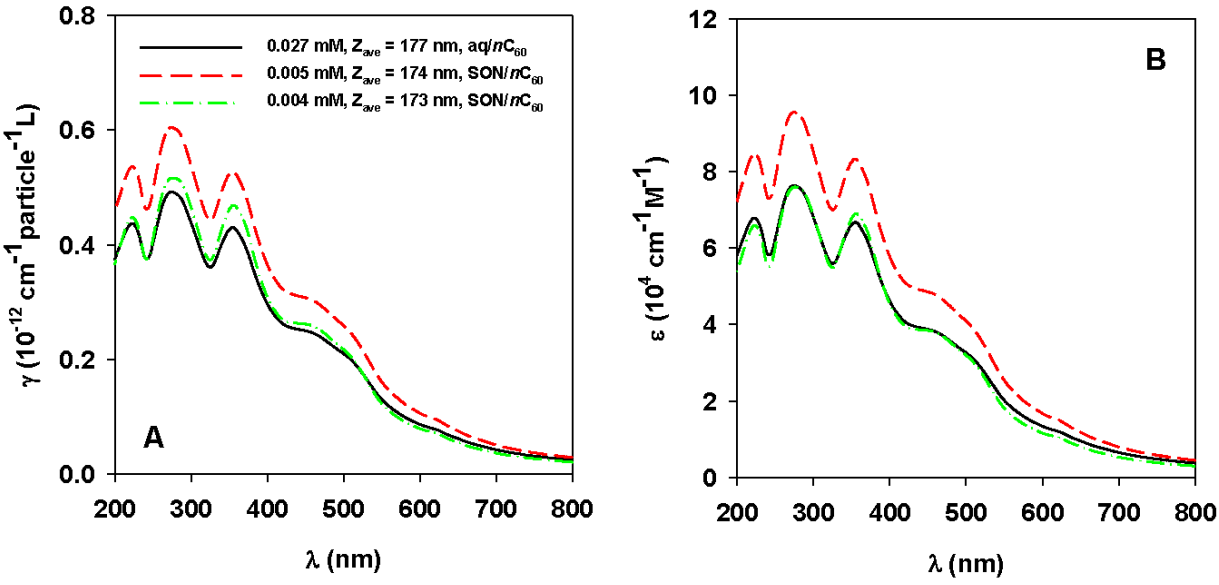

Figure B.3 (A) Particle extinction spectra and (B) molar extinction spectra of SON/nC$_{60}$ suspensions and an aq/nC$_{60}$ suspension with similar Z$_{ave}$.

The lack of reproducibility is observed in SON/nC$_{60}$ suspensions. Two SON/nC$_{60}$ suspensions produced under identical conditions have very similar average particle sizes (174.0 ± 1.2 and 173.0 ± 1.6 nm) and EM values (-3.148 ± 0.039 × 10^{-8} and -3.030 ± 0.041 m^2/V-s). Their TOC values are 0.005 and 0.004 mM, respectively. However, their extinction spectra are still quite different.

Calculation of the average particle extinction coefficient for a heterogeneous aq/*n*C_{60} suspension based upon its size distribution.

Assumptions:

(1) Aq/*n*C_{60} suspensions only contain spherical particles with different sizes.

(2) Size distributions from DLS measurements are treated as discrete functions $p_i = f(D_i)$, where p_i is the fraction of particles with the diameter of D_i.

Based on Beer-Lambert Law, the absorbance at a specific wavelength (A) of a suspension is

$$A = l \sum_i N_i \cdot \gamma_i = l N_{total} \Gamma \quad \text{(B.1)}$$

where l is the pathlength (= 1 cm), γ_i (particle^{-1}cm^{-1}L) is the extinction coefficient per particle with diameter of D_i (nm), N_i (particles/L) is the number concentration of particles with diameter of D_i, N_{total} (particles/L) is the total number concentration of the aq/*n*C_{60} suspension, and Γ (particle^{-1}cm^{-1}L) is the number weighted average particle extinction coefficient of the aq/*n*C_{60}. The relationships among N_{total}, N_i, and p_i are shown in Eqns. B.2 and B.3.

$$N_{total} = \sum_i N_i \quad \text{(B.2)}$$

$$N_i = N_{total} \cdot p_i \quad \text{(B.3)}$$

From Eqn. B.1, there is

$$\Gamma = \frac{\sum_i N_i \cdot \gamma_i}{N_{total}} \quad \text{(B.4)}$$

The objective of this calculation is to obtain spectra of Γ for aq/*n*C_{60} suspensions. In order to do so, we must calculate N_i for each sample first.

Particle concentration calculation:

The number particle concentration N_{total} of an aq/nC$_{60}$ suspension is calculated based upon the balance of C$_{60}$ molecule concentration ([C$_{60}$]$_{molecule}$, molecules/L). From the mass concentration determined by TOC, there is:

$$[C_{60}]_{molecule} = \frac{TOC}{M_w} \cdot N_A \quad \text{(B.5)}$$

where TOC is the mass concentration of C$_{60}$ determined by TOC (g/L), M_w is the molecular weight of C$_{60}$ (720 g/mole), and N_A is the Avogadro constant (6.02×10^{23} mole^{-1}). Form the particle number concentration's point of view,

$$[C_{60}]_{molecule} = \sum_i N_i \cdot n_i \quad \text{(B.6)}$$

where n_i (molecules/particle) is the number of C$_{60}$ molecules contained in a spherical (*fcc*) aq/nC$_{60}$ particle with the diameter of D_i:

$$n_i = \frac{4\pi}{3}\left(\frac{D_i}{2}\right)^3 \frac{4}{L^3} \quad \text{(B.7)}$$

where L is the lattice constant of C$_{60}$ (1.417 nm). Combining Eqns. B.3, and B.5-B.7, the total nC$_{60}$ particle number concentration is:

$$N_{total} = \frac{\frac{TOC}{M_w} \cdot N_A}{\frac{4\pi}{3} \cdot \frac{4}{L^3}\left[\sum_i \left(\frac{D_i}{2}\right)^3 \cdot p_i\right]} \quad \text{(B.8)}$$

Then the N_i can be calculated for the aq/nC$_{60}$ suspension by Eqn. B.3.

We have 36 aq/nC$_{60}$ samples with known TOC values and size distributions range from 28.21 to 825 nm (D_i, i_{max} = 24, from DLS). At a specific wavelength (λ), there is a system of linear equations:

$$N_{1,1}\gamma_1(\lambda) + N_{1,2}\gamma_2(\lambda) + \cdots + N_{1,24}\gamma_{24}(\lambda) = A_1(\lambda)$$

$$N_{2,1}\gamma_1(\lambda) + N_{2,2}\gamma_2(\lambda) + \cdots + N_{2,24}\gamma_{24}(\lambda) = A_2(\lambda)$$

$$\vdots \qquad \vdots \qquad \vdots \qquad \vdots$$

$$N_{36,1}\gamma_1(\lambda) + N_{36,2}\gamma_2(\lambda) + \cdots + N_{36,24}\gamma_{24}(\lambda) = A_{36}(\lambda)$$

(9)

where $N_{j,i}$ is the number concentration of particles with the diameter of D_i in the j^{th} aq/nC$_{60}$ sample (j_{max}= 36), and A_j is the absorbance at wavelength λ for the the j^{th} aq/nC$_{60}$ sample. These equations represent aq/nC$_{60}$ suspension from different batches. For this system, we have 36 equations for 24 unknowns. Therefore, we can only obtain the optimal solutions for γ_i by linear least squares. The γ_i values are then applied in Eqn. B.4 to calculate the Γ values for each sample at each wavelength to obtain the Γ-λ spectra.

Results:

γ_i values. Based upon research results on other nanoparticles, at a specific wavelength, extinction coefficient values for particles of different sizes should increase with particle size. Figure B.4 presents γ_i values at four different wavelengths. They all vary in broad ranges and do not increase with D_i. γ_i at other wavelengths show the similar lack of patterns.

Theoretically, the plot of calculated γ_i values vs. wavelength λ is the extinction spectrum of a monodisperse suspension consisting of spherical particles with the diameter of D_i. This spectrum should have the similar shape of spectra obtained by UV-Vis spectrophotometer. Figure B.5 presents γ_i spectra obtained by the equations system B.9. Only several γ_i spectra (D_i = 28.21, 50.75, 91.28, 141.8, and 164.2 nm) exhibit similar shapes to the UV-Vis spectra of aq/*n*C_{60}. When D_i > 250 nm, the calculated γ_i have large values in the longer wavelength range (500 to 800 nm), which is consistent with the results from MiePlot.

If all assumptions were satisfied, the system of linear Eqns. B.9 would have a unique solution, which are the actual extinction coefficients for spherical aq/*n*C_{60} particles with the diameter of D_i. However, in our calculation, the scattered γ_i values in Figure B.4 and the lack of similar shape to that of the UV-Vis spectra of actual aq/*n*C_{60} suspensions in Figure B.5 indicate that the obtained γ_i values are the optimal values to fit linear least squares for Eqns. B.9, instead of the actual extinction coefficients of aq/*n*C_{60} particles with the diameter of D_i. And the obtained γ_i values from Eqns. B.9 are dependent upon the data set used in the linear least squares calculation (will be discussed in following sections). Therefore, the calculated γ_i can only be used to calculate the Γ for these 36 aq/*n*C_{60} samples. They should not be used to predict the extinction coefficient for other samples with different size distributions.

The failure to calculate the actual values of γ_i is primarily caused by the dissatisfaction of the assumptions due to the high heterogeneity of aq/*n*C_{60} suspensions and the irregularly shaped aq/*n*C_{60} particles.

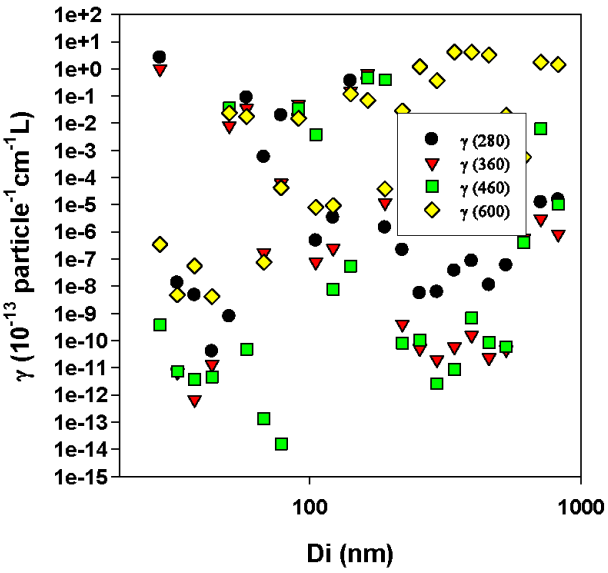

Figure B.4 γ_i as a function of D_i at four specific wavelengths.

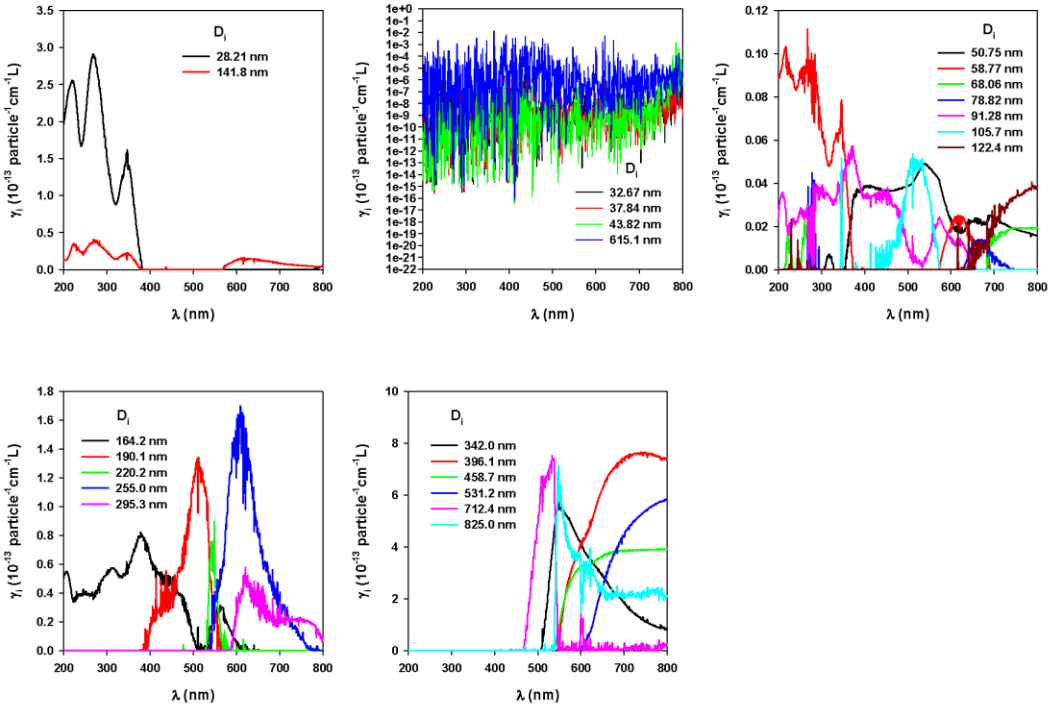

Figure B.5 Calculated γ_i spectra.

Γ-λ spectra. Figures B.6-8 show the Γ-λ spectra, in which Γ values are calculated by Eqn. B.4 using γ_i values obtained previously based upon size distributions by DLS measurements. The

results suggest that aq/nC$_{60}$ suspensions with different particle size distributions do not have converged extinction spectra. Figure B.9A shows there is no obvious relationship between Γ and Z_{ave} values. However, Γ value at a specific wavelength increases linearly with number weighted average particle size D_{Number} ($D_{Number} = \frac{\sum_i D_i N_i}{\sum_i N_i}$) (Figure B.9B).

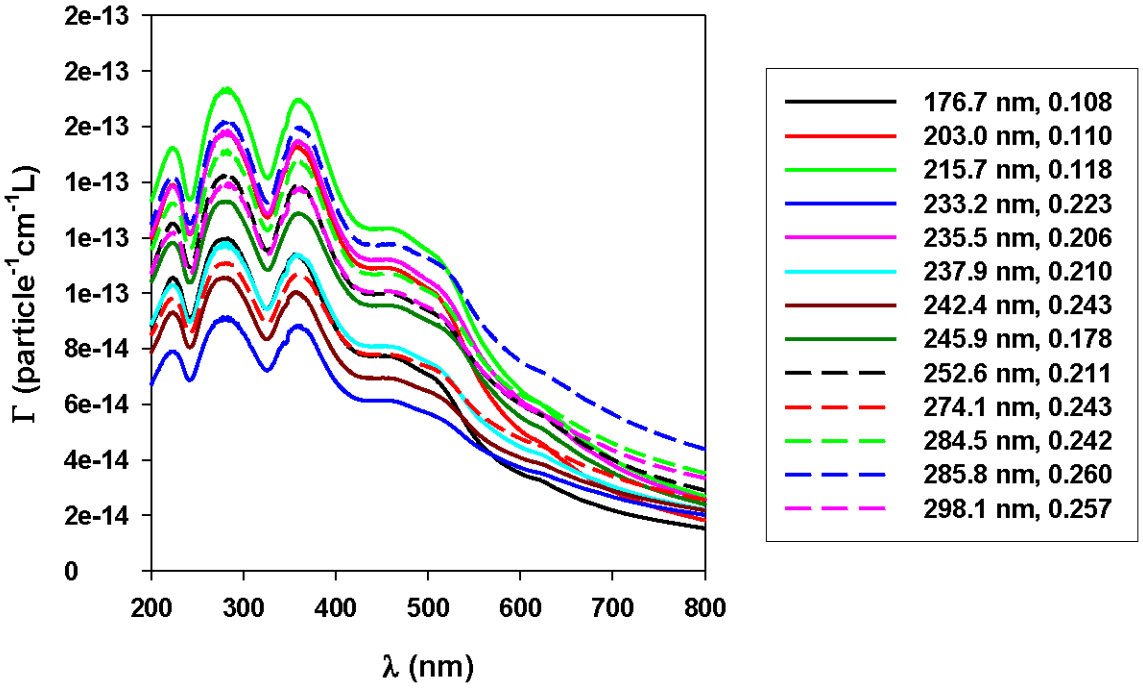

Figure B.6 Γ spectra: settled samples with Z_{ave} from 177 nm to 298 nm.

The dependence of calculated Γ on the data sets of $N_{j,i}$ (in Eqns. B.9). As discussed earlier, instead of having a unique solution, the system of linear Eqns. B.9 has optimal γ_i values, which are obtained by linear least squares and greatly depends upon the data set of $N_{j,i}$. Eqns. B.9 were arranged by the D_{number} value of aq/nC$_{60}$ samples: the first equation represented the Beer-Lambert law base on size distribution (Eqn. B.1) for the aq/nC$_{60}$ with the smallest D_{number} value, and the last (36th) equation represented the Beer-Lambert law for the aq/nC$_{60}$ with the largest D_{number} value. And three calculations of γ_i were conducted using different $N_{j,i}$ and A_j sets: (1) all 36 equations, (2) the first 30 equations, excluding the data from samples with largest D_{number}, and (3)

the last 30 equations, excluding the data from samples with smallest D_{number}. The three sets of γ_i from these calculations are quite different from each other (data are not shown). Figure B.10 presents the Γ spectra of three samples obtained by the γ_i sets calculated from three different $N_{j,i}$ and A_j sets described above. For sample with the smallest D_{number} (Figure B.10A), Γ spectra represented by black solid line and red dash line are obtained from γ_i calculated from $N_{j,i}$ and A_j sets (1) and (2), which include the information of this sample, while the one represented by the green dash line, which is quite different from the other two, is the value predicted by γ_i calculated from $N_{j,i}$ and A_j sets (3) excluding size distribution data of this sample. For sample with the D_{number} = 132 nm, all three data sets used to calculate Γ spectra in Figure B.10B include the $N_{j,i}$ and A_j data of this sample. The three calculated Γ for this sample are quite similar. The exclusion of information of the sample with the D_{number}(max) = 179 nm during the calculation using data set (3) causes the differences between Γ spectra represented by the red dash line and the other two (Figure B.10C).

Spectra in Figure B.10 suggest that our method to calculated Γ is greatly dependent upon the data set and that it could only be used to calculate Γ values for samples with known size distribution, C_{60} concentration, and original UV-Vis spectra and should not be used to predict the Γ value for samples with unknown size distributions.

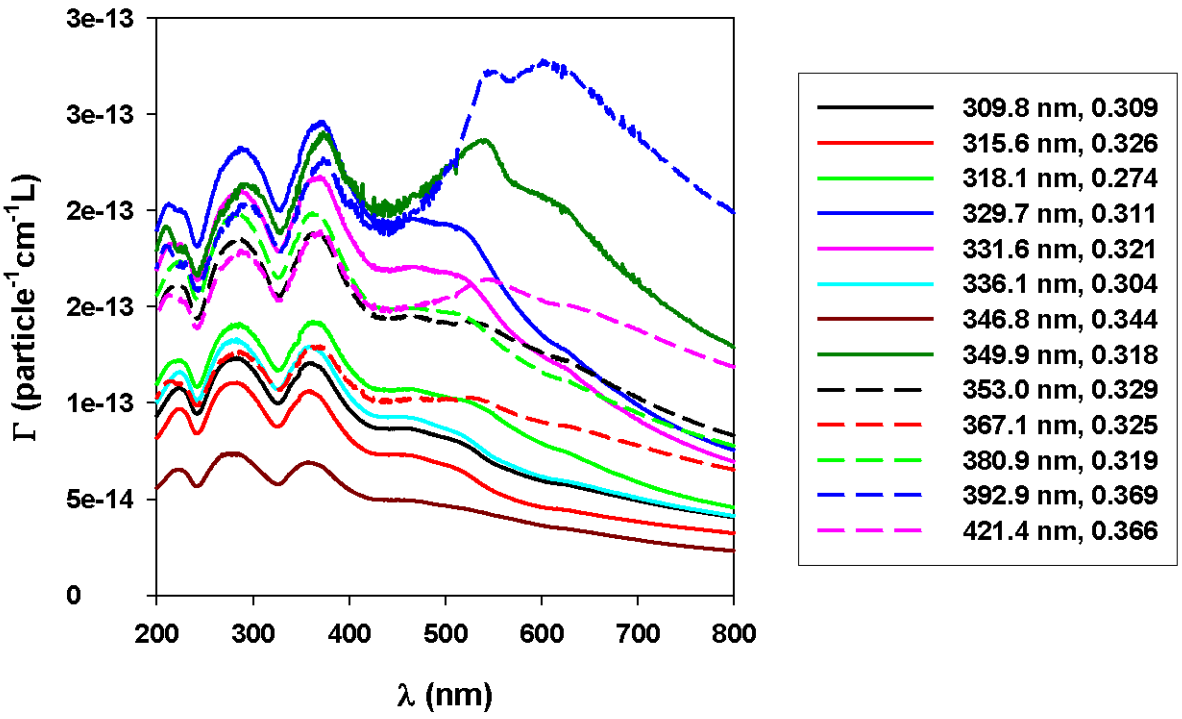

Figure B.7 Γ spectra: settled samples with Z_{ave} from 310 to 421 nm.

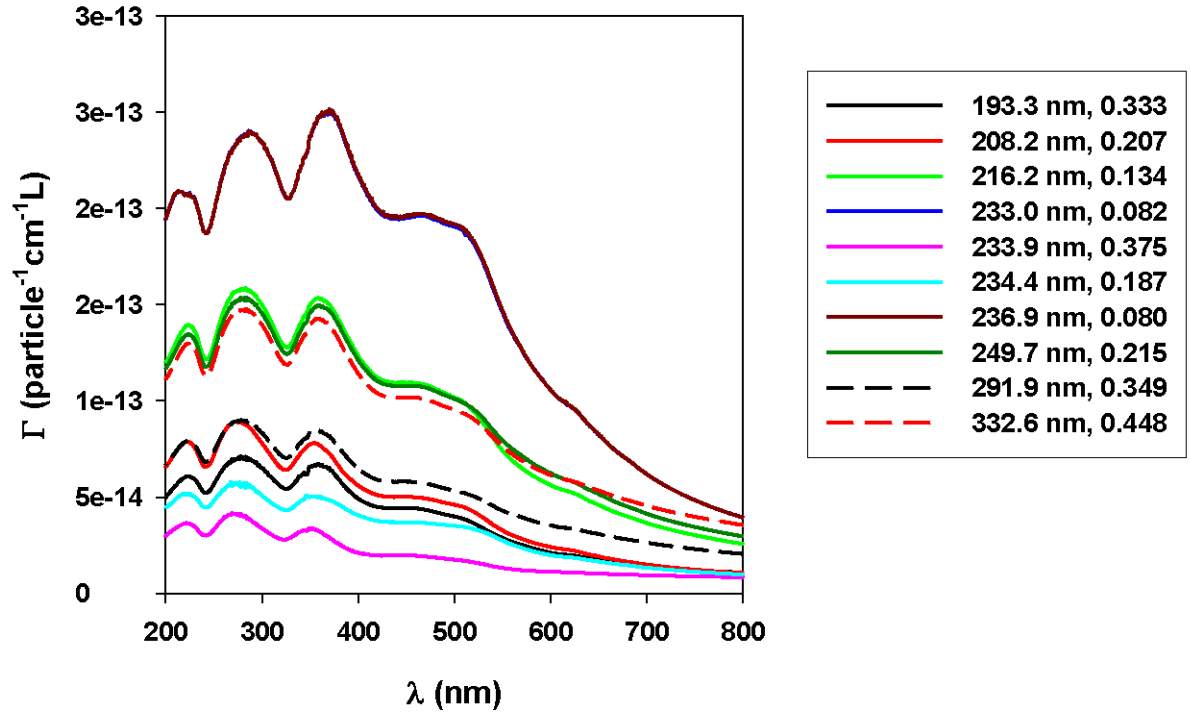

Figure B.8 Γ spectra: centrifuged samples.

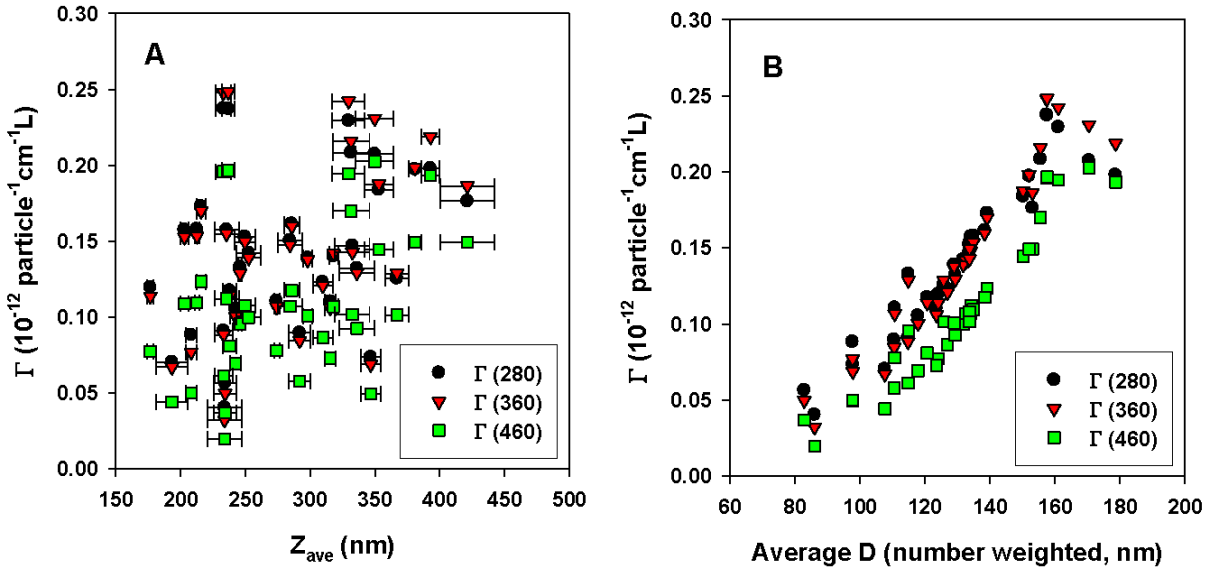

Figure B.9 Γ values at 280, 360, and 460 nm as a function of (A) Z_{ave} (The Z_{ave} value represented in this figure is the average of three measurements and the error bar represents the standard deviation of three measurements.) and (B) number weighted average particle diameter.

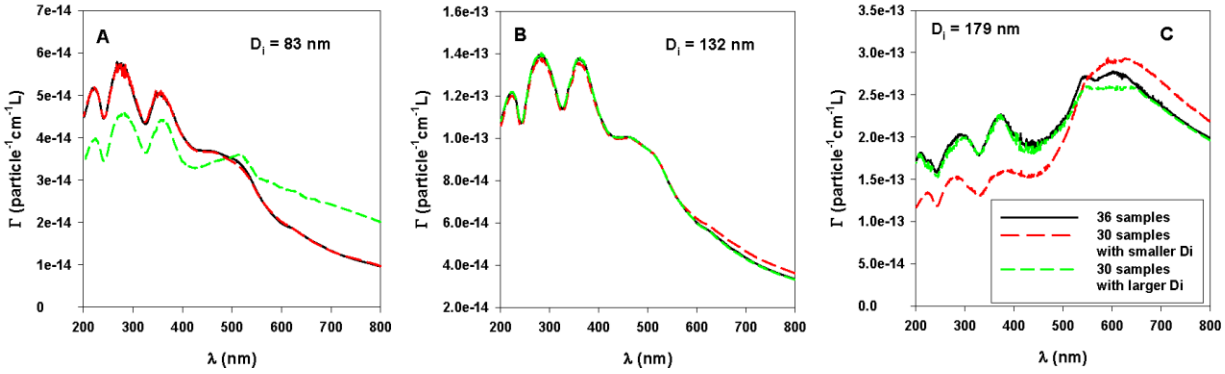

Figure B.10 Γ spectra calculated based on three different data sets. Black solid line: data from all 36 samples are used in calculation; red dash line: data from 30 samples with smaller D_{number} are used in calculation; Green dash line: data from 30 samples with larger D_{number} are used in calculation. (A) D_{number} = 83 nm; (B) D_{number} = 132 nm; (C) D_{number} = 179 nm.

The validity of Γ calculation. Normalized UV-Vis absorption spectra: $Relative\ ABS(\lambda) = \frac{ABS(\lambda)}{ABS(360)} = \frac{l\sum_i N_i\gamma_i(\lambda)}{l\sum_i N_i\gamma_i(360)} = \frac{\sum_i N_i\gamma_i(\lambda)}{\sum_i N_i\gamma_i(360)}$. Normalized Γ spectra: $Relative\ \Gamma(\lambda) = \frac{\Gamma(\lambda)}{\Gamma(360)} = \frac{l\sum_i p_i\gamma_i(\lambda)}{l\sum_i p_i\gamma_i(360)} = \frac{\sum_i p_i\gamma_i(\lambda)}{\sum_i p_i\gamma_i(360)}$. Therefore, $\frac{Relative\ ABS(\lambda)}{Relative\ \Gamma(\lambda)} = \frac{\sum_i N_i\gamma_i(\lambda)}{\sum_i p_i\gamma_i(\lambda)} \cdot \frac{\sum_i p_i\gamma_i(360)}{\sum_i N_i\gamma_i(360)}$. Because of the relationship between N_i and p_i from Eqn. B.3, there is $\frac{Relative\ ABS(\lambda)}{Relative\ \Gamma(\lambda)} = 1$, indicating that the

normalized absorption spectrum and normalized Γ spectrum for the same aq/nC$_{60}$ suspension should be identical. This result can be used as a criterion to justify the validity of the Γ calculation based upon particle size distributions: Great differences between normalized UV-Vis spectrum and normalized Γ spectrum indicate that Γ values obtained by Eqn B.4 using γ_i from Eqns. B.9 are not valid.

The comparison between the normalized UV-Vis spectra and Γ spectra (Figure B.11) show that the fraction of larger particles (D_i > 400 nm) is a key factor that affects the validity of the calculation. Figures B.11A and B.11B (top row) show that samples with P_{400} (fraction of particles with D_i > 400 nm) less than 0.5% have identically or quite similarly shaped normalized UV-Vis spectra and Γ spectra. For samples with 0.5% < P_{400} <1%, the two normalized spectra are still similar in the 200-400 nm region (Figure B.11C, bottom row left). While the normalized spectra show significantly large values in the 500-800 nm region for samples with P_{400} > 1% (Figure B.11D, bottom row right), indicating that the calculated Γ values for these samples in the 500-800 nm region are not valid.

However, the identical shape of normalized UV-Vis spectra and Γ spectra is only the necessary condition of the validity of Γ calculation. The Γ calculations for samples shown in Figures B.11A and B.11B are not necessarily valid.

$\frac{Relative\ ABS(\lambda)}{Relative\ \Gamma(\lambda)} = 1$ also indicates that samples has different normalized UV-Vis spectra would not have converged Γ spectra. Similar conclusions can be drawn for both ε and γ spectra for different aq/nC$_{60}$ samples. These results suggest that the positions of absorption maxima, the bandwidths, and the relative absorption intensities of a spectrum do not change during the conversion from original UV-Vis spectra to extinction (ε, γ, or Γ) spectra.

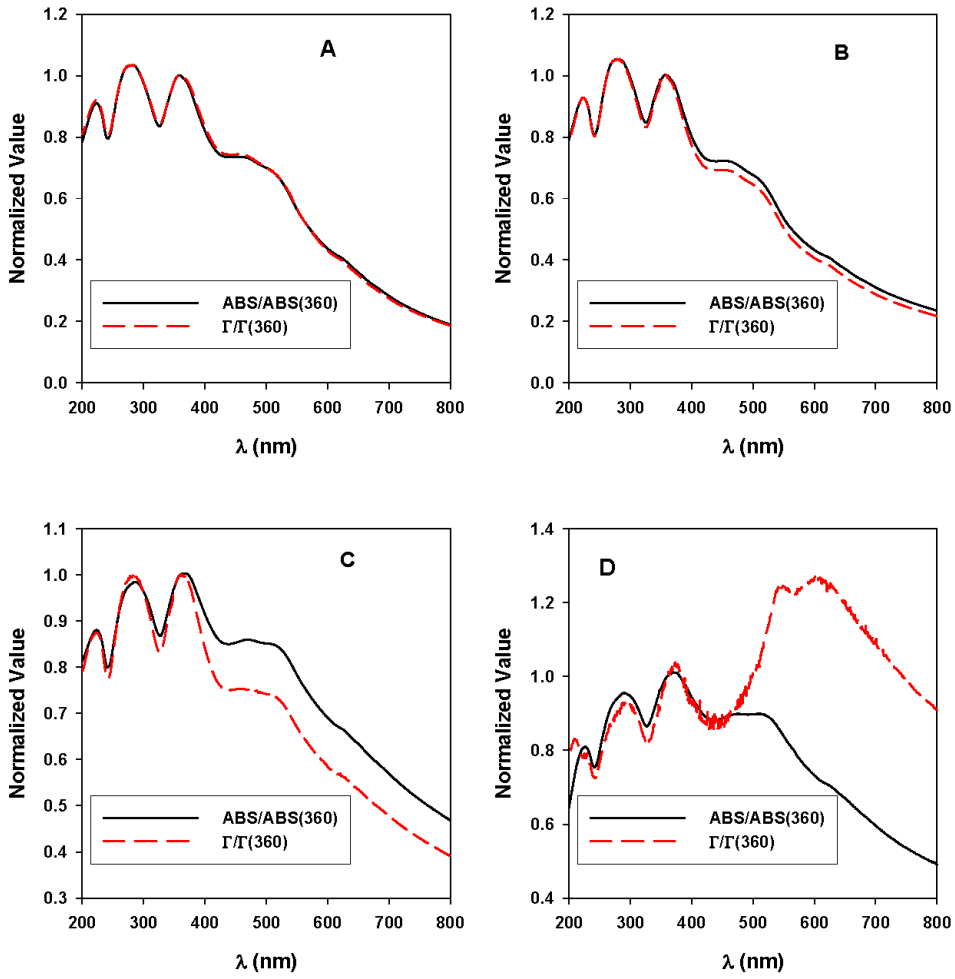

Figure B.11 Normalized original UV-Vis absorption spectra and calculated Γ spectra for different samples.

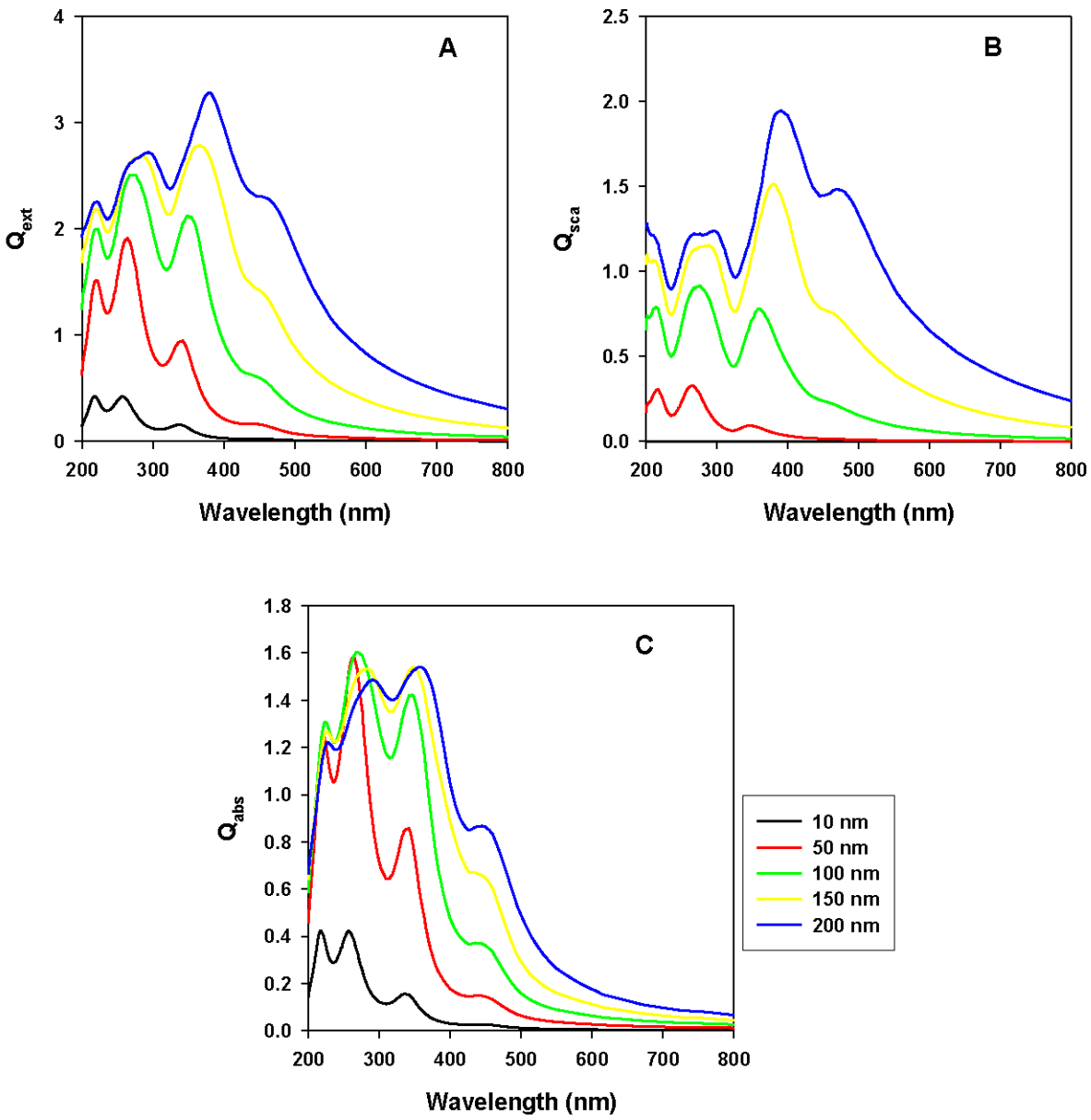

Figure B.12 Extinction, scattering, and absorption spectra of monodisperse spherical aq/*n*C_{60} nanoparticles plotted by Mieplot.

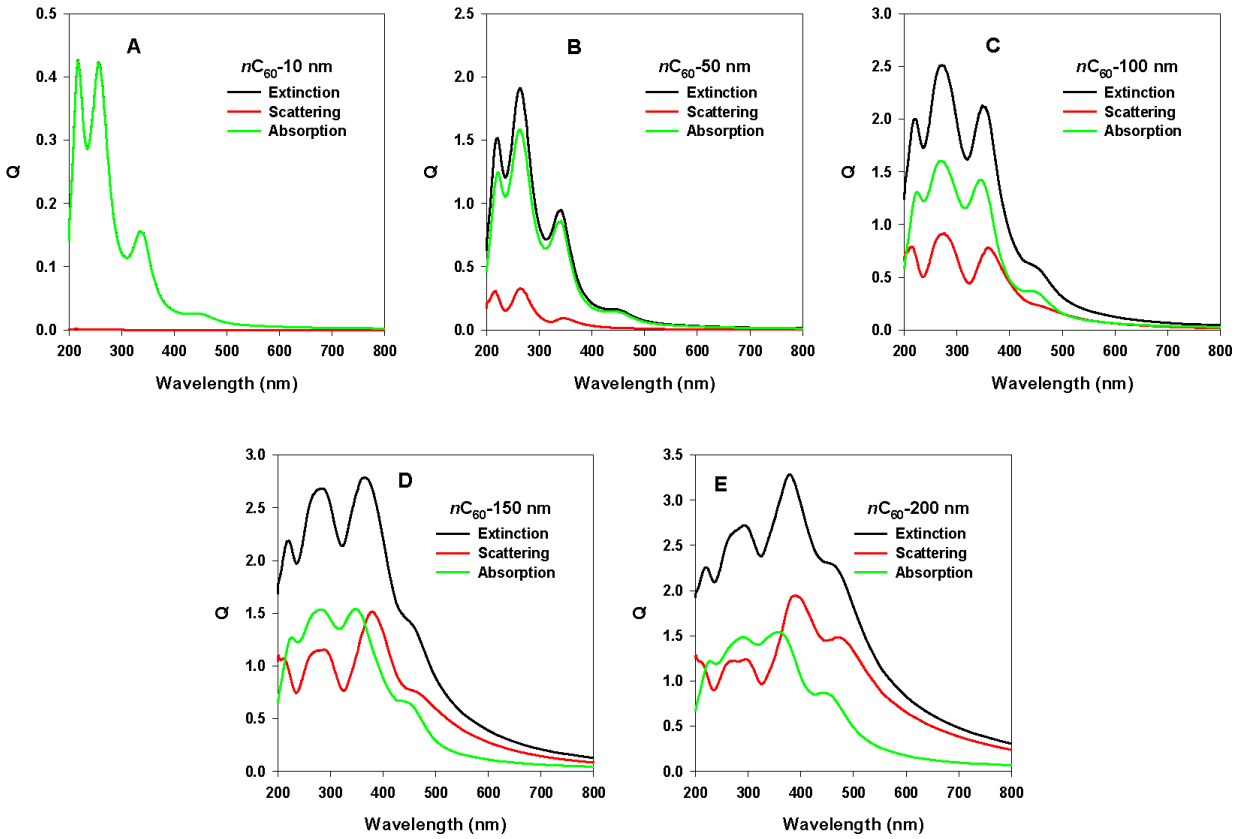

Figure B.13 Extinction, scattering, and absorption spectra of monodisperse spherical aq/nC$_{60}$ nanoparticles with different size plotted by Mieplot

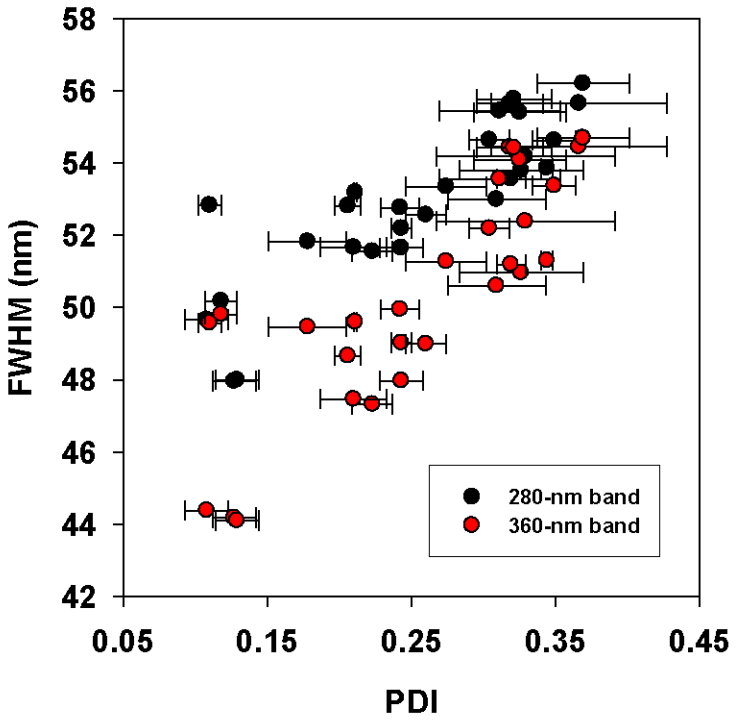

Figure B.14 The full widths at half maximum (FWHM) of the 360- and 280-nm bands as a function of the polydispersity indices. The horizontal error bar represents the standard deviation of three measurements for each sample. (The PDI value represented in this figure is the average of three measurements and the error bar represents the standard deviation of three measurements.)

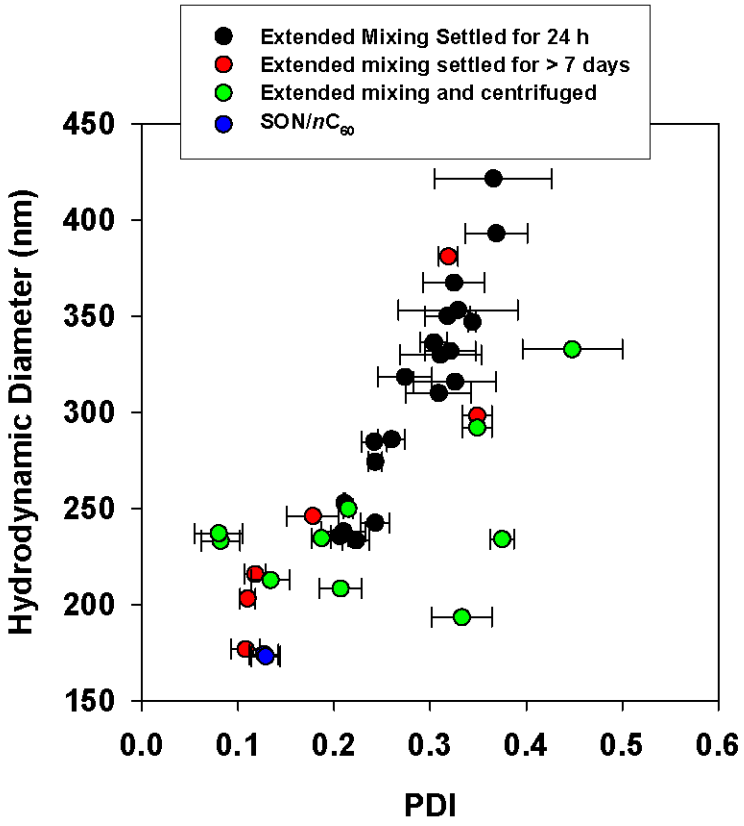

Figure B.15 Average particle size as a function of polydispersity of nC_{60}. (The PDI value represented in this figure is the average of three measurements and the error bar represents the standard deviation of three measurements.)

The Estimation of Z_{ave} for an aq/$n$$C_{60}$ suspension based on the absorption maximum positions of its UV-Vis Spectra

The position of an absorption maximum (λ_{max}) is the information that can be directly obtained from a spectrum of an aq/$n$$C_{60}$ suspension. Although it has been reported that $\lambda_{max}(280)$ and $\lambda_{max}(360)$ increased with Z_{ave} (Figure 4.5A), the linear relationships between $\lambda_{max}(280)$/ $\lambda_{max}(360)$ are not good enough to be directly used to predict average particle size of an aq/$n$$C_{60}$ suspension. However, using the bandwidth as a medium, the linear relationship between λ_{max} and the bandwidth (FWHM) of the same absorption band and that between FWHM and Z_{ave} (Table B.1) can be used to predict the average particle size of an aq/$n$$C_{60}$ sample with its UV-Vis spectral properties.

Table B.1 Regression results for Figures 4.4C and 4.4A

	Linear Relationships		R^2
Figure 4.4C	FWHM(280) = (0.4758 ±0.0596)$\lambda_{max}(280)$ + (-82.11 ±16.98)[a]	(B.10)	R^2 = 0.9186
	FWHM(360) = (0.4631 ±0.0797)$\lambda_{max}(360)$ + (-117.35 ±28.96)	(B.11)	R^2 = 0.8569
Figure 4.4A	Z_{ave} = (32.14 ±7.09)FWHM(280) + (-1417.97 ±378.52)	(B.12)	R^2 = 0.7849
	Z_{ave} = (21.13 ±4.50)FWHM(360) + (-785.24 ±229.20)	(B.13)	R^2 = 0.7988

[a]The error of the fit parameters represents 95% confidence interval.

A calculation example:

For the aq/$n$$C_{60}$ shown in Figure 4.2A with [C_{60}] = 0.055 mM and Z_{ave} = 274.1 nm, its $\lambda_{max}(280)$ and $\lambda_{max}(360)$ were 283 and 359 nm, respectively. Using this two values we calculated that the FWHM(280) and FWHM(360) by Eqns. B.10 and B.11, respectively. And the two FWHM values were then applied in Eqns. B.12 and B.13 to calculated Z_{ave}. The Z_{ave} values calculated from $\lambda_{max}(280)$ and $\lambda_{max}(360)$ for this sample were 271.5 and 256.6 nm, which were both in the error range less than 10% of the Z_{ave} determined by DLS. Table B.2 lists the estimated Z_{ave} by this method and their errors compared with the measured DLS values.

Table B.2 Comparison between DLS determined Z_{ave} and Z_{ave} estimated by UV-Vis spectral properties.

Sample No.	Position of absorption maximum (nm)		Z_{ave} determined by DLS (nm)	Z_{ave} estimated (nm)		Estimation Error (%)	
	$\lambda_{max}(280)$	$\lambda_{max}(360)$		by $\lambda_{max}(280)$	by $\lambda_{max}(280)$	by $\lambda_{max}(280)$	by $\lambda_{max}(280)$
1	276	356	176.7	168.3	226.8	-4.8	28.3
2	285	360	203	301.0	266.6	48.3	31.3
3	281	359	245.9	242.0	256.6	-1.6	4.4
4	278	358	215.7	197.8	246.7	-8.3	14.4
5	286	366	353	315.8	326.3	-10.5	-7.5
6	285	360	309.8	301.0	266.6	-2.8	-13.9
7	283	359	274.1	271.5	256.6	-0.9	-6.4
8	288	370	421.4	345.3	366.2	-18.1	-13.1
9	288	370	367.1	345.3	366.2	-5.9	-0.3
10	287	367	336.1	330.5	336.3	-1.7	0.1
11	289	372	392.9	360.0	386.1	-8.4	-1.7
12	289	371	329.7	360.0	376.1	9.2	14.1
13	287	362	315.6	330.5	286.5	4.7	-9.2
14	289	372	349.9	360.0	386.1	2.9	10.3
15	289	372	331.6	360.0	386.1	8.6	16.4
16	287	362	346.8	330.5	286.5	-4.7	-17.4
17	284	362	318.1	286.3	286.5	-10.0	-9.9
18	284	359	284.5	286.3	256.6	0.6	-9.8
19	284	359	285.8	286.3	256.6	0.2	-10.2
20	285	360	252.6	301.0	266.6	19.2	5.5
21	285	359	235.5	301.0	256.6	27.8	9.0
22	283	358	242.4	271.5	246.7	12.0	1.8
23	279	358	233.2	212.5	246.7	-8.9	5.8
24	281	360	237.9	242.0	266.6	1.7	12.1
25	287	368	380.9	330.5	346.3	-13.2	-9.1
26	285	362	298.1	301.0	286.5	1.0	-3.9

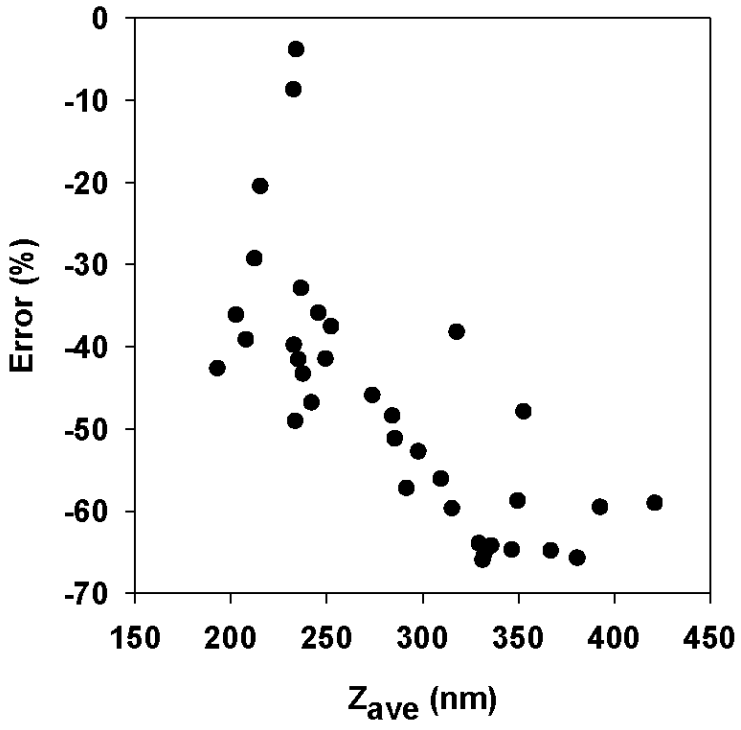

Figure B.16 Error of calculated [C_{60}] based upon the ε(360) of aq/*n*C_{60} with the smallest Z_{ave} (176.7 nm) as a function of average particle size. Error = (calculated [C_{60}]-[C_{60}] determined by TOC)/ [C_{60}] determined by TOC.

Appendix C: Supporting Information for Chapter 6

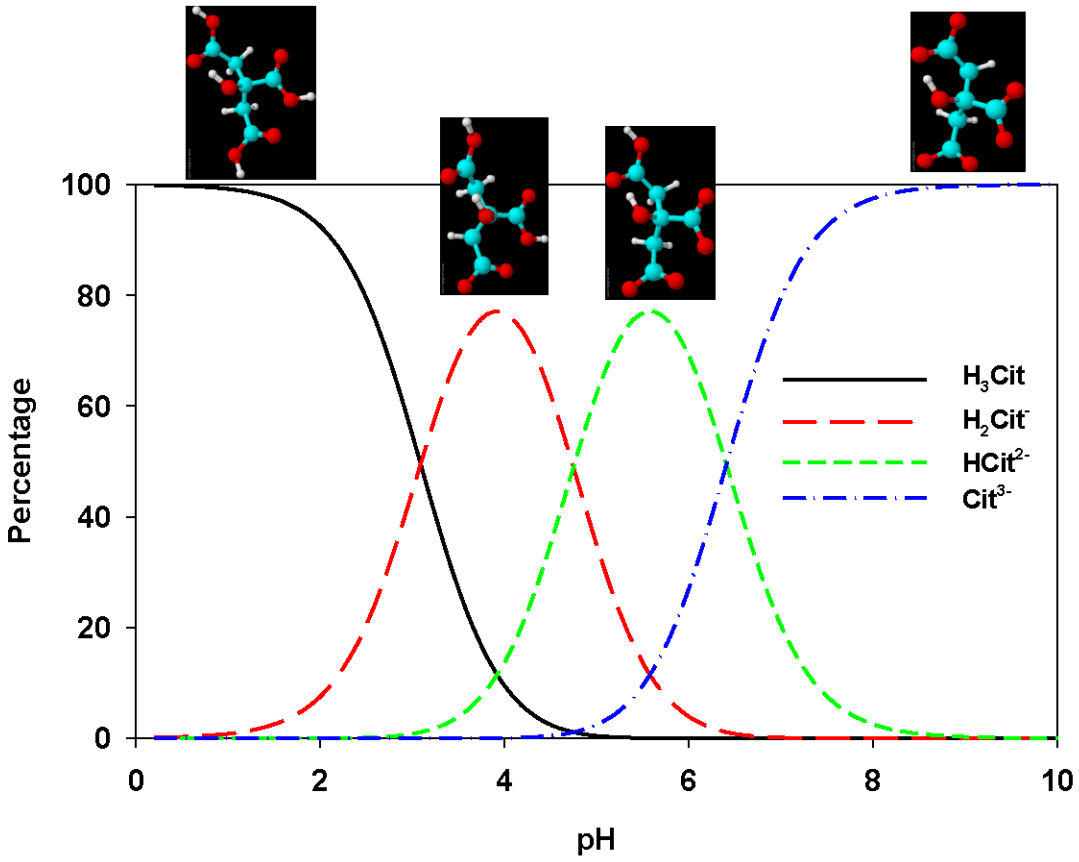

Figure C.1 Distribution of citrate as a function of solution pH.

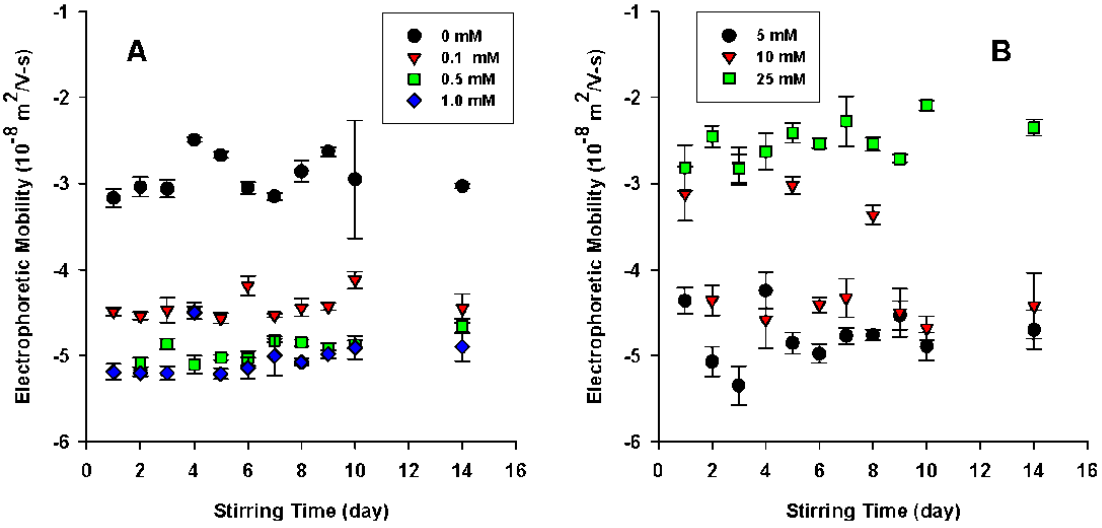

Figure C.2 EM of nC_{60} as a function of stirring time: (A) [Na_3Cit] = 0-1.0 mM and (B) [Na_3Cit] = 5-25 mM. (Each data point represents the average of three measurements for one sample and the error bar represents the standard deviation. Note: To enhance the clarity of the figures, data for cit/nC_{60} produced in 0.01, 0.03, 0.05, 0.07, 0.3, 0.7, 3.0, and 15.0 mM Na_3Cit solutions are not presented.)

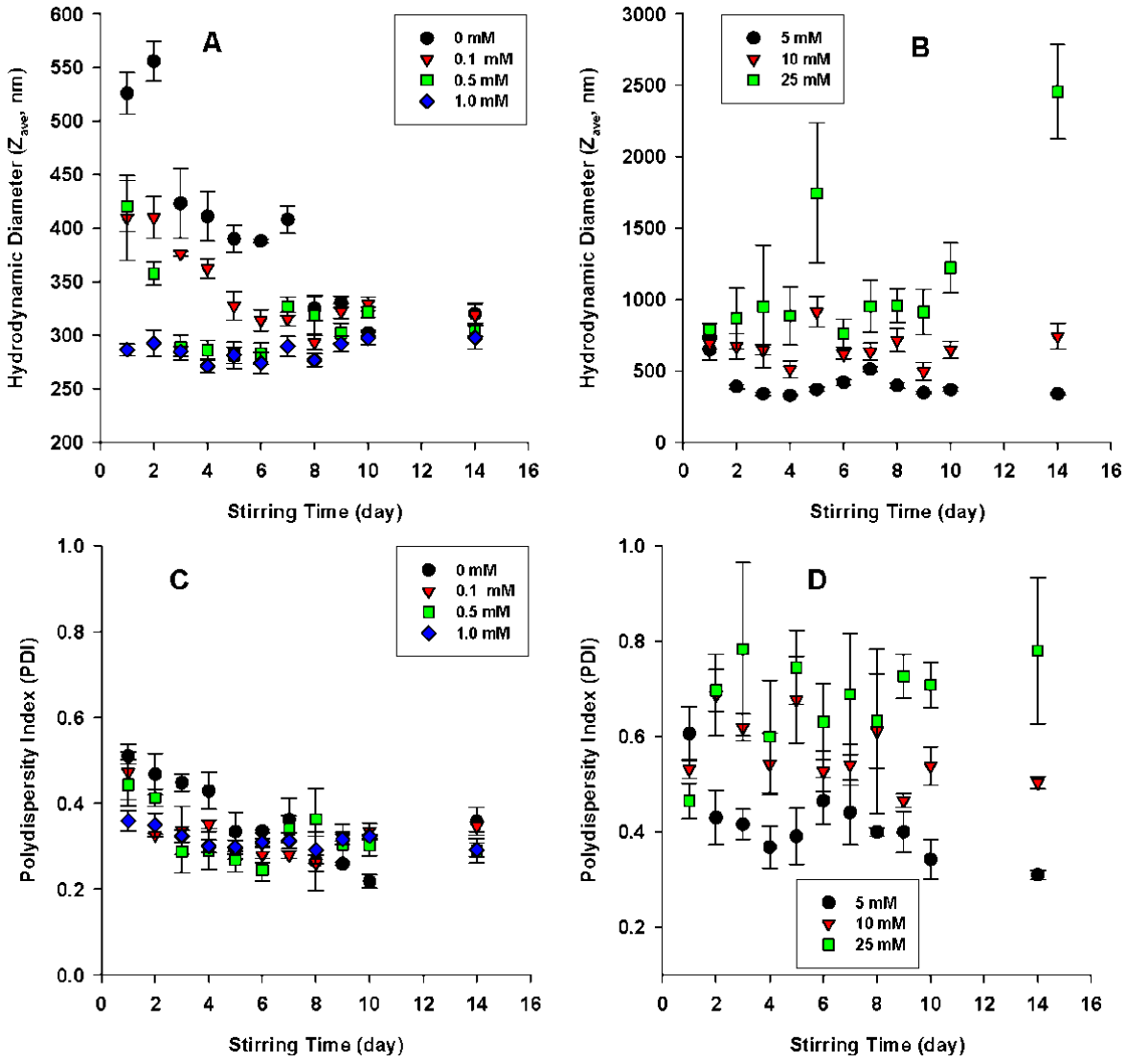

Figure C.3 Average particle size of nC$_{60}$ as a function of stirring time: (A) [Na$_3$Cit] = 0-1.0 mM, (B) [Na$_3$Cit] = 5-25 mM; Polydispersity index of nC$_{60}$ as a function of stirring time: (C) [Na$_3$Cit] = 0-1.0 mM, (D) [Na$_3$Cit] = 5-25 mM. (Each data point represents the average of three measurements for one sample and the error bar represents the standard deviation. Note: To enhance the clarity of the figures, data for cit/nC$_{60}$ produced in 0.01, 0.03, 0.05, 0.07, 0.3, 0.7, 3.0, and 15.0 mM Na$_3$Cit solutions are not presented.)

pH Regulation by Citrate.

In the experiments discussed in the main paper (Chapter 6), Na_3Cit was used to adjust the citrate concentration. Unfortunately, the variation in Na_3Cit simultaneously alters both pH and $[Na^+]$ and thus the results shown in Figure 6.2 cannot be unambiguously attributed to citrate changes alone. To evaluate the pH-regulating role of citrate, cit/nC$_{60}$ was produced in citrate buffers over the [total citrate] (= $[Na_3Cit]$ + $[H_3Cit]$) range of 0.1-25 mM. The use of citrate buffers produced solutions with a fixed [total citrate], but variable pH and ionic strength by adjusting the fractions of H_3Cit and Na_3Cit. In these buffers, solution pH increased with the ratio of $[Na_3Cit]$ to [total citrate] and ranged from 2.66 (25 mM H_3Cit) to 7.87 (25 mM Na_3Cit).

Over the [total citrate] range from 0.1 to 1.0 mM, the EM value of a cit/nC$_{60}$ suspension was solely dependent on its pH (Figure C.4A). This relationship between EM and pH is consistent with the variable $[Na_3Cit]$ experiment and collectively these results indicate that pH, which is fixed by the citrate content, regulates the cit/nC$_{60}$ surface charge at low $[Na^+]$. Interestingly, despite the fact that their solution pH and EM varied widely, cit/C$_{60}$ suspensions produced in these buffers generally had a similar average size of ≈300 nm after 14-day stirring (Range: 250 to 350 nm; Figure C.4B). Cit/nC$_{60}$ produced in 1 mM H_3Cit was an exception; its larger average particle size (860 ± 3.3 nm) can be attributed to its weak surface charge (-0.01 ± 0.02 $\times 10^{-8}$ m^2/V-s) that destabilized the particles. The general insensitivity of Z_{ave} to pH, [total citrate], and $[Na^+]$ under these conditions corroborates the results previously obtained in variable $[Na_3Cit]$ experiments. In the cit/nC$_{60}$ suspensions produced in buffers with [total citrate] ≥ 5 mM the EM values generally became more negative with an increase in pH as well. However, as discussed previously, the high $[Na^+]$ in these suspensions resulted in low nC$_{60}$ concentrations, leading to significant fluctuations in EM and large Z_{ave} values with large error bars (data not shown).

In buffers with pH < 3, EM of cit/nC$_{60}$ fluctuated between negative and positive values during the stirring period. Under these conditions, nC$_{60}$ had a weak and unstable surface charge. Nonetheless, after 14-day stirring the supernatants of these samples were yellow to light brown in color – indicative of cit/nC$_{60}$. The presence of cit/nC$_{60}$ in these supernatants was confirmed by UV-Vis and TEM (not shown). nC$_{60}$ particles in these solutions had a low electrostatic barrier against aggregation and ultimately aggregated and settled out of solutions after 9-months of storage in the dark, leaving clear supernatants. For samples with more negative EM values, a significant amount of cit/nC$_{60}$ particles remained in supernatants after 9-months settling. The disparity between these cit/nC$_{60}$ suspensions suggests that although surface charge does not necessarily dictate nC$_{60}$ formation, it does affect its ultimate aggregation and deposition.

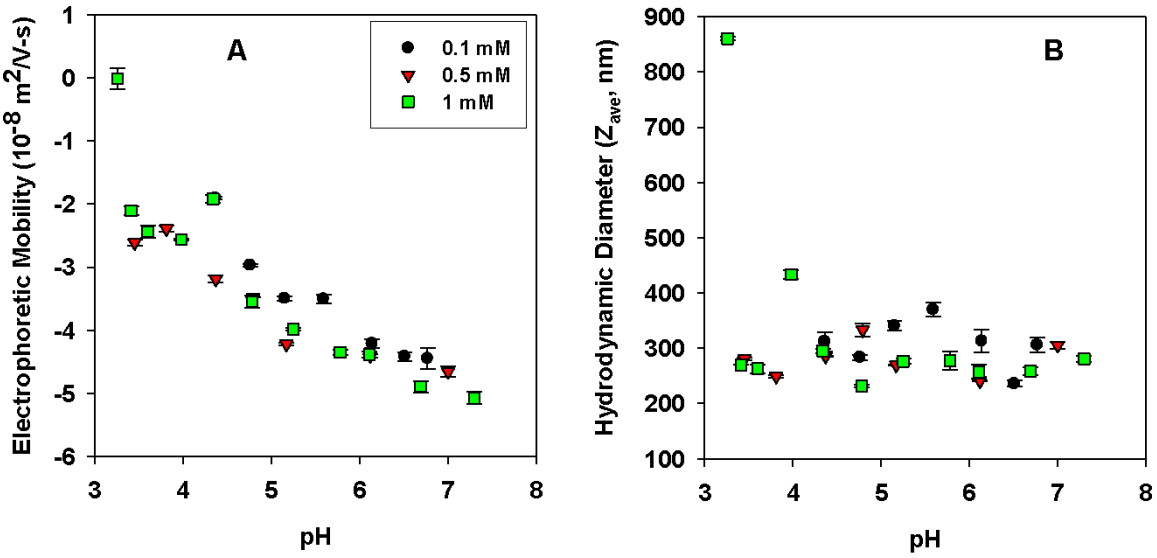

Figure C.4 (A) EM and (B) Z_{ave} of cit/nC$_{60}$ in citrate buffers after 14-days stirring as a function of pH. (Each data point represents the average of three measurements for one sample and the error bar represents the standard deviation.)

[Na^+] Effects.

In the citrate buffer and variable [Na_3Cit] experiments, [Na^+] was set by [Na_3Cit]. To isolate the effects of [Na^+] we conducted experiments wherein [Na^+] was varied in solutions with fixed [total citrate] = 0.5 mM at pH values of 3.6 (set by 0.5 mM H_3Cit) and 6.9 (set by 0.5 mM Na_3Cit). These experiments were conducted at an elevated temperature of 50 ºC to accelerate nC_{60} production. We note that the surface charge and average size of the particles produced at 50 ºC were similar to those produced at 30 ºC (Figure C.5). Similar to the trends described previously, pH dictated the nC_{60} surface charge in solutions with [Na^+] ≤ 15 mM (Figure C.6A). The EM values for the low pH samples were less negative than those for the high pH samples irrespective of [Na^+]. For solutions with [Na^+] ≥ 15 mM, however, EM became increasingly positive. This can be explained by the screening effect of the counterion since high ionic strengths are expected to decrease the surface charge.[59,60,64]

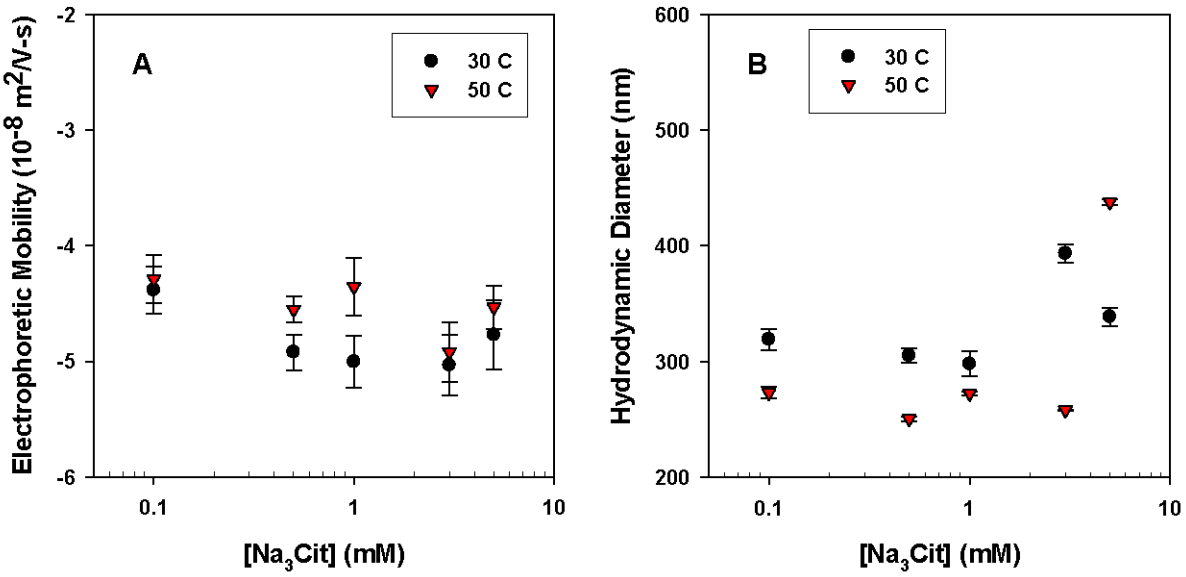

Figure C.5 (A) Surface charge and (B) average particle size of nC_{60} produced at different temperatures as a function of [Na_3Cit]. (Each data point represents the average of three measurements for one sample and the error bar represents the standard deviation.)

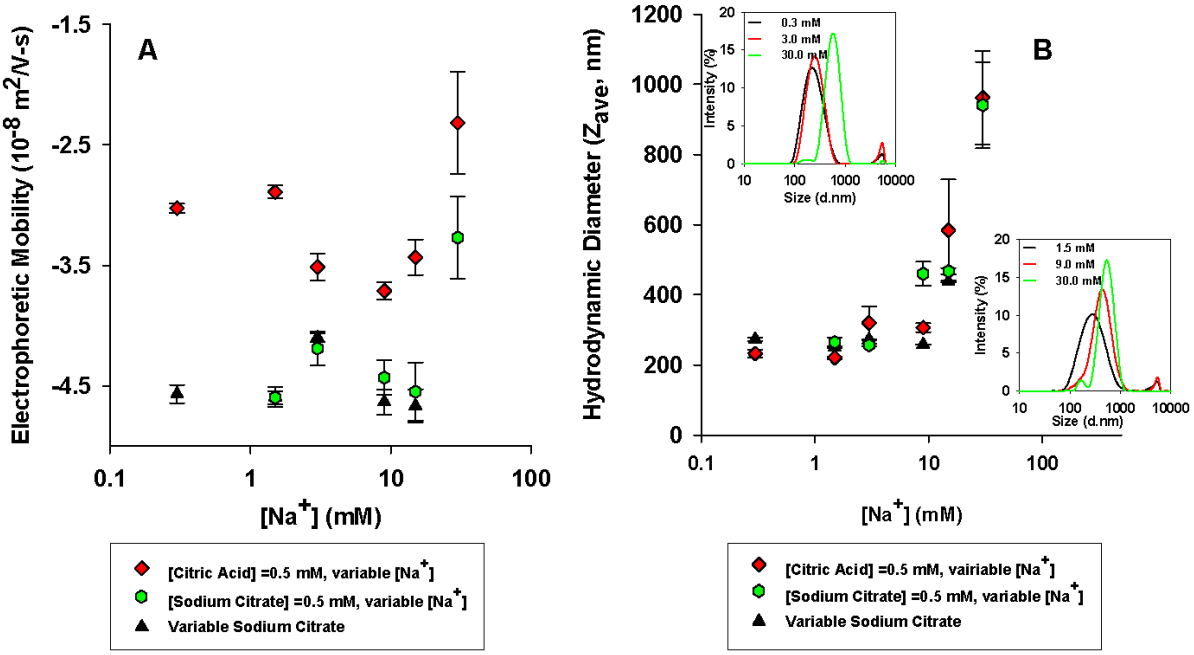

Figure C.6 (A) EM and (B) Z_{ave} of nC_{60} on day 14 as a function of [Na^+]; Intensity weighted particle size distribution of cit/nC_{60} produced in H_3Cit solutions with variable [Na^+] (left inset) and in Na_3Cit solutions with variable [Na^+] (right inset) after 14-day stirring and 24-h settling. (Each data point represents the average of three measurements for one sample and the error bar represents the standard deviation.)

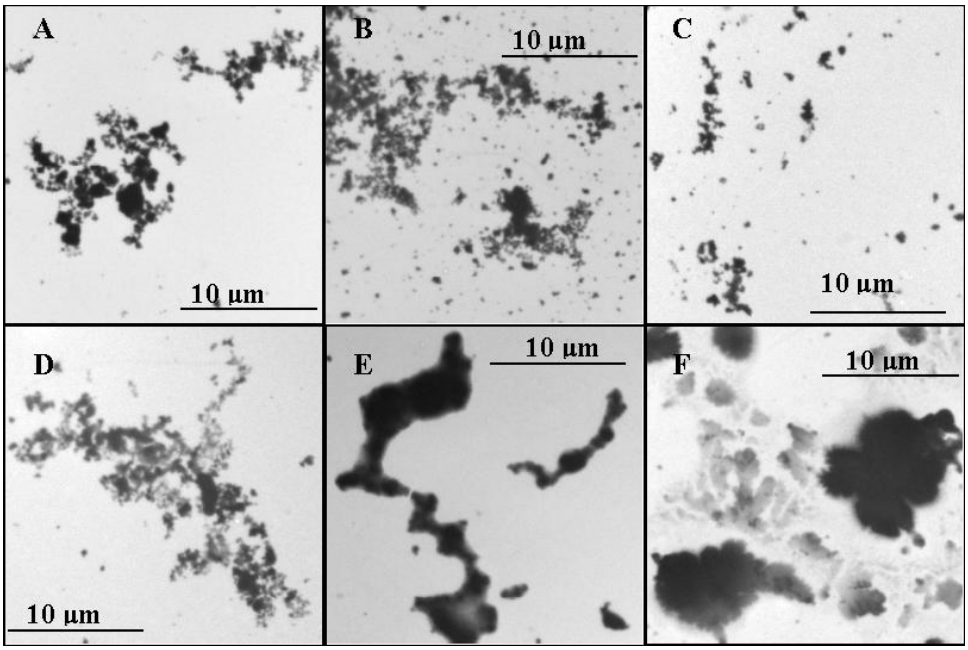

Figure C.7 Low resolution TEM images of cit/nC_{60} formed in 0.5 mM citric acid solutions with variable [Na^+]: (A) 0.3 mM, (B) 1.5 mM, (C) 3.0 mM, (D) 9.0 mM, (E) 15.0 mM, and (F) 30.0 mM.

Corroborating the previously presented results, Z_{ave} was insensitive to solution pH and was only affected by $[Na^+]$ for $[Na^+] > 10$ mM. Importantly, a less negative surface charge does not necessarily result in the formation of larger particles. For example, cit/nC$_{60}$ produced in a solution with 0.5 mM H_3Cit and 3 mM NaCl, had a smaller average size (220.0 ± 4.4 nm) than cit/nC$_{60}$ (265.0 ± 13.6 nm) produced in a solution with the same [total citrate] and $[Na^+]$, yet higher pH. However, the EM of the former (-2.89 ± 0.05 × 10^{-8} m^2/V-s) was considerably less negative than that of the latter (-4.60 ± 0.06 × 10^{-8} m^2/V-s). Figure C.6B and its insets show that in both solution series as $[Na^+]$ increased particle size distributions shifted to larger sizes. The argument that high $[Na^+]$ facilitates the formation of large cit/nC$_{60}$ particles is further supported by TEM images of cit/nC$_{60}$ produced in 0.5 mM H_3Cit solutions with variable $[Na^+]$. Figure C.7 shows images of a typical mesh on a given TEM grid. As shown in the low resolution images in Figures C.7A-D (0.3 mM ≤ [Na+] ≤ 9 mM), the majority of cit/nC$_{60}$ were small particles or aggregates comprised of these particles. The similarities in these aggregate structures and morphologies were consistent to their similar EM values and relatively small Z_{ave}. As $[Na^+]$ increased to 15 and 30 mM, however, large solid particles, whose formation was facilitated by the minimal surface charge became the predominant particle type.

Collectively the variable $[Na_3Cit]$, pH, ionic strength, and $[Na^+]$ studies have shown that solution pH is the primary parameter determining the surface charge of nC$_{60}$, that Z_{ave} is generally insensitive to EM and pH when $[Na^+] \leq 15$ mM, and that charge screening is an important factor that affects the nC$_{60}$ surface charge and increases its average size when $[Na^+]$ exceeds 15 mM.

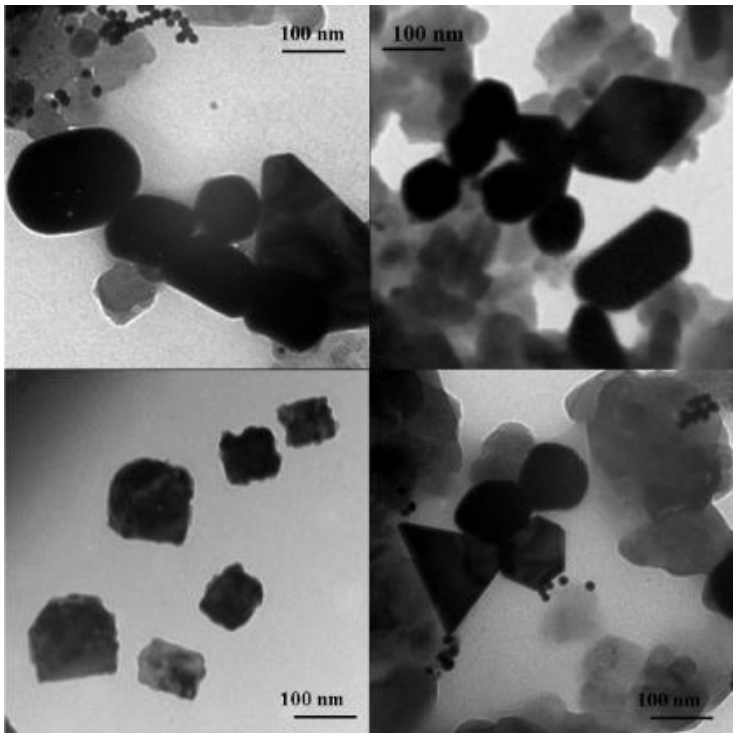

Figure C.8 TEM images of regularly shaped cit/*n*C_{60}.

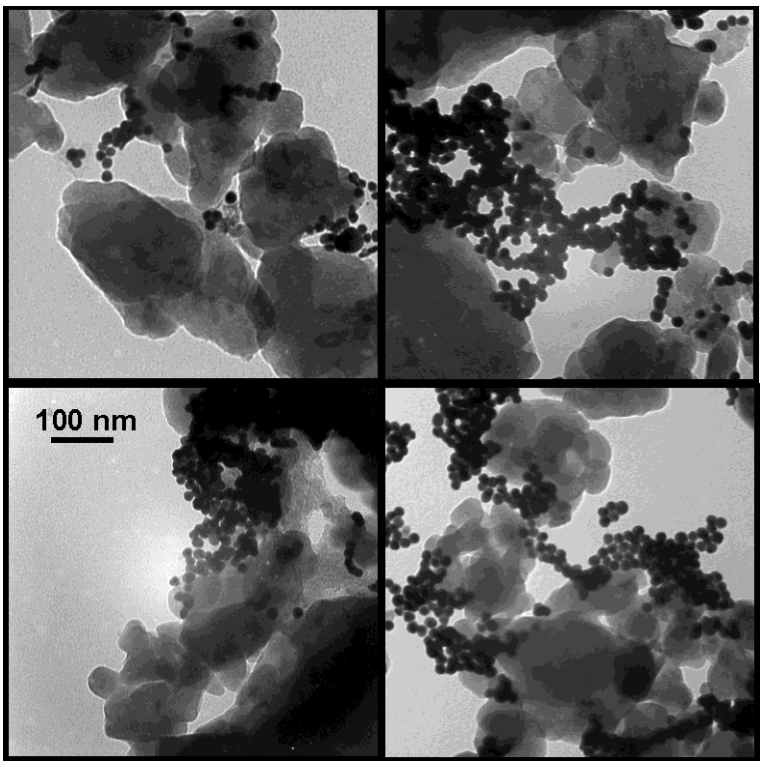

Figure C.9 TEM images of spherical particles in select areas near cracks and crevices in the large particles.

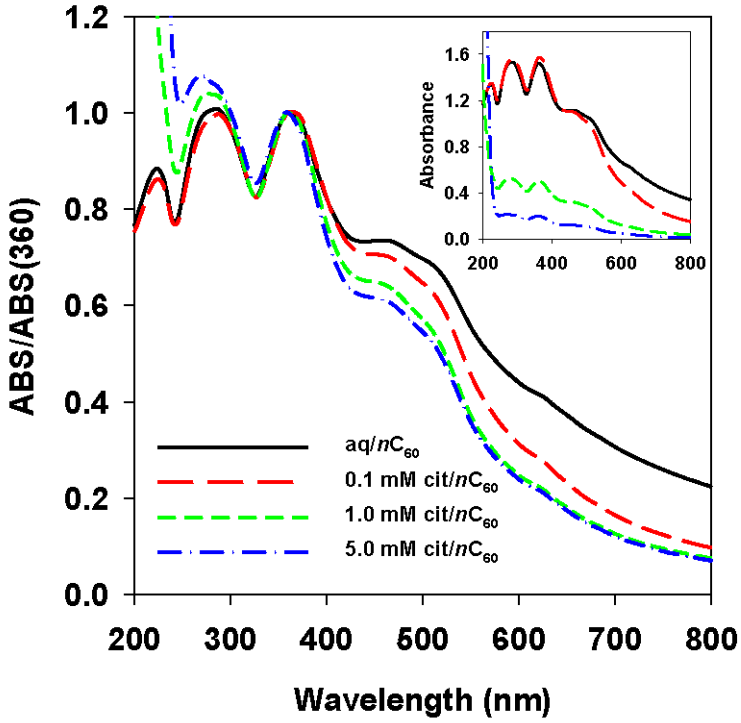

Figure C.10 Normalized spectra (For each sample, its absorbance (ABS) at a specific wavelength is divided by ABS at 360 nm.) for nC_{60} suspensions produced in four different solutions. Inset: the original UV-Vis spectra for these four suspensions.

Centrifugation of nC$_{60}$.

nC$_{60}$ suspensions were fractionated based on particle size by centrifugation. For an ideal suspension consisting of spherical particles, according to Stokes' law,[155] after a centrifugation period of t, the radius a of the largest particles remaining in the supernatant is proportional to the following parameter S:

$$a \propto S = \left[\frac{18\eta}{(\rho_0 - \rho_f)R\omega^2}\right]^{\frac{1}{2}} \quad \text{(C.1)}$$

where ρ_0 is the density of the particle; ρ_f is the fluid density; η is the fluid viscosity; ω is the angular velocity; and R is the distance from the rotor axis. In this experiment, ω and R were fixed while ρ_f and η remained roughly constant within the [Na$_3$Cit] range of 0 to 5 mM.[189] Therefore, particle sizes obtained from Eqn. C.1 for the four tested suspensions (aq/nC$_{60}$, 0.1 mM cit/nC$_{60}$, 1.0 mM cit/nC$_{60}$, and 5.0 mM cit/nC$_{60}$) should be the same despite their different solution chemistries if they all only contained spherical nC$_{60}$ particles. Based upon our observation, there was a decrease in average particle size with centrifugation time for all nC$_{60}$ suspensions (Figure C.11). However, despite its largest initial particle size, aq/nC$_{60}$ had the fastest decrease in Z_{ave} following centrifugation. The extent of reduction in Z_{ave} decreased with [Na$_3$Cit].

The discrepancy between the observed Z_{ave} in Figure C.11 and the theoretically calculated results based on Eqn. C.1 could be accounted for the difference surface charges of these particles and their inherent heterogeneity due to extended mixing. As discussed in the main paper the surface charge of nC$_{60}$ becomes more negative with [Na$_3$Cit]. The more negatively charged surfaces of 1.0 and 5.0 mM cit/nC$_{60}$ impede them from aggregating and precipitating during

centrifugation. On the other hand, based upon the modified Stokes' law, Eqn. C.2[190] calculates the velocity of an irregularly shaped particle during centrifugation.

$$v = \frac{K(\rho_0 - \rho_f)a_{eq}^2 R\omega^2}{18\eta}, K = 0.843lg\left(\frac{A_{eq}}{A \times 0.065}\right) \quad \text{(C.2)}$$

where a_{eq} and A_{eq} correspond to the diameter and area of the sphere with same volume as the particle, respectively. And K ≈ 2-4 for different shapes. This equation indicates that irregularly shaped particles with a_{eq} moves faster towards the bottom of centrifuge tubes than spheres with radius of a_{eq}. As presented in Figure 6.3, the small spherical particles that exist in 1.0 and 5.0 cit/nC$_{60}$ suspensions are more capable of resisting precipitation.

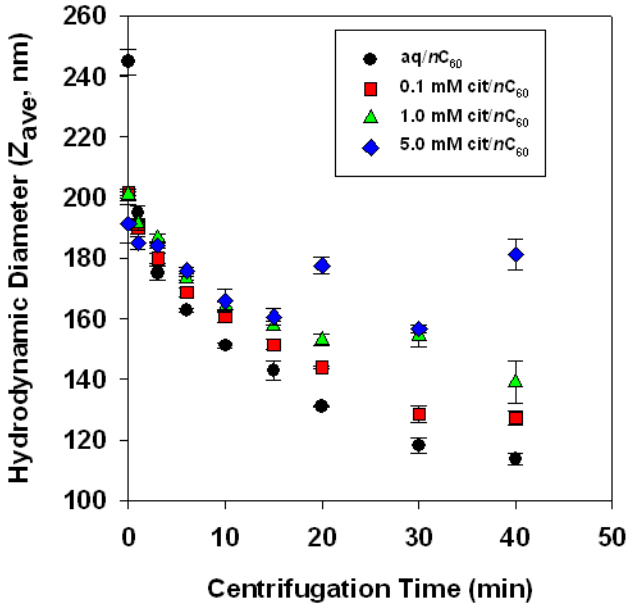

Figure C.11 Average particle size of nC$_{60}$ as a function of centrifugation time (The error bar represents the standard deviation of three measurements.).

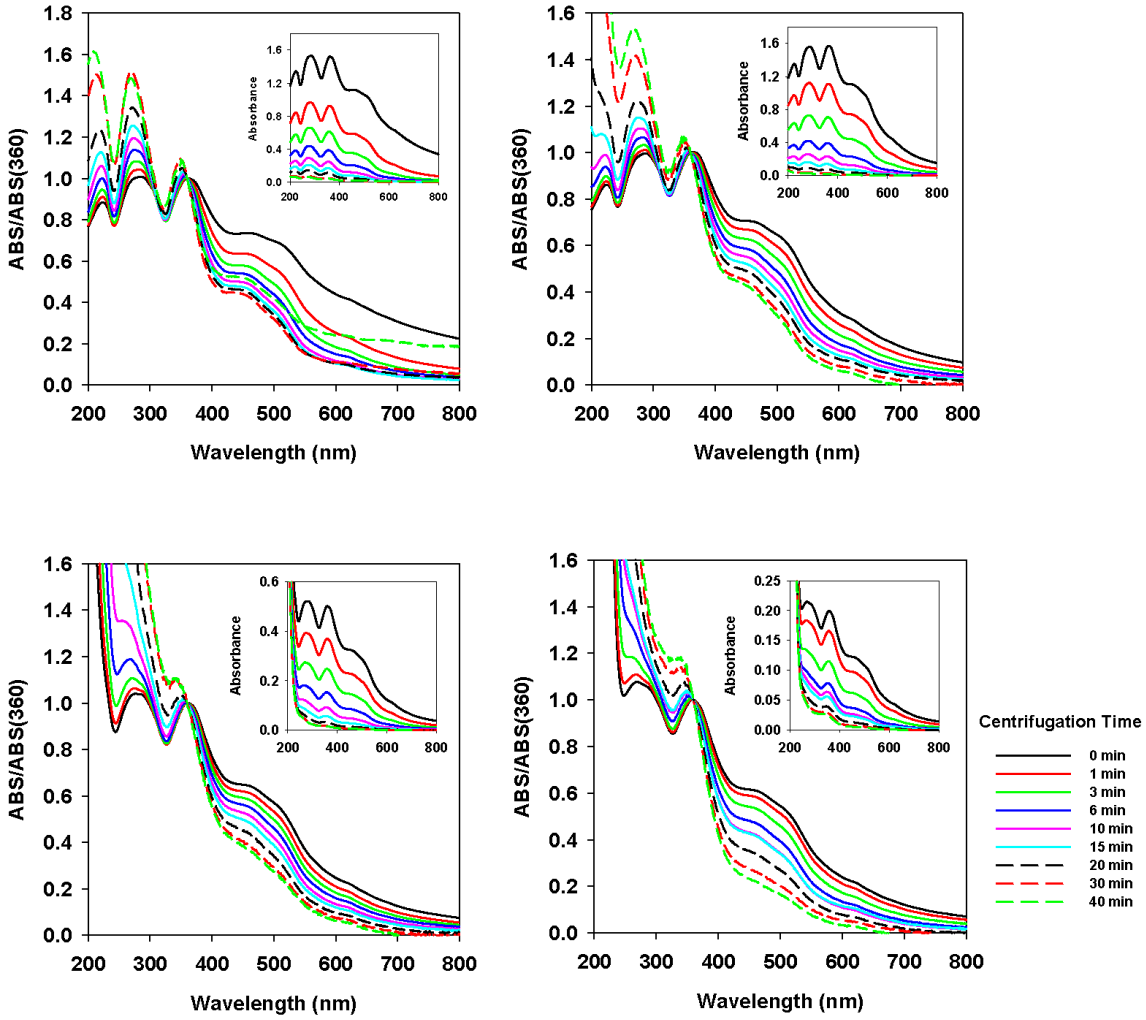

Figure C.12 Normalized UV-Vis spectra of centrifuged nC_{60}: (A) aq/nC_{60}, (B) 0.1 mM cit/nC_{60}, (C) 1.0 mM cit/nC_{60}, and (D) 1.0 mM cit/nC_{60}. Insets: the original UV-Vis spectra of centrifuged nC_{60} suspensions.

Aggregation behavior of nC$_{60}$

Experimental Methods. nC$_{60}$ stock suspensions, including aq/nC$_{60}$, 0.1, 0.5, and 1.0 mM cit/nC$_{60}$, were tested in aggregation kinetic experiments. The initial average size of these suspensions were 223.5 ± 3.4, 212.7 ± 0.4, 200.7 ± 5.4, and 180.8 ± 0.7 nm, respectively. Time-resolved DLS measurements were obtained to determine their aggregation kinetics. nC$_{60}$ suspensions and NaCl solutions were mixed at a volumetric ratio of 3:1 by hand. The mixtures were then transferred to a capillary disposable cuvette and the DLS measurement was started immediately. The tested [Na^+] ranged from 20 to 800 mM. The aggregation experiment for each mixture took one hour and the interval between two consecutive measurements was 15 seconds. The intensity-weighted hydrodynamic diameter of the mixture determined by the cumulant method was used to determine aggregation kinetics and attachment efficiencies for these nC$_{60}$ samples.

Results and Discussion. Time-resolved DLS is the most commonly used method to investigate the aggregation behavior of nanoparticles. The initial rate of increase in the hydrodynamic diameter (Z_{ave}) of a suspension with respect to time t is proportional to its initial particle number concentration N_0 and the initial aggregation rate constant k_{11}.[86] In the present study, for each type of nC$_{60}$ suspensions, N_0 was approximately fixed by a constant volumetric ratio in mixtures of the nC$_{60}$ stock suspension and the NaCl solution (V_{nC60}:V_{NaCl} = 3:1). Under these conditions, the attachment efficiency α was calculated as:

$$\alpha = \frac{1}{W} = \frac{k_{11}}{(k_{11})_{fast}} = \frac{k_{11}N_0}{(k_{11})_{fast}N_0} = \frac{\left(\frac{dZ_{ave}(t)}{dt}\right)_{t\to 0}}{\left(\frac{dZ_{ave}(t)}{dt}\right)_{t\to 0,fast}} \quad \text{(C.3)}$$

where W is the stability ratio and the subscript "fast" refers to diffusion-limited aggregation conditions. In previous studies,[30,31,112] the initial phase of aggregation was determined as the period before Z_{ave} reaches 1.25 times the initial average particle size ($Z_{ave, t=0}$). However, in the present study, because of high particle concentrations in stock nC$_{60}$ suspensions, it took less than 2 minutes for most samples to reach $1.25Z_{ave, t=0}$. Data collected during this time period were too few in number to accurately estimate k_{11}. Therefore, we slightly expanded the range to $2Z_{ave, t=0}$ to define the initial aggregation phase.

Figure C.13 presents aggregation profiles for four nC$_{60}$ suspensions. aq/nC$_{60}$, 0.1 mM cit/nC$_{60}$, and 0.5 mM cit/nC$_{60}$ readily aggregate at salt concentrations < 60 mM, whereas 1.0 mM cit/nC$_{60}$ did not start aggregating until [NaCl] exceeded 100 mM. Due to the dependence of the k_{11} value upon particle concentration (which varied greatly between the four nC$_{60}$ suspensions, Figure C.10 inset), we compared concentration normalized attachment efficiencies (α) instead of k_{11} to investigate the different aggregation behaviors of nC$_{60}$ produced in these solutions. In Figure C.14, attachment efficiencies are presented as a function of [NaCl]. Attachment efficiencies were calculated using Eqn. C.3, in which the $(k_{11})_{fast}$ value for each nC$_{60}$ suspension was defined at [NaCl] = 500 mM. In the absence of citrate, the aggregation behavior of aq/nC$_{60}$ was in good agreement with DLVO theory, which was similar to that of tol/nC$_{60}$[112] and SON/nC$_{60}$.[185] In the reaction-limited regime, α values of aq/nC$_{60}$ and 0.1 mM cit/nC$_{60}$ generally increased with [NaCl]. Once [NaCl] reached the CCC, the attachment efficiency was stable around 1. A previous study reported that the presence of NOM significantly reduced the aggregation nC$_{60}$.[30] However, in the present study, the presence of citrate did not prevent cit/nC$_{60}$ from aggregating. For 0.1 mM cit/nC$_{60}$ the critical coagulation concentration (CCC) of 100 mM was slightly lower than the CCC of 160 mM determined for aq/nC$_{60}$. In the reaction-limited regime (α < 1), 0.1 mM

cit/nC$_{60}$ had a higher α value than aq/nC$_{60}$ at the same [NaCl] level, indicating that 0.1 mM cit/nC$_{60}$ nanoparticles were more prone to attach to one another than aq/nC$_{60}$ nanoparticles. This behavior is contradictory to what might be expected based upon the surface charges of these nanoparticles: more negatively charged 0.1 mM cit/nC$_{60}$ particles should have lower α value than aq/nC$_{60}$ at the same [NaCl] level. Aggregation behavior of 0.5 and 1.0 mM cit/nC$_{60}$ did not strictly follow DLVO theory. No clear CCC values were observed for these two cit/nC$_{60}$ suspensions and they did not have an obvious diffusion-limited regime. We arbitrarily chose k_{11} values at [NaCl] = 500 mM as their $(k_{11})_{fast}$, α values of these two suspensions shown in Figure C.14 were relative values of k_{11} and were therefore not comparable to those of aq/nC$_{60}$ and 0.1 mM cit/nC$_{60}$. The propensity of 0.1 mM cit/nC$_{60}$ to aggregate and the inconsistent aggregation behavior of 0.5 and 1.0 mM cit/nC$_{60}$ could not be simply explained by their more negatively charged surfaces. Morphological differences (small spherical particles in 0.5 and 1.0 mM cit/nC$_{60}$ vs. larger irregular particle in aq/nC$_{60}$) could be responsible for the different aggregation behaviors.[191,192] The association between citrate and C$_{60}$ could be another origin.

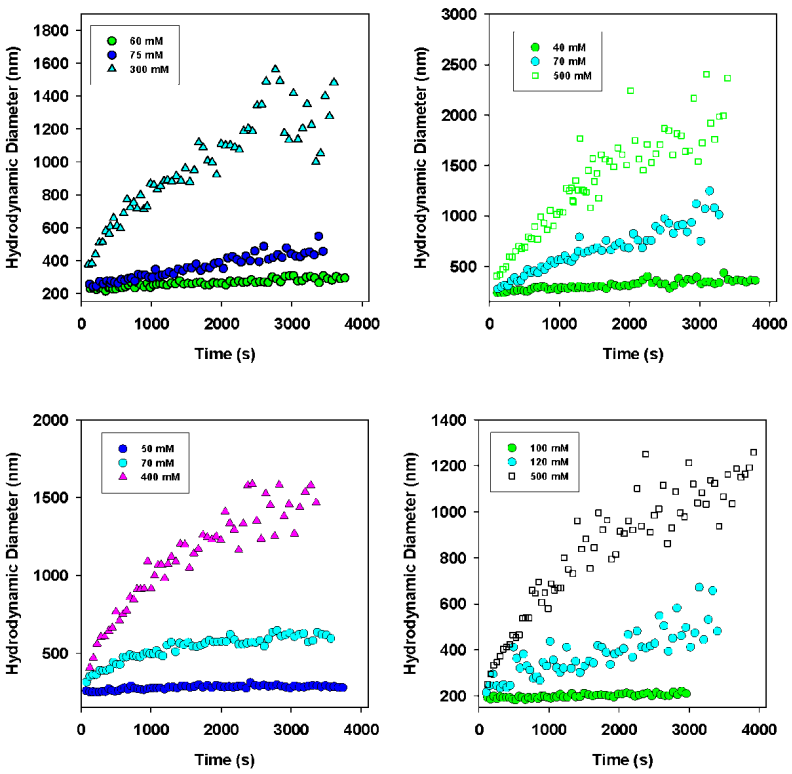

Figure C.13 Aggregation profiles of (A) aq/*n*C_{60}; (B) 0.1 mM cit/*n*C_{60}; (C) 0.5 mM cit/*n*C_{60}; and (D) 1.0 mM cit/*n*C_{60}.

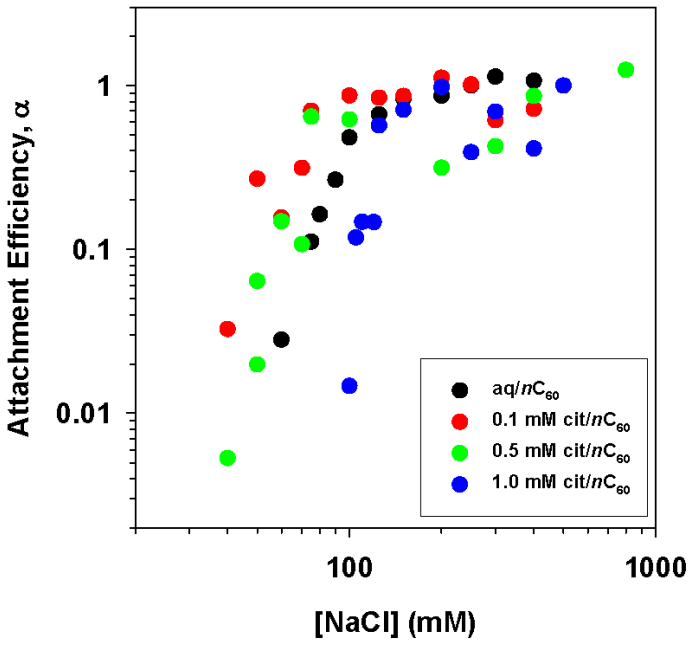

Figure C.14 Attachment efficiencies of *n*C_{60} as a function of NaCl concentration.

Ionic Strength Effects.

Experimental Method. nC_{60} stock suspensions (aq/nC_{60}, 0.1, 0.5, 1.0, and 5.0 mM cit/nC_{60}) were mixed with NaCl solutions at a volume ratio of 4:1. [Na^+] in these mixtures ranged from 0 to 100 mM.

Results and Discussion. Previous studies[58,59] reported that aq/nC_{60} and other nC_{60} produced via solvent exchange became less negatively charged with [Na^+] when [Na^+] exceeded 1 mM. In the present study, we observed different behaviors after adding NaCl to stock nC_{60} suspensions. Here we note that for some samples there were great variations between three EM measurements (Figure C.15). A nice single peak was obtained in the first measurement while the other two measurements showed overlapping multipeaks which ranged from -100 mV to above 0 mV. At the same time, the conductivities of these samples increased significantly during the measurements. Peak splitting and broadening and the increase in solution conductivity were repeatedly observed in samples with [Na^+] ranging from 15-30 mM. These changes were likely caused by the destruction of the electrical double layers of nC_{60} particles during EM measurement. Therefore, we observed large error bars for these samples in Figure C.16.

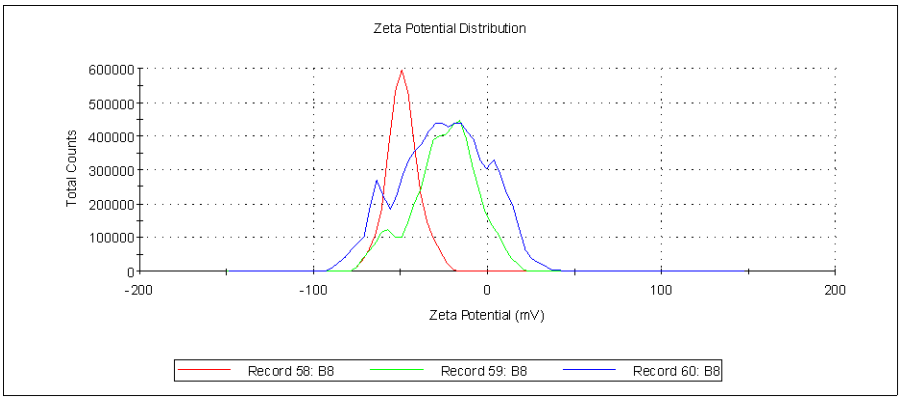

Figure C.15 Zeta potential distribution of cit/nC_{60} in 30 mM NaCl.

Surface charge of nC$_{60}$ produced in different solutions varied in dissimilar patterns. Aq/nC$_{60}$ and 0.1 mM cit/nC$_{60}$ exhibited a slight but statistically significant increase in their surface charge as [Na^+] increased from 0.1 to 10 mM. Beyond 10 mM [Na^+], the EM values became increasing less negative with further increases in [Na^+] (Figures C.16A and C.16B). This latter behavior (i.e., an increase in EM with an increase in [Na^+]) was observed over the entire tested range (Figures C.16C-E). To our knowledge, the more negative charged surfaces with increasing [Na^+] are first reported in the present study. The slightly less charged aq/nC$_{60}$ and 0.1 mM cit/nC$_{60}$ in solutions with low ionic strengths can be explained by a theoretical calculation of the potential of electrical double layer interactions for a sphere-plate system,[193] which indicates that low ionic strength will destabilize nanoparticles.

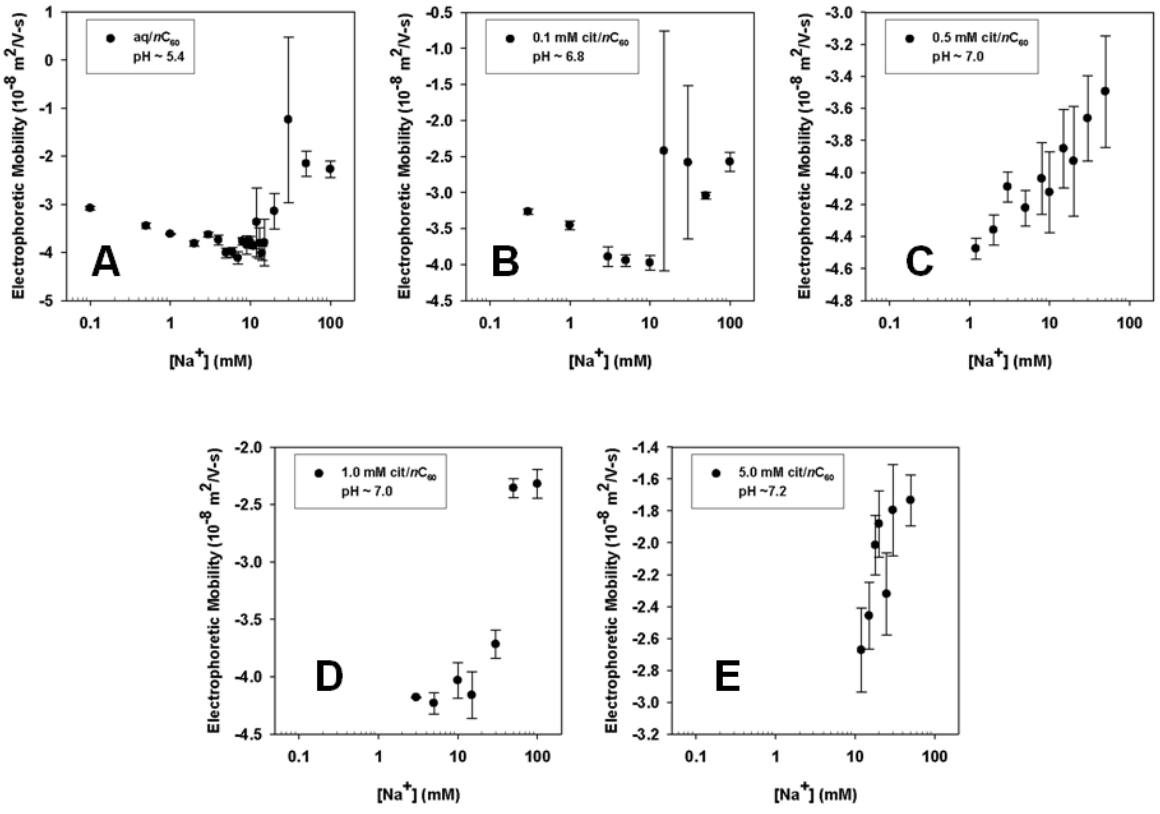

Figure C.16 Surface charge of nC$_{60}$ as a function of [Na^+] in nC$_{60}$-NaCl mixture. (Each data point represents the average of three measurements for one sample and the error bar represents the standard deviation.)

Exhaustive Extraction.

Experimental Methods. nC$_{60}$ was extracted into toluene in the presence of 200 mM NaCl. The mixture, consisting of 3 mL of nC$_{60}$ stock suspension, 0.2 mL of 3.2 M NaCl solution, and 3 mL of toluene, was vortexed in a test tube for 1 min settled for 15 min to allow the two phases to separate and then the organic phase was transferred to an aqua-regia cleaned test tube. The aqueous phase was then combined with 3 mL of toluene for a second extraction. Extraction operations were repeated for three times and the lack of any detectable nC$_{60}$ characteristic absorption bands in the UV-Vis spectrum of aqueous phase after three extraction cycles indicates that all of the nC$_{60}$ was extracted from the aqueous phase. The C$_{60}$ concentration ([C$_{60}$]$_{tol}$) in each toluene extract was determined based upon its UV-Vis absorbance at 336 nm and a calibration curve established by a series of C$_{60}$-toluene solutions with known [C$_{60}$]. In these experiments the total [nC$_{60}$]$_{TOT}$ was calculated as the sum of [C$_{60}$]$_{tol}$ from the three extracts. The recovery efficiency of each extraction is defined as the ratio of [C$_{60}$]$_{tol}$ in each toluene extract to [nC$_{60}$]$_{TOT}$ for each nC$_{60}$ suspension.

Results and Discussion. The extraction efficiency of each extraction was calculated as the ratio of [C$_{60}$] in each extract to [C$_{60}$]$_{TOT}$ and presented in Figure C.17. For cit/nC$_{60}$ produced in solutions with moderate [Na$_3$Cit] (0.5-5.0 mM), more than 95% of nC$_{60}$ was extracted to toluene in the first extraction. In contrast, only ≈ 50% of the aq/nC$_{60}$ produced and 0.1 mM Cit/nC$_{60}$ was extracted in the first extraction, with the remainder extracted in the second and third operations. It could be hypothesized that the difference in extraction efficiency for the first extraction was caused by the variable initial [nC$_{60}$] in these samples. However, results of exhaustive extractions for diluted aq/nC$_{60}$ suspensions suggest that the initial [nC$_{60}$] for aqueous nC$_{60}$ samples had little effect on their extraction efficiencies. For nC$_{60}$ produced in different solutions, 1.0 mM cit/nC$_{60}$

with UV-Vis absorbance at 360 nm (ABS(360)) of 0.83 had higher extraction efficiency than 0.1 mM cit/nC$_{60}$ with ABS(360) = 0.55. We conclude that the observed variation in the first extraction efficiency indicates the differential capacity of the different types of nC$_{60}$ to solvation in toluene. The results suggest that surface characteristics of nC$_{60}$ produced in solutions with low or no [Na$_3$Cit] are dissimilar from those of cit/nC$_{60}$ produced in solutions with moderate [Na$_3$Cit]. This dissimilarity is due to the possible association between citrate and nC$_{60}$. The particle-solution interface of aq/nC$_{60}$ contains only surface associated water molecules (Figure C.18A), while at sufficient citrate concentrations (> 0.1 mM) citrate present at the interface are high enough (Figure C.18C) to affect the extraction efficiency. The comparatively higher initial extraction efficiencies for cit/nC$_{60}$ produced in 0.5-5.0 mM Na$_3$Cit suggest that the association between citrate and nC$_{60}$ is readily destroyed by high [Na^+].

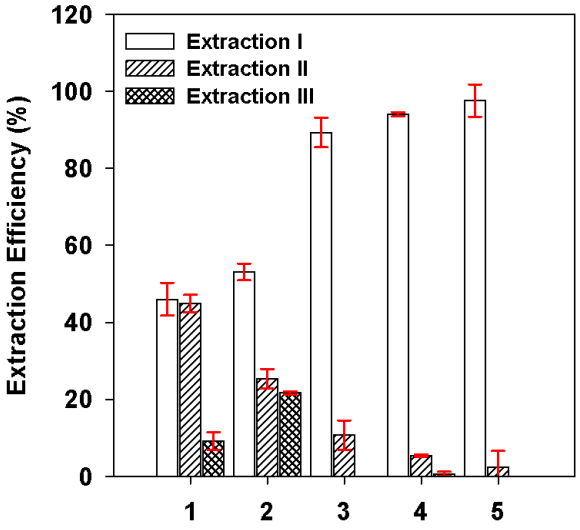

Figure C.17 Extraction efficiencies of individual extraction steps (I, II, and III) for different nC$_{60}$ suspensions. 1 = aq/nC$_{60}$, 2 = 0.1 mM cit/nC$_{60}$, 3 = 0.5 mM cit/nC$_{60}$, 4 = 1.0 mM cit/nC$_{60}$, and 5 = 5.0 mM cit/nC$_{60}$; The vertical bar represents the average of duplicates and the error bar represents the standard deviation of the duplicates.

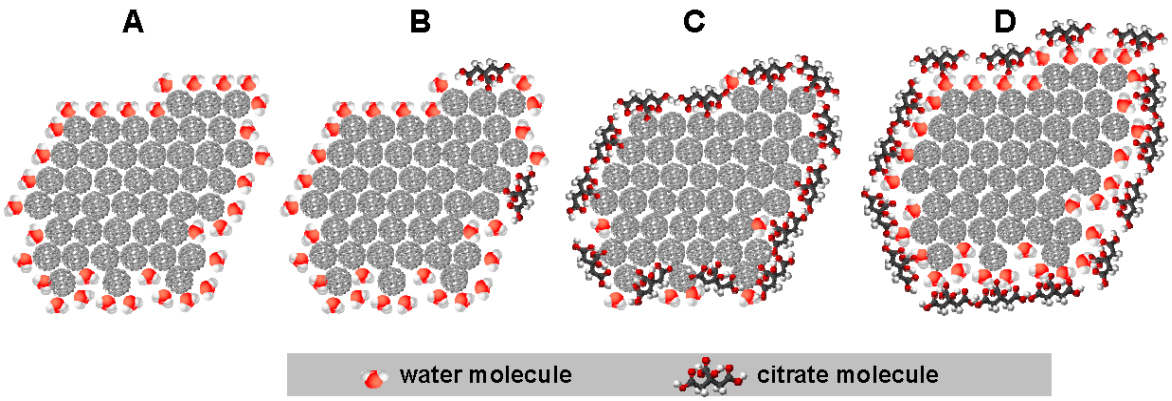

Figure C.18 Models of nC_{60} particles surfaces for (A) aq/nC_{60}, (B) cit/nC_{60} produced in solutions with low [Na_3Cit] levels, (C), cit/nC_{60} produced in solutions with moderate [Na_3Cit], and (D) aq/nC_{60} with the addition of Na_3Cit after extended mixing.

Adsorption of citrate on nC_{60}.

Isolation. To quantitatively estimate citrate adsorption to nC_{60}, cit/nC_{60} particles were removed from aqueous solutions by ultrafiltration or centrifugation. A cit/nC_{60} stock suspension was ultrafiltrated through a membrane with a cutoff size of 1 kDa. at 2×10^5 Pa; A cit/nC_{60} stock suspension was centrifuged at 10000 rpm for 30 min. The supernatant was then transferred to a new centrifugation tube and centrifuged at the same speed for 20 min. The filtrate and supernatant were transferred to aqua-regia cleaned test tubes for further characterization. UV-Vis analysis of the filtrate from ultrafiltration or the supernatant from centrifugation indicated that all cit/nC_{60} particles were retained on the membrane or in the pellet. Accordingly, the changes in [citrate] in the ultrafiltrate and supernatant reflect the amount of citrate associated with nC_{60}.

Results and Discussion. Citrate stabilization of nanoparticle suspensions is an established phenomenon and involves both pH modification and the association of citrate with the nanoparticle surface.[154,165] Jiang et al.[168] recently determined that citric acid treated carbon nanotubes (CNT) exhibit more negative zeta potentials than pristine CNT. They hypothesized that citrate associated with the CNT surface, but did not suggest a mechanism. The adsorption of NOM, proteins, and organic pollutants on surfaces of nC_{60} has been studied previously.[28,83,91,194-196] Adsorbates interact with nC_{60} via hydrophobic interactions, electrostatic interactions, π-π bonding, or hydrogen bonding. The mechanism by which citrate associates with C_{60} is presently unknown; however, because of its hydrophilic surfaces, its negatively charged surface, and the molecular structure of citrate, hydrophobic interaction, electrostatic interaction and π-π bonding are not likely to be the sources of the association between citrate and nC_{60}. The –COOH groups in citrate molecule can act as hydrogen-bonding donors and form hydrogen bonds with C_{60} molecule, which act as hydrogen bonding acceptor.[197] For electron deficient substrates, the

carbonyl-π interaction was found to be energetically favorable.[169] Fullerite C_{60}, which is electron deficient[198] and has structures similar to aromatic rings, may associate with citrate through the carbonyl-π cloud interaction. It is also well established that C_{60} serves as an electron acceptor in electron-donor acceptor complexes with a variety of organic molecules[171-174] and it appears that citrate can serve as an electron donor enabling production of supramolecular nC_{60} structures. The conversion from the *fcc* crystal structure for aq/nC_{60} to the *hcp* crystal structure for cit/nC_{60} also supports this contention.

Cit/nC_{60} produced in solutions with different [Na_3Cit] levels were isolated from solutions by centrifugation. [Citrate] in original cit/nC_{60} suspensions and their supernatants after centrifugation are present in Figure C.19. An obvious decrease in [citrate] was only observed in the 0.1 mM cit/nC_{60} samples. Less than 10% of the initial citrate remained in the supernatants. In other samples, the decreases in [citrate] were less than 0.05 mM, quite low compared with [Na_3Cit] in original cit/nC_{60} suspensions. Similar results were observed in ultrafiltration experiments as well. The obvious decreases in [citrate] in ultrafiltrates were only observed for the 0.05 mM and 0.1 mM cit/nC_{60} samples. Collectively, these results indicate that the amount of citrate adsorbed on the surface of nC_{60} is trivial or that the association between citrate and nC_{60} is weak and can be readily destroyed by ultrafiltration and centrifugation.

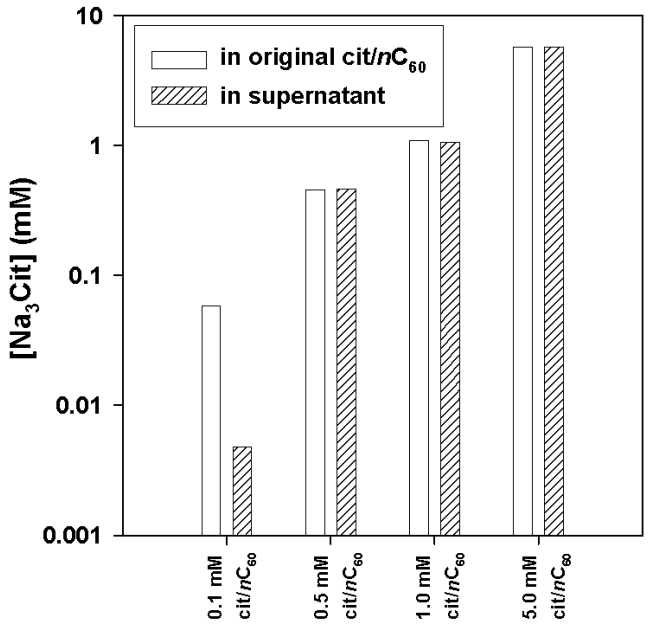

Figure C.19 [Na_3Cit] in original cit/nC_{60} suspensions and centrifuged supernatants.

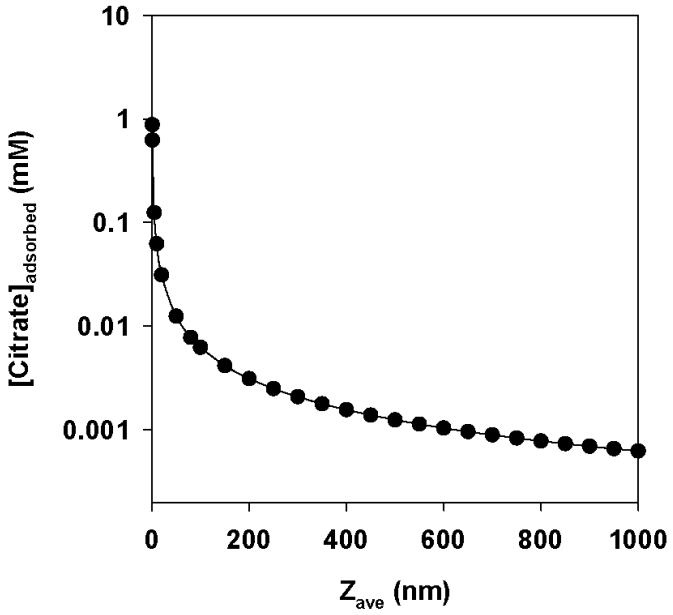

Figure C.20 Calculated [citrate] adsorbed by nC_{60} as a function of particle size.

Table C.1 contains a simplified estimation of the adsorbed citrate on the surface of cit/nC_{60}. Based upon this calculation, when the particle size is larger than 10 nm, citrate adsorbed by cit/nC_{60} is less than 0.01 mM (Figure C.20). In cit/nC_{60} produced via extended mixing, [C_{60}] is

usually lower than 20 mg/L and the Z_{ave} is around 200 nm. Therefore, in reality, $[citrate]_{adsorbed}$ would be lower than 0.001 mM. This may explain the fact that we did not observe much difference in [citrate] between the original cit/*n*C_{60} suspension and its ultrafiltrate/supernatant from centrifugation.

Table C.1 Adsorption of citrate on the surfaces of *n*C_{60} calculation

Some constants and values used in this calculation:

- Size of a C_{60} molecule: 0.71 nm;
- Avogadro's number: $N_A = 6.02 \times 10^{23}$ mol^{-1};
- The lattice constant of C_{60} crystal (*fcc*): l = 1.417 nm;
- Surface area of a citrate molecule: $A_{citrate} = 0.38$ nm^2 $molecule^{-1}$
- Initial fullerene concentration of cit/*n*C_{60} suspension: $[C_{60}] = 400$ mg/L.

Assumptions in this estimation:

- The cit/*n*C_{60} particles are spherical with the same size. The Z_{ave} represents the diameter of these particles.
- Monolayer adsorption.

Calculation: (use 300 nm particle as an example)

2 Number C_{60} molecules in *n*C_{60} suspensions of 400 mg/L: $= N_0 = \frac{[C_{60}]}{Mw_{C_{60}}} \times N_A = 3.34 \times 10^{20}$ molecules/L

3 One spherical particle of 300 nm contains n_0 C_{60} molecules: $n_0 = \frac{4\pi}{3}\left(\frac{Z_{ave}}{2}\right)^3 \frac{4}{l^3} = 1.99 \times 10^7$ molecules/particle

4 Number concentration of 300 nm spherical *n*C_{60} particles: $[nC_{60}]_{particle} = \frac{N_0}{n_0} = 1.68 \times 10^{13}$ particles/L = 2.80×10^{-11} mol/L.

5 One 300 nm spherical *n*C_{60} will adsorb $n_{citrate}$ molecule: $n_{citrate} = \frac{A_{surface(nC_{60})}}{A_{surface(citrate)}} = \frac{4\pi\left(\frac{Z_{ave}}{2}\right)^2}{A_{surface(citrate)}} = = 7.44 \times 10^5$ citrate molecule/particle

6 $[Citrate]_{adsorbed} = n_{citrate} \times [nC_{60}]_{particle} = 2.08 \times 10^{-5}$ mol/L = 0.002 mM.

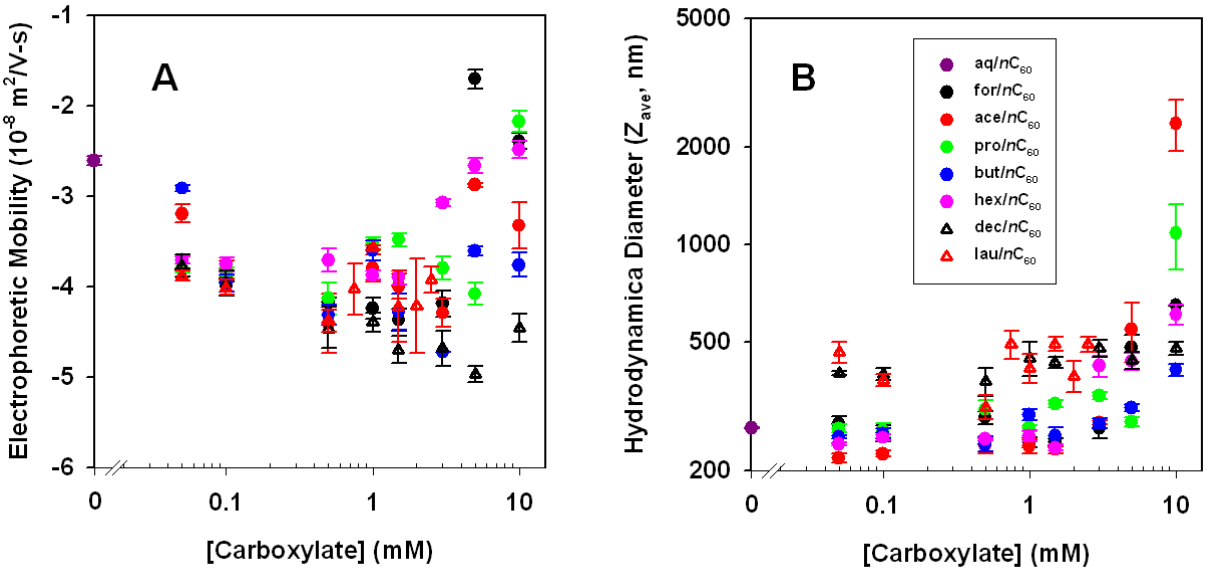

Figure C.21 (A) Surface charge and (B) average particle size of nC_{60} produced in different carboxylate solutions as a function of the concentration of carboxylate. (Each data point represents the average of three measurements for one sample and the error bar represents the standard deviation.)

References

(1) Kroto, H. W.; Heath, J. R.; Obrien, S. C.; Curl, R. F.; Smalley, R. E., C60 - Buckminsterfullerene. *Nature* **1985,** 318, (6042), 162-163.

(2) Dzwilewski, A.; Wagberg, T.; Edman, L., Photo-induced and resist-free imprint patterning of fullerene materials for use in functional electronics. *J. Am. Chem. Soc.* **2009,** 131, (11), 4006-4011.

(3) Da Ros, T.; Prato, M., Medicinal chemistry with fullerenes and fullerene derivatives. *Chem. Commun.* **1999**, (8), 663-669.

(4) Nazarov, G. V.; Galan, S. E.; Nazarova, E. V.; Karkishchenko, N. N.; Muradov, M. M.; Stepanov, V. A., Nanosized forms of drugs (A Review). *Pharmaceutical Chemistry Journal* **2009,** 43, (3), 163-170.

(5) Murakami, T.; Tsuchida, K., Recent advances in inorganic nanoparticle-based drug delivery systems. *Mini-Rev. Med. Chem.* **2008,** 8, (2), 175-183.

(6) Rade, I.; Natasa, R.; Biljana, G.; Aleksandar, D.; Borut, S., Bioapplication and activity of fullerenol C60(OH)(24). *African Journal of Biotechnology* **2008,** 7, (25), 4940-4950.

(7) Gao, Y. Y.; Ou, Z. Z.; Yang, G. Q.; Liu, L. H.; Jin, M. M.; Wang, X. S.; Zhang, B. W.; Wang, L. X., Efficient photocleavage of DNA utilizing water soluble riboflavin/naphthaleneacetate substituted fullerene complex. *J. Photochem. Photobiol. A-Chem.* **2009,** 203, (2-3), 105-111.

(8) Mayer, A. C.; Toney, M. F.; Scully, S. R.; Rivnay, J.; Brabec, C. J.; Scharber, M.; Koppe, M.; Heeney, M.; McCulloch, L.; McGehee, M. D., Bimolecular crystals of fullerenes in conjugated polymers and the implications of molecular mixing for solar cells. *Adv. Funct. Mater.* **2009,** 19, (8), 1173-1179.

(9) Dennler, G.; Scharber, M. C.; Brabec, C. J., Polymer-fullerene bulk-heterojunction solar cells. *Adv. Mater.* **2009,** 21, (13), 1323-1338.

(10) Goyal, R. N.; Gupta, V. K.; Bachheti, N.; Sharma, R. A., Electrochemical sensor for the determination of dopamine in presence of high concentration of ascorhic acid using a fullerene-C60 coated gold electrode. *Electroanalysis* **2008,** 20, (7), 757-764.

(11) Sherigara, B. S.; Kutner, W.; D'Souza, F., Electrocatalytic properties and sensor applications of fullerenes and carbon nanotubes. *Electroanalysis* **2003,** 15, (9), 753-772.

(12) Mauter, M. S.; Elimelech, M., Environmental applications of carbon-based nanomaterials. *Environ. Sci. Technol.* **2008,** 42, (16), 5843-5859.

(13) Takada, H.; Mimura, H.; Xiao, L.; Islam, R. M.; Matsubayashi, K.; Ito, S.; Miwa, N., Innovative anti-oxidant: Fullerene is as "Radical Sponge" on the skin. Its high level of safety, stability and potential as premier anti-aging and whitening cosmetic ingredient. *Fuller. Nanotub. Carbon Nanostruct.* **2006,** 14, (2-3), 335-341.

(14) Halford, B., Fullerene for the face. *Chem. Eng. News* **2006,** 84, (13), 47-47.

(15) Tremblay, J. F., Mitsubishi chemical aims at breakthrough. *Chem. Eng. News* **2002,** 80, (49), 16-17.

(16) Murayama, H.; Tomonoh, S.; Alford, J. M.; Karpuk, M. E. In *Fullerene production in tons and more: From science to industry*, 6th Biennial International Workshop on Fullerenes and Atomic Clusters, St Petersburg, RUSSIA, Jun 30-Jul 04, 2003; Marcel Dekker Inc: St Petersburg, RUSSIA, 2003; pp 1-9.

(17) Taylor, R.; Walton, D. R. M., The chemistry of fullerenes. *Nature* **1993,** 363, (6431), 685-693.

(18) Prato, M., [60] Fullerene chemistry for materials science applications. *J. Mater. Chem.* **1997,** 7, (7), 1097-1109.

(19) Kavan, L.; Dunsch, L., Spectroelectrochemistry of carbon nanostructures. *Chemphyschem* **2007,** 8, (7), 975-998.

(20) Johnson, R. D.; Meijer, G.; Bethune, D. S., C60 has icosahedral symmetry. *J. Am. Chem. Soc.* **1990,** 112, (24), 8983-8984.

(21) Johnson, R. D.; Bethune, D. S.; Yannoni, C. S., Fullerne structure and dynamics - A magnetic-resonance potpourri. *Accounts Chem. Res.* **1992,** 25, (3), 169-175.

(22) Heymann, D., Solubility of fullerenes C60 and C70 in seven normal alcohols and their deduced solubility in water. *Fullerene Sci. Technol.* **1996,** 4, (3), 509-515.

(23) Ruoff, R. S.; Malhotra, R.; Huestis, D. L.; Tse, D. S.; Lorents, D. C., Anomalous solubility behavior of C60. *Nature* **1993,** 362, (6416), 140-141.

(24) Heymann, D., Solubility of C-60 in alcohols and alkanes. *Carbon* **1996,** 34, (5), 627-631.

(25) Scrivens, W. A.; Tour, J. M.; Creek, K. E.; Pirisi, L., Synthesis of C-14-labeled C60, its suspension in water, and its uptake by human keratinocytes. *J. Am. Chem. Soc.* **1994,** 116, (10), 4517-4518.

(26) Andrievsky, G. V.; Kosevich, M. V.; Vovk, O. M.; Shelkovsky, V. S.; Vashchenko, L. A., On the production of an aqueous colloidal solution of fullerenes. *J. Chem. Soc., Chem. Commun.* **1995**, (12), 1281-1282.

(27) Deguchi, S.; Alargova, R. G.; Tsujii, K., Stable dispersions of fullerenes, C60 and C70, in water. Preparation and characterization. *Langmuir* **2001,** 17, (19), 6013-6017.

(28) Cheng, X. K.; Kan, A. T.; Tomson, M. B., Naphthalene adsorption and desorption from aqueous C60 fullerene. *J. Chem. Eng. Data* **2004,** 49, (3), 675-683.

(29) Terashima, M.; Nagao, S., Solubilization of [60]fullerene in water by aquatic humic substances. *Chem. Lett.* **2007,** 36, (2), 302-303.

(30) Chen, K. L.; Elimelech, M., Influence of humic acid on the aggregation kinetics of fullerene (C60) nanoparticles in monovalent and divalent electrolyte solutions. *J. Colloid. Interface Sci.* **2007,** 309, (1), 126-134.

(31) Chen, K. L.; Elimelech, M., Interaction of fullerene (C60) nanoparticles with humic acid and alginate coated silica surfaces: Measurements, mechanisms, and environmental Implications. *Environ. Sci. Technol.* **2008,** 42, (20), 7607-7614.

(32) Nath, S.; Pal, H.; Sapre, A. V., Effect of solvent polarity on the aggregation of C60. *Chem. Phys. Lett.* **2000,** 327, (3-4), 143-148.

(33) Nath, S.; Pal, H.; Sapre, A. V., Effect of solvent polarity on the aggregation of fullerenes: A comparison between C60 and C70. *Chem. Phys. Lett.* **2002,** 360, (5-6), 422-428.

(34) Patnaik, A., Structure and dynamics in self-organized C60 fullerenes. *J. Nanosci. Nanotechnol.* **2007,** 7, (4-5), 1111-1150.

(35) Ying, Q. C.; Marecek, J.; Chu, B., Solution behavior of buckminsterfullerene (C60) in benzene. *J. Chem. Phys.* **1994,** 101, (4), 2665-2672.

(36) Nath, S.; Pal, H.; Palit, D. K.; Sapre, A. V.; Mittal, J. P., Aggregation of fullerene, C60, in benzonitrile. *J. Phys. Chem. B* **1998,** 102, (50), 10158-10164.

(37) Bokare, A. D.; Patnaik, A., Evidence for C60 aggregation from solvent effects in [Ps-C60] molecular complex formation. *Carbon* **2003,** 41, (13), 2643-2651.

(38) Bokare, A. D.; Patnaik, A., Self-organization of C60 nanoparticles in carbon disulfide solution. *J. Phys. Chem. B* **2003,** 107, (25), 6079-6086.

(39) Bulavin, L. A.; Adamenko, II; Yashchuk, V. M.; Ogul'chansky, T. Y.; Prylutskyy, Y. I.; Durov, S. S.; Scharff, P. In *Self-organization C60 nanoparticles in toluene solution*, International Conference on Special Problems in Physics of Liquids, Odessa, Ukraine, May 31-Jun 04, 1999; Odessa, Ukraine, 1999; pp 187-191.

(40) Alfe, M.; Apicella, B.; Barbella, R.; Bruno, A.; Ciajolo, A., Aggregation and interactions of C60 and C70 fullerenes in neat N-methylpyrrolidinone and in N-methylpyrrolidinone/toluene mixtures. *Chem. Phys. Lett.* **2005,** 405, (1-3), 193-197.

(41) Alargova, R. G.; Deguchi, S.; Tsujii, K., Stable colloidal dispersions of fullerenes in polar organic solvents. *J. Am. Chem. Soc.* **2001,** 123, (43), 10460-10467.

(42) Zulian, L.; Ruzicka, B.; Ruocco, G., About the formation of C60 fine particles with reprecipitation method in ethanol/carbon disulfide mixture. *J. Photochem. Photobiol. A-Chem.* **2007,** 187, (2-3), 402-405.

(43) Beck, M. T. In *Solubility and molecular state of C60 and C70 in solvents and solvent mixtures*, 8th International Symposium on Solubility Phenomena, Niigata, Japan, Aug 05-08, 1998; Niigata, Japan, 1998; pp 1881-1887.

(44) Ruoff, R. S.; Tse, D. S.; Malhotra, R.; Lorents, D. C., Solubility of C60 in a variety of solvents. *J. Phys. Chem.* **1993,** 97, (13), 3379-3383.

(45) Cusan, C.; Da Ros, T.; Spalluto, G.; Foley, S.; Janto, J. M.; Seta, P.; Larroque, C.; Tomasini, M. C.; Antonelli, T.; Ferraro, L.; Prato, M., A new multi-charged C60 derivative: Synthesis and biological properties. *Eur. J. Org. Chem.* **2002**, (17), 2928-2934.

(46) Arrais, A.; Diana, E., Highly water soluble C60 derivatives: A new synthesis. *Fuller. Nanotub. Carbon Nanostruct.* **2003,** 11, (1), 35-46.

(47) Nakamura, E.; Isobe, H., Functionalized fullerenes in water. The first 10 years of their chemistry, biology, and nanoscience. *Accounts Chem. Res.* **2003,** 36, (11), 807-815.

(48) Belousov, V. P.; Belousova, I. M.; Kris'ko, A. V.; Kris'ko, T. K.; Murav'eva, T. D.; Sirotkin, A. K., Aqueous micellar solution C60: Preparation, properties, and capability for generation of singlet oxygen. *Russ. J. Gen. Chem.* **2006,** 76, (2), 251-257.

(49) Andersson, T.; Nilsson, K.; Sundahl, M.; Westman, G.; Wennerstrom, O., C60 embedded in gamma-cyclodextrin- A water-soluble fullerene. *J. Chem. Soc., Chem. Commun.* **1992**, (8), 604-606.

(50) Buvari-Barcza, A.; Rohonczy, J.; Rozlosnik, N.; Gilanyi, T.; Szabo, B.; Lovas, G.; Braun, T.; Samu, J.; Barcza, L., Aqueous solubilization of [60]fullerene via inclusion complex formation and the hydration of C60. **2001**, (2), 191-196.

(51) Yamakoshi, Y. N.; Yagami, T.; Fukuhara, K.; Sueyoshi, S.; Miyata, N., Solubilization of fullerenes into water with polyvinylpyrrolidone applicable to biological tests. *J. Chem. Soc., Chem. Commun.* **1994**, (4), 517-518.

(52) Ungurenasu, C.; Airinei, A., Highly stable C60/poly(vinylpyrrolidone) charge-transfer complexes afford new predictions for biological applications of underivatized fullerenes. *J. Med. Chem.* **2000,** 43, (16), 3186-3188.

(53) Li, H. G.; Jia, X. F.; Li, Y.; Shi, X. W.; Hao, J. C., A salt-free zero-charged aqueous onion-phase enhances the solubility of fullerene C60 in water. *J. Phys. Chem. B* **2006,** 110, (1), 68-74.

(54) Eastoe, J.; Crooks, E. R.; Beeby, A.; Heenan, R. K., Structure and photophysics in C60-micellar solutions. *Chem. Phys. Lett.* **1995,** 245, (6), 571-577.

(55) Beeby, A.; Eastoe, J.; Heenan, R. K., Solubilization of C60 in aqueous micellar solution. *J. Chem. Soc., Chem. Commun.* **1994**, (2), 173-175.

(56) Mchedlov-Petrossyan, N. O.; Klochkov, V. K.; Andrievsky, G. V., Colloidal dispersions of fullerene C60 in water: Some properties and regularities of coagulation by electrolytes. *J. Chem. Soc.Faraday T* **1997,** 93, (24), 4343-4346.

(57) Andrievsky, G. V.; Klochkov, V. K.; Karyakina, E. L.; Mchedlov-Petrossyan, N. O., Studies of aqueous colloidal solutions of fullerene C60 by electron microscopy. *Chem. Phys. Lett.* **1999,** 300, (3-4), 392-396.

(58) Brant, J.; Lecoanet, H.; Hotze, M.; Wiesner, M., Comparison of electrokinetic properties of colloidal fullerenes (nC60) formed using two procedures. *Environ. Sci. Technol.* **2005,** 39, (17), 6343-6351.

(59) Brant, J. A.; Labille, J.; Bottero, J. Y.; Wiesner, M. R., Characterizing the impact of preparation method on fullerene cluster structure and chemistry. *Langmuir* **2006,** 22, (8), 3878-3885.

(60) Fortner, J. D.; Lyon, D. Y.; Sayes, C. M.; Boyd, A. M.; Falkner, J. C.; Hotze, E. M.; Alemany, L. B.; Tao, Y. J.; Guo, W.; Ausman, K. D.; Colvin, V. L.; Hughes, J. B., C60 in water: Nanocrystal formation and microbial response. *Environ. Sci. Technol.* **2005,** 39, (11), 4307-4316.

(61) Avdeev, M. V.; Khokhryakov, A. A.; Tropin, T. V.; Andrievsky, G. V.; Klochkov, V. K.; Derevyanchenko, L. I.; Rosta, L.; Garamus, V. M.; Priezzhev, V. B.; Korobov, M. V.; Aksenov, V. L., Structural features of molecular-colloidal solutions of C60 fullerenes in water by small-angle neutron scattering. *Langmuir* **2004,** 20, (11), 4363-4368.

(62) Dhawan, A.; Taurozzi, J. S.; Pandey, A. K.; Shan, W. Q.; Miller, S. M.; Hashsham, S. A.; Tarabara, V. V., Stable colloidal dispersions of C60 fullerenes in water: Evidence for genotoxicity. *Environ. Sci. Technol.* **2006,** 40, (23), 7394-7401.

(63) Tseluikin, V. N.; Chubenko, I. S.; Gun'kin, I. F.; Pankst'yanov, A. Y., Colloidal dispersion of fullerene C60 free of organic solvents. *Russ. J. Appl. Chem.* **2006,** 79, (2), 325-326.

(64) Brant, J.; Lecoanet, H.; Wiesner, M. R., Aggregation and deposition characteristics of fullerene nanoparticles in aqueous systems. *J. Nanopart. Res.* **2005,** 7, (4-5), 545-553.

(65) Andrievsky, G. V.; Klochkov, V. K.; Bordyuh, A. B.; Dovbeshko, G. I., Comparative analysis of two aqueous-colloidal solutions of C60 fullerene with help of FTIR reflectance and UV-Vis spectroscopy. *Chem. Phys. Lett.* **2002,** 364, (1-2), 8-17.

(66) Ko, W. B.; Heo, J. Y.; Nam, J. H.; Lee, K. B., Synthesis of a water-soluble fullerene [C60] under ultrasonication. *Ultrasonics* **2004,** 41, (9), 727-730.

(67) Belousova, I. M.; Belousov, V. P.; Kiselev, V. M.; Murav'eva, T. D.; Kislyakov, I. M.; Sirotkin, A. K.; Starodubtsev, A. M.; Kris'ko, T. K.; Bagrov, I. V.; Ermakov, A. V., Structural and optical properties of solid-phase singlet oxygen photosensitizers based on fullerene aqueous suspensions. *Opt. Spectrosc.* **2008,** 105, (5), 711-719.

(68) Labille, J.; Masion, A.; Ziarelli, F.; Rose, J.; Brant, J.; Villieras, F.; Pelletier, M.; Borschneck, D.; Wiesner, M. R.; Bottero, J. Y., Hydration and dispersion of C60 in aqueous systems: The nature of water-fullerene interactions. *Langmuir* **2009,** 25, (19), 11232-11235.

(69) Labille, J.; Brant, J.; Villieras, F.; Pelletier, M.; Thill, A.; Masion, A.; Wiesner, M.; Rose, J.; Bottero, J. Y., Affinity of C60 fullerenes with water. *Fuller. Nanotub. Carbon Nanostruct.* **2006,** 14, (2-3), 307-314.

(70) Manson, T. J., *Chemistry with Ultrasound*. Elsevier: London, 1990.

(71) Chae, S. R.; Badireddy, A. R.; Budarz, J. F.; Lin, S. H.; Xiao, Y.; Therezien, M.; Wiesner, M. R., Heterogeneities in fullerene nanoparticle aggregates affecting reactivity, bioactivity, and rransport. *Acs Nano* **2010,** 4, (9), 5011-5018.

(72) Leach, S.; Vervloet, M.; Despres, A.; Breheret, E.; Hare, J. P.; Dennis, T. J.; Kroto, H. W.; Taylor, R.; Walton, D. R. M., Electronic-spectra and transition of the fullerene C60. *Chem. Phys.* **1992,** 160, (3), 451-466.

(73) Zhao, B. Z.; Bilski, P. J.; He, Y. Y.; Feng, L.; Chignell, C. F., Photo-induced reactive oxygen species generation by different water-soluble fullerenes (C60) and their cytotoxicity in human keratinocytes. *Photochem. Photobiol.* **2008,** 84, (5), 1215-1223.

(74) Kato, H.; Nakamura, A.; Takahashi, K.; Kinugasa, S., Size effect on UV-Vis absorption properties of colloidal C60 particles in water. *Phys. Chem. Chem. Phys.* **2009,** 11, (25), 4946-4948.

(75) Bulavin, L.; Adamenko, I.; Prylutskyy, Y.; Durov, S.; Graja, A.; Bogucki, A.; Scharff, P., Structure of fullerene C60 in aqueous solution. *Phys. Chem. Chem. Phys.* **2000,** 2, (8), 1627-1629.

(76) Scharff, P.; Risch, K.; Carta-Abelmann, L.; Dmytruk, I. M.; Bilyi, M. M.; Golub, O. A.; Khavryuchenko, A. V.; Buzaneva, E. V.; Aksenov, V. L.; Avdeev, M. V.; Prylutskyy, Y. I.; Durov, S. S. In *Structure of C60 fullerene in water: spectroscopic data*, Symposium on Advanced Multifunctional Nanocarbon Materials and Nanosystems held at the 2003 EMRS Spring Meeting, Strasbourg, FRANCE, Jun 10, 2004; Pergamon-Elsevier Science Ltd: Strasbourg, FRANCE, 2004; pp 1203-1206.

(77) Gun'kin, I. F.; Loginova, N. Y., Effect of nature of organic solvent on the absorption spectrum of C60 fullerene. *Russ. J. Gen. Chem.* **2006,** 76, (12), 1911-1913.

(78) Lee, J.; Kim, J. H., Effect of encapsulating agents on dispersion status and photochemical reactivity of C60 in the aqueous phase. *Environ. Sci. Technol.* **2008,** 42, (5), 1552-1557.

(79) Deguchi, S.; Mukai, S.; Yamazaki, T.; Tsudome, M.; Horikoshi, K., Nanoparticles of fullerene C60 from engineering of antiquity. *J. Phys. Chem. C* **2010,** 114, (2), 849-856.

(80) Duncan, L. K.; Jinschek, J. R.; Vikesland, P. J., C60 colloid formation in aqueous systems: Effects of preparation method on size, structure, and surface, charge. *Environ. Sci. Technol.* **2008,** 42, (1), 173-178.

(81) Bouchard, D.; Ma, X.; Issacson, C., Colloidal properties of aqueous fullerenes: Isoelectric points and aggregation kinetics of C60 and C60 Derivatives. *Environ. Sci. Technol.* **2009,** 43, (17), 6597-6603.

(82) Ma, X.; Bouchard, D., Formation of aqueous suspensions of fullerenes. *Environ. Sci. Technol.* **2009,** 43, (2), 330-336.

(83) Deguchi, S.; Yamazaki, T.; Mukai, S.; Usami, R.; Horikoshi, K., Stabilization of C60 nanoparticles by protein adsorption and its implications for toxicity studies. *Chem. Res. Toxicol.* **2007,** 20, (6), 854-858.

(84) Kadish K. M., R. R. S., *Fullerenes Chemistry, Physics, and Technology*. John Wiley & Sons: New York, 2000.

(85) Yoshida, Z. I.; Takekuma, H.; Takekuma, S. I.; Matsubara, Y., Molecular recognition of C60 with gamma-cyclodextrin. **1994,** 33, (15-16), 1597-1599.

(86) Elimelech, M.; Gregory, J.; Jia, X.; Willams, R. A., *Particle Deposition and Aggregatuion - Measurement, Modelling and Simulation*. Butterworth-Heinemann: Oxford, England, 1995.

(87) Lyon, D. Y.; Adams, L. K.; Falkner, J. C.; Alvarez, P. J. J., Antibacterial activity of fullerene water suspensions: Effects of preparation method and particle size. *Environ. Sci. Technol.* **2006,** 40, (14), 4360-4366.

(88) Cheng, X. K.; Kan, A. T.; Tomson, M. B., Uptake and sequestration of naphthalene and 1,2-dichlorobenzene by C60. *J. Nanopart. Res.* **2005,** 7, (4-5), 555-567.

(89) Xie, B.; Xu, Z. H.; Guo, W. H.; Li, Q. L., Impact of natural organic matter on the physicochemical properties of aqueous C60 nanoparticles. *Environ. Sci. Technol.* **2008,** 42, (8), 2853-2859.

(90) Lecoanet, H. F.; Wiesner, M. R., Velocity effects on fullerene and oxide nanoparticle deposition in porous media. *Environ. Sci. Technol.* **2004,** 38, (16), 4377-4382.

(91) Hu, X. L.; Liu, J. F.; Mayer, P.; Jiang, G., Impacts of some environmentally relevant parameters on the sorption of polycyclic aromatic hydrocarbons to aqueous suspensions of fullerene. *Environ. Toxicol. Chem.* **2008,** 27, (9), 1868-1874.

(92) Hofmann, T.; von der Kammer, F., Estimating the relevance of engineered carbonaceous nanoparticle facilitated transport of hydrophobic organic contaminants in porous media. *Environ. Pollut.* **2009,** 157, (4), 1117-1126.

(93) Bensasson, R. V.; Bienvenue, E.; Dellinger, M.; Leach, S.; Seta, P., C60 in model biological -systems - A visible-UV absorption absorption study of solvent-dependent parameters and solute aggregation. *J. Phys. Chem.* **1994,** 98, (13), 3492-3500.

(94) Rao, C. N. R., *Ultra-violet and Visible Spectroscopy*. Butterworth & Co Lyd: Boston, 1975.

(95) Sassara, A.; Zerza, G.; Chergui, M.; Leach, S., Absorption wavelengths and bandwidths for interstellar searches of C60 in the 2400-4100 angstrom region. *Astrophys. J. Suppl. Ser.* **2001,** 135, (2), 263-273.

(96) Renge, I., Solvent effects on the absorption maxima of fullerene C60 and C70. *J. Phys. Chem.* **1995,** 99, (43), 15955-15962.

(97) Sivaraman, N.; Dhamodaran, R.; Kaliappan, I.; Srinivasan, T. G.; Rao, P. R. V.; Mathews, C. K., Solubility of C60 in organic-solvents. *Journal of Organic Chemistry* **1992,** 57, (22), 6077-6079.

(98) Gallagher, S. H.; Armstrong, R. S.; Lay, P. A.; Reed, C. A., Solvent effects on the electronic-spectrum of C60. *J. Phys. Chem.* **1995,** 99, (16), 5817-5825.

(99) Scharff, P.; Carta-Abelmann, L.; Siegmund, C.; Matyshevska, O. P.; Prylutska, S. V.; Koval, T. V.; Golub, A. A.; Yashchuk, V. M.; Kushnir, K. M.; Prylutskyy, Y. I., Effect of X-ray and UV irradiation of the C-60 fullerene aqueous solution on biological samples. *Carbon* **2004,** 42, (5-6), 1199-1201.

(100) Kilpatrick, P. K.; Miller, W. G.; Talmon, Y., Staining and drying-induced artifacts in electron-microscopy of surfactant dispersions. 2. Change in phase-behavior produced by variation in pH modifiers, stain, and concentration. *Journal of Colloid and Interface Science* **1985,** 107, (1), 146-158.

(101) Chang, X.; Vikesland, P. J., Effects of carboxylic acids on nC(60) aggregate formation. *Environ. Pollut.* **2009,** 157, (4), 1072-1080.

(102) Achiba, Y.; Nakagawa, T.; Matsui, Y.; Suzuki, S.; Shiromaru, H.; Yamauchi, K.; Nishiyama, K.; Kainosho, M.; Hoshi, H.; Maruyama, Y.; Mitani, T., Visible, UV, and VUV absorption-spectra of C60 thin-films grown by the molecular-beam epitaxy (MBE) technique. *Chem. Lett.* **1991**, (7), 1233-1236.

(103) Chen, Z.; Westerhoff, P.; Herckes, P., Quantification of C60 fullerene concentrations in water. *Environ. Toxicol. Chem.* **2008,** 27, (9), 1852-1859.

(104) Hassellov, M.; Readman, J. W.; Ranville, J. F.; Tiede, K., Nanoparticle analysis and characterization methodologies in environmental risk assessment of engineered nanoparticles. *Ecotoxicology* **2008,** 17, (5), 344-361.

(105) Reichardt, C., *Solvents and Solvent Effects in Organic Chemistry 2nd ed*. VCH Verlagsgesellaschaft: Weinheim, 1988.

(106) Seshadri, R.; Rao, C. N. R.; Pal, H.; Mukherjee, T.; Mittal, J. P., Interaction of C60 and C70 with aromatic amines in the ground and excited states. Evindence for fullerene--benzene interaction in the ground state. *Chem. Phys. Lett.* **1993,** 205, (4-5), 395-398.

(107) Zhang, B.; Cho, M.; Fortner, J. D.; Lee, J.; Huang, C. H.; Hughes, J. B.; Kim, J. H., Delineating oxidative processes of aqueous C60 preparations: Role of THF peroxide. *Environ. Sci. Technol.* **2009,** 43, (1), 108-113.

(108) Wi, S.; Spano, J.; Ducker, W. A., Hindered rotation of water near C60. *J. Phys. Chem. C* **2010,** 114, (35), 14986-14991.

(109) Hungerbuhler, H.; Guldi, D. M.; Asmus, K. D., Incorporation of C60 into artificial lipid-membranes. *J. Am. Chem. Soc.* **1993,** 115, (8), 3386-3387.

(110) Heiney, P. A.; Fischer, J. E.; McGhie, A. R.; Romanow, W. J.; Denenstein, A. M.; McCauley, J. P.; Smith, A. B.; Cox, D. E., Orientational ordering transition in solid C60. *Phys. Rev. Lett.* **1991,** 66, (22), 2911-2914.

(111) Hotze, E. M.; Bottero, J. Y.; Wiesner, M. R., Theoretical framework for nanoparticle reactivity as a function of aggregation state. *Langmuir* **2010,** 26, (13), 11170-11175.

(112) Chen, K. L.; Elimelech, M., Aggregation and deposition kinetics of fullerene (C60) nanoparticles. *Langmuir* **2006,** 22, (26), 10994-11001.

(113) Jafvert, C. T.; Kulkarni, P. P., Buckminsterfullerene's (C60) octanol-water partition coefficient (Kow) and aqueous solubility. *Environ. Sci. Technol.* **2008,** 42, (16), 5945-5950.

(114) Lee, J.; Cho, M.; Fortner, J. D.; Hughes, J. B.; Kim, J. H., Transformation of aggregate C60 in the aqueous phase by UV irradiation. *Environ. Sci. Technol.* **2009,** 43, (13), 4878-4883.

(115) Isaacson, C. W.; Kleber, M.; Field, J. A., Quantitative analysis of fullerene nanomaterials in environmental systems: A critical review. *Environ. Sci. Technol.* **2009,** 43, (17), 6463-6474.

(116) Bouchard, D.; Ma, X., Extraction and high-performance liquid chromatographic analysis of C60, C70, and [6,6]-phenyl C61-butyric acid methyl ester in synthetic and natural waters. *J. Chromatogr. A* **2008,** 1203, (2), 153-159.

(117) Isaacson, C. W.; Usenko, C. Y.; Tanguay, R. L.; Field, J. A., Quantification of fullerenes by LC/ESI-MS and its application to in vivo toxicity assays. *Anal. Chem.* **2007,** 79, (23), 9091-9097.

(118) Wang, C.; Shang, C.; Westerhoff, P., Quantification of fullerene aggregate nC(60) in wastewater by high-performance liquid chromatography with UV-vis spectroscopic and mass spectrometric detection. *Chemosphere* **2010,** 80, (3), 334-339.

(119) Spohn, P.; Hirsch, C.; Hasler, F.; Bruinink, A.; Krug, H. F.; Wick, P., C60 fullerene: A powerful antioxidant or a damaging agent? The importance of an in-depth material characterization prior to toxicity assays. *Environ. Pollut.* **2009,** 157, (4), 1134-1139.

(120) Pospisil, L.; Gal, M.; Hromadova, M.; Bulickova, J.; Kolivoska, V.; Cvacka, J.; Novakova, K.; Kavan, L.; Zukalova, M.; Dunsch, L., Search for the form of fullerene C60 in aqueous medium. *Phys. Chem. Chem. Phys.* **2010,** 12, (42), 14095-14101.

(121) Chang, X.; Vikesland, P. J., UV-Vis spectroscopic properties of nC60 produced via extended mixing. *submitted* **2011**.

(122) Yu, W. W.; Qu, L.; Guo, W.; Peng, X., Experimental determination of the extinction coefficient of CdTe, CdSe, and CdS nanocrystals. *Chem. Mat.* **2003,** 15, (14), 2854-2860.

(123) Cademartiri, L.; Montanari, E.; Calestani, G.; Migliori, A.; Guagliardi, A.; Ozin, G. A., Size-dependent extinction coefficients of PbS quantum dots. *J. Am. Chem. Soc.* **2006,** 128, (31), 10337-10346.

(124) Torres, V. M.; Posa, M.; Srdjenovic, B.; Simplicio, A. L., Solubilization of fullerene C60 in micellar solutions of different solubilizers. *Colloid Surf. B-Biointerfaces* **2010,** 82, (1), 46-53.

(125) Micali, N.; Mallamace, F.; Castriciano, M.; Romeo, A.; Scolaro, L. M., Separation of scattering and absorption contributions in UV/visible spectra of resonant systems. *Anal. Chem.* **2001,** 73, (20), 4958-4963.

(126) Striolo, A.; Ward, J.; Prausnitz, J. M.; Parak, W. J.; Zanchet, D.; Gerion, D.; Milliron, D.; Alivisatos, A. P., Molecular weight, osmotic second virial coefficient, and extinction coefficient of colloidal CdSe nanocrystals. *J. Phys. Chem. B* **2002,** 106, (21), 5500-5505.

(127) Wang, Y.; Herron, N., Nanometer-sized semiconductor clusters -Materials synthesis, quantum size effects, and photophysical properties. *J. Phys. Chem.* **1991,** 95, (2), 525-532.

(128) Link, S.; El-Sayed, M. A., Spectral properties and relaxation dynamics of surface plasmon electronic oscillations in gold and silver nanodots and nanorods. *J. Phys. Chem. B* **1999,** 103, (40), 8410-8426.

(129) Liu, X.; Atwater, M.; Wang, J.; Huo, Q., Extinction coefficient of gold nanoparticles with different sizes and different capping ligands. *Colloid Surf. B-Biointerfaces* **2007,** 58, (1), 3-7.

(130) Jain, P. K.; Lee, K. S.; El-Sayed, I. H.; El-Sayed, M. A., Calculated absorption and scattering properties of gold nanoparticles of different size, shape, and composition: Applications in biological imaging and biomedicine. *J. Phys. Chem. B* **2006,** 110, (14), 7238-7248.

(131) Schmelz, O.; Mews, A.; Basche, T.; Herrmann, A.; Mullen, K., Supramolecular complexes from CdSe nanocrystals and organic fluorophors. *Langmuir* **2001,** 17, (9), 2861-2865.

(132) Dai, Q.; Wang, Y.; Li, X.; Zhang, Y.; Pellegrino, D. J.; Zhao, M.; Zou, B.; Seo, J.; Wang, Y.; Yu, W. W., Size-dependent composition and molar extinction coefficient of PbSe semiconductor nanocrystals. *Acs Nano* **2009,** 3, (6), 1518-1524.

(133) Moreels, I.; Lambert, K.; Smeets, D.; De Muynck, D.; Nollet, T.; Martins, J. C.; Vanhaecke, F.; Vantomme, A.; Delerue, C.; Allan, G.; Hens, Z., Size-dependent optical properties of colloidal PbS quantum dots. *Acs Nano* **2009,** 3, (10), 3023-3030.

(134) Kelly, K. L.; Coronado, E.; Zhao, L. L.; Schatz, G. C., The optical properties of metal nanoparticles: The influence of size, shape, and dielectric environment. *J. Phys. Chem. B* **2003,** 107, (3), 668-677.

(135) Lee, K. S.; El-Sayed, M. A., Dependence of the enhanced optical scattering efficiency relative to that of absorption for gold metal nanorods on aspect ratio, size, end-cap shape, and medium refractive index. *J. Phys. Chem. B* **2005,** 109, (43), 20331-20338.

(136) Ren, S. L.; Wang, Y.; Rao, A. M.; McRae, E.; Holden, J. M.; Hager, T.; Wang, K. A.; Lee, W. T.; Ni, H. F.; Selegue, J.; Eklund, P. C., Ellipsometric determiantion of the optical-constants of C60 (buckministerfullerene) films. *Appl. Phys. Lett.* **1991,** 59, (21), 2678-2680.

(137) Markovic, B. T.; Jokanovic, V.; Jovanovic, S.; Kleut, D.; Dramicanin, M.; Markovic, Z., Surface chemical modification of fullerene by mechanochemical treatment. *Appl. Surf. Sci.* **2009,** 255, (17), 7537-7541.

(138) Nath, N.; Chilkoti, A., Label-free biosensing by surface plasmon resonance of nanoparticles on Glass: Optimization of nanoparticle size. *Anal. Chem.* **2004,** 76, (18), 5370-5378.

(139) Rance, G. A.; Marsh, D. H.; Khlobystov, A. N., Extinction coefficient analysis of small alkanethiolate-stabilised gold nanoparticles. *Chem. Phys. Lett.* **2008,** 460, (1-3), 230-236.

(140) Scharff, P.; Risch, K.; Carta-Abelmann, L.; Dmytruk, I. M.; Bilyi, M. M.; Golub, O. A.; Khavryuchenko, A. V.; Buzaneva, E. V.; Aksenov, V. L.; Avdeev, M. V.; Prylutskyy, Y. I.; Durov, S. S., Structure of C-60 fullerene in water: spectroscopic data. *Carbon* **2004,** 42, (5-6), 1203-1206.

(141) Oberdorster, E.; Zhu, S. Q.; Blickley, T. M.; McClellan-Green, P.; Haasch, M. L., Ecotoxicology of carbon-based engineered nanoparticles: Effects of fullerene (C60) on aquatic organisms. *Carbon* **2006,** 44, (6), 1112-1120.

(142) Ojeda, C. B.; Rojas, F. S., Determination of rhodium: Since the origins until today: Spectrophotometric methods. *Talanta* **2005,** 67, (1), 1-19.

(143) Girinath, P.; Ahmad, R., Effect of lysine side chain length on intra-helical glutamate-lysine ion pairing interactions. *Biochemistry* **2007,** 46, (37), 10528-10537.

(144) Pace, C. N.; Vajdos, F.; Fee, L.; Grimsley, G.; Gray, T., How to measure and predict the molar absorption-coefficient of a protein. *Protein Sci.* **1995,** 4, (11), 2411-2423.

(145) Colvin, V. L., The potential environmental impact of engineered nanomaterials. *Nat. Biotechnol.* **2003,** 21, (10), 1166-1170.

(146) Kamanina, N. V., Photoinduced phenomena in fullerene-doped PDLC: potentials for optoelectronic applications. *Opto-Electron. Rev.* **2004,** 12, (3), 285-289.

(147) Andrievsky, G.; Klochkov, V.; Derevyanchenko, L., Is the C60 fullerene molecule toxic?! *Fuller. Nanotub. Carbon Nanostruct.* **2005,** 13, (4), 363-376.

(148) Zakharian, T. Y.; Seryshev, A.; Sitharaman, B.; Gilbert, B. E.; Knight, V.; Wilson, L. J., A fullerene-paclitaxel chemotherapeutic: Synthesis, characterization, and study of biological activity in tissue culture. *J. Am. Chem. Soc.* **2005,** 127, (36), 12508-12509.

(149) Collins, M. R.; Amy, G. L.; Steelink, C., Molecular-weight distribution, carboxylic acidity, and humic substances content of aquatic organic-matter - Implications for removal during water-treatment. *Environ. Sci. Technol.* **1986,** 20, (10), 1028-1032.

(150) Lee, S.; Cho, J. W.; Elimelech, M., Combined influence of natural organic matter (NOM) and colloidal particles on nanofiltration membrane fouling. *J. Membr. Sci.* **2005,** 262, (1-2), 27-41.

(151) Kang, S.; Mauter, M. S.; Elimelech, M., Microbial cytotoxicity of carbon-based nanomaterials: Implications for river water and wastewater effluent. *Environ. Sci. Technol.* **2009,** 43, (7), 2648-2653.

(152) Gao, J.; Youn, S.; Hovsepyan, A.; Llaneza, V. L.; Wang, Y.; Bitton, G.; Bonzongo, J. C. J., Dispersion and toxicity of selected manufactured nanomaterials in natural river water samples: Effects of water chemical composition. *Environ. Sci. Technol.* **2009,** 43, (9), 3322-3328.

(153) Li, D.; Lyon, D. Y.; Li, Q.; Alvarez, P. J. J., Effect of soil sorption and aquatic natural organic matter on the antibacterial activity of a fullerene water suspension. *Environ. Toxicol. Chem.* **2008,** 27, (9), 1888-1894.

(154) Mudunkotuwa, I. A.; Grassian, V. H., Citric acid adsorption on TiO2 nanoparticles in aqueous suspensions at acidic and circumneutral pH: Surface Coverage, surface speciation, and its impact on nanoparticle-nanoparticle interactions. *J. Am. Chem. Soc.* **2010,** 132, (42), 14986-14994.

(155) Hiemenz, P. C.; Rajagopalan, R., *Principles of Colloid and Surface Chemistry*. Marcel Dekker, Inc.: New York, 1997.

(156) Isaacson, C.; Zhang, W.; Powell, T.; Ma, X.; Bouchard, D., Temporal changes in aqu/C60 physical-chemical, deposition, and transport characteristics in aqueous systems. *Environ. Sci. Technol.* **2011,** ASAP.

(157) Burns, J. L.; Yan, Y.-d.; Jameson, G. J.; Biggs, S., A light scattering study of the fractal aggregation behavior of a model colloidal system. *Langmuir* **1997,** 13, (24), 6413-6420.

(158) Thill, A.; Spalla, O., Aggregation due to capillary forces during drying of particle submonolayers. *Colloid Surf. A-Physicochem. Eng. Asp.* **2003,** 217, (1-3), 143-151.

(159) Wang, C.; Ravi, P.; Tam, K. C., Morphological transformation of [60]fullerene-containing poly(acrylic acid) induced by the binding of surfactant. *Langmuir* **2006,** 22, (7), 2927-2930.

(160) El-Sayed, M. A., Some interesting properties of metals confined in time and nanometer space of different shapes. *Accounts Chem. Res.* **2001,** 34, (4), 257-264.

(161) Narayanan, R.; El-Sayed, M. A., Catalysis with transition metal nanoparticles in colloidal solution: Nanoparticle shape dependence and stability. *J. Phys. Chem. B* **2005,** 109, (26), 12663-12676.

(162) Domingos, R. F.; Baalousha, M. A.; Ju-Nam, Y.; Reid, M. M.; Tufenkji, N.; Lead, J. R.; Leppard, G. G.; Wilkinson, K. J., Characterizing manufactured nanoparticles in the environment: Multimethod determination of particle sizes. *Environ. Sci. Technol.* **2009,** 43, (19), 7277-7284.

(163) Skokan, E. V.; Arkhangelskii, I. V.; Izotov, D. E.; Chelovskaya, N. V.; Nikulin, M. M.; Velikodnyi, Y. A., Stability of hexagonal modification of fullerite C60. *Carbon* **2005,** 43, (4), 803-808.

(164) Chang, X.; Vikesland, P. J., Uncontrolled variability in the extinction spectra of aq/nC60. *manuscript* **2011**.

(165) Ji, X. H.; Song, X. N.; Li, J.; Bai, Y. B.; Yang, W. S.; Peng, X. G., Size control of gold nanocrystals in citrate reduction: The third role of citrate. *J. Am. Chem. Soc.* **2007,** 129, (45), 13939-13948.

(166) Jiang, X. C.; Chen, C. Y.; Chen, W. M.; Yu, A. B., Role of citric acid in the formation of silver nanoplates through a synergistic reduction approach. *Langmuir* **2009,** 26, (6), 4400-4408.

(167) Pillai, Z. S.; Kamat, P. V., What factors control the size and shape of silver nanoparticles in the citrate ion reduction method? *J. Phys. Chem. B* **2004,** 108, (3), 945-951.

(168) Jiang, L.; Gao, L., Modified carbon nanotubes: an effective way to selective attachment of gold nanoparticles. *Carbon* **2003,** 41, (15), 2923-2929.

(169) Gautrot, J. E.; Hodge, P.; Cupertino, D.; Helliwell, M., Experimental evidence for carbonyl-pi electron cloud interactions. *New J. Chem.* **2006,** 30, (12), 1801-1807.

(170) Jiang, L. Q.; Gao, L., Modified carbon nanotubes: an effective way to selective attachment of gold nanoparticles. *Carbon* **2003,** 41, (15), 2923-2929.

(171) Balch, A. L.; Lee, J. W.; Noll, B. C.; Olmstead, M. M., Disorder in a crystalline form of buckminsterfullerene - C60.4C6H6. *J. Chemi. Soc.Chem.Comm.* **1993**, (1), 56-58.

(172) Crane, J. D.; Hitchcock, P. B.; Kroto, H. W.; Taylor, R.; Walton, D. R. M., Preparation and characterization of C60(ferrocene)2. *J. Chem. Soc., Chem. Commun.* **1992**, (24), 1764-1765.

(173) Schulz-Dobrick, M.; Panthofer, M.; Jansen, M., Supramolecular arrangement of C60 and phenol into a square packing arrangement pi-pi interacting and hydrogen-bonded rods in C60 center dot 5C(6)H(5)OH. *Eur. J. Inorg. Chem.* **2005**, (20), 4064-4069.

(174) Pekker, S.; Kovats, E.; Oszlanyi, G.; Benyei, G.; Klupp, G.; Bortel, G.; Jalsovszky, I.; Jakab, E.; Borondics, F.; Kamaras, K.; Bokor, M.; Kriza, G.; Tompa, K.; Faigel, G., Rotor-stator molecular crystals of fullerenes with cubane. *Nat. Mater.* **2005,** 4, (10), 764-767.

(175) Porter, A. E.; Gass, M.; Muller, K.; Skepper, J. N.; Midgley, P.; Welland, M., Visualizing the uptake of C60 to the cytoplasm and nucleaus of human monocyte-derived macrophage cells using energy-filtered transmission electron microscopy and electron tomography. *Environ. Sci. Technol.* **2007,** 41, (8), 3012-3017.

(176) Porter, A. E.; Muller, K.; Skepper, J.; Midgley, P.; Welland, M., Uptake of C60 by human monocyte macrophages, its localization and implications for toxicity: Studied by high resolution electron microscopy and electron tomography. *Acta Biomater.* **2006,** 2, (4), 409-419.

(177) Chae, S. R.; Hotze, E. M.; Wiesner, M. R., Evaluation of the oxidation of organic compounds by aqueous suspensions of photosensitized hydroxylated-C60 Fullerene aggregates. *Environ. Sci. Technol.* **2009,** 43, (16), 6208-6213.

(178) Lee, J.; Fortner, J. D.; Hughes, J. B.; Kim, J. H., Photochemical production of reactive oxygen species by C60 in the aqueous phase during UV irradiation. *Environ. Sci. Technol.* **2007,** 41, (7), 2529-2535.

(179) Lecoanet, H. F.; Bottero, J. Y.; Wiesner, M. R., Laboratory assessment of the mobility of nanomaterials in porous media. *Environ. Sci. Technol.* **2004,** 38, (19), 5164-5169.

(180) Espinasse, B.; Hotze, E. M.; Wiesner, M. R., Transport and retention of colloidal aggregates of C-60 in porous media: Effects of organic macromolecules, ionic composition, and preparation method. *Environ. Sci. Technol.* **2007,** 41, (21), 7396-7402.

(181) Li, Q. L.; Xie, B.; Hwang, Y. S.; Xu, Y. J., Kinetics of C60 fullerene dispersion in water enhanced by natural organic matter and sunlight. *Environ. Sci. Technol.* **2009,** 43, (10), 3574-3579.

(182) Isaacson, C. W.; Bouchard, D. C., Effects of humic acid and sunlight on the generation and aggregation state of aqu/C60 nanoparticles. *Environ. Sci. Technol.* **2010,** 44, (23), 8971-8976.

(183) Lyon, D. Y.; Brunet, L.; Hinkal, G. W.; Wiesner, M. R.; Alvarez, P. J. J., Antibacterial activity of fullerene water suspensions (nC(60)) is not due to ROS-mediated damage. *Nano Lett.* **2008,** 8, (5), 1539-1543.

(184) Tervonen, K.; Waissi, G.; Petersen, E. J.; Akkanen, J.; Kukkonen, J. V. K., Analysis of fullerene C60 and kinetic measurement for its accumulation and depuration in daphnia magna. *Environ. Toxicol. Chem.* **2010,** 29, (5), 1072-1078.

(185) Qu, X. L.; Hwang, Y. S.; Alvarez, P. J. J.; Bouchard, D.; Li, Q. L., UV irradiation and humic acid mediate aggregation of aqueous fullerene (nC(60)) nanoparticles. *Environ. Sci. Technol.* **2010,** 44, (20), 7821-7826.

(186) Chang, X.; Vikesland, P. J., Association of citrate with nC60: Surface charge, morphology, and spectral characteristics. *manuscript* **2011**.

(187) Zhang, L.; Wang, L.; Zhang, P.; Kan, A. T.; Chen, W.; Tomson, M. B., Facilitated Transport of 2,2',5,5'-polychlorinated biphenyl and phenanthrene by fullerene nanoparticles through sandy soil columns. *Environ. Sci. Technol.* **2011,** 45, (4), 1341-1348.

(188) Hu, X. L.; Liu, J. F.; Zhou, Q. F.; Lu, S. Y.; Liu, R.; Cui, L.; Yin, D. Q.; Mayer, P.; Jiang, G. B., Bioavailability of organochlorine compounds in aqueous suspensions of fullerene:

Evaluated with medaka (Oryzias latipes) and negligible depletion solid-phase microextraction. *Chemosphere* **2010,** 80, (7), 693-700.

(189) Salabat, A.; Shamshiri, L.; Sahrakar, F., Thermodynamic and transport properties of aqueous trisodium citrate system at 298.15 K. *J. Mol. Liq.* **2005,** 118, (1-3), 67-70.

(190) Sharma, V.; Park, K.; Srinivasarao, M., Shape separation of gold nanorods using centrifugation. *Proc. Natl. Acad. Sci. U. S. A.* **2009,** 106, (13), 4981-4985.

(191) Zhou, D. X.; Keller, A. A., Role of morphology in the aggregation kinetics of ZnO nanoparticles. *Water Res.* **2010,** 44, (9), 2948-2956.

(192) Vold, M. J., Van der Waals' attraction between anisometric particles. *J. Colloid Sci.* **1954,** 9, (5), 451-459.

(193) Lin, S.; Wiesner, M. R., Exact analytical expressions for the potential of electrical double layer interactions for a sphere-plate system. *Langmuir* **2010,** 26, (22), 16638-16641.

(194) Cheng, X. K.; Kan, A. T.; Tomson, M. B., Study of C60 transport in porous media and the effect of sorbed C60 on naphthalene transport. *J. Mater. Res.* **2005,** 20, (12), 3244-3254.

(195) Yang, K.; Zhu, L.; Xing, B., Adsorption of polycyclic aromatic hydrocarbons by carbon nanomaterials. *Environ. Sci. Technol.* **2006,** 40, (6), 1855-1861.

(196) Pan, B.; Lin, D.; Mashayekhi, H.; Xing, B., Adsorption and hysteresis of bisphenol A and 17a-ethinyl estradiol on carbon nanomaterials. *Environ. Sci. Technol.* **2008,** 42, (15), 5480-5485.

(197) Yang, K.; Xing, B. S., Adsorption of organic compounds by carbon nanomaterials in aqueousphase: Polanyi theory and its application. *Chem. Rev.* **2010,** 110, (10), 5989-6008.

(198) Fowler, P. W.; Ceulemans, A., Electron deficiency of the fullerenes. *J. Phys. Chem.* **1995,** 99, (2), 508-510.